Mechanical Behavior of Polypropylene and Epoxy-based Woven Glass Fiber Reinforced Composites Under High-Velocity Impact Loading

by

Saikanth Paruchuru

A thesis submitted in partial fulfillment
of the requirements for the degree of
Master of Science in Engineering
(Mechanical Engineering)
in the University of Michigan–Dearborn
2019

Master's Thesis Committee:
Associate Professor German Reyes-Villanueva, Chair
Professor Hong-Tae Kang
Assistant Professor Tanjore V. Jayaraman

DEDICATION

To my parents, Mr.Venkateswara Rao Paruchuru and Mrs. Anuradha Paruchuru

and

To my brother, Lakshmi Kanth Paruchuru

for their love and support

ACKNOWLEDGMENTS

I want to express my deepest gratitude and sincere thanks to my mentor, advisor Dr. German Reyes-Villanueva for his technical, financial and moral support. My research work could never be possible without his encouragement. From the bottom of my heart, I will always be grateful to him. I will forever be indebted to him for giving me a rewarding experience. I appreciate him for understanding me and his patience.

I would like to especially thank Dr. Tanjore V. Jayaraman for evaluating my thesis, for his valuable advices, guidance, and support to be a better Graduate Student Instructor. I would also like to express my gratitude to Dr. Hong-Tae Kang for evaluating my thesis.

I want to thank Prakash Mallik Pariti for sharing his valuable experience, for his support and encouragement throughout the thesis. I would also like to thank my friend Sree Sruthi Modala for her encouragement and assistance. I want to express my profound gratitude to my beloved friend Manoghna Myneni. I also would like to thank the Manufacturing Systems and Engineering Laboratory team (Matt Brown, Shawn Simone, Jesse Cross and Josh Postel) whose assistance helped me along the way.

I would like to especially thank my friends Sai Sandeep Bandi,Aqheel Mohammad, Sai Shubhash Karumanchi, Dr.Phani Krishna Sharma Telluri, Sandeep Kolluri, Prasanna Sai Galla, Subramanyam Srinivas Mellacheruvu, Akhil Kumar Reddy Anumula, Prashanth Kumar Gardhas, Kundhan Reddy Choodi, Mukarram Shadaab, Bharat Pochu, Shahzan Iqbal Khaja, Sushma Reddy Vancha, Akhila Dhayapulay Gopi Krishna Nimmagadda, Gaushik Mandava, Nagendra Babu, Prashanth Karanam and Vishnu Pingili for their encouragement.

TABLE OF CONTENTS

DEDICATION……..…..ii

ACKNOWLEDGEMENTS…….iii

LIST OF FIGURES……vi

LIST OF TABLES……..xvi

ABSTRACT……..….xvii

CHAPTER 1. INTRODUCTION…….……...1

1.1 Composites……1

1.2 A Brief History of Composite Materials……1

1.3 Types of Materials……..3
1.3.1 Fibers……...…….....3
1.3.2 Matrix material……..…….…5
1.4 Hybrid Composites……5

1.5 Advanced Composites for Military Applications…….....8
1.5.1 Polymer Matrix Composites…….....8
1.6 Advantages and Disadvantages associated with advanced polymer matrix composites
……...9

1.7 Applications of Polymer Matrix Composites……..…….10

1.8 Requirements of Materials for Defense Applications……...10

1.9 Summary…….....11

References……..12

CHAPTER 2. LITERATURE REVIEW……..……..15

Objectives……...……...18

References……..19

CHAPTER 3. EXPERIMENTAL PROCEDURE…….21

3.1 Manufacturing of Composites……..……21

3.1.1 Manufacturing of Shield Strand S® / Epoxy Composites…….....22
3.1.2 Manufacturing of Twintex® Composites……25

3.2 Cutting of Composites…….....27

3.3 Drilling……..……...27

3.4 Design and Manufacturing of Projectiles…….…….28

3.5 Single Stage Gas Gun Setup……...……..29

3.6 Photron Fast Cam Viewer……32

3.7 E9800 MK2 Velocity Sensor……32

3.8 Impact Energy…….....33

3.9 Ballistic Limit……..…….....33

3.10 Digital Image Correlation……..….....34

References……..….....36

CHAPTER 4. RESULTS AND DISCUSSIONS…….....….37

4.1 Pressure and Velocity Relationship for the spherical head and sharp nose projectiles…….....37

4.2 Ballistic Testing……....38

4.2.1 Impact behavior of Twintex® 2.5 mm thick composites with the spherical head projectile…….....…..43
4.2.2 Impact behavior of Shield Strand S® / Epoxy 2.5 mm thick composites with the spherical head projectile……..54
4.2.3 Impact behavior of Twintex® 4.5 mm thick composites with the spherical head projectile……..71
4.2.4 Impact behavior of Shield Strand S® / Epoxy 4.5 mm thick composites with the spherical head projectile……..84
4.2.5 Impact behavior of Twintex® 2.5 mm thick composites with the sharp nose projectile……106
4.2.6 Impact behavior of Twintex® 4.5 mm thick composites with the sharp nose projectile……116
4.2.7 Impact behavior of Shield Strand S® / Epoxy 2.5 mm thick composites with the sharp nose projectile……...…….……130

4.2.8 Impact behavior of Shield Strand S® / Epoxy 4.5 mm thick composites with the sharp nose projectile……..145

References……....170

CHAPTER 5. CONCLUSIONS…….……...…171

LIST OF FIGURES

Figure 1 Death mask made of cartonnage……..…..2

Figure 2 World War-II Military Aircraft……..…3

Figure 3 Laminated composites with different ply orientation…….…..6

Figure 4 Honeycomb sandwich structures…….….6

Figure 5 Spread Tow Fabrics for Ultralight Composites…….…...7

Figure 6 Steel wire mesh reinforced polyethylene composite pipe…….……...7

Figure 7 Polymer matrix composites of short fibers, continuous fibers, and particles…….…..9

Figure 8 Reinforcements used in the project based on (a) TPP 60 1485 E-glass fibers and (b) Shield Strand S® fibers…….….21

Figure 9 Epoxy resin mixture on a Digital weighing scale……....22

Figure 10 Aluminum mold with Teflon coating ……..…..23

Figure 11 Carver Hydraulic Press…….….24

Figure 12 Hand layup method (Sheild Strand S® fibers with Epoxy resin)…….….24

Figure 13 Shield Strand S® / Epoxy composite…….……..…..25

Figure 14 (a) Prepreg method and (b) Twintex® composite.……...……...…...26

Figure 15 Rigid 7 Inch Wet Tile Saw …….…..…..27

Figure 16 Endmill drilling holes in composites ……...……..……...28

Figure 17 Manufacturing of projectiles (a) Bench Lathe machining the projectile (b) Spherical head and Sharp nose Projectiles.……...…….29

Figure 18 Pictures of Single stage gas gun system and equipment of high velocity impact testing (a) Rectangular chamber for Impact testing (b) Arrangement of high-speed cameras (c) Single stage gas gun system.…….……...……..30

Figure 19 Apx Photron high speed camera……..……..32

Figure 20 E9800 MK2 Velocity sensor ……..…....33

Figure 21 250 x 200 mm Digital Image Correlation calibration panel…….…...34

Figure 22 Speckle pattern …….…....35

Figure 23 Sample pretest results using Digital Image Correlation…….....35

Figure 24 The relationship between pressure and velocity for the spherical head projectile …….……...37

Figure 25 The relationship between pressure and velocity for the sharp nose projectile ……38

Figure 26 Impact velocities used to test the composites with the spherical head projectile …….……...……38

Figure 27 Impact velocities used to test the composites with the sharp nose projectile …….…….....39

Figure 28 The relationship between Maximum displacement and Impact velocity for Twintex® 2.5 mm thick composites impacted with the spherical head projectile and sharpnose projectile ..40

Figure 29 The relationship between Maximum displacement and Impact velocity for Twintex® 4.5 mm thick composites impacted with the spherical head projectile and sharpnose projectile..41

Figure 30 The relationship between Maximum displacement and Impact velocity for Shield Strand S® / Epoxy 2.5 mm thick composites impacted with the spherical head and Sharp nose projectile…….....….42

Figure 31 The relationship between Maximum displacement and Impact velocity for Shield Strand S®/Epoxy 4.5 mm thick composites impacted with the spherical head and sharp nose projectile……..…….42

Figure 32 Twintex® based 2.5 mm thick composite impacted at a velocity of 67.28 m/s with the spherical head projectile…….…..……..44

Figure 33 Displacement vs Stage graph of Twintex® based 2.5 mm thick composite impacted at velocity 67.28 m/s with the spherical head projectile……..…….…..45

Figure 34 3D deformation stages of Twintex® based 2.5 mm thick composite impacted at a velocity 67.28 m/s with the spherical head projectile……..…….....46

Figure 35 Twintex® based 2.5 mm thick composite impacted at a velocity of 76.12 m/s with the spherical head projectile…….……...47

Figure 36 Displacement vs Stage graph of Twintex® based 2.5 mm thick composite impacted at velocity 76.12 m/s with the spherical head projectile…….……...48

Figure 37 3D deformation stages of Twintex® based 2.5 mm thick composite impacted at a velocity 76.12 m/s with the spherical head projectile…….…..…..49

Figure 38 Twintex® based 2.5 mm thick composite impacted at a velocity of 83.78 m/s with the spherical head projectile…….……....50

Figure 39 Displacement vs Stage graph of Twintex® based 2.5 mm thick composite impacted at velocity 83.78 m/s with the spherical head projectile……..…….……....51

Figure 40 3D deformation stages of Twintex® based 2.5 mm thick composite impacted at a velocity 83.78 m/s with the spherical head projectile…….……...52

Figure 41 (a) Twintex® 2.5 mm composite impacted at a velocity of 93.86 m/s with the spherical head projectile (b) High speed camera image (c) Section of impacted composite …….....……...53

Figure 42 Shield Strand S® / Epoxy based 2.5 mm thick composite impacted at a velocity of 74.32 m/s with the spherical head projectile…….....……..55

Figure 43 Displacement vs Stage graph of Shield Strand S® / Epoxy based 2.5 mm thick composite impacted at a velocity 74.32 m/s with the spherical head projectile……...…....…56

Figure 44 3D deformation stages of Shield Strand S® / Epoxy based 2.5 mm thick composite impacted at a velocity 74.32 m/s with the spherical head projectile…….....……...57

Figure 45 Shield Strand S® / Epoxy based 2.5 mm thick composite impacted at a velocity of 88.4 m/s with the spherical head projectile……...…..58

Figure 46 Displacement vs Stage graph of Shield Strand S® / Epoxy based 2.5 mm thick composite impacted at a velocity 88.4 m/s with the spherical head projectile……..…….…..59

Figure 47 3D deformation stages of Shield Strand S® / Epoxy based 2.5 mm thick composite impacted at a velocity 88.4 m/s with the spherical head projectile……...…..60

Figure 48 Shield Strand S® / Epoxy based 2.5 mm thick composite impacted at a velocity of 94.20 m/s with the spherical head projectile……..…...61

Figure 49 Displacement vs Stage graph of Shield Strand S® / Epoxy based 2.5 mm thick composite impacted at a velocity 94.20 m/s with the spherical head projectile……..…….62

Figure 50 3D deformation stages of Shield Strand S® / Epoxy based 2.5 mm thick composite impacted at a velocity 94.20 m/s with the spherical head projectile…….…….63

Figure 51 Shield Strand S® / Epoxy based 2.5 mm thick composite impacted at a velocity of 101.5 m/s with the spherical head projectile……..……..……....64

Figure 52 Displacement vs Stage graph of Shield Strand S® / Epoxy based 2.5 mm thick composite impacted at a velocity 101.5 m/s with the spherical head projectile…….…65

Figure 53 3D deformation stages of Shield Strand S® / Epoxy based 2.5 mm thick composite impacted at a velocity 101.5 m/s with the spherical head projectile……..……..……..…….66

Figure 54 Shield Strand S® / Epoxy based 2.5 mm thick composite impacted at a velocity of 105 m/s with the spherical head projectile…….……..……..…67

Figure 55 Displacement vs Stage graph of Shield Strand S® / Epoxy based 2.5 mm thick composite impacted at a velocity 105 m/s with the spherical head projectile…….……....68

Figure 56 3D deformation stages of Shield Strand S® / Epoxy based 2.5 mm thick composite impacted at a velocity 105 m/s with the spherical head projectile…….69

Figure 57 (a) Shield Strand S ®/ Epoxy based 2.5 mm thick composite impacted at a velocity of 118.5 m/s with the spherical head projectile (b) Section of impacted composite……..70

Figure 58 Twintex® based 4.5 mm thick composite impacted at a velocity of 60.91m/s with the spherical head projectile…….71

Figure 59 Displacement vs Stage graph of Twintex® based 4.5 mm thick composite impacted at a velocity 60.91 m/s with the spherical head projectile…….……72

Figure 60 3D deformation stages of Twintex® based 4.5 mm thick composite impacted at a velocity 60.91 m/s with the spherical head projectile…….73

Figure 61 Twintex® based 4.5 mm thick composite impacted at a velocity of 75.42 m/s with the spherical head projectile…….74

Figure 62 Displacement vs Stage graph of Twintex® based 4.5 mm thick composite impacted at a velocity 75.42 m/s with the spherical head projectile…….75

Figure 63 3D deformation stages of Twintex® based 4.5 mm thick composite impacted at a velocity 75.42 m/s with the spherical head projectile…….76

Figure 64 Twintex® based 4.5 mm thick composite impacted at a velocity of 87.45 m/s with the spherical head projectile…….77

Figure 65 Displacement vs Stage graph of Twintex® based 4.5 mm thick composite impacted at a velocity 87.45 m/s with the spherical head projectile……..…….78

Figure 66 3D deformation stages of Twintex® based 4.5 mm thick composite impacted at a velocity 87.45 m/s with the spherical head projectile…….…79

Figure 67 Twintex® based 4.5 mm thick composite impacted at a velocity of 98.88 m/s with the spherical head projectile…….…80

Figure 68 Displacement vs Stage graph of Twintex® based 4.5 mm thick composite impacted at a velocity 98.88 m/s with the spherical head projectile…….....81

Figure 69 3D deformation stages of Twintex® based 4.5 mm thick composite impacted at a velocity 98.88 m/s with the spherical head projectile…….…82

Figure 70 (a) Twintex® based 4.5 mm thick composite impacted at a velocity of 107.8 m/s with the spherical head projectile (b) Section of impacted composite…..……..…….83

Figure 71 Shield Strand S® / Epoxy based 4.5 mm thick composite impacted at a velocity of 79.35 m/s with the spherical head projectile……..…….……..84

Figure 72 Displacement vs Stage graph of Shield Strand S® / Epoxy based 4.5 mm thick composite impacted at a velocity 79.35 m/s with the spherical head projectile..……...….85

Figure 73 3D deformation stages of Shield Strand S® / Epoxy based 4.5 mm thick composite impacted at a velocity 79.35 m/s with the spherical head projectile.……..…...86

Figure 74 Shield Strand S® / Epoxy based 4.5 mm thick composite impacted at a velocity of 91.58 m/s with the spherical head projectile…….……...….87

Figure 75 Displacement vs Stage graph of Shield Strand S® / Epoxy based 4.5 mm thick composite impacted at a velocity 91.58 m/s with the spherical head projectile……..…88

Figure 76 3D deformation stages of Shield Strand S® / Epoxy based 4.5 mm thick composite impacted at a velocity 91.58 m/s with the spherical head projectile…….....89

Figure 77 Shield Strand S® / Epoxy based 4.5 mm thick composite impacted at a velocity of 103.7 m/s with the spherical head projectile……..…..90

Figure 78 Displacement vs Stage graph of Shield Strand S® / Epoxy based 4.5 mm thick composite impacted at a velocity 103.7 m/s with the spherical head projectile…...……..….91

Figure 79 3D deformation stages of Shield Strand S® / Epoxy based 4.5 mm thick composite impacted at a velocity 103.7 m/s with the spherical head projectile..……..…..92

Figure 80 Shield Strand S® / Epoxy based 4.5 mm thick composite impacted at a velocity of 116.3 m/s with the spherical head projectile…….……...93

Figure 81 Displacement vs Stage graph of Shield Strand S® / Epoxy based 4.5 mm thick composite impacted at a velocity 116.3 m/s with the spherical head projectile…….…….94

Figure 82 3D deformation stages of Shield Strand S® / Epoxy based 4.5 mm thick composite impacted at a velocity 116.3 m/s with the spherical head projectile…...…….……..95

Figure 83 Shield Strand S® / Epoxy based 4.5 mm thick composite impacted at a velocity of 126.7 m/s with the spherical head projectile……...…….……96

Figure 84 Displacement vs Stage graph of Shield Strand S® / Epoxy based 4.5 mm thick composite impacted at a velocity 126.7 m/s with the spherical head projectile...……..…….97

Figure 85 3D deformation stages of Shield Strand S® / Epoxy based 4.5 mm thick composite impacted at a velocity 126.7 m/s with the spherical head projectile……..…98

Figure 86 Shield Strand S® / Epoxy based 4.5 mm thick composite impacted at a velocity of 144.8 m/s with the spherical head projectile……...99

Figure 87 Displacement vs Stage graph of Shield Strand S® / Epoxy based 4.5 mm thick composite impacted at a velocity 144.8 m/s with the spherical head projectile……....100

Figure 88 3D deformation stages of Shield Strand S® / Epoxy based 4.5 mm thick composite impacted at a velocity 144.8 m/s with the spherical head projectile……....101

Figure 89 Shield Strand S® / Epoxy based 4.5 mm thick composite impacted at a velocity of 156.7 m/s with the spherical head projectile……..…….……..102

Figure 90 Displacement vs Stage graph of Shield Strand S® / Epoxy based 4.5 mm thick composite impacted at a velocity 156.7 m/s with the spherical head projectile……..…...103

Figure 91 3D deformation stages of Shield Strand S® / Epoxy based 4.5 mm thick composite impacted at a velocity 156.7 m/s with the spherical head projectile...……..……...104

Figure 92 (a) Shield Strand S ®/ Epoxy based 4.5 mm thick composite impacted at a velocity of 164.5 m/s with the spherical head projectile (b) Section of impacted composite…….….105

Figure 93 Twintex® based 2.5 mm thick composite impacted at a velocity of 60.96 m/s with the sharp nose projectile……...……..…106

Figure 94 Displacement vs Stage graph of Twintex® based 2.5 mm thick composite impacted at a velocity 60.96 m/s with the sharp nose projectile…….…….……...107

Figure 95 3D deformation stages of Twintex® based 2.5 mm thick composite impacted at a velocity 60.96 m/s with the sharp nose projectile…….…….…..….108

Figure 96 Twintex® based 2.5 mm thick composite impacted at a velocity of 71.22 m/s with the sharp nose projectile…….……...…….109

Figure 97 Displacement vs Stage graph of Twintex® based 2.5 mm thick composite impacted at a velocity 71.22 m/s with the sharp nose projectile…….……..…..…110

Figure 98 3D deformation stages of Twintex® based 2.5 mm thick composite impacted at a velocity 71.22 m/s with the sharp nose projectile…….……111

Figure 99 Twintex® based 2.5 mm thick composite impacted at a velocity of 81.09 m/s with the sharp nose projectile…….……112

Figure 100 Displacement vs Stage graph of Twintex® based 2.5 mm thick composite impacted at a velocity 81.09 m/s with the sharp nose projectile…….…..113

Figure 101 3D deformation stages of Twintex® based 2.5 mm thick composite impacted at a velocity 81.09 m/s with the sharp nose projectile…….……...114

Figure 102 (a) Twintex® based 2.5 mm thick composite impacted at a velocity of 92.1 m/s with the sharp nose projectile (b) High speed camera image (c) Section of impacted composite…….…….....115

Figure 103 Twintex® based 4.5 mm thick composite impacted at a velocity ……117

Figure 104 Displacement vs Stage graph of Twintex® based 4.5 mm thick composite impacted at a velocity 58.07m/s with the sharp nose projectile…….....118

Figure 105 3D deformation stages of Twintex® based 4.5 mm thick composite impacted at a velocity 58.07 m/s with the sharp nose projectile……..……..119

Figure 106 Twintex® based 4.5 mm thick composite impacted at a velocity of 66.35 m/s with the sharp nose projectile……120

Figure 107 Displacement vs Stage graph of Twintex® based 4.5 mm thick composite impacted at a velocity 66.35 m/s with the sharp nose projectile……...……...121

Figure 108 3D deformation stages of Twintex® based 4.5 mm thick composite impacted at a velocity 66.35 m/s with the sharp nose projectile…….…….……..122

Figure 109 Twintex® based 4.5 mm thick composite impacted at a velocity of 74.29 m/s with the sharp nose projectile……...…..123

Figure 110 Displacement vs Stage graph of Twintex® based 4.5 mm thick composite impacted at a velocity 74.29 m/s with the sharp nose projectile…….…….....124

Figure 111 3D deformation stages of Twintex® based 4.5 mm thick composite impacted at a velocity 74.29 m/s with the sharp nose projectile…….…….…….…….…125

Figure 112 Twintex® based 4.5 mm thick composite impacted at a velocity of 93.77 m/s with the sharp nose projectile……...…….…….126

Figure 113 Displacement vs Stage graph of Twintex® based 4.5 mm thick composite impacted at a velocity 93.77 m/s with the sharp nose projectile…….…….…….....127

Figure 114 3D deformation stages of Twintex® based 4.5 mm thick composite impacted at a velocity 93.77 m/s with the sharp nose projectile…….……...….128

Figure 115 (a) Twintex® based 4.5 mm composite impacted at a velocity of 103.25 m/s with the sharp nose projectile (b) Section of impacted composite…..…….....……..129

Figure 116 Shield Strand S® / Epoxy based 2.5 mm thick composite impacted at a velocity of 56.7 m/s with the sharp nose projectile…….…….…..130

Figure 117 Displacement vs Stage graph of Shield Strand S® / Epoxy based 2.5 mm thick composite impacted at a velocity 56.7 m/s with the sharp nose projectile……..……..…131

Figure 118 3D deformation stages of Shield Strand S® / Epoxy based 2.5 mm thick composite impacted at a velocity 56.7 m/s with the sharp nose projectile…….……..……..132

Figure 119 Shield Strand S® / Epoxy based 2.5 mm thick composite impacted at a velocity of 68.5 m/s with the sharp nose projectile…….…...133

Figure 120 Displacement vs Stage graph of Shield Strand S® / Epoxy based 2.5 mm thick composite impacted at a velocity 68.5 m/s with the sharp nose projectile…….134

Figure 121 3D deformation stages of Shield Strand S® / Epoxy based 2.5 mm thick composite impacted at a velocity 68.5 m/s with the sharp nose projectile…….135

Figure 122 Shield Strand S® / Epoxy based 2.5 mm thick composite impacted at a velocity of 79.28 m/s with the sharp nose projectile…….....……..…..136

Figure 123 Displacement vs Stage graph of Shield Strand S® / Epoxy based 2.5 mm thick composite impacted at a velocity 79.28 m/s with the sharp nose projectile……..…137

Figure 124 3D deformation stages of Shield Strand S® / Epoxy based 2.5 mm thick composite impacted at a velocity 79.28 m/s with the sharp nose projectile…….....138

Figure 125 Shield Strand S® / Epoxy based 2.5 mm thick composite impacted at a velocity of 90.57 m/s with the sharp nose projectile…….…..139

Figure 126 Displacement vs Stage graph of Shield Strand S® / Epoxy based 2.5 mm thick composite impacted at a velocity 90.57 m/s with the sharp nose projectile…….140

Figure 127 3D deformation stages of Shield Strand S® / Epoxy based 2.5 mm thick composite impacted at a velocity 90.57 m/s with the sharp nose projectile….……..….141

Figure 128 Shield Strand S® / Epoxy based 2.5 mm thick composite impacted at a velocity of 114.4 m/s with the sharp nose projectile…….…….142

Figure 129 3D deformation stages of Shield Strand S® / Epoxy based 2.5 mm thick composite impacted at a velocity 114.4 m/s with the sharp nose projectile….…….…….143

Figure 130 (a) Shield Strand S® / Epoxy based 2.5 mm composite impacted at a velocity of 125.1 m/s with the sharp nose projectile (b) Section of impacted composit……..144

Figure 131 Shield Strand S® / Epoxy based 4.5 mm thick composite impacted at a velocity of 80.5 m/s with the sharp nose projectile……..…..……145

Figure 132 Displacement vs Stage graph of Shield Strand S® / Epoxy based 4.5 mm thick composite impacted at a velocity 80.5 m/s with the sharp nose projectile…….....146

Figure 133 3D deformation stages of Shield Strand S® / Epoxy based 4.5 mm thick composite impacted at a velocity 80.5 m/s with the sharp nose projectile…..……..…147

Figure 134 Shield Strand S® / Epoxy based 4.5 mm thick composite impacted at a velocity of 95.69 m/s with the sharp nose projectile……..……....148

Figure 135 Displacement vs Stage graph of Shield Strand S® / Epoxy based 4.5 mm thick composite impacted at a velocity 95.69 m/s with the sharp nose projectile……...149

Figure 136 3D deformation stages of Shield Strand S® / Epoxy based 4.5 mm thick composite impacted at a velocity 95.69 m/s with the sharp nose projectile…….……...150

Figure 137 Shield Strand S® / Epoxy based 4.5 mm thick composite impacted at a velocity of 109.4 m/s with the sharp nose projectile……..……...…..151

Figure 138 Displacement vs Stage graph of Shield Strand S® / Epoxy based 4.5 mm thick composite impacted at a velocity 109.4 m/s with the sharp nose projectile……..152

Figure 139 3D deformation stages of Shield Strand S® / Epoxy based 4.5 mm thick composite impacted at a velocity 109.4 m/s with the sharp nose projectile….……..…….153

Figure 140 Shield Strand S® / Epoxy based 4.5 mm thick composite impacted at a velocity of 121.6 m/s with the sharp nose projectile…….…….….154

Figure 141 Displacement vs Stage graph of Shield Strand S® / Epoxy based 4.5 mm thick composite impacted at a velocity 121.6 m/s with the sharp nose projectile…….155

Figure 142 3D deformation stages of Shield Strand S® / Epoxy based 4.5 mm thick composite impacted at a velocity 121.6 m/s with the sharp nose projectile……...….156

Figure 143 Shield Strand S® / Epoxy based 4.5 mm thick composite impacted at a velocity of 134.24 m/s with the sharp nose projectile……..…...157

Figure 144 Displacement vs Stage graph of Shield Strand S® / Epoxy based 4.5 mm thick composite impacted at a velocity 134.24 m/s with the sharp nose projectile……...…..158

Figure 145 3D deformation stages of Shield Strand S® / Epoxy based 4.5 mm thick composite impacted at a velocity 134.24 m/s with the sharp nose projectile…….....159

Figure 146 Shield Strand S® / Epoxy based 4.5 mm thick composite impacted at a velocity of 152.4 m/s with the sharp nose projectile……...…….……..160

Figure 147 Displacement vs Stage graph of Shield Strand S® / Epoxy based 4.5 mm thick composite impacted at a velocity 152.4 m/s with the sharp nose projectile.……....161

Figure 148 3D deformation stages of Shield Strand S® / Epoxy based 4.5 mm thick composite impacted at a velocity 152.4 m/s with the sharp nose projectile…..…….162

Figure 149 (a) Shield Strand S ®/ Epoxy based 4.5 mm composite impacted at a velocity of 173. 4 m/s with the sharp nose projectile (b) Section of impacted composite…..……..…….163

Figure 150 Relation between Perforation energy and specific perforation energy for Twintex® composites impacted with the spherical head and sharp nose projectiles…….…..164

Figure 151 Relation between Perforation energy and specific perforation energy for Shield Strand S® / Epoxy composites impacted with the spherical head and sharp nose projectiles……...165

Figure 152 Three point bending testing on composite using an Instron 5967 universal testing machine…….……..……167

Figure 153 Relation between experimental and theroritical ballistic limit for Twintex® based composites impacted with the spherical head and sharp nose projectile…….…...168

Figure 154 Relation between experimental and theroritical ballistic limit for Shield Strand S® / Epoxy based composites impacted with the spherical head and sharp nose projectile……..168

LIST OF TABLES

Table 1 The relationship between the Impact velocities and the maximum displacements when the Twintex® and Shield Strand S® / Epoxy composites are impacted with the spherical head Projectiles……..…….…....39

Table 2 The relationship between the Impact velocities and the maximum displacements when the Twintex® and Shield Strand S® / Epoxy composites are impacted with the sharp nose projectiles. ……..…….....39

Table 3 Relationship between Impact velocity and Impact energy for Shield Strand S® / Epoxy and E Glass fiber / Polypropylene tested with the spherical head projectile…….....165

Table 4 Relationship between Impact velocity and Impact energy for Shield Strand S® / Epoxy and E Glass fiber / Polypropylene tested with the sharp nose projectile……..…165

ABSTRACT

Assessment of high-velocity impact resistance is necessary for light-weight structures that may be subjected to the impact loading conditions. Polymer matrix composites are one of the most commonly used materials in light weight applications. They are classified into various types based on the type of fibers, the quantity of fibers, the orientation of fibers, and type of matrix or resin used. The fibers that are generally preferred for the ballistic applications are aramid fibers, carbon fibers, and glass fibers. The objective of this research project is to study the ballistic properties of glass fiber thermoplastic and thermoset based woven polymer matrix composites using Shield Strand S ® / Epoxy, E-glass fibers / Polypropylene (Twintex ®) composites by spherical head and sharp nose projectiles. Composites were manufactured with a number of fiber layers using hand layup and compression method. Ballistic testing was performed with a single stage gas system, and impact velocities ranged between 50 m/s-180 m/s. After each test, impact velocity and impact energy was analyzed using a velocity sensor. Modes of failure and ballistic limit of the composites were investigated using high-speed cameras (APX-Photron) and digital image correlation, maximum transient out of plane displacements at each stage of impact and final back face displacement of the specimens after the impact were revealed. Finally, Analytical modeling was used to predict the ballistic limit of these composite materials.

CHAPTER 1

INTRODUCTION

1.1 Composites

A composite can be defined as a material which is manufactured by combining two or more constituents. These materials exhibit better properties than the individual components alone. The primary reason for using composites is that they have high stiffness and superior strength when compared with metals and their alloys. The weight of composites is also less compared with them [1]. Composites can be either natural or artificial. Heavy loads or forces may damage the composite materials entirely, or they may ruin a few layers. This phenomenon is referred to as Delamination. Depending on the application of composite materials, to predict and prevent the failure, various mechanical tests are performed on them [2].

1.2 A Brief History of Composite Materials

The first composite material was made by the Egyptians based on straw and mud for construction purposes. Wood and bamboo are a few examples of raw materials which were used by the ancient humans to make natural composites, also used those composites for the same purpose [2]. Around 3400 B.C ancient Mesopotamians created plywood by gluing pieces of wood together. Later, in between 2181-2055 B.C, ancient Egyptians made a material called Cartonnage which contained linen covered with plaster material. Cartonnage was used as a source to make death masks and portraits as shown in Figure 1[3,4].

Figure 1. Death mask made of cartonnage [4].

In 1500 B.C, people in Egypt and Mesopotamia used straws to reinforce boats and mud bricks. In 1200 B.C, Mongols made archery bows by combining materials like bamboo, silk, cattle tendons and horns [5].

In the 1800s, builders experimented laminating the kraft papers with a natural resin called shellac to make paper laminate, In a period between 1870-1890, the first synthetic resins were created which could be converted from a liquid state to a solid state and included celluloid and melamine [5].

In the 19th century, plastics like vinyl polystyrene and polyester were developed [3]. In 1907, Leo Hedrick Backeland invented Bakelite ® which was used in the Rolls Royce in 1917. In the 1920's, polymer resins were further developed. In the 1930's, glass fibers were combined with polyester by the Owens Illinois Glass company, and the result was a durable and lightweight composite. The same company in 1942 used those composites in the manufacturing of boats [6].

Between 1945-1948, during the period of World War-II, fiber reinforced plastics were used for military applications figure 2 shows World War-II military aircraft [6]. In the 1950's, metal matrix composites gained reputation, and they were used in the U.S Navy and U.S Airforce. Advanced composites came into light in the 1960's as they were made with high modulus whiskers and filaments. Later the whiskers were replaced with graphite fibers which provided significant advantages [7].

Figure 2. World War-II Military Aircraft [8].

In 1961, carbon fibers were commercially available in the market. By 1970 graphite fiber composites became notable. Kevlar® was also developed at the same time. In the 1980's, military equipment was manufactured using aramids. Later, polyethylene and liquid crystal polymers replaced aramids since they also exhibited properties like good fatigue resistance, corrosion resistance and they were light in weight. Nomex® and Teflon® were also invented in the same period [9]. First microfill composite was developed in the 1990s which was used to fill tooth cavities [10].

In the early 2000's, Nanotechnology gained popularity and Carbon nanotubes were created during this period. Nanoparticles were mixed with fibers and resins which gave birth to new composites [7]. Until 2010, carbon and glass fiber reinforced plastics were the best source available and showed excellent performance, but they couldn't meet the demands of future requirements. To overcome that situation, advanced composite materials continue to be developed and research is still pursued on them for further development [7].

1.3 Types of Materials

1.3.1 Fibers

Fibers are the primary reinforcing material in composite materials. Fibers possess high specific strength and stiffness. Properties of fiber layers vary with direction and orientation. Depending on applications or requirements, fiber layers are made in different types of weaves; for example, Twill, Satin and Plain weave, etc. Fibers are further classified as long fibers or continuous fibers, and short fibers [11].

Glass Fibers

Glass fibers are one of the most commonly type of reinforcement used in industrial applications and they exhibit good impact resistance. They are used in the manufacturing of structural composites. Glass fibers are manufactured by melting raw glass along with silica and other minerals in a furnace. After melting, these fibers are extruded from small orifices. The material obtained from these orifices is referred to as fiber strands. Individual strands are winded together to obtain Tows. Depending on the type of weaves required, rows and columns of tows are arranged. Fibers are also chopped if small fibers are desired. Glass fibers are classified into E(electrical) glass, S(strength) glass, C (chemical) glass, M (modulus) glass, A (alkali) glass, D (dielectric) glass, R glass, T glass, ECR glass for military applications R glass, T glass and S glass are used [11].

Carbon Fibers

The major constituent of carbon fibers is carbon. Due to the strong covalent bond between the carbon atoms they exhibit high specific strength. Depending on the precursor material used, carbon fibers have been classified into four types. Precursor material can be defined as organic or inorganic compounds from which thin filaments or nanofibers are obtained. PAN-based carbon fibers contain acrylonitrile as the primary polymer and little content of other monomers which maintains oxidation. Depending on the type of pitch, carbon fibers are classified into isotropic pitch, mesophase pitch and anisotropic pitch. Vapor grown carbon fibers contain a minute amount of iron deposited on fibers due to pyrolysis of hydrocarbon gas. Cellulose-based carbon fibers were one of the oldest types carbon fibers. All the carbon fibers are manufactured using a standard technique which includes a high-temperature heat treatment with few changes or pretreatment in each method of manufacturing. For example, PAN method starts with the abstraction of fibers from wet spun followed by preheating between 200°C to 400°C and finally heated between 1500°C to 3000°C [12,13].

Aramid fibers

Aramid fibers are the first organic material used as reinforcement for advanced composites with adequate tensile strength and modulus. They are classified into two types: meta-aramid fibers and para-aramid fibers. In meta-aramid fibers, the orientation of fibers is improper or randomly, whereas in para-aramid fibers the fibers are oriented in a pattern. Kevlar® is an example of meta-

aramid fibers and Nomex® is an example of para-aramid fibers. The two methods used for manufacturing aramid fibers wet spinning and dry spinning processes. In the wet spinning process, the mixture of raw materials is spun through water or weak acid to remove inorganic salts whereas, in the dry spinning process, raw materials are spun directly which leaves inorganic salts in the material. Sulfuric acid is used as a solvent in both the methods and further operations like drawing and post curing are also performed. The wet spinning process is preferable for para-aramid fibers, and the dry spinning process is used to make weaker meta-aramid fibers. Aramid fibers provide excellent impact resistance, but tensile strength is decidedly less compared to glass and carbon fibers [14-16].

1.3.2 Matrix material

Matrix acts as a continuous phase in a composite. It protects the fiber from physical attacks, chemical damages and it also transfers loads to the discontinuous phase in a composite. The matrix reduces crack development and cracks propagation.

Thermoset Polymers

Thermoset polymers contain long-chain polymers cross-linked in a three-dimensional pattern. They are manufactured in two phases In first phase polymerization of long-chain takes place, and in the second phase cross-links between the long chain polymers are formed. Unlike thermoplastics, in thermosets, curing takes place which cannot be reversed since the bonds between mere units are strong. Few thermosets can cure at room temperature, for example, epoxy and few thermosets require very high temperature for curing. Thermosets are stable at high temperatures. Typical thermosets are epoxies, polyesters, polyamides, silicones, aminos, alkyds, and phenolics [17].

Thermoplastic polymers

Similar to thermosets, thermoplastic polymers contain long chained molecules but the bond strength between the molecules is lower. Hence, compared with thermoset polymers, thermoplastic polymers have lower strength and stiffness. Thermoplastics can be melted by heating beyond their glass transition temperature and can be fabricated into any required shape. In thermoplastics, the melting and solidification process can be reversed unlike thermosets, but repeated melting and

solidification leads to a reduction of properties. Examples of thermoplastics are polystyrene, PVC (Poly Vinyl Chloride), polystyrene, polypropylene, polyamides, polyesters, polycarbonates, polyethylene, polyimides, arycyclics, ABS(Acrylonitrile-Butadiene-Styrene), cellulosics and fluorocarbons [17].

1.4 Hybrid Composites

Research has shown that regular composite materials sometimes do not meet the desired demands which lead to the development of hybrid materials [18]. Hybrid composites consists of dissimilar materials. Properties of these composites depend upon the composition and the properties of individual materials which are used for fabrication [19]. Application of a hybrid composite depend on the mechanical, chemical and physical stability of the fibers and matrix system.

Hybrid composites are classified into several types, these

1)Tow by Tow composites

In tow by tow composites, the tows of different fibers are arranged randomly or in a regular way to make a hybrid fiber layer.

2) Laminated composites

In the laminated composites, fiber layers with different fiber orientations and distinct types are stacked together in the form of piles to obtain a single hybrid composite as shown in Figure 3.

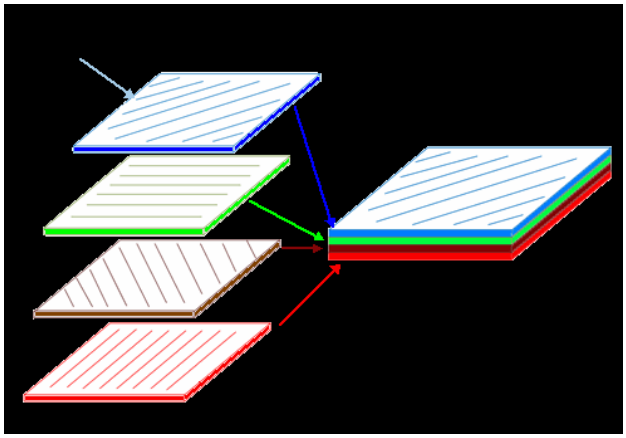

Figure 3. Laminated composites with different ply orientations and distinct fibers [20].

3) Sandwich composite

In the Sandwich composites, a core material is sandwiched between two similar or dissimilar materials with a resin as shown in Figure 4.

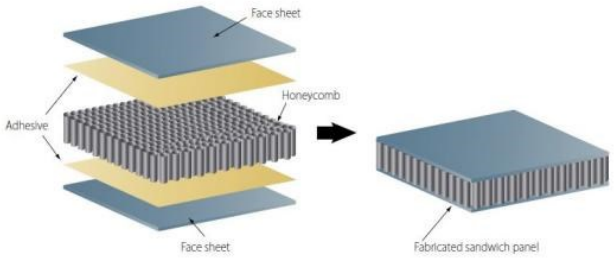

Figure 4. Honeycomb sandwich structures [21].

4) Mixed hybrid composite

In the mixed hybrid composites, a variety of fibers are mixed randomly so that the fibers are distinct which can lead to improvement in mechanical properties as shown in Figure 5.

Figure 5. Spread tow fabrics for ultralight composites [19].

5) Other types

There are various types of other composites that are made by using reinforcing metals, ribs, wires or the combination of all the materials which are mentioned in either fibers or resins [23]. It was suggested that growth in the field of hybrid materials would solve the problems associated with manufacturing processes and reduces wastage [24]. Figure 6 shows steel wire mesh reinforced polyethylene composite pipe which is one of the example for the other types of hybrid composite

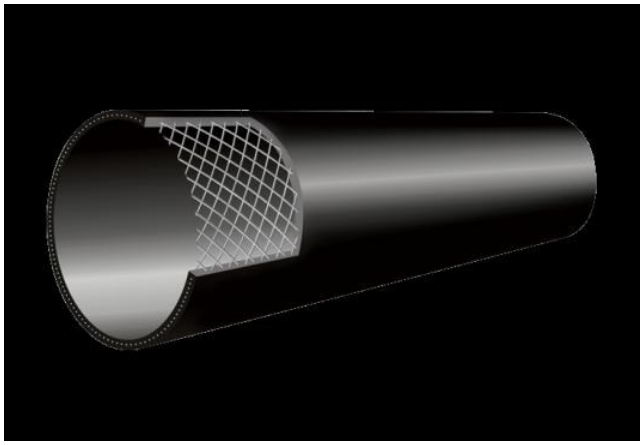

Figure 6. Steel wire mesh reinforced polyethylene composite pipe [23].

1.5 Advanced Composites for Military applications

Composites have been used in defense applications since the 1950's. They overcame the problems associated with using conventional materials individually [25]. Growing demands for better properties lead to the development of advanced composite materials. Advanced composites also play a vital role in the defense automotive and aviation industry. Latest military automotive and aviation applications use composite materials both for interior and exterior components [26]. Examples of combat aircraft and vehicles made of advanced composites include Boeing AH-64 Apache, S-11, F-27 Boeing 787 Dreamliner, Airbus A400M, Boeing 787 Dreamliner, Komatsu D355A, C130, C17 and Foxhound [27].

1.5.1 Polymer Matrix Composites

A polymer matrix composite is a composite material made by combining fibers and polymer matrix [28,29]. Reinforced plastics are a combination of resins and fibers with low stiffness whereas the advanced composite materials are a combination of resins and fibers with high strength and stiffness [27]. Figure 7 shows polymer matrix composites made of short fibers, continuous fibers and particles. Polymer matrix composites usually contain a higher percentage of fibers compared to the matrix for better properties. Carbon, graphite, glass and aramids fibers are few types of fibers which are regularly used in polymer matrix composites. Depending on the requirement and application, the volume fraction of fibers and matrix changes. The polymer matrix can be either a thermoset or a thermoplastic polymer. Few examples of thermosets include

polyesters, epoxies, polyamides, etc. [27,29] whereas, thermoplastics include polyesters, polyphenylene, etc. Thermoplastics have high expectations in future applications they may replace epoxy resins which are currently used for regular applications [27,29]. Properties of a polymer matrix composite depend on the properties of fibers, the orientation of fibers, the percentage of fibers and properties of the matrix [28].

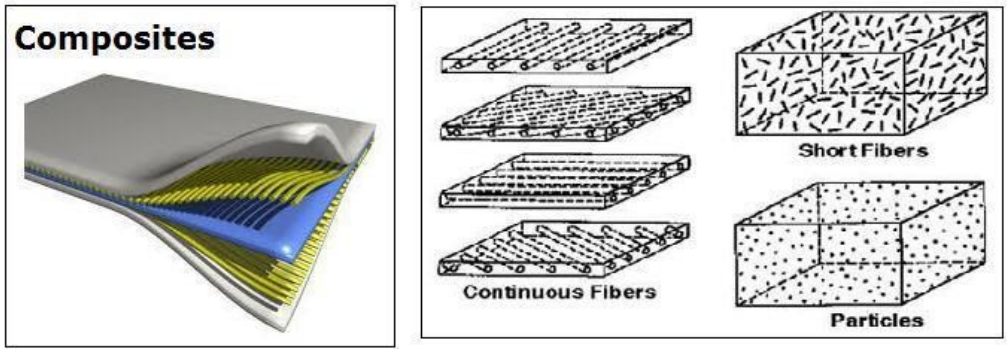

Figure 7. Polymer matrix composites of short fibers, continuous fibers, and particles [29].

1.6 Advantages and disadvantages associated with advanced Polymer Matrix Composites

Advanced composite materials are gaining attention in the automotive, aviation, defense and sporting goods industries due to their additional advantages compared with metals, and conventional materials [30]. The advantages and disadvantages associated with advanced polymer matrix composite materials are:

Advantages of Polymer Matrix Composites

- Light in weight.

- High tensile strength and fracture toughness.

- Excellent corrosion resistance and can withstand extreme climatic conditions.

- Possess good abrasion and puncture resistance.

-Complicated shapes can be easily obtained from these composites.

- Long service life and lower maintenance cost [28,31,32].

Disadvantages of Polymer Matrix Composites

- Low thermal resistance, low coefficient of expansion, at high-temperature, cracking takes places and debonding between fibers occurs [33,34].

- Require experts for mass production and the manufacturing process should be performed with extra safety.

-Delamination occurs where the fiber layers are weakly bonded, and it is challenging to inspect the composite since complex inspection techniques are required.

-Lower compression strength [31,32].

1.7 Applications of Polymer Matrix Composites

Polymer matrix composites have been used for defense applications since the 1970s. Applications of polymer matrix composites are more significant compared with any other type advanced composite material.

The general applications of polymer matrix composites include sporting goods, commercial aircrafts, construction, reciprocating equipment, helicopters, medical devices.

Some special applications of PMC's include:

Space Applications: Space transportation systems, space stations.

Military: Bioproduction, Air crafts, bulletproof materials, and tanks.

Futuristic applications: Rigid-rod molecules, oriented molecules, novel matrices structures, high-temperature matrices [27].

Aerospace: Military aircraft, naval applications, automotive industry [27,33].

1.8 Requirements of composite materials for Defense Applications

It has been observed that the materials used for defense applications have undergone several changes since the 1500's until now. The main reason for development or changes in the materials

is to improve parameters like reduction in weight, cost, performance, defense, safety and life [34]. Designing, analysis, and manufacturing was a tough task in olden days, but with improvements in technology like CAD (Computer Aided Design) and CAE (Computer Aided Engineering) tools, the job became simple. Apart from the cost and weight of the composites, to design and manufacture a composite material for defense applications, the main parameters that are to be taken into consideration are [35]. Static tensile strength, stiffness, corrosion resistance, shear strength, fatigue resistance, fracture toughness, environmental resistance, compression strength, stability, low maintenance, easy to manufacture [36] and crashworthiness [37].

1.9 Summary

There are many composites which are used in the manufacturing of materials required for regular applications. Polymer matrix composites are one of the most commonly used lightweight materials for Defense applications. Polymer matrix composites are advanced materials based on thermoplastic and thermosetting resins reinforced with synthetic fibers. The matrix ensures proper bonding between the fibers and acts as a load-bearing component. It also behaves as a medium that transfers the load to fibers. Due to thin layers of fibers, the weight of these polymer matrix composites is lower compared with traditional metals and few other composites. They also exhibit properties like excellent fatigue resistance and excellent impact resistance. These factors favor the main requirements of materials used for defense applications [29,38]. In industry, polymer matrix composites are manufactured using techniques like injection molding, compression molding, sheet forming, thermo stamping, filament winding, resin transfer molding, vacuum baggage, compression resin transfer molding, and autoclave [39].

References

[1] F C Campbell, 2010, “Introduction to Composite Materials” Chapter 1, *ASM International*

[2] K K Chawla, 1998, “Composite materials: Science and Engineering” *Springer*, New York 2nd Edition

[3] N Hu, 2012, “Composites and their applications” Published by Intech

[4] J Putnam, 2004, “Hayman”, Mummy (Rev. ed.). New York, Pub. p. 70. ISBN 0756607078.

[5] M Balasubramaniyum, 2014, “Composite Materials and Processing”, *CRC Press Taylor & Francis Group*, International Standard Book Number-13: 978-1-4398-8054-8

[6] Composites lab, 2016 “History of composites” American composite manufacturing Association

[7] E Pete Scala, 1996, “A Brief History of Composites in the U.S.—The Dream and the Success” *The Minerals, Metals & Materials Society*

[8] Military Aircraft pictures, 2018, Sitessen ltd

[9] F J Milnar, 2014, “The History and Evolution of Direct Composites” Volume 10, Issue 1

[10] Min-JungKimaRyan, Jin-Young, KimaJack, Ferracaneb, In-BogLeea, 2017 ″Thermographic analysis of the effect of composite type, layering method, and curing light on the temperature rise of photo-cured composites in tooth cavities” Volume 33, Issue 10, Pages e373-e383

[11] F T Wallenberger, James C. Watson, and Hong Li, PPG Industries, 2001, “Glass Fibers”, *ASM Handbook*, Vol. 21: Composites (#06781G)

[12] Michioinagaki, 2000, “Chapter 4 - Carbon Fibers”, *New Carbons - Control of Structure and Functions*, Pages 82-123

[13] O Paris, H Petersik, 2009, “10 - The structure of carbon fibers”, *Handbook of Textile Fibre Structure, Natural, Regenerated, Inorganic and Specialist Fibres*, Volume 2 in Woodhead Publishing Series in Textiles, Pages 353-377

[14] M Ertekin, 2017, “7 - Aramid fibers”, Fiber Technology for Fiber-Reinforced Composites, *Woodhead Publishing Series in Composites Science and Engineering*, Pages 153-167

[15] T Tam, A Bhatnagar, 2006, “7 - High-performance ballistic fibers”, Lightweight Ballistic Composites, Lightweight Ballistic Composites, Military and Law-Enforcement Applications, *Woodhead Publishing Series in Composites Science and Engineering*, Pages 189-209

[16] M Anjum, 2015, “Aramid Fibers-An overview”, *School of Textile and Design*

[17] S Kalpakjain, S R. Schmid, 2008, “Manufacturing Process for Engineering Materials” *Pearson Education, Inc*, ISBN 0-13-227271-7

[18] G Kickelbick, 2007 “Hybrid Materials. Synthesis, Characterization, and Applications” *Wiley-VCH Verlag GmbH & Co. KGaA,* Weinheim ISBN: 978-3-527-31299-3

[19] M Nanko, 2009 “Definitions and Categories of Hybrid Materials” *The Azo materials journal online*, Written by AZoM

[20] R M Koid, 2013, “An ant colony algorithm applied to lay-up optimization of laminated composite plates” *Latin American Journal of Solids and Structures*, On-line version ISSN 1679-7825

[21] L A Khan, 2018, “Processing of Sandwich Structures”, Honeycombs and Honeycomb Materials Information

[22] M J John, R D. Anandjiwala, Sabu Thomas, 2009 “Hybrid Composites” Chapter- 12

[23] M Pagliaro, J Marie Nedelec, 2017 “Hybrid Materials” Nanoscale, 6, 6219

[24] B S. Kukreja, 2018, “Composites in the Aircraft Industry,” Categories: MECH370, Materials processing, 178(2017) 346-381

[25] Composite world, 2017, “Aerospace Composites” Gardner Business Media, Inc.

[26] M Mrazova, 2013, “Advanced composite materials of the future in aerospace industry,” INCAS Bulletin; Bucharest Vol. 5, Iss. 3, (2013): 139-150.

[27] R Wang, Ya-Ping-Zheng, Shui-Rong Zheng, 2016, “Introduction to polymer matrix composites” Chapter-1, Polymer matrix composites and technology, *Woodhead Publishing in Materials*, Pg no 1-25

[28] J Y Sheikh-Ahmad, 2009, “Introduction to Polymer composites” *Chapter-1, Machining of Polymer Composites*, Pg no 1-34

[29] Princeton education,1985, “Polymer Matrix Composites” *Advanced Materials by Design - Chapter 3*

[30] S Rana, R Fangueiro, 2016, “Advanced Composite Materials for Aerospace Engineering: Processing, Properties, and Applications” *Woodhead publishing series in Composites Science and Engineering: Number 70*

[31] M Kohar, 2017, “Polymer matrix composites advantages and disadvantages” *Brainly.in*

[32] J Woodruffm, 2018, “Advantages & Disadvantages of Polymer Composites” Bizfluent-Leaf Group

[33] A G Koniuszewska , J W Kaczmar, 2016, “Application of Polymer-Based Composite Materials in Transportation” *Progress in Rubber, Plastics and Recycling Technology*, Vol. 32, No. 1

[34] D Paul, L Kelly, V Venkayya, 2002, “Evolution of U.S. Military Aircraft Structures Technology”, *Journal of Aircraft*, Vol. 39, No. 1

[35] The National Academies of Sciences, Engineering, and medicine, 1992, “Aeronautical Technologies for the Twenty-First Century”, Chapter: 9 Materials and Structures

[36] L Jenkinson, P Simpkin, D Rhodes, 1999, “ Civil Jet Aircraft Design” *Great Britain: Arnold Publishers*. p. 55. ISBN 0-340-74152-X.

[37] National Academy Press, 1987, “Advanced Organic Composite Materials for Aircraft the structures- Future the programs”, *National Research Council (U.S.). Committee on the Status and Viability of Composite Materials for Aircraft Structures*

[38] Ru Min Wang, Shui-Kong Zheng, Ya-Ping, 2005, “Polymer Matrix composites and technology” *Wood head publishing in Materials*

[39] S Advani ,2012, “Manufacturing Techniques for Polymer Matrix Composites (PMCs)” 1st Edition

CHAPTER 2

LITERATURE REVIEW

In an attempt to reduce the damage caused by a weapon, in 6th century for the first time, Persians and Greeks used linen layer clothes for protection. Later in the 9th-century people from Ellice and Gilber islands used coconut palm fibers to make protective layers on clothes. Later animals hide in the form of layers were used by Chinese and Americans as body armor in that period. In 400 BC Ukraine's developed chain mail armor. Taking it as reference, Romans introduced mail shirts. Brigandine armor (made of stacked metal plates in leather) was invented by the Greeks around 500 B.C. Iron and steel were used in Brigandine armor. With modifications, metal plate armor trend continued for a long period [1]. In the 1500s, with advancement in weapon technology, metal plate armor could'nt satisfy the desired requirements of protection. In the 1800s, Japenese developed silk material which demonstrated good impact resistance, but the cost of material was expensive [2]. In 1898 British made the prototype of armored car with iron, by 1902 with modifications in materials, armored cars were available in the market [3]. In 1909, Military aircraft were made of aluminum, nickel, and titanium by the U.S.A. Later in the same century, those metals were replaced with Al-2024 and Al-7075 in the majority of defense aircraft's [4]. In 1960s, new fibers were discovered which was proved to be ballistic resistant. Extending the work on those fibers, in 1970's kevlar fibers were developed. By 1976 kevlar became the source that provides excellent ballistic resistance with less weight [1,2]. With the improvement in weapon technology, kevlar alone couldn't meet the desired requirements. In order to overcome the difficulties associated with kevlar, hybrid and advanced composite materials were used. There are several advanced composites that are used for defense applications like MMC's(Metal matrix composites), CMC's(Ceramic matrix composites), PMC's(Polymer matrix composites), FML(Fiber metal laminates), newly developing NHAF-X(Nano adaptive hybrid fabric), Central reinforced Aluminum, Spider silk fibers, Hybrid composite steel sheets etc [5,6].

There are many polymer matrix composites manufactured until this decade, but research is pursued on them to understand the performance and improve the properties. Until now many tests have been performed on them altering the type of fibers, quantity of fiber layers, orientation of fibers and type of matrix or resin. High-velocity impact tests are generally performed using two apparatus which are Hopkinson bar setup and Gas gun technique. It is observed that in Hopkinson bar setup, shear stresses occurs at the gripping area, and the dimensions of specimens should be large for testing whereas newly developed Gas gun systems do not have these disadvantages. Force/displacement data can also be obtained from advanced Gas gun systems. They can be used to test specimens of various sizes, so they are much preferred for high-velocity impact testing [7].. H.L Gower and D.S Cronin studied the high-velocity impact behavior of kevlar 29 and kevlar 129 with conical and spherical projectiles at velocities 130 m/s and 250 m/s, they observed that back face displacement of the specimen after the impact of kevlar 29 was more compared with kevlar 129 [8]. Xie and Meng performed ballistic testing on carbon/carbon composites at high temperatures, they concluded that impact velocity plays a key role in impact resistance of specimen rather than the dimensions of projectile and in all conditions impact resistance increased with increase in temperature along with ballistic testing, they also performed tensile testing to determine the residual strength at high temperatures [9]. Moallemzadeh investigated high-velocity impact behavior of E-glass / Polyester under preloading (which includes a tensile load or compressive load or combination of both) with a spherical projectile at velocities ranging between 185 m/s – 235 m/s and they observed that preloading has less effect on impact resistance of the specimens [10]. Higuchi and Obake in their work on high-velocity impact behavior on carbon fiber reinforced plastics showed various failure modes that can occur in PMC's during ballistic testing [11]. Ramadhan and Abutalib studied Kevlar-29 / Epoxy composites high-velocity impact behavior with 7.62 mm diameter steel cylindrical projectile at velocities ranging between 180 m/s-400 m/s and found that energy absorption increases with increase in velocity of projectile [12]. Alireza and Nargis investigated the properties of glass fiber reinforced polymers with a sharp tip projectile at velocities ranging between 80 m/s to 160 m/s and revealed composite wave propagation and the ballistic performance of woven and cross-ply composites based on E-glass. They found that woven composites had better impact resistance compared with cross ply composites [13].

Leman and Salman studied the high-velocity impact behavior of the combination of Kenaf / Kevlar- 29 fibers and they stated that stacking of fiber layers with different fiber orientations affects impact resistance. They have concluded that few orders of stacking of fiber layers with different fiber orientations lead to a heavy loss in ballistic properties and few of them lead to improvement in properties [14]. Nakamura and Keiji observed independent damages and fan-shaped delaminations in ballistic testing on carbon fiber reinforced plastics [15]. Gunnarsson and Ziemski performed ballistic testing on polycarbonate at velocities ranging from 50.1 m/s to 81.2 m/s using digital image correlation to monitor the maximum back face displacement of the plates during the impact event [16]. Kaboglu and Mohagheghian investigated the high-velocity impact behavior of fiber metal laminates also using a digital image correlation system at velocities ranging from 116 m/s to 267 m/s in order to understand the full-field out-of-plane displacement, out-of-plane displacement profile during loading and unloading and as well as central maximum out-of-plane displacement of the material. They concluded that the energy absorption changes in FML's with an increase in the number of metal and fiber layers [17].

From the literature review, it is observed that impact resistance varies with the grade of fibers, dimensions of projectiles have no effect on impact resistance, but the shape of projectiles effects the impact resistance. Failure modes change with different impact energies. Plain weave as well as cross-ply weave have better high-velocity impact resistance. Digital image correlation technique was used to understand maximum out of plane displacement during an impact event. Considering the background review, this work mainly focuses on the ballistic testing of a different grade of glass fibers with distinct matrix and different projectiles at varying velocities to understand the mechanical properties and failure modes of the composite.

Objectives

The main objective of this research project is to study the ballistic properties of glass fiber thermoset and thermoplastic-based woven polymer matrix composites to understand their mechanical behavior so that they can be used in light weight structures that may be subjected to the impact loading conditions. Thermoplastic and thermoset based woven composites will be manufactured with a number of fiber layers using hand layup and compression method.

To study the ballistic properties of these composites, a single stage gas gun system a system will be used. Universal projectiles like sharp nose and the spherical head will be used for the ballistic testing. After each test, impact velocity and energy of the projectiles will be analyzed with a velocity sensor. Failure modes of the composites after each test will be studied, and the ballistic limit of the specimens will be investigated. Using Digital Image Correlation, maximum transient out of plane displacements at all stages of impact and final back face displacement of the composites after the impact will be revealed. Analytical modeling will be performed to predict the ballistic limit of these composite materials.

References

[1] C Devina ,P Holly ,R Reem , 2012, “The History and Application- Bulletproof Nanotechnology”

[2] Bullet Safe, 2019, “An article on History of Bullet Proof West”

[3] E John, Lord Montagu, D B Wise , 1995, “Daimler Century: The Full History of Britain's Oldest Car Maker” *Haynes Publications.* ISBN 978-1-85260-494-3.

[4] Federal Aviation Administration, “Aviation Maintenance Technician Handbook – Airframe”, Volume 1 Table of Contents

[5] S Rana, R Fangueiro, 2016, “Advanced Composite Materials for Aerospace Engineering: Processing, Properties, and Applications” *Woodhead publishing series in Composites Science and Engineering: Number 70*

[6] B S Kukreja, 2018, “Composites in the Aircraft Industry”, Categories: MECH370, Materials processing, 178(2017) 346-381

[7] W J Cantwell, J Morton, 1991, “The impact resistance of composite materials---a review” Composites. Volume 22. number

[8] H L Gower, D.S Cronin, 2007, “Ballistic Impact Response of Laminated Composite Panels” Science Direct, *International Journal of Impact Engineering*, 35(2008) 1000-1008

[9] WH Xie, SH Meng, 2016, “High-velocity Impact Test on High-Temperature carbon-carbon composites” Composites Part-B 98(2016) 30-38

[10] A R Malekzadeh, S A R Sabet, 2017, “Preloaded composite panels under high-velocity impact” *International Journal of Impact Engineering* 114 (2018) 153–159

[11] R Higuchi, T Okabe, A. Yoshimura, 2017, “Progressive failure under high-velocity impact on composite laminates: Experiment and phenomenological metamodeling” *Engineering Fracture Mechanics* 178(2017) 346-381

[12] A A Ramadhan, AR Abutalib, 2012, “High-Velocity Response of Kevlar-29/epoxy and Aluminum 6061 -T6 aluminum laminated panels” *Materials and Design* 43(2013)307-321

[13] A Sabet, Nargis, M Hossain, 2011, “Effect on Reinforcement type on high-velocity impact response of GRP Plates using a sharp tip projectile” *International Journal of Impact Engineering* 38(2011) 715-722

[14] S D Salman, Z Leman, MTH Sultan, MR Ishak, F Cardona, 2017, “Effect of kenaf fibers on trauma penetration depth and ballistic impact resistance for laminated composites” *Textile Research Journal*,Vol. 87(17) 2051–2065 The Author(s) 2016 Reprints and permissions: sagepub.co.uk/journals Permissions.nav DOI: 10.1177/0040517516663155

[15] T Nakamura, K Ogi , 2013, “Characterization of high-velocity impact damage CFRP laminates: Part 1- Experiment” Composites: Part A 48(2013) 93-10

[16] A Gunnarsson, B Ziemski, T Weerasooriya, P Moy, 2009, “Deformation and Failure of Polycarbonate during Impact as a Function of Thickness” , *Proceedings of the Society for Experimental Mechanics in Annual Conference*, Albuquerque, New Mexico USA

[17] C Kaboglu, I Mohagheghian, J Zhou, Z Gua, W Cantwell, S John, B R. K. Blackman, A J. Kinloch, J P. Dear, 2017, “High-velocity impact deformation and perforation of fiber metal laminates”, *J Mater* Sci (2018) 53:4209–4228.

CHAPTER 3

EXPERIMENTAL PROCEDURE

3.1 Manufacturing of Composites

In this research project, woven thermoset and thermoplastic-based composites shown in Figure 8 were manufactured using Shield Strand S® glass fibers / Fiber glast epoxy [1,2] and E- glass fibers/polypropylene (Twintex®), TPP 60 1485 AF [3].

Where,

T: fabric

PP: polypropylene matrix

60: glass content in weight (%)

1485: nominal weight (g/m²)

AF: roving type

For manufacturing both the composites, fiber layers were cut according to the mold size from its raw material (fabric rolls) which was obtained from the manufacturer.

(a) (b)

Figure 8. Reinforcements used in this project based on (a) TPP 60 1485 E-glass fibers and (b) Shield Strand S® fibers.

The number of fiber layers for manufacturing the composites were considered based on the thickness requirements.

3.1.1 Manufacturing of Shield Strand S®/ Epoxy composites

In this research project, for both thermoplastic and thermoset based composites, the volume fraction of fibers is 60%, and the volume fraction of resin was 40%. After obtaining the total mass of fiber layers from the calculations, based on volume fraction, the amount of resin mixture required was estimated. Fiber glast epoxy resin 2000 and its respective curing agent or hardener (2060) were used in manufacturing of the thermoset composite material. Hardener acts as a catalyst that reduces the time taken for the fabrication of composite. For the calculations, the predefined density of epoxy resin was considered, and with the help of volume estimated in calculations, the mass of resin mixture was established using density, mass and volume relationship.

The epoxy and the hardener were mixed in a 3:1 ratio according to the recommendations given by the manufacturer To make the resin mixture, the epoxy was poured into measuring cup and weighed on a scale; adjustments were made with a spoon until the required quantity was present in the cup as shown in Figure 9. Similarly, curing agent was also poured in a new measuring cup and weighed on the scale as well until the required amount of curing agent was present. After the measurement, the curing agent was slowly poured into epoxy and adequately mixed with the help of a stick avoiding the formation of air bubbles.

Figure 9. Epoxy resin mixture on a Digital weighing scale.

In order to prevent the composite from sticking to the mold, during manufacturing, it was coated with Teflon® sticker on the top plate, on the bottom plate and all sides of the mold. To provide additional resistance against sticking to the mold, Teflon® spray was also sprayed on all the sides and corners of the mold as shown in Figure 10.

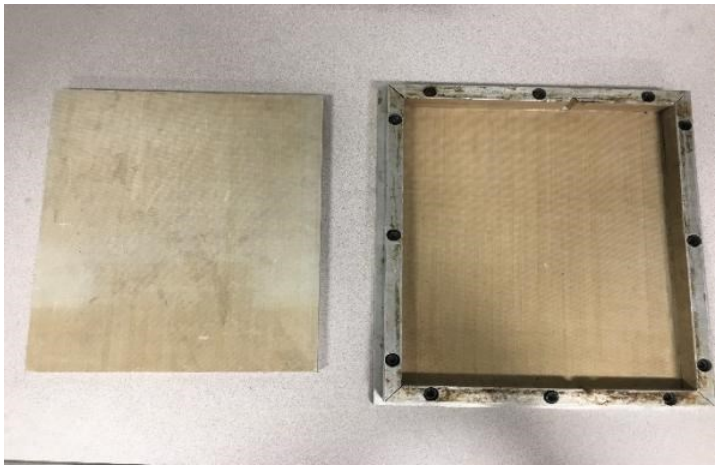

Figure 10. Aluminum mold with Teflon coating.

A Carver hydraulic press shown in Figure 11 was used to apply pressure while curing the composite. Press contains two bolsters in which the mold was placed. The bolsters are connected to the threaded rods, with the help of lever at the bottom, lower bolster can be either moved up or down. A pressure gauge is located near the lever which shows the amount of pressure applied. The two Bolsters are connected to the power unit. The power unit helps to control the temperature of two bolsters. Depending on the curing temperature of the resin mixture which is recommended, the temperature was adjusted in the power unit, and the two bolsters were preheated before placing the mold in hydraulic press.

Figure 11. Carver hydraulic press.

Fiber layers along with resin mixture were placed in the mold using hand lay-up method as shown in Figure 12. Here, layers of reinforcements were alternated with the epoxy resin and hand rolled to remove the excess resin and any air that could have been trapped. After the required number of fiber layers along with resin mixture in between them were stacked in the bottom plate of the mold, the top plate of the mold was placed.

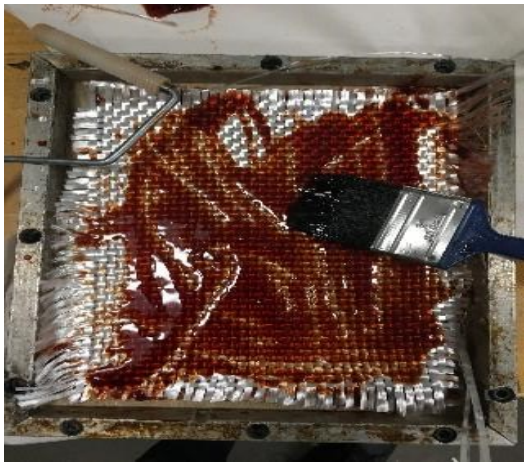

Figure 12. Hand layup method (Sheild Strand S® fibers with Epoxy resin).

The mold was placed in the hydraulic press which was preheated to a temperature of 100°C and with the help of lever at the bottom, a pressure of 7 MPa was applied on the mold. The mold was left in the hydraulic press for one hour according to the manufacturer recommendations.

After curing, the knob at the bottom of the press was rotated in a clockwise direction to release the pressure, and the temperature control was switched off. The mold was left in the press until it attained room temperature. After this, it was taken out from the press, and the composite was extracted from the mold as shown in Figure 13. In order to remove the edges of manufactured composite as well as to cut the composite into required dimensions for testing, a Diamond coated cutter was used.

Figure 13. Sheild Strand S ® / Epoxy composite.

3.1.2 Manufacturing of Twintex® composites

TPP 160 1485 AF (Twintex®) it is a comingled prepreg. For manufacturing, The top plate and bottom plate of mold was coated with Teflon® stickers to prevent the composite from sticking to the mold and Teflon® spray was also sprayed at the edges and corners of the mold to make sure that composite doesn't get attached to the corners and sides of the mold. Depending on the thickness requirements, a number of fiber layers were placed in the bottom plate of the mold as shown in Figure 14. A thermocouple was used to monitor the temperature of composite. The wire of the thermocouple was placed in between the prepreg layers and, the top plate of the mold was closed followed by placing the mold in the preheated carver hydraulic press. The hydraulic press was preheated at 195°C. A pressure of 7 MPa was applied to the mold during melting and solidification.

When the thermocouple displayed temperature around 175°C, thermocouple wire was pulled out, and the power unit of the hydraulic press was switched off. The mold was left inside the press until it attained room temperature (20°C-25°C). When the mold reached the room temperature, the pressure of the press was released, and mold was taken out from the press followed by extraction of the composite from the mold.The final composite obtained is also shown in Figure 14.

(a)

(b)

Figure 14. (a) Prepreg method and (b) Twintex® composite.

3.2 Cutting of Composites

In order to prepare specimens for testing, a diamond coated cutter [4] shown in Figure 15 was used for cutting and performing surface finishing operations on both the thermoplastic and thermoset based composites. To cut the composite, motor and laser guideway was switched ON, and the sliding table with composite secured on it was moved towards the cutter and when the composite was cut, the sliding table was pulled back followed by taking out the composite, similar procedure was followed for cutting all the composite specimens required for testing.

Figure 15. Rigid 7 Inch Wet Tile Saw.

For ballistic testing, all the specimens were cut into 100 mm x100 mm panels taking ASTM 7136-M and ASTMD 8101 standards as reference [5,6].

3.3 Drilling

In order to hold the composite specimens in the fixture for high-velocity impact testing, holes were made in them using a Mx8 solid carbide drill bit. Eight holes were drilled in each specimen so that it could be securedly fastened to the fixture with the help of bolts. Holes were drilled in a circular pattern provided by the fixture design.

To obtain the circular holes pattern,a Jet 690179 Jim-4vs-1 Mill shown in the Figure 16 was used. Here, a program was selected in the end mill to get the circular holes pattern. Specimens were clamped on the mill table with a set of toggle clamps, and holes were punched continuously as per the hole pattern by the mill.

Figure 16. Endmill drilling holes in composite speciemens.

3.4 Design and Manufacturing of Projectiles

In this research project, two types of projectiles will be used for high-velocity impact testing. The spherical head and sharp nose projectiles shown in Figure 17 were designed using CATIA V5 and fabricated using a Jet GHB-1340A geared head bench lathe. Projectiles were made from a stainless steel rod. The rear diameter of both the projectiles was 11.90 mm which was proposed according to the radius of gas gun barrel.

The mass of Spherical head projectile was 23.6 grams

The mass of Sharp nose projectile was 16.8 grams

(a)

(b)

Figure 17. Manufacturing of projectiles (a) Bench Lathe machining the projectile (b) Spherical head and Sharpnose Projectiles.

3.5 Single stage gas gun Setup

In order to perform low-velocity, high-velocity impact testing, an in-house developed pneumatic system (gas gun) was used. The single stage gas gun setup is shown in Figure 18. This system contains a compressor that is connected to a valve that is used to operate the air flow, The gas booster is used to increase the pressure of compressed air in the pressure chamber. The solenoid

valve controls the release of the air pressure required for the test. A digital pressure meter was located near the solenoid valve displays the pressure inside the pressure chamber. Depending on the required velocity for the impact test, the pressure of compressed air inside the pressure chamber was adjusted using the valve. The system also includes a safety valve to release the excess amount of compressed air present in the pressure chamber. The solenoid valve is connected to a barrel with a length of approximately 1.82 m. The test specimens were clamped in the fixture prior to testing an placed in the impact chamber which prevents any damage to surroundings caused by the projectile during and after a test as shown in Figure 18. A velocity sensor was also placed in the impact chamber to detect the impact velocity of the projectile just before impact . Two APX-RS Photron high-speed cameras were placed at the back of the impact chamber to capture the impact test. A pair of high beam focusing 150W LED lights, and 250W lamps were placed close to the impact chamber to increase the brightness to be able to record the event as shown in Figure 18.

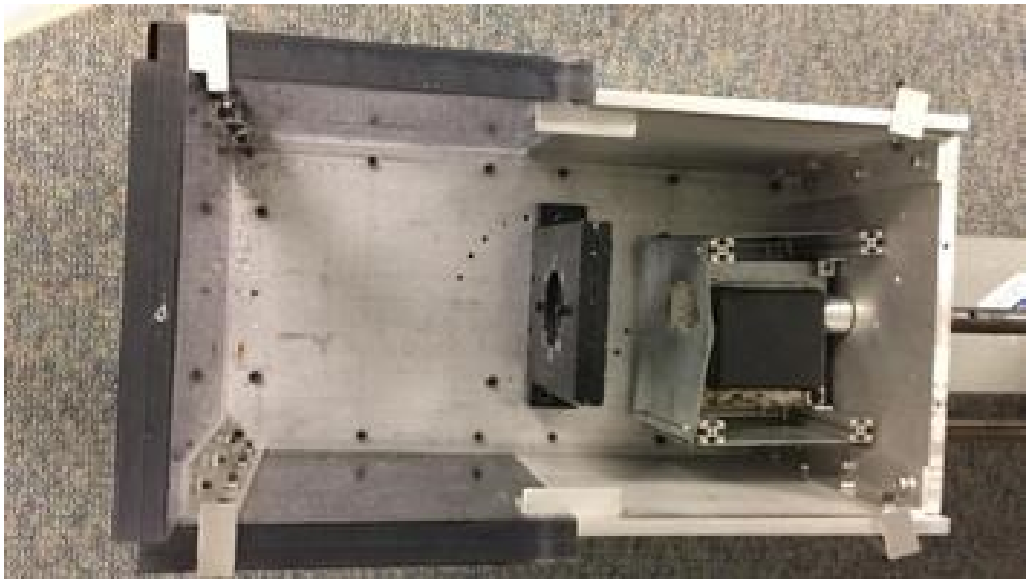

(a)

(b)

(c)

Figure 18. Pictures of Single stage gas gun system and equipment of high-velocity impact testing (a) Impact chamber (b) Arrangement of high-speed cameras (c) Single stage gas gun system.

3.6 Photron Fastcam Viewer

The Photron fast cam viewer is a software used for Photron APX-RS cameras (high-speed cameras). These cameras can capture 1-100,000 frames per second. They were connected to two control units, and these control units were connected to a system with the help of IEEE 391 cable. The two cameras are named as camera 1 and camera 2. Both camera 1 and camera 2 were located behind the impact test chamber. Camera 1 acts as the master camera and camera 2 acts as a slave camera. A 20 mm focal lens was used in the cameras. After connecting the two cameras to the computer, the control units was switched ON. Images of the specimen were observed in the software while focussing. A frame rate of 30,000 frames per second and a resolution of 256 x 256 was used for all the tests in this project [7]. Apx photron high speed camera shown in Figure 19.

Figure 19. Apx photron high speed camera.

3.7 E9800 MK2 Velocity Sensor

The velocity with which the projectile hits the test specimen is referred to a impact velocity. Here, the impact velocity was measured using an E9800 MK2 velocity sensor shown in Figure 20. It contains a screen which displays the impact velocity and energy values in required units [8]. It works on a simple mechanism which is based on a distance and time relationship of the projectile.

Figure 20. E9800 MK2 Velocity sensor.

3.8 Impact Energy

The impact energy of the projectiles was found using the velocity sensor. Here, the impact energy is given by

$$\text{Impact energy} = \frac{1}{2}mv^2$$

where,

m = Mass of the projectile

v = Velocity of projectile

3.9 Ballistic limit

The ballistic limit can be defined as the velocity at which the projectile perforates through the material by at least 50% of the time. In other terms, at the velocity below the ballistic limit, the projectile doesn't pierce or perforate through the specimen.

3.10 Digital Image Correlation

Digital image correlation is a non-contact type deformation measurement technique. DIC can be used to measure the displacement and time relationship which can be used to calculate strain [9]. Aramis V6-1.0.1-2 software was used [10]. Before taking the images for measuring the displacement, the cameras were calibarted. Depending on the dimensions of the specimen for which the deformation needs to be measured, the calibration panel was selected. In this project, the calibration panel used to calibrate the high-speed cameras was of 250 x 200 millimeters shown in Figure 21.

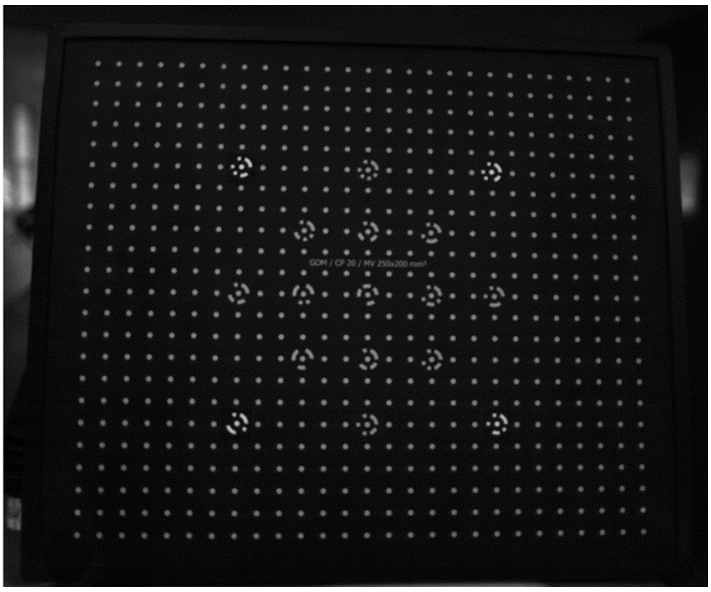

Figure 21. 250 x 200 millimeters DIC calibration panel.

After the calibration, the position of the cameras was readjusted to focus on the test specimen. A frame rate of 30,000 fps and a resolution of 256x256. “Trigger mode” was set to manual. To obtain the deformation data, specimens were spray painted with a unique speckle pattern. This pattern contained big dots of two coatings of black paint and two coatings of white paint alternatively as shown in Figure 22.

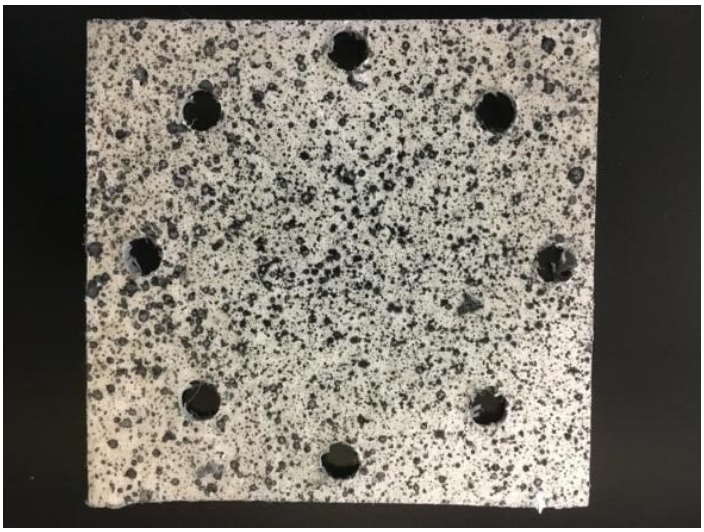

Figure 22. Speckle pattern.

Specimens with the pattern were clamped in the fixture, and initially two images were captured before testing. These images were imported to the DIC software. The pretest was performed to ensure that the cameras were monitoring the target area shown in Figure 23. After the completion of the impact test, the required images were selected from the PFV software and were saved in ".Tiff " format. The saved data was imported to DIC software. After the data was computed, an option in the software was selected to obtain displacement plot at all the stages. Stage points were set on the 3D deformation data to understand the change in displacement at various stages. A graph between Z displacement and stage was obtained from the software after completion of each test.

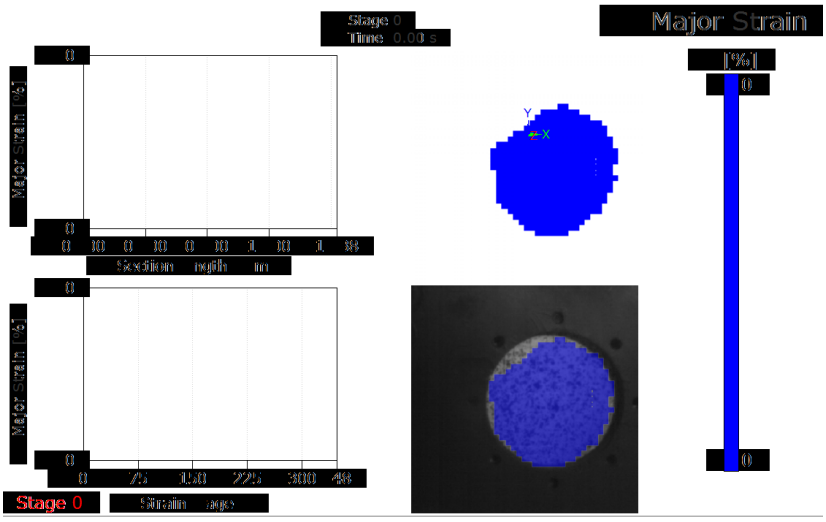

Figure 23. Sample pretest results using DIC.

References

[1] Fibre Glast Developments Corporation, 2010, “System 2000 Epoxy Resin”, Product Data Sheet, 800.214.8579

[2] OCV Reinforcements, 2010, “ Shield Strand S: High-Performance Reinforcements”, Product Information

[3] OCV Reinforcements, 2008, “Twintex T PP Glass Fabrics”, Product Information

[4] Rigid, 2013, “7 in. Tile Saw R4030”, Operator’s Manual

[5] ASTM D7136/D7136M standards, 2015, “Standard Test Method for Measuring the Damage Resistance of a Fiber-Reinforced Polymer Matrix Composite to a Drop-Weight Impact Event”

[6] ASTM D8101/D8101M—18 standards, 2018, “Standard Test Method for Measuring the Penetration Resistance of Composite Materials to Impact by a Blunt Projectile”

[7] Photron Limited, 2013, “ Photron FASTCAM Analysis Operation Manual V1.3.1”

[8]Hong Kong FF Electronic Products, 2012, “E9800-MKII Multifunctional chronoscope”, Instructions.

[9] GOM mbh, “Technical document on strain computation”.

[10] GOM mbh, 2009, “ARAMIS V 6.1 User manual”.

CHAPTER 4

RESULTS AND DISCUSSIONS

4.1 Pressure and velocity relationship for the spherical head and sharp nose projectiles

The objective of this research project is to investigate the ballistic properties of thermoplastic and thermoset based composite materials. High velocity impact testing was conducted using a single stage gas-gun with spherical head and sharp nose projectiles. First, to estimate the velocity of the projectile required for the test, the pressure and velocity calibration relationship was investigated. Spherical head and sharp nose projectiles were propelled under different pressures towards wood blocks placed in the impact chamber until the pressure vs velocity calibration relationship was established. It was noticed that for the spherical head projectile, the pressure required to attain certain velocity was higher than the pressure required to reach that velocity for the sharp nose projectile. Considering the pressure vs velocity relationship for the two projectiles are plotted in figures 24 and 25

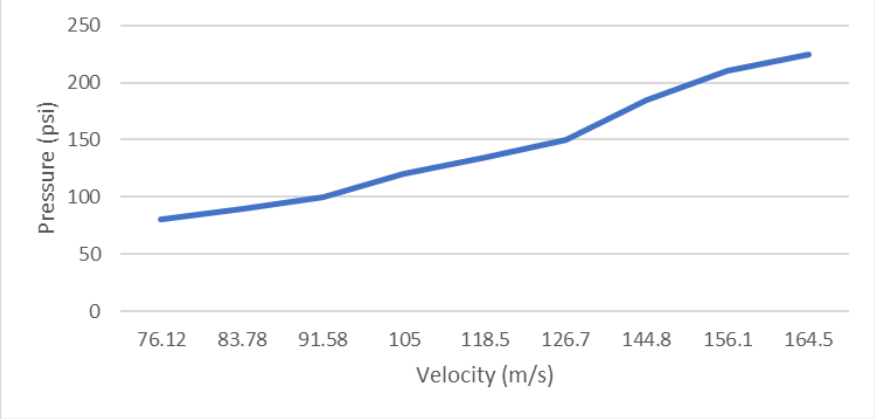

Figure 24. Pressure vs velocity relationship for the spherical head projectile.

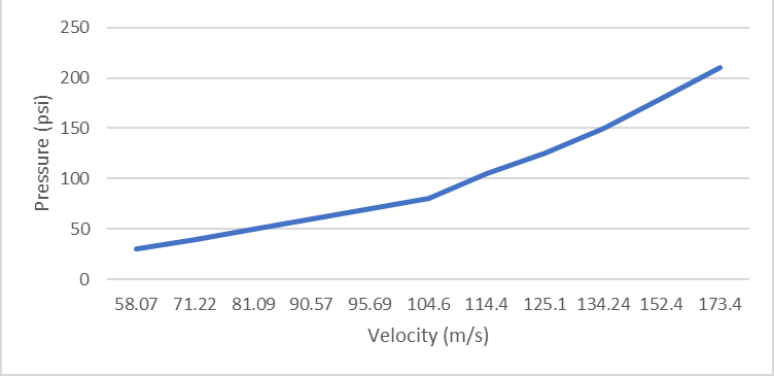

Figure 25. Pressure vs velocity relationship for the sharp nose projectile.

4.2 Ballistic Testing

Once the pressure vs velocity calibration was established for both the projectiles, the high velocity impact response of the woven thermoplastic and thermoset composites was investigated using a single stage gas gun setup as shown in Figure 18.

A frame rate of 30,000 fps was used by the high speed camears during all the impact testing events. For all the composites which were tested, displacement vs strain stage graph were plotted where, each strain stage is approximately 0.000033 s.

Impact velocities were increased until complete perforation of the specimens was achieved.

Figure 26 shows the range of velocities used in the research study with a spherical head projectile. Included in the figure are the impact energies associated with impact event.

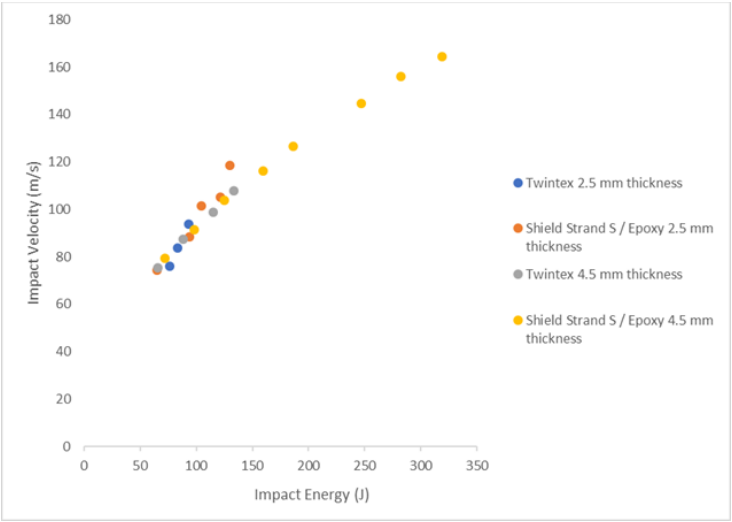

Figure 26. Impact velocities used to test the composites with the spherical head projectile.

Table 1 shows the summary of the results of the high velocity impact testing on the woven thermoplastic and thermoset composites using a spherical head projectile.

Maximum displacement of composites at different impact velocities with the Spherical head projectile			
Twintex 2.5 mm thick specimens		**Shield Strand S/Epoxy 2.5 mm thick specimens**	
Impact Velocity (m/s)	**Maximum Displacement(mm)**	**Impact Velocity (m/s)**	**Maximum Displacement(mm)**
67.28	11.14	74.32	8.81
76.12	14.5	88.4	11.2
83.78	17.2	94.2	12.2
93.86	approximately 18	101.5	13.63
		105	15.6
		118.5	approximately 17
Twintex 4.5 mm thick specimens		**Shield Strand S/Epoxy 4.5 mm thick specimens**	
Impact Velocity (m/s)	**Maximum Displacement(mm)**	**Impact Velocity (m/s)**	**Maximum Displacement(mm)**
67.68	7.91	79.35	7.74
75.42	8.59	91.58	8.8
87.45	12.46	103.7	10.72
98.88	13.8	116.3	11.88
107.8	approximately 15	126.7	13.99
		144.8	14.8
		156.1	15.63
		164.5	approximately 17

Figure 27 shows the range of velocities used in the research study with a sharp nose projectile. Included in the figure are the impact energies associated with impact event.

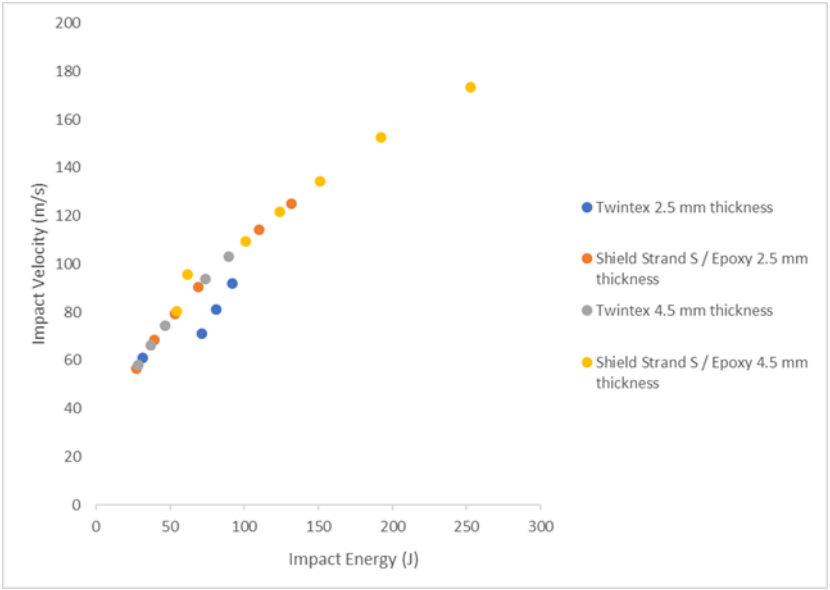

Figure 27. Impact velocities used to test composites with the sharp nose projectile.

Table 2 shows the summary of the results of the high velocity impact testing on the woven thermoplastic and thermoset composites using a sharp nose projectile.

Maximum displacement of composites at different impact velocities with the Sharp nose projectile			
Twintex 2.5 mm thick specimens		**Shield Strand S/Epoxy 2.5 mm thick specimens**	
Impact Velocity (m/s)	**Maximum Displacement (mm)**	**Impact Velocity (m/s)**	**Maximum Displacement (mm)**
60.96	7.19	56.7	5.09
71.22	7.74	68.5	6.28
81.09	12.64	79.28	7.68
92.1	approximately 14	90.57	7.99
		114.4	approximately 10
		125.1	approximately 13
Twintex 4.5 mm thick specimens		**Shield Strand S/Epoxy 4.5 mm thick specimens**	
Impact Velocity (m/s)	**Maximum Dsiplacement(mm)**	**Impact Velocity (m/s)**	**Maximum Displacement (mm)**
58.07	4.87	80.5	5.08
66.35	6.924	95.69	5.527
74.29	7.002	109.4	7.12
93.77	8.29	121.6	8.39
103.25	approximately 9	134.24	11.1
		152.4	12.16
		173.4	approximately 14

Figure 28 shows the relationship between impact velocity and maximum transient out of plane displacement for Twintex® based 2.5 mm thick composites impacted with the spherical head and sharp nose projectile. At a velocity 93.86 m/s, Twintex® based 2.5 mm composite attained its ballistic limit and when impacted with the sharpnose projectile, the composite reached its ballistic limit at a velocity of 92.1 m/s.

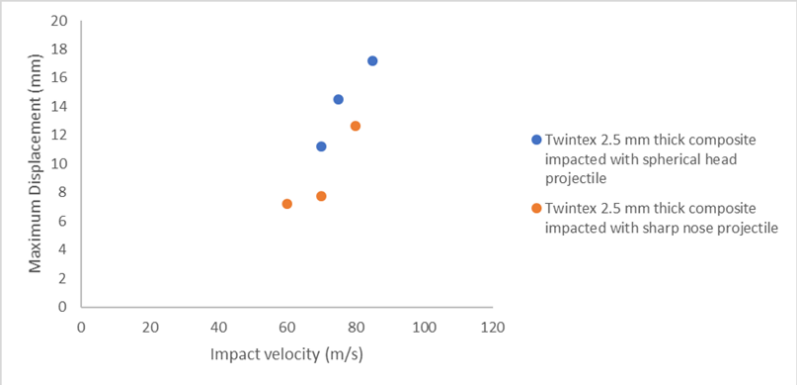

Figure 28. The relationship between Maximum displacement and Impact velocity for Twintex® 2.5 mm thick composites impacted with the spherical head projectile and sharpnose projectile

Figure 29 shows the relationship between impact velocities and maximum transient out of plane displacements for Twintex® 4.5mm thick composites impacted with the spherical head projectile and the sharp nose projectile. At a velocity 107.8 m/s, composite attained its ballistic limit and when impacted with the sharpnose projectile, the composite reached its ballistic limit at a velocity of 103.25 m/s.

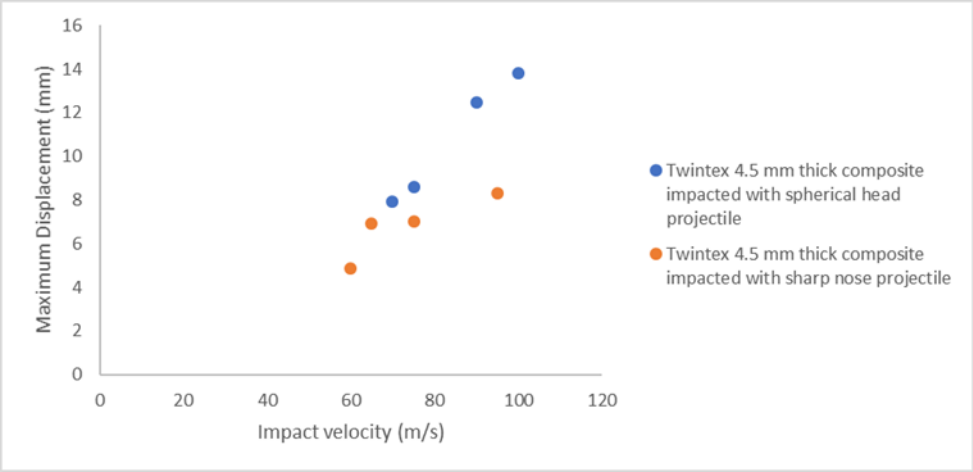

Figure 29. The relationship between Maximum displacement and Impact velocity for Twintex® 4.5 mm thick composites impacted with the spherical head projectile and sharp nose projectile.

From the figures 28 and 29, it is evident the maximum out of plane displacement is more when the Twintex® composites were impacted with the spherical head projectile.

Figure 30 shows the relationship between impact velocities and maximum transient out of plane displacements for Shield Strand S ®/ Epoxy based 2.5 mm thick composites impacted with the spherical head projectile and the sharp nose projectile. At a velocity 118.5 m/s, Shield Strand S ®/ Epoxy based 2.5 mm thick composite attained its ballistic limit and when impacted with the sharpnose projectile, the composite reached its ballistic limit at a velocity of 125.1 m/s.

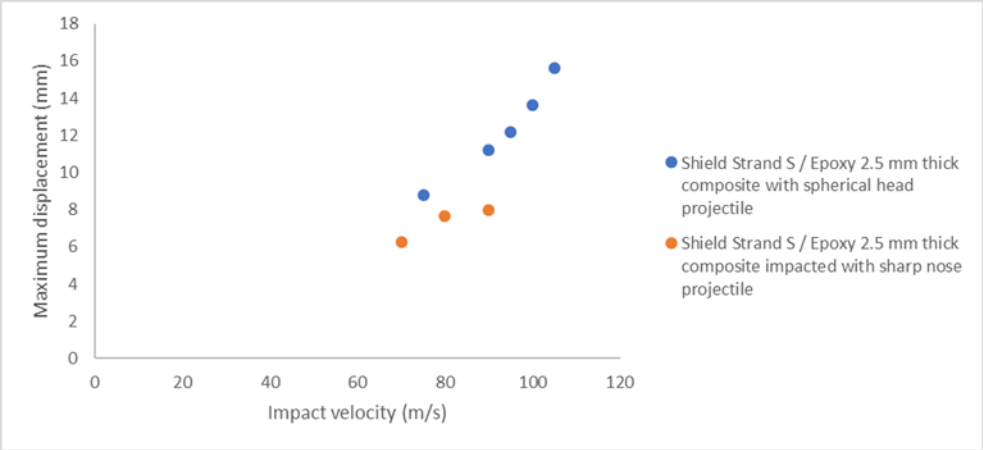

Figure 30. The relationship between Maximum displacement and Impact velocity for Shield Strand S ®/ Epoxy based 2.5 mm thick composites impacted with the spherical head and sharp nose projectile.

Figure 31 shows the relationship between impact velocities and maximum transient out of plane displacements for Shield Strand S ®/ Epoxy based 4.5 mm thick composites impacted with the spherical head projectile and the sharp nose projectile. At a velocity 164.5 m/s, Shield Strand S ®/ Epoxy based 4.5 mm thick composite attained its ballistic limit and when impacted with the sharpnose projectile, the composite reached its ballistic limit at a velocity of 173.4 m/s.

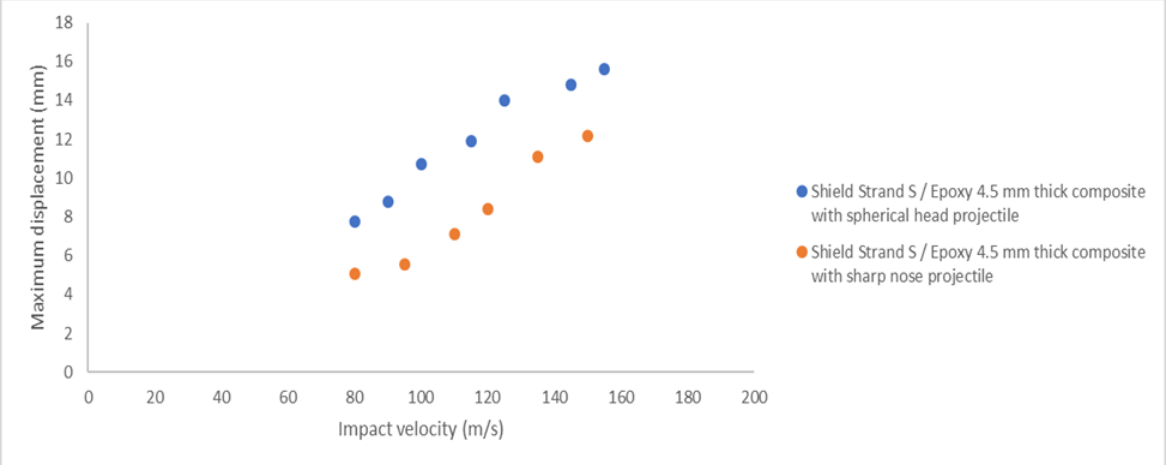

Figure 31. The relationship between Maximum displacement and Impact velocity for Shield Strand S® / Epoxy 4.5 mm thick composites impacted with the spherical head projectile and sharp nose projectile.

From figures 30 and 31, it is also evident that the maximum out of plane displacement is more when composites were impacted with the spherical head projectile. Maximum out of plane displacement is less in Shield Strand S® / Epoxy based composites when compared to Twintex® composites and it is also fascinating to note that Shield Strand S® / Epoxy 2.5 mm thick composites and Twintex® 4.5 mm thick composites showed approximately same maximum out of plane displacement at same velocities when impacted with both the projectiles even though Twintex® 4.5 mm thick composites has less impact resistance compared to the Shield Strand S® / Epoxy 2.5 mm thick composites.

In order to get a better understanding of the mechanical behavior of the woven thermoplastic and thermoset composite materials when subjected to high velocity impact loading conditions a detailed examination will be presented. First results will be given for the 2.5 mm thick Twintex® based composites impacted with spherical head and sharp nose projectile. Then experimental results for the 2.5 mm thick Shield Strand S® / Epoxy based composites impacted also with spherical and sharp nose projectile will be detailed. Following this experimental results will be offered for the 4.5 mm thick thermoplastic and thermoset based composites subjected to high velocity impact testing with spherical head and sharp nose projectiles.

4.2.1 Impact behaviour of Twintex® 2.5 mm thick composites with the Spherical head projectile

Figure 32 shows the low magnification optical images of the Twintex® based 2.5 mm thick specimen impacted with the spherical head projectile at a velocity of 67.28 m/s. It is observed that on the side of impact there are multiple slits with no signs of major damages. On the opposite side, no damage is evident.

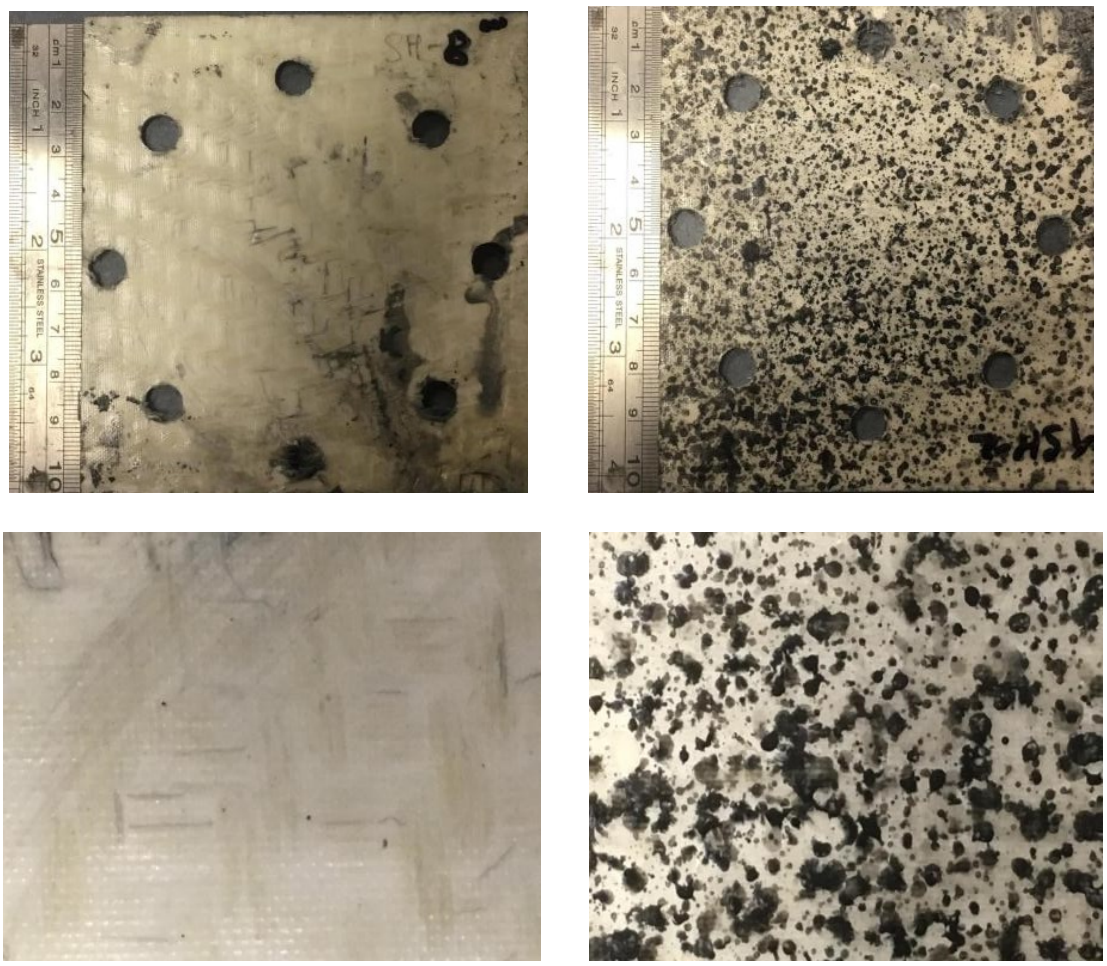

Figure 32. Twintex® based 2.5 mm thick composite impacted at a velocity of 67.28 m/s with the spherical head projectile.

Figure 33 shows the variation of the maximum transient out-of-plane displacement with stage time for the specimen illustrated in Figure 32. In this case, the maximum out of plane displacement was close to 11.14 mm. Vibrations are noticed which depicts that specimen had absorbed most of the impact energy of the spherical head projectile without showing signs of major damage.

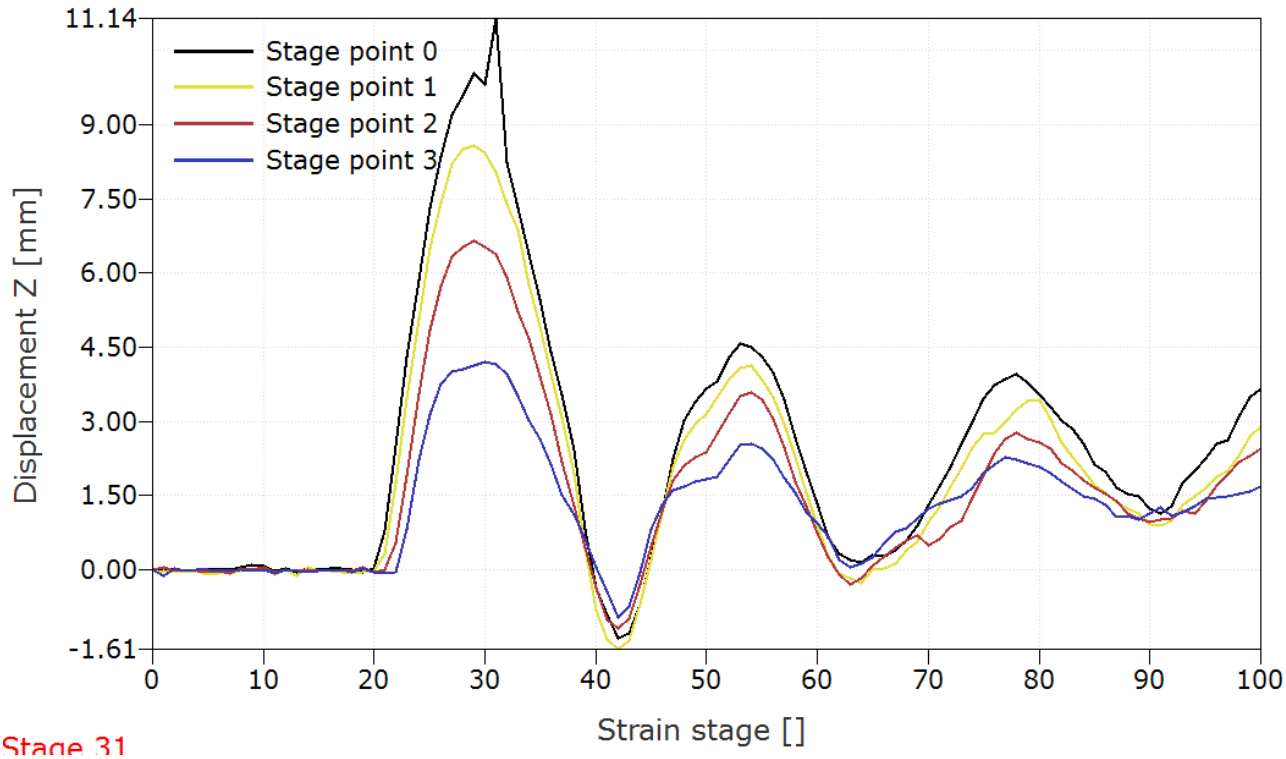

Figure 33. Displacement vs Stage graph of Twintex® based 2.5 mm thick composite impacted at velocity 67.28 m/s with the spherical head projectile.

Figure 34 shows some deformation stages representing the impact event on the 2.5 mm thick Twintex® based composites tested at a velocity of 67.28 m/s with the spherical head projectile. From the figure, it is evident how the out-of-plane deformation increased until the maximum transient out-of-plane displacement was reached in stage 29 with a value of 11.14 mm. Following this, the displacement decreased in stage 41 with the final displacement taking a value close to 4.5 mm in the region of impact.

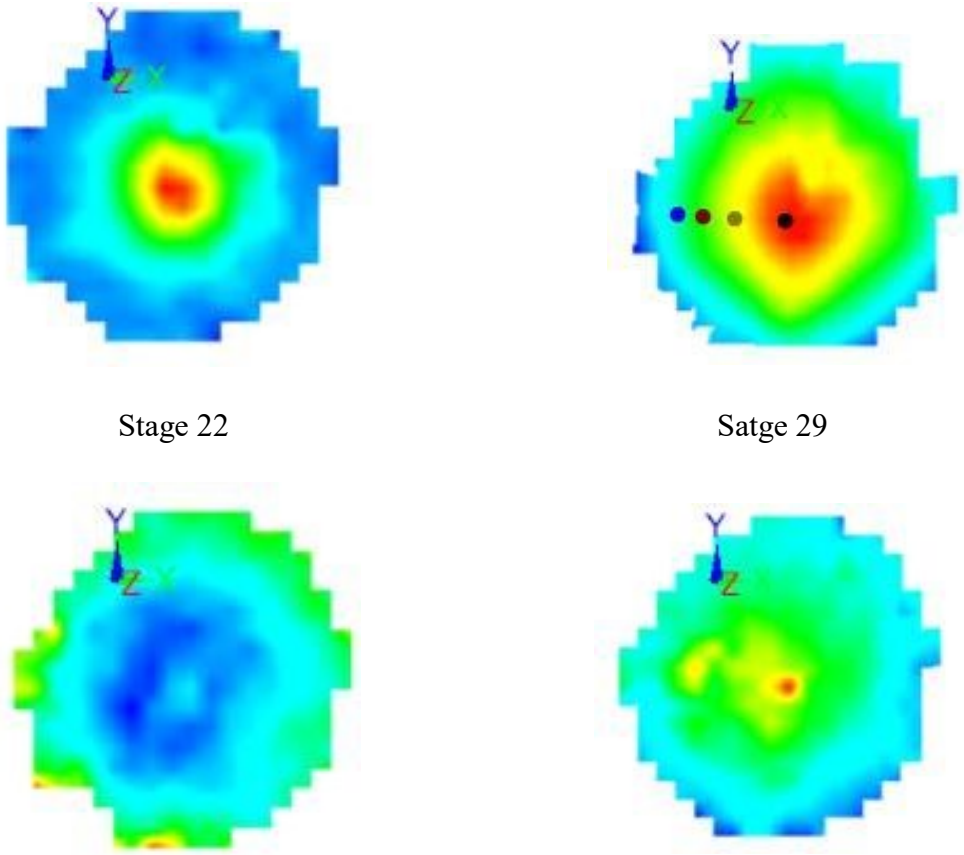

Figure 34. 3D deformation stages of Twintex® based 2.5 mm thick composite impacted at a velocity of 67.28 m/s with the spherical head projectile.

Figure 35 shows the low magnification optical images of the Twintex® based 2.5 mm thick specimen impacted with the spherical head projectile at a velocity of 76.12 m/s. From the figure, it is evident that on the point of contact of the projectile, there are multiple splits due to matrix cracking and on the opposite side no signs of damage are observed because the amount of impact energy is less to fracture or damage the material completely.

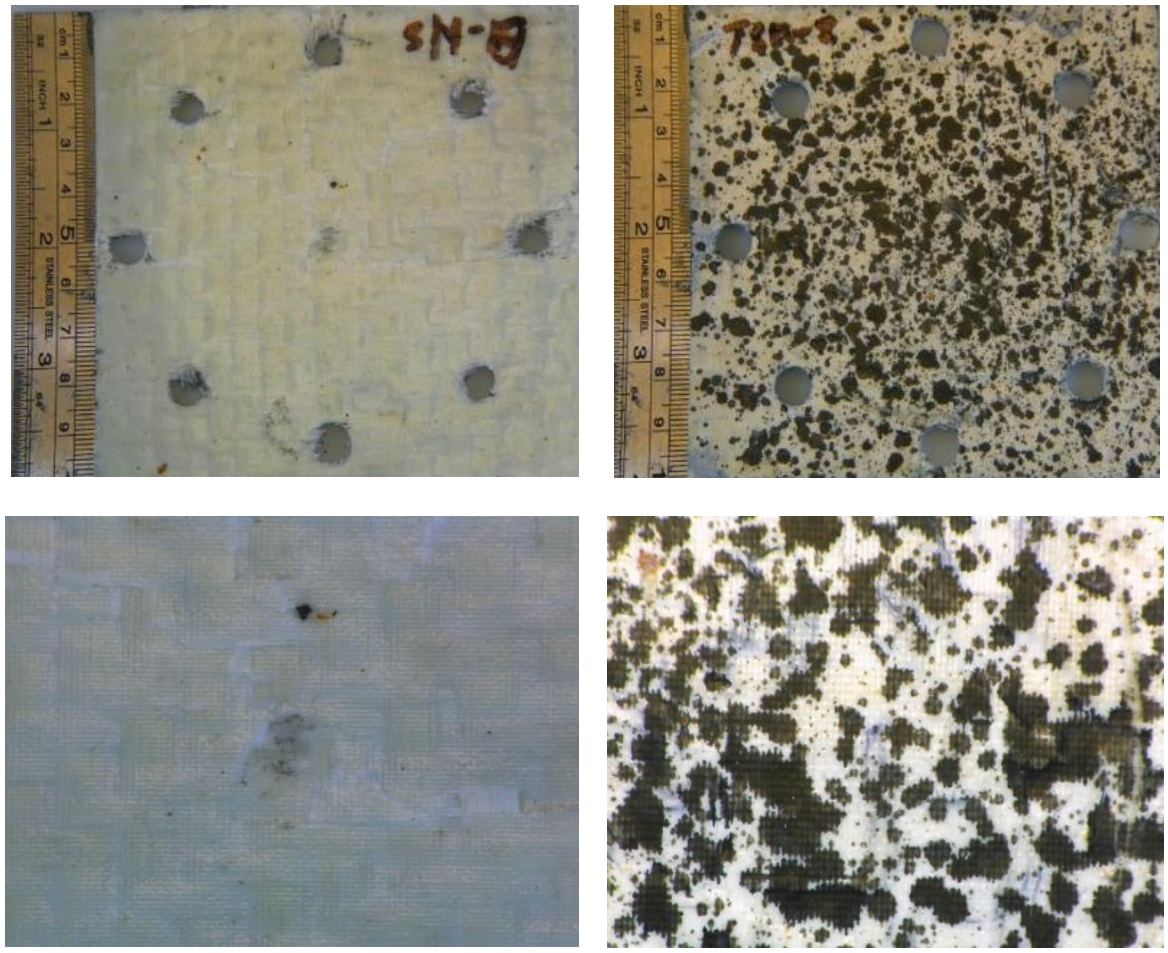

Figure 35. Twintex® based 2.5 mm thick composite impacted at a velocity of 76.12 m/s with the spherical head projectile.

Figure 36 shows the variation of the maximum transient out-of-plane displacement with stage time for the specimen illustrated in Figure 29 . For this case, the maximum out of plane displacement was measured as 14.5 mm.

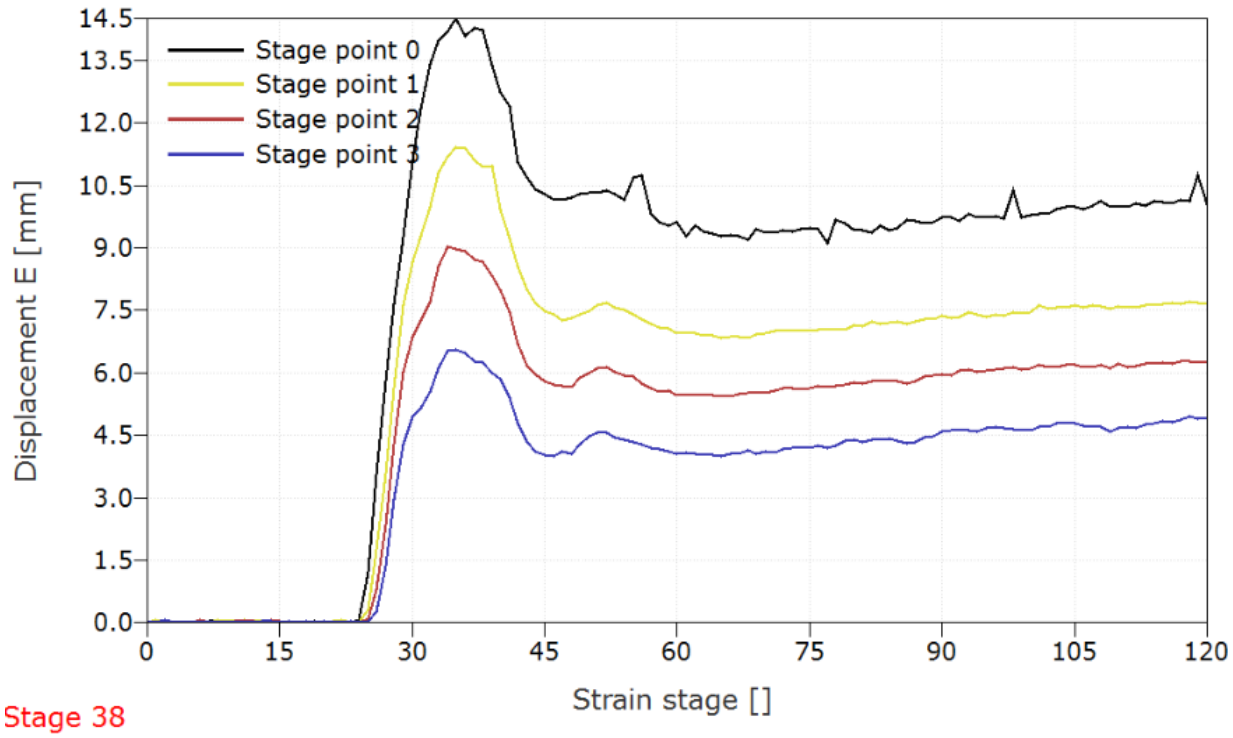

Figure 36. Displacement vs Stage graph of Twintex® based 2.5 mm thick composite impacted at velocity 76.12 m/s with the spherical head projectile.

Figure 37 shows some deformation stages representing the impact event on the 2.5 mm thick Twintex® based composites tested at a velocity of 76.12 m/s with the spherical head projectile. From the figure, it is evident how the out-of-plane deformation increased until the maximum transient out-of-plane displacement was reached in stage 35 with a value of 14.5 mm. Following this, the displacement decreased in stage 46 with the final displacement taking a value close to 10.50 mm in the region of impact.

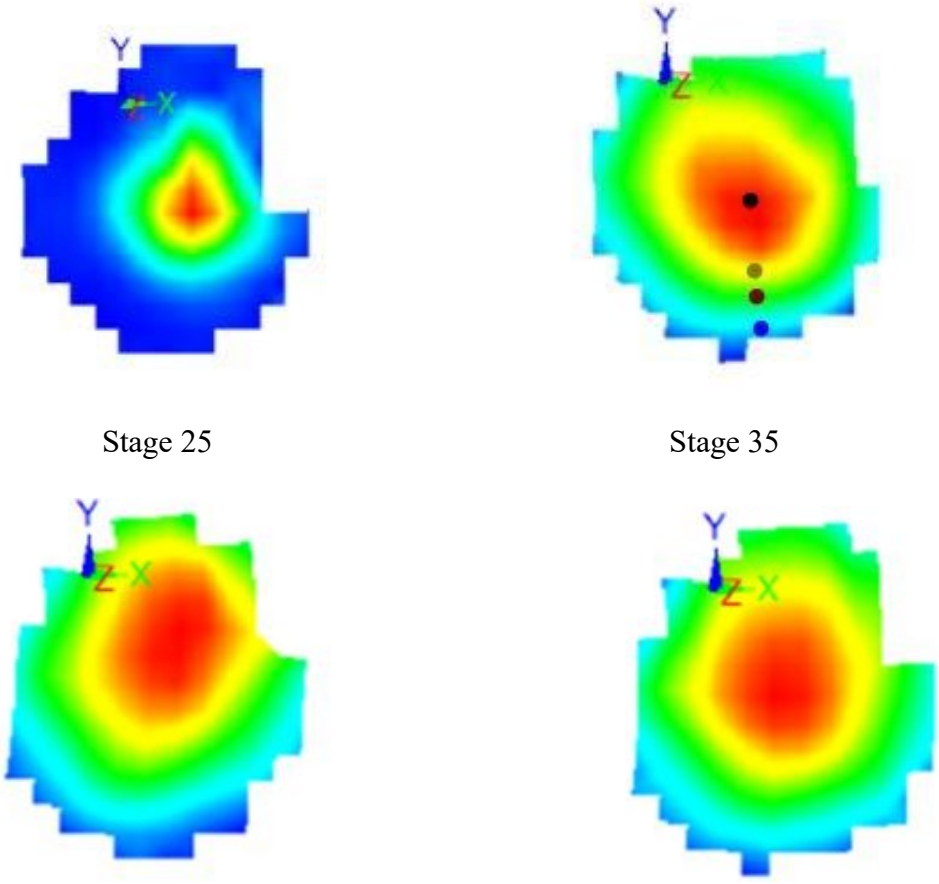

Figure 37. 3D deformation stages of Twintex® based 2.5 mm thick composite impacted at a velocity of 76.12 m/s with the spherical head projectile.

Figure 38 shows the Impact behavior of the Twintex® based 2.5 mm thick specimen impacted with a spherical head projectile at a velocity of 83.78 m/s. From the figure, it is observed that there are multiple splits near the point of impact due to matrix cracking and a small amount of fiber ruptures at the point of impact are noticed. On the opposite side, a small fiber rupture is evident.

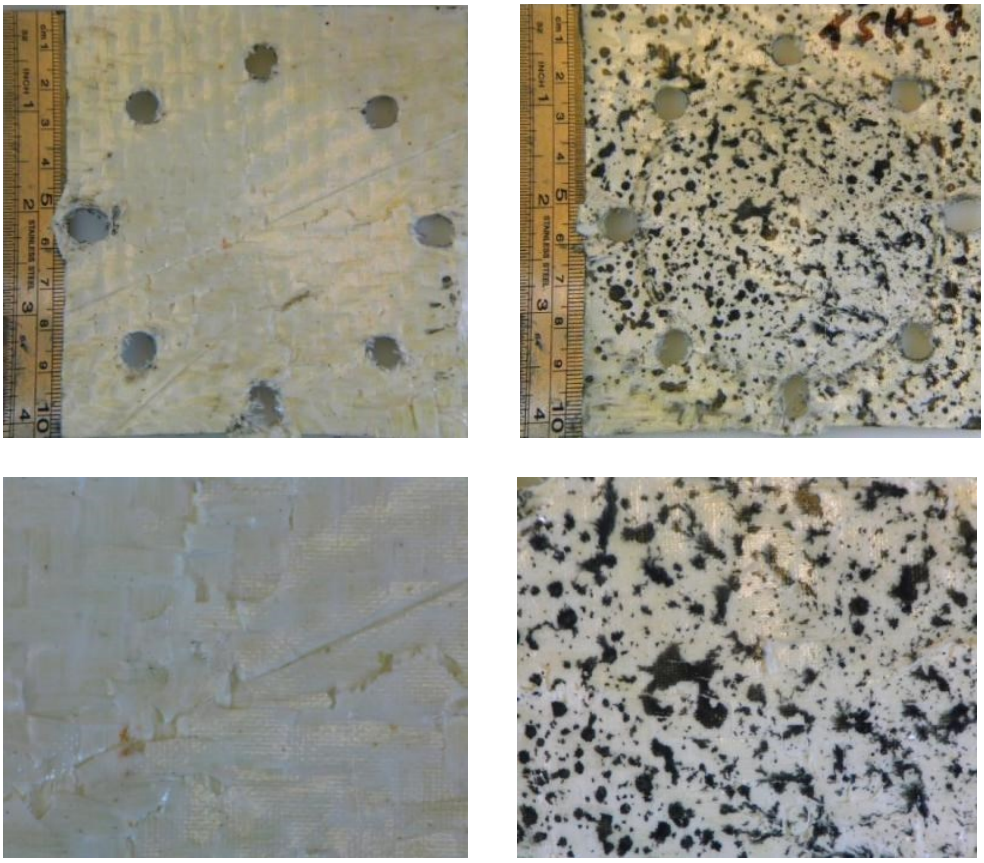

Figure 38. Twintex® based 2.5 mm composite impacted at a velocity of 83.78 m/s with the spherical head projectile.

Figure 39 shows the variation of the maximum transient out-of-plane displacement with stage time for the specimen illustrated in Figure 29. Here, the maximum out of plane transient displacement is 17.2 mm which increased by 2.65 mm compared with the previous specimen which was impacted with a velocity of 76.12m/s. Final displacement was around 12 mm at the point of impact.

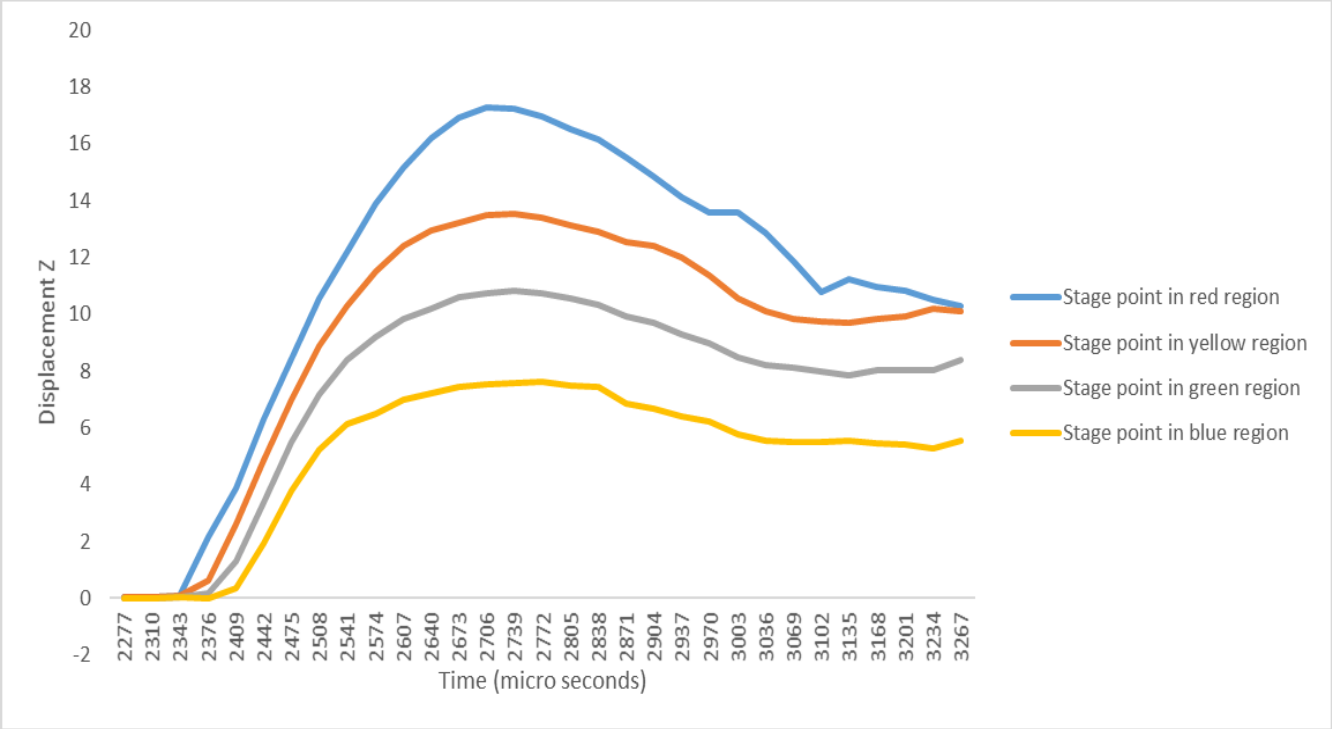

Figure 39. Displacement vs stage graph of Twintex® based 2.5 mm thick composite impacted at velocity 83.78 m/s with the spherical head projectile.

Figure 40 shows a number of deformation stages representing the impact event on the 2.5 mm thick Twintex® based composites tested at a velocity of 83.78 m/s with a spherical head projectile. From the figure, it is evident how the out-of-plane deformation increased until the maximum transient out-of-plane displacement was reached in stage 82 with a value of 17.2 mm. Following this, the displacement decreased in stage 93 with the final displacement taking a value close to 12 mm in the region of impact.

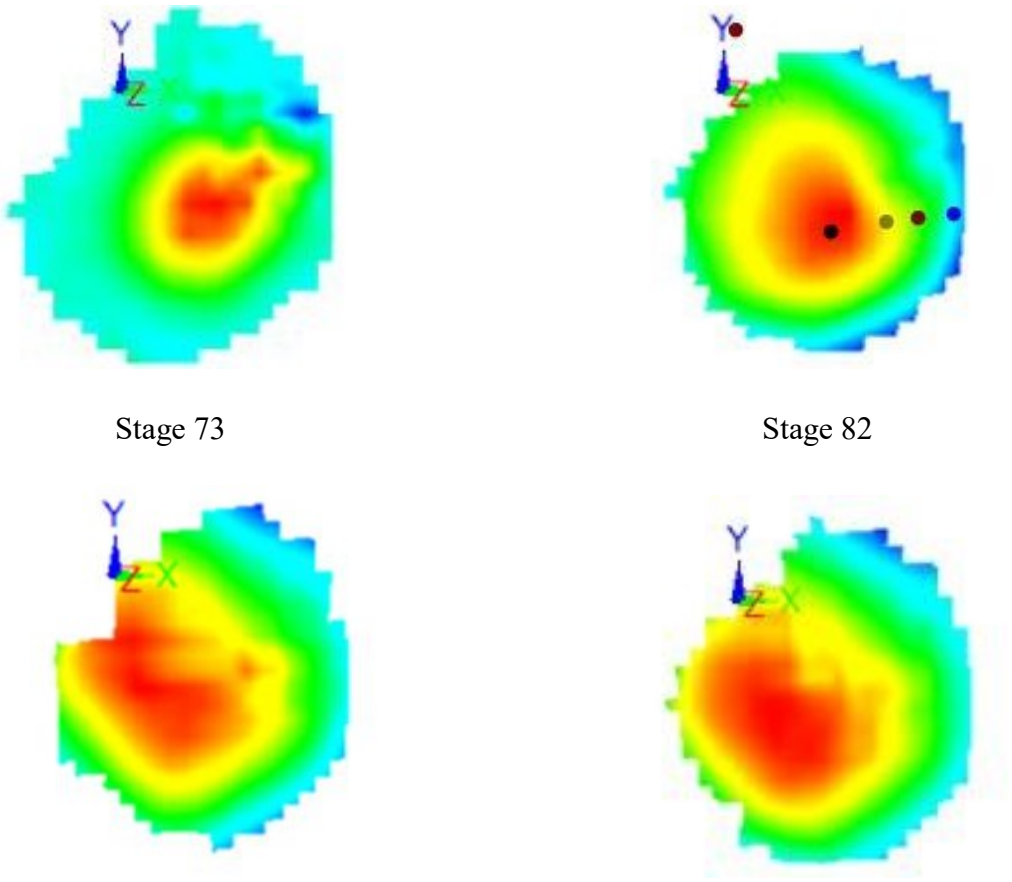

Figure 40. 3D deformation stages of Twintex® 2.5 mm thick composite tested at velocity 83.78 m/s with the spherical head projectile.

Figure 41 shows the impact behavior of the Twintex® based 2.5 mm thick specimen impacted with a spherical head projectile at a velocity of 93.86 m/s. At this velocity the woven composite reached its ballistic limit which lead to the projectile through the specimen. At the region of contact of the projectile, there are multiple splits due to matrix cracking and minute fiber ruptures. At the point of the contact of the projectile, fiber ruptures are evident. On the opposite side, fiber ruptures and fiber pull outs are noticed at and near the point of impact. This mode of failure of composite resembles petaling failure since the tensile strength of the composite was exceded. Figure 41 includes a number of optical micrograph of the section of the speimen as well as image of the impact event obtained from the high speed cameras.

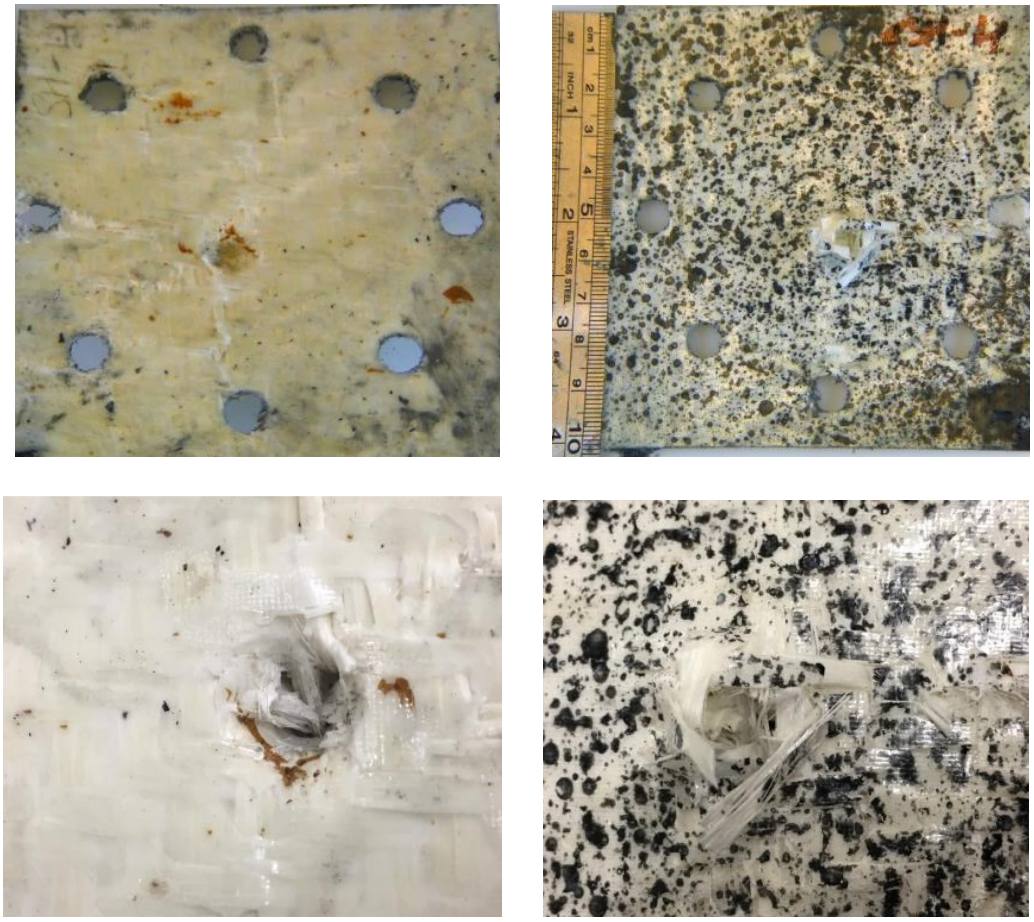

(a)

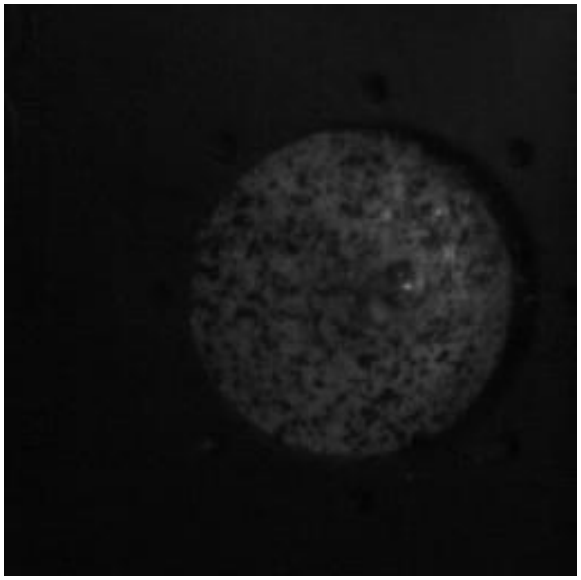

(b)

(c)

Figure 41. (a) Twintex® 2.5 mm composite impacted at a velocity of 93.86 m/s with the spherical head projectile (b) High speed camera image (c) Section of impacted composite.

4.2.2 Impact behavior of Sheild Strand S® / Epoxy 2.5 mm thick composites with the Spherical head projectile

Figure 42 shows the low magnification optical images Shield Strand S®/epoxy based 2.5 mm thick specimen impacted with the spherical head projectile at a velocity of 74.32 m/s. From the figure, it is evident that there is a negligible amount of damage at the region and point of contact of the projectile along with minute delamination. On the opposite side, no signs of damages were observed. The reason for not showing any signs of damage is because the specimen absorbed the total impact energy of the projectile.

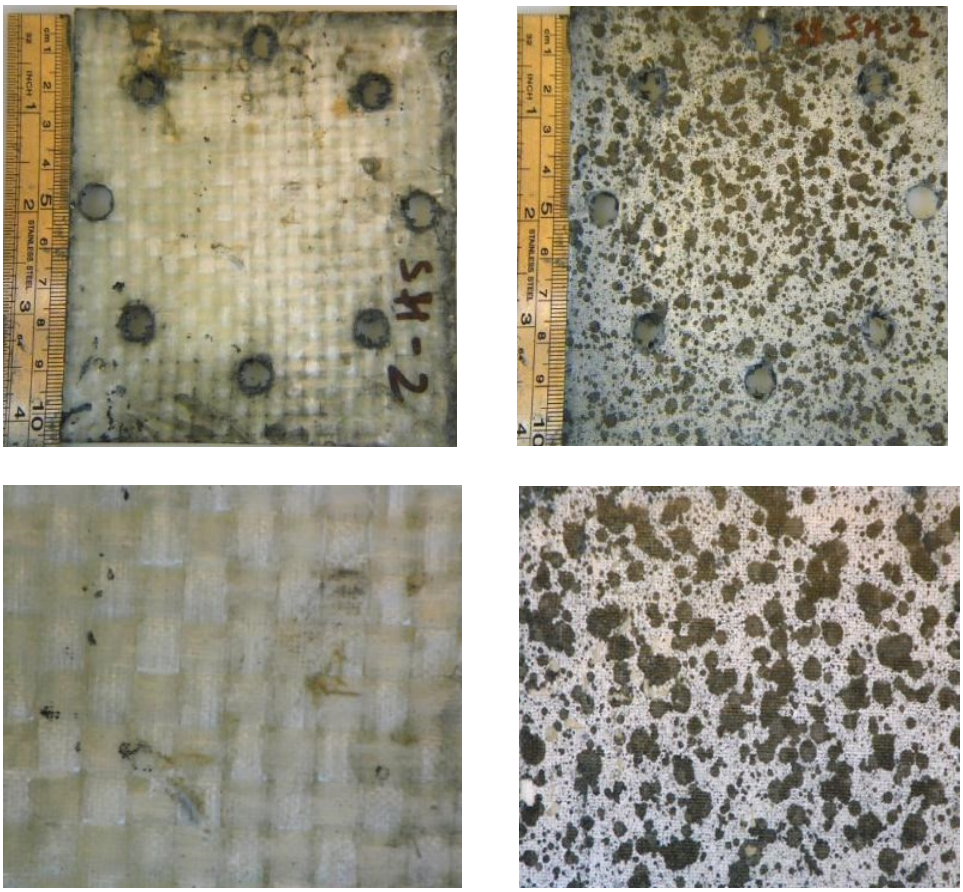

Figure 42. Shield Strand S® / Epoxy based 2.5 mm composite impacted at a velocity of 74.32 m/s with spherical head projectile.

The maximum transient out-of-plane displacement with stage time for specimen is presented in Figure 43. In this case, the maximum out-of-plane displacement reached a value of 8.81 mm. Figure 43 also highlights some deformations and vibrations associated with the impact waves after the impact event.

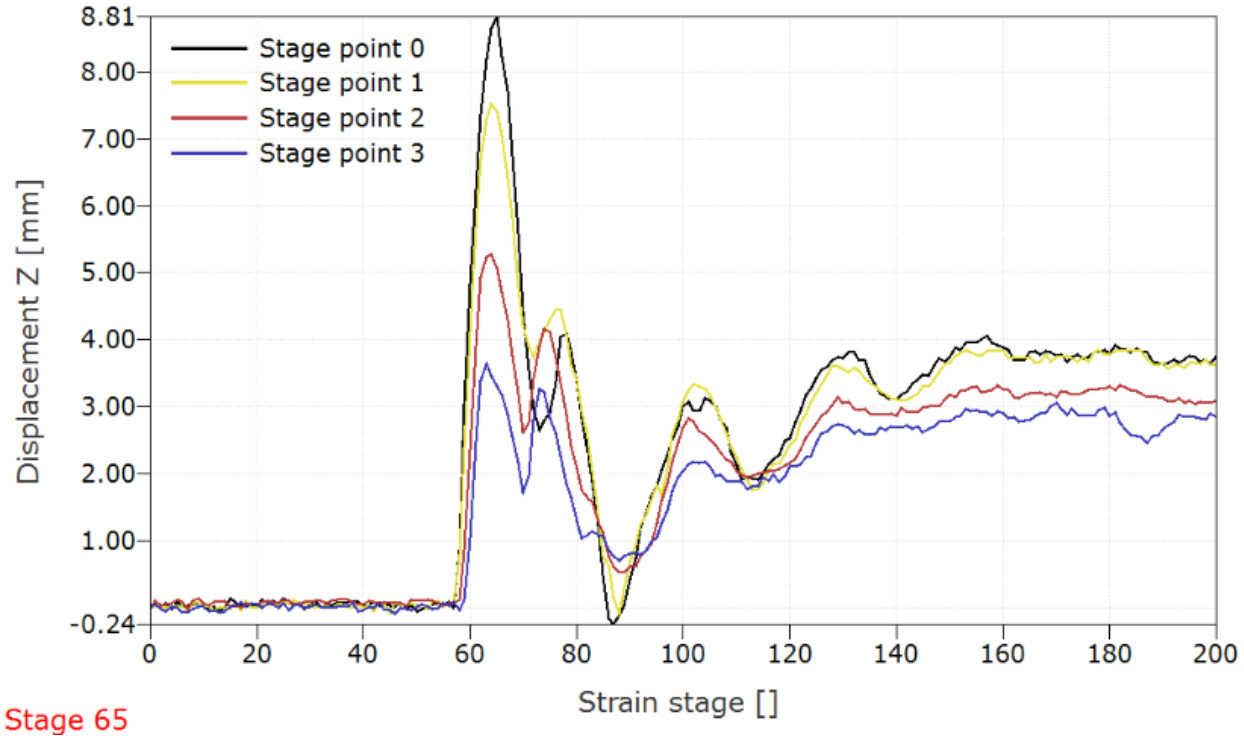

Figure 43. Displacement vs Stage graph of Shield Strand S® / Epoxy based 2.5 mm thick composite impacted at velocity 74.32 m/s with the spherical head projectile.

Figure 44 shows a number of deformation stages representing the impact event on the Shield Strand S / Epoxy based 2.5 mm thick composite tested at a velocity of 74.32 m/s with a spherical head projectile. From the figure, it is evident how the out-of-plane deformation increased until a value of 8.81 mm was reached. Following this, the displacement decreased as shown in stage 88. The final displacement was close to 4.00 mm at the point of impact.

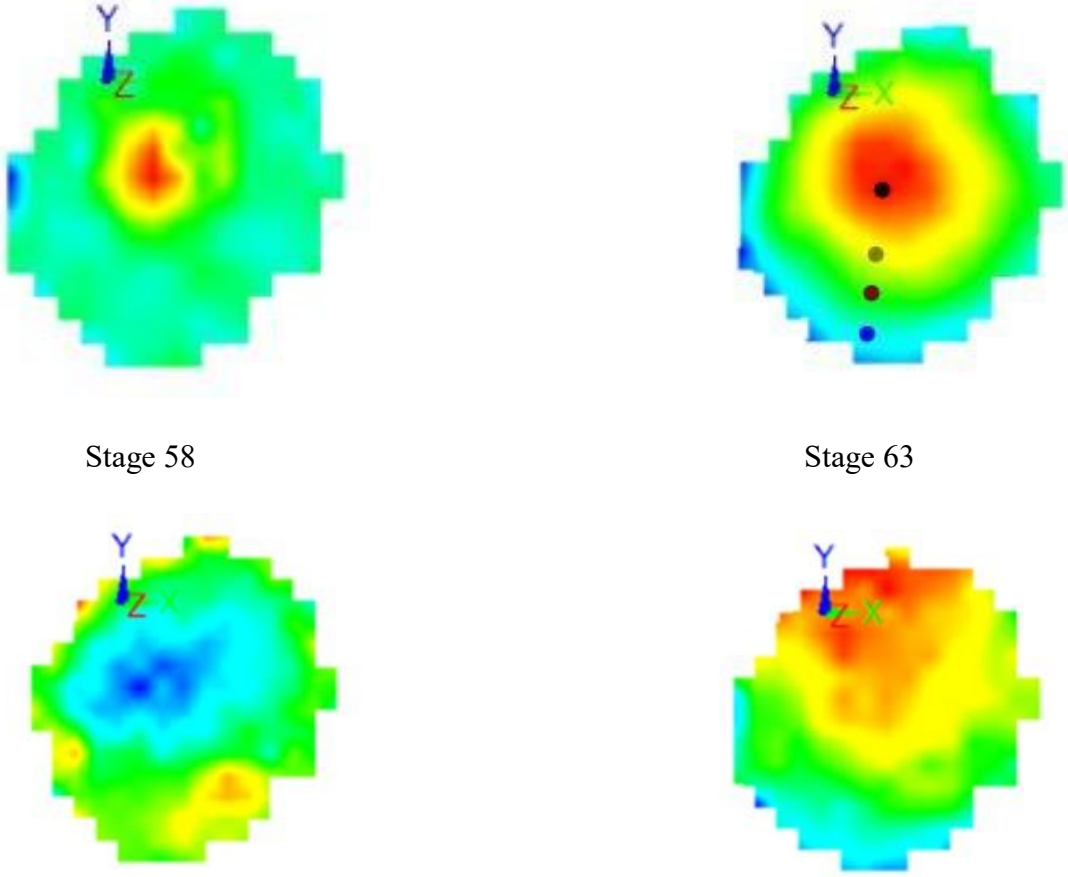

Figure 44. 3D deformation stages of Shield Strand S® / Epoxy based 2.5 mm thick composite impacted at velocity 74.32 m/s with the spherical head projectile.

Figure 45 shows the low magnification optical images oof Shield Strand S® / Epoxy based 2.5 mm thick specimen impacted with the spherical head projectile at a velocity of 88.40 m/s. From the figure, a minute amount of delaminations and fiber ruptures are noticed at region and point of contact of the projectile. In the opposite side, no damages are observed. Delamination occurred in the top layer of the specimen because it absorbed most of the impact energy of the projectile before transferring the energy to the other layers.

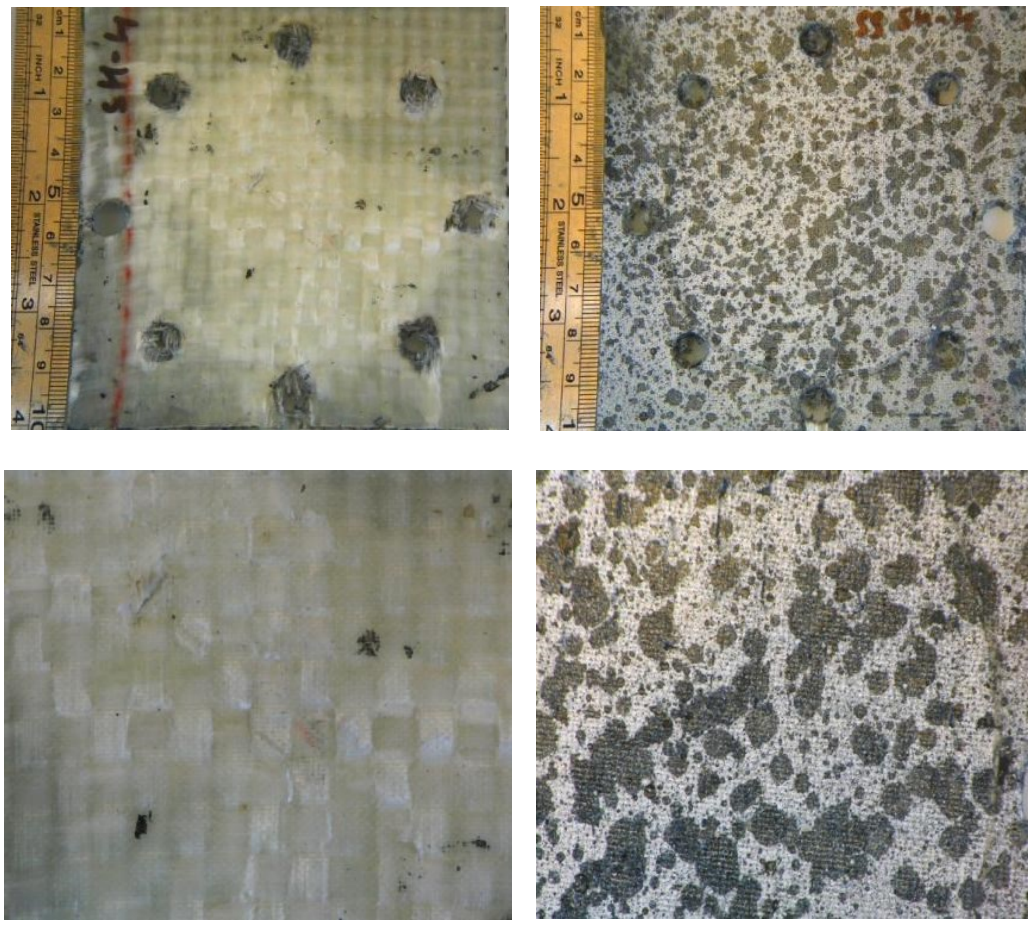

Figure 45. Shield Strand S® / Epoxy based 2.5 mm composite impacted at the velocity of 88.40 m/s with the spherical head projectile.

The maximum transient out-of-plane displacement with stage time for the specimen is presented in Figure 46. In this case, the maximum out-of-plane displacement reached a value of 11.2 mm. Here, a vibration associated with the impact wave is evident. Due to damage done to the top layer of impact, the number of impact waves were reduced compared to the same specimen impacted at a velocity of 74.32 m/s.

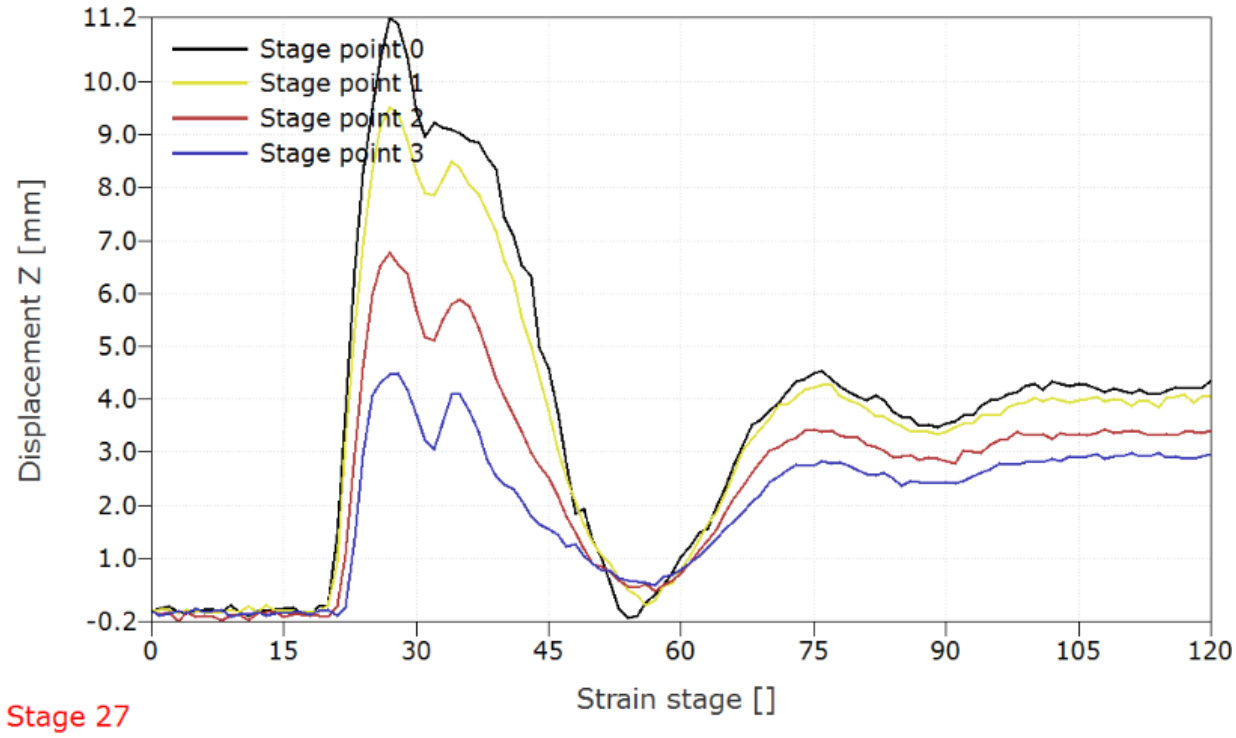

Figure 46. Displacement vs Stage graph of Shield Strand S® / Epoxy based 2.5 mm thick composite impacted at velocity 88.40 m/s with the spherical head projectile.

Figure 47 shows a number of deformation stages representing the impact event on the Shield Strand S® / Epoxy based 2.5 mm thick composite tested at a velocity of 88.40 m/s with the spherical head projectile. From the figure, it is evident how the out-of-plane deformation increased until a value of 11.2 mm was reached. Following this, the displacement decreased as shown in stage 56. The final displacement was close to 4.50 mm at the point of impact. Partial deformation data in stage 22 could not be captured due to the reflection of lights when it deformed.

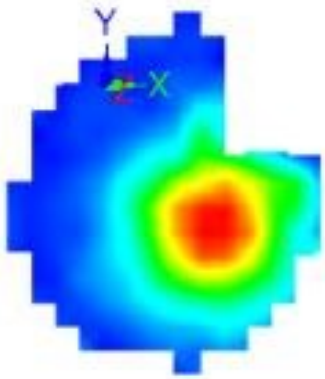

Stage 22

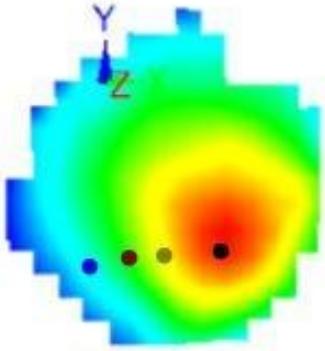

Stage 27

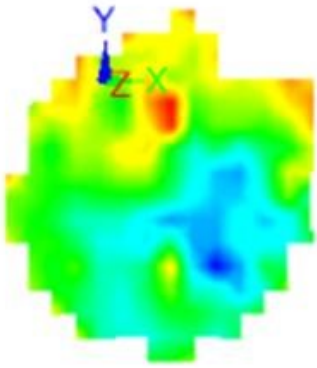

Stage 56

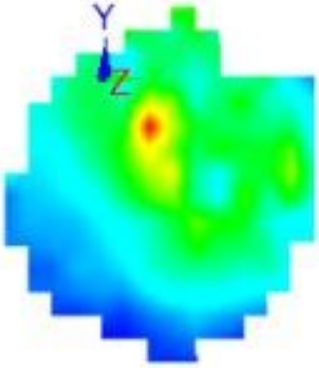

Stage 120

Figure 47. 3D deformation stages of Shield Strand S® / Epoxy based 2.5 mm thick composite impacted at velocity 88.40 m/s with the spherical head projectile.

Figure 48 shows the low magnification optical images of Shield Strand S®/epoxy based 2.5 mm thick specimen impacted with the spherical head projectile at a velocity of 94.20 m/s. From the figure, it is observed that there are small fiber ruptures at the area of impact along with delamination in the top layer, whereas on the opposite side, minute fiber ruptures are evident. This impact velocity is close to the ballistic limit impact velocity of the Twintex® based 2.5 mm thick specimen impacted with the spherical head projectile.

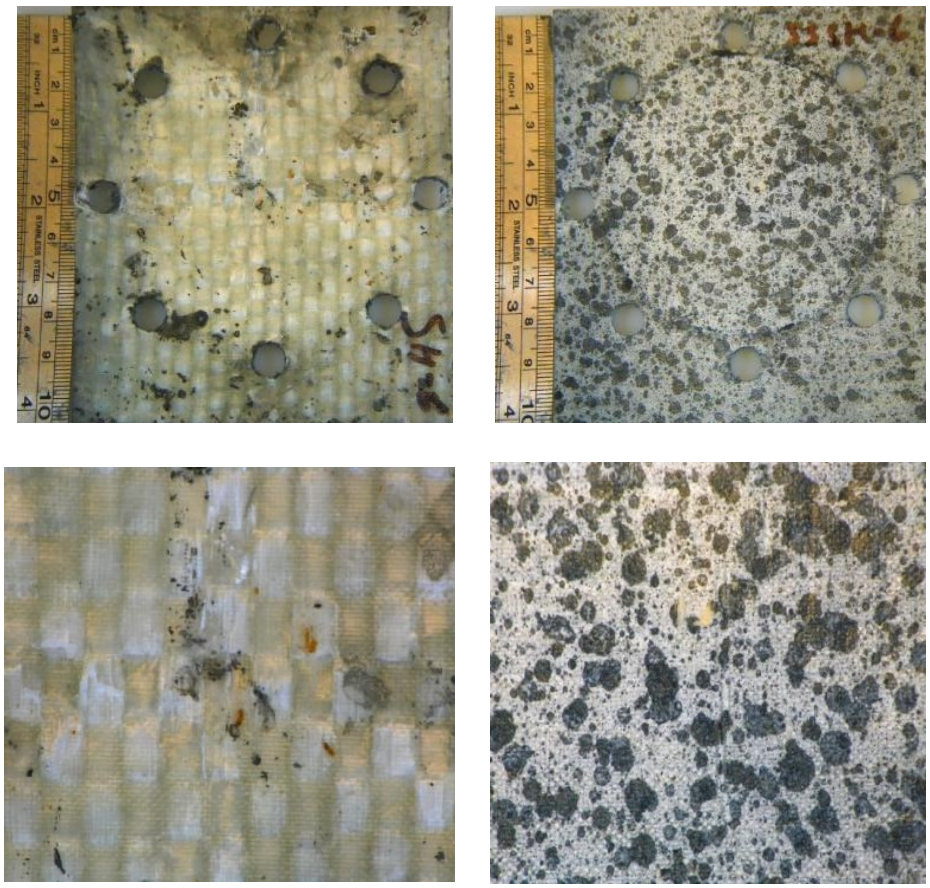

Figure 48. Shield Strand S ®/ Epoxy based 2.5 mm composite impacted at the velocity of 94.20 m/s with the spherical head projectile.

The maximum transient out-of-plane displacement with stage time for specimen presented in Figure 49. In this case, the maximum out-of-plane displacement reached a value of 12.01 mm.

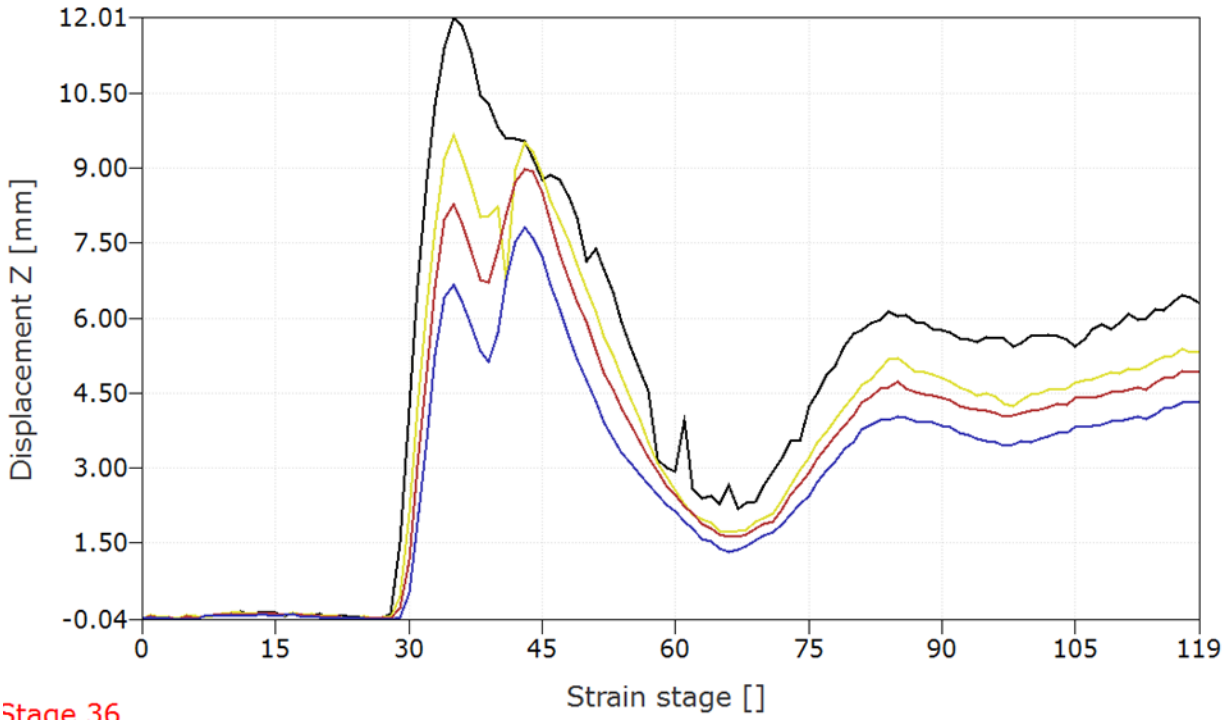

Figure 49. Displacement vs Stage graph of Shield Strand S® / Epoxy based 2.5 mm thick composite impacted at velocity 94.20 m/s with the spherical head projectile.

Figure 50 shows some deformation stages representing the impact event on the Shield Strand S® / Epoxy based 2.5 mm thick composite tested at a velocity of 105 m/s with the spherical head projectile. From the figure, it is evident how the out-of-plane deformation increased until a value of 12.00 mm was reached. Following this, the displacement decreased as shown in stage 66. The final displacement was close to 6.5 mm at the point of impact.

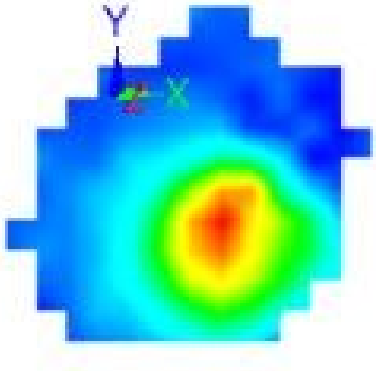

Stage 29

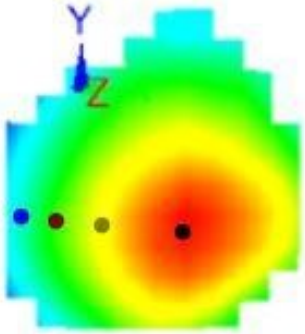

Stage 36

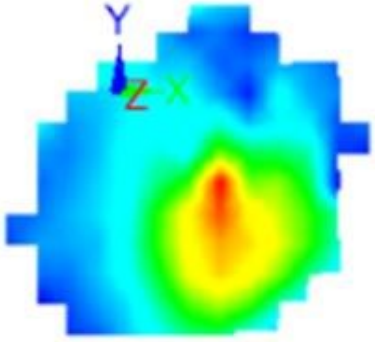

Stage 66

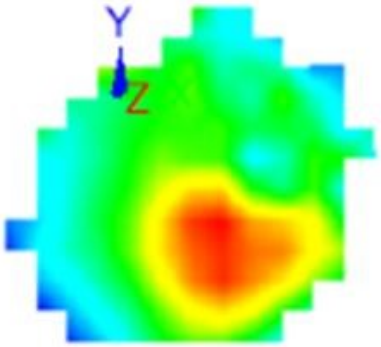

Stage 119

Figure 50. 3D deformation stages of Shield Strand S ®/ Epoxy based 2.5 mm thick composite impacted at a velocity 94.20 m/s with the spherical head projectile.

Figure 51 shows the low magnification optical images of Shield Strand S®/epoxy based 2.5 mm thick specimen impacted with the spherical head projectile at a velocity of 101.54 m/s. From the figure, it is evident that there are minute fiber ruptures and delamination on the region of impact of the projectile. It is noticed that with an increase in the impact velocity, the amount of delamination in the top layer increased. On the speckle pattern side, at the point of contact of the projectile and a few areas in the same region, fiber ruptures are observed.

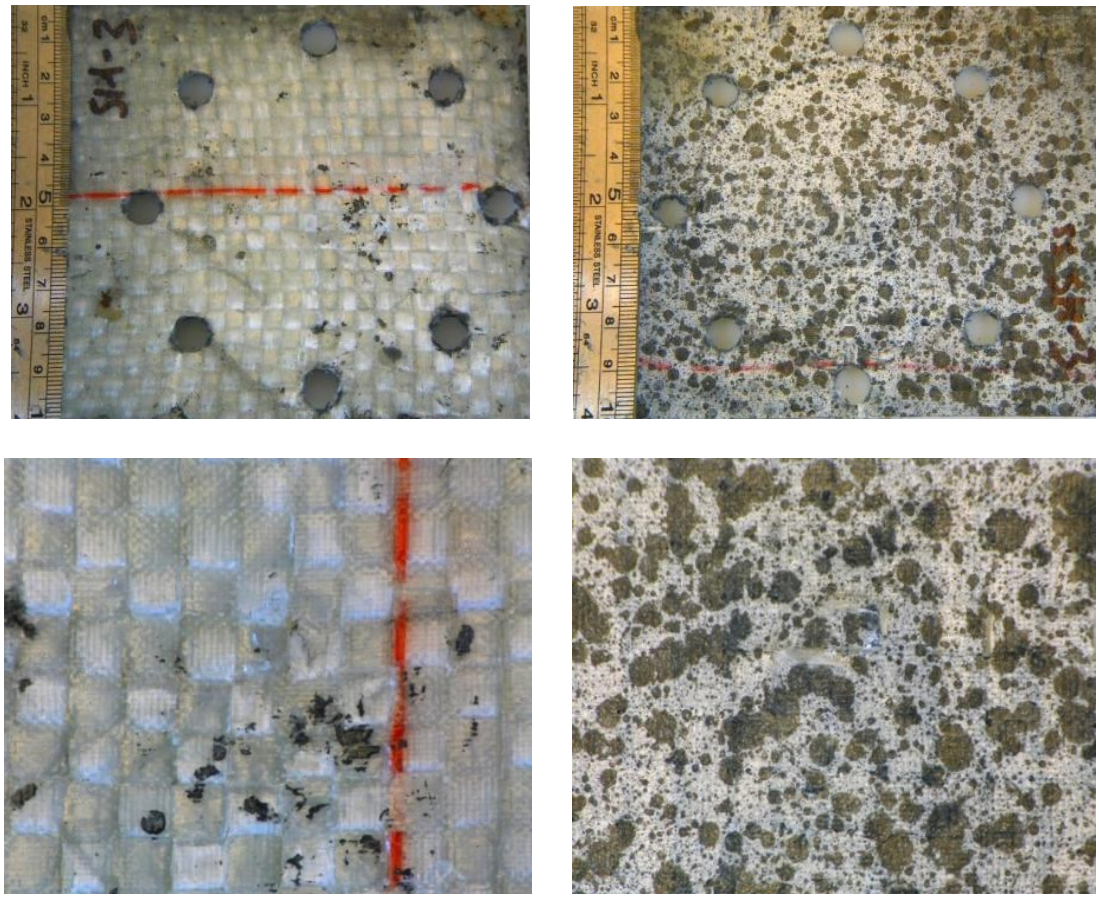

Figure 51. Shield Strand S® / Epoxy based 2.5 mm thick composite impacted at a velocity of 101.54 m/s with the spherical head projectile.

The maximum transient out-of-plane displacement with stage time for specimen presented in Figure 52. In this case, the maximum out-of-plane displacement reached a value of 13.63 mm. Here, a vibration associated with the impact wave is evident. In this case, the number of impact waves reduced due to the energy absorbing capacity of the specimen.

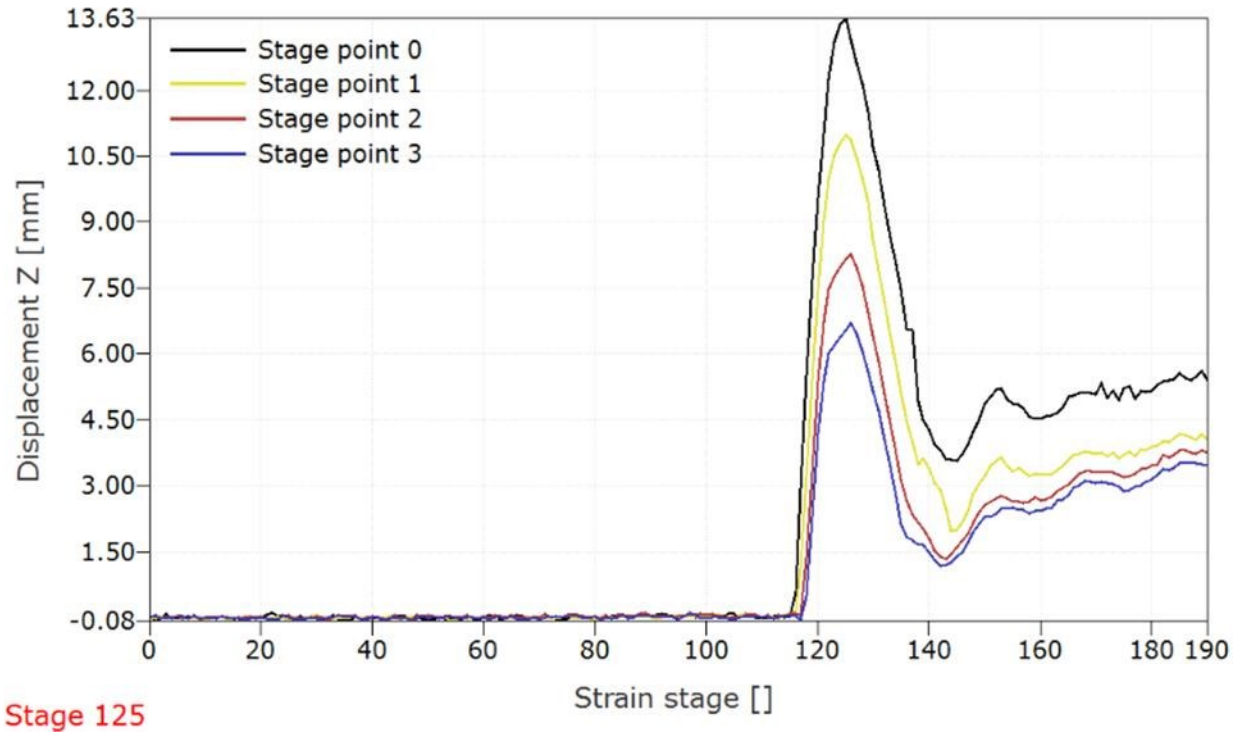

Figure 52. Displacement vs Stage graph of Shield Strand S® / Epoxy based 2.5 mm thick composite impacted at velocity 101.54 m/s with the spherical head projectile.

Figure 53 shows a number of deformation stages representing the impact event on the Shield Strand S® / Epoxy based 2.5 mm thick composite tested at a velocity of 94.20 m/s with the spherical head projectile. From the figure, it is evident how the out-of-plane deformation increased until a value of 13.63 mm was reached. Following this, the displacement decreased as shown in stage 142. The final displacement was close to 5.50 mm at the point of impact.

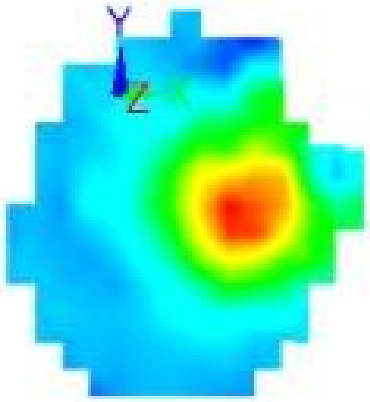

Stage 117

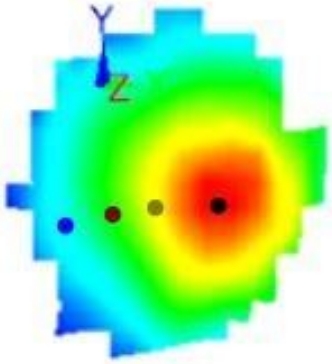

Stage 125

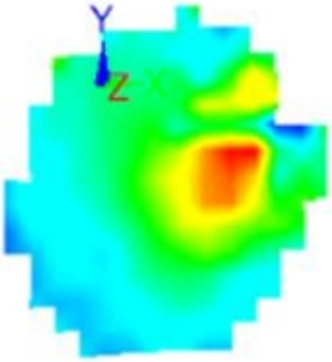

Stage 142

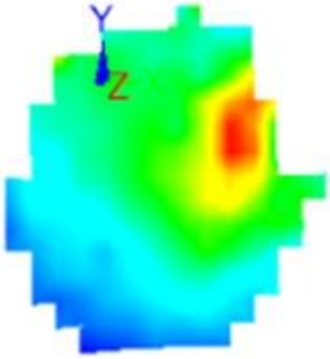

Stage 190

Figure 53. 3D deformation stages of Shield Strand S® / Epoxy 2.5 mm thick composite tested at velocity 101.54 m/s with the Spherical head projectile.

Figure 54 shows the low magnification optical images of Shield Strand S®/Epoxy based 2.5 mm thick specimen impacted with the spherical head projectile at a velocity of 105 m/s. From the figure, it is evident that on the point of contact of the projectile, delamination occurred and minute matrix cracks are noticed on the area of impact. On the opposite side, minute fiber ruptures are present on the point of contact of the projectile along with minute matrix cracks at the area of impact.

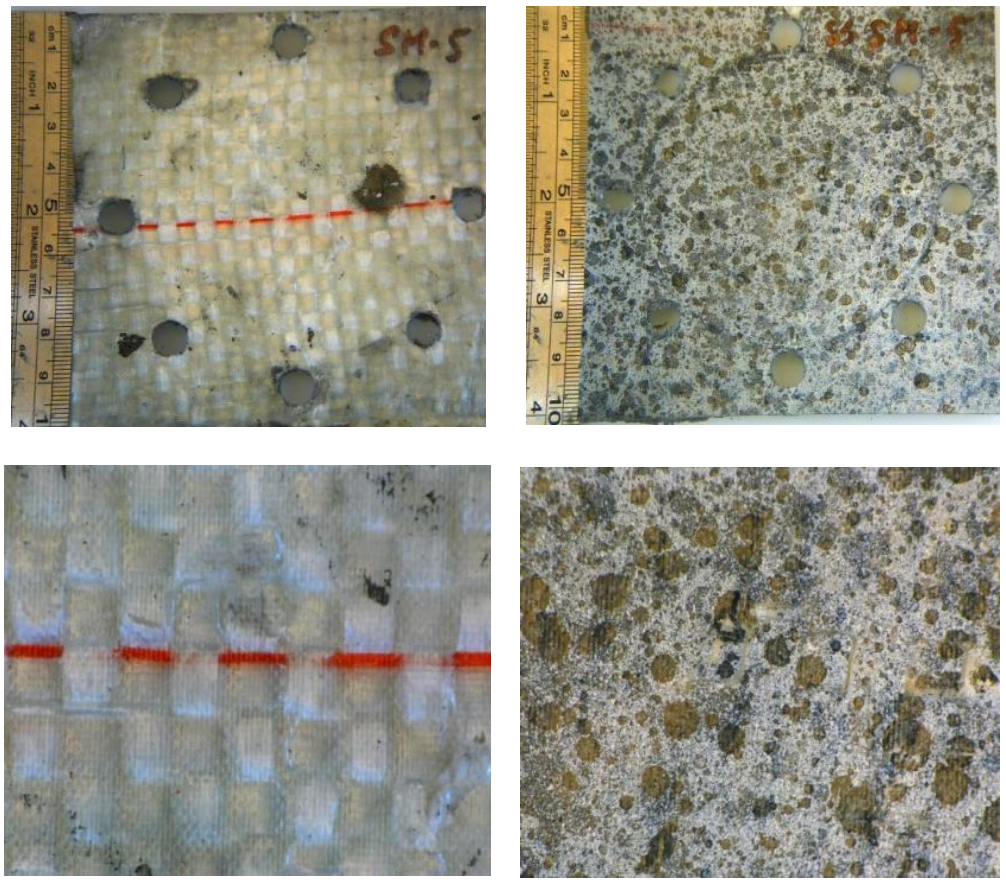

Figure 54. Shield Strand S ®/ Epoxy based 2.5 mm composite impacted at a velocity of 105 m/s with the spherical head projectile.

The maximum transient out-of-plane displacement with stage time for specimen presented in Figure 55. In this case, the maximum out-of-plane displacement reached a value of 15.60 mm. Similar to the thermoset based 2.5 mm thick specimen impacted at 94.20 m/s, a vibration associated with the impact wave is evident.

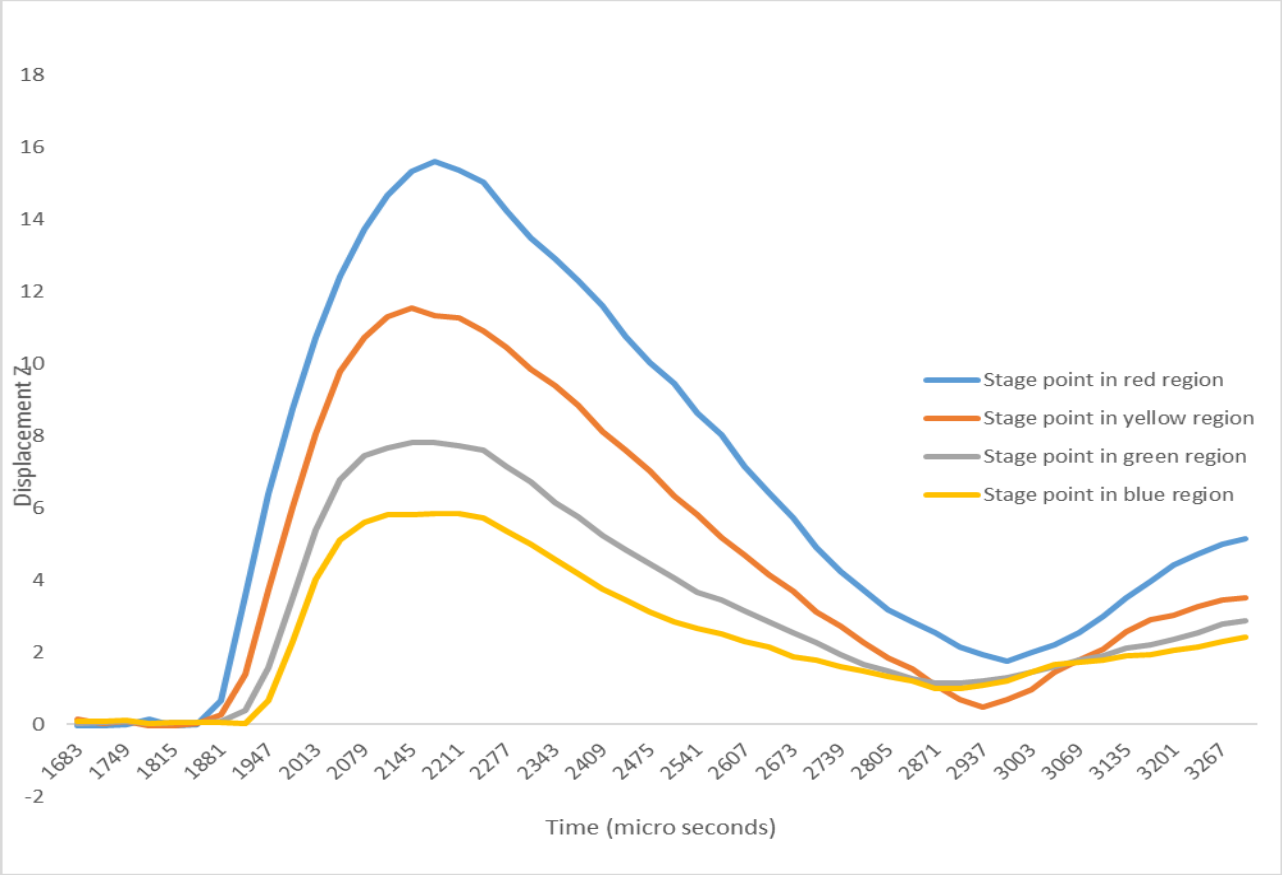

Figure 55. Displacement vs Stage graph of Shield Strand S ®/ Epoxy based 2.5 mm thick composite impacted at a velocity 105 m/s with the spherical head projectile.

Figure 56 shows a number of deformation stages representing the impact event on the Shield Strand S ®/ Epoxy based 2.5 mm thick composite tested at a velocity of 101.54 m/s with the spherical head projectile. From the figure, it is evident how the out-of-plane deformation increased until a value of 15.60 mm was reached. Following this, the displacement decreased as shown in stage 95. The final displacement was close to 7.0 mm at the point of impact.

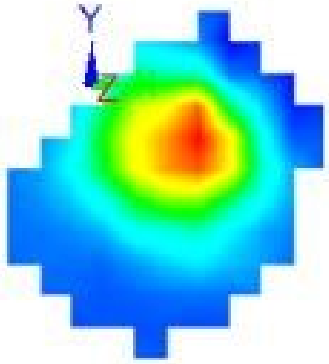

Stage 58

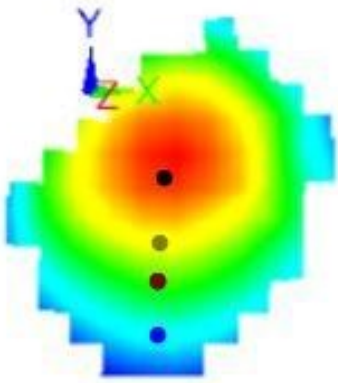

Stage 66

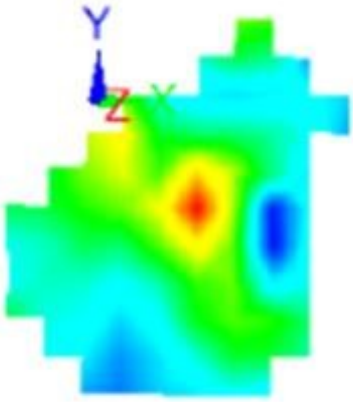

Stage 95

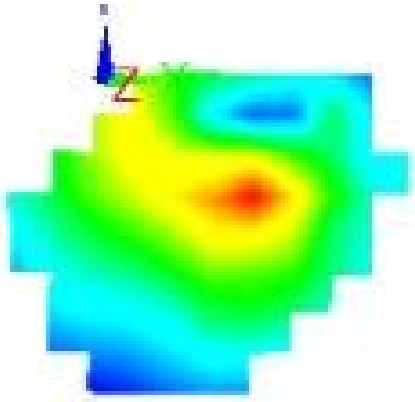

Stage 150

Figure 56. 3D deformation stages of Shield Strand S® / Epoxy based 2.5 mm thick composite impacted at velocity 105 m/s with the spherical head projectile.

Figure 57 shows the low magnification optical images of Shield Strand S®/Epoxy based 2.5 mm thick specimen impacted with the spherical head projectile at a velocity of 118.5 m/s. At this velocity, specimen reached its ballistic limit. From the figure, at the region of impact of the projectile, star-shaped delamination is evident with signs of fiber ruptures at the point of impact. On the speckle pattern side, fiber ruptures are evident in the region of impact along with heavy fiber ruptures at the point of contact. Petaling failure mode is noticed as well as fragmentation was

visualized during the test. Figure 57 includes optical micrograph of the section of impacted specimen.

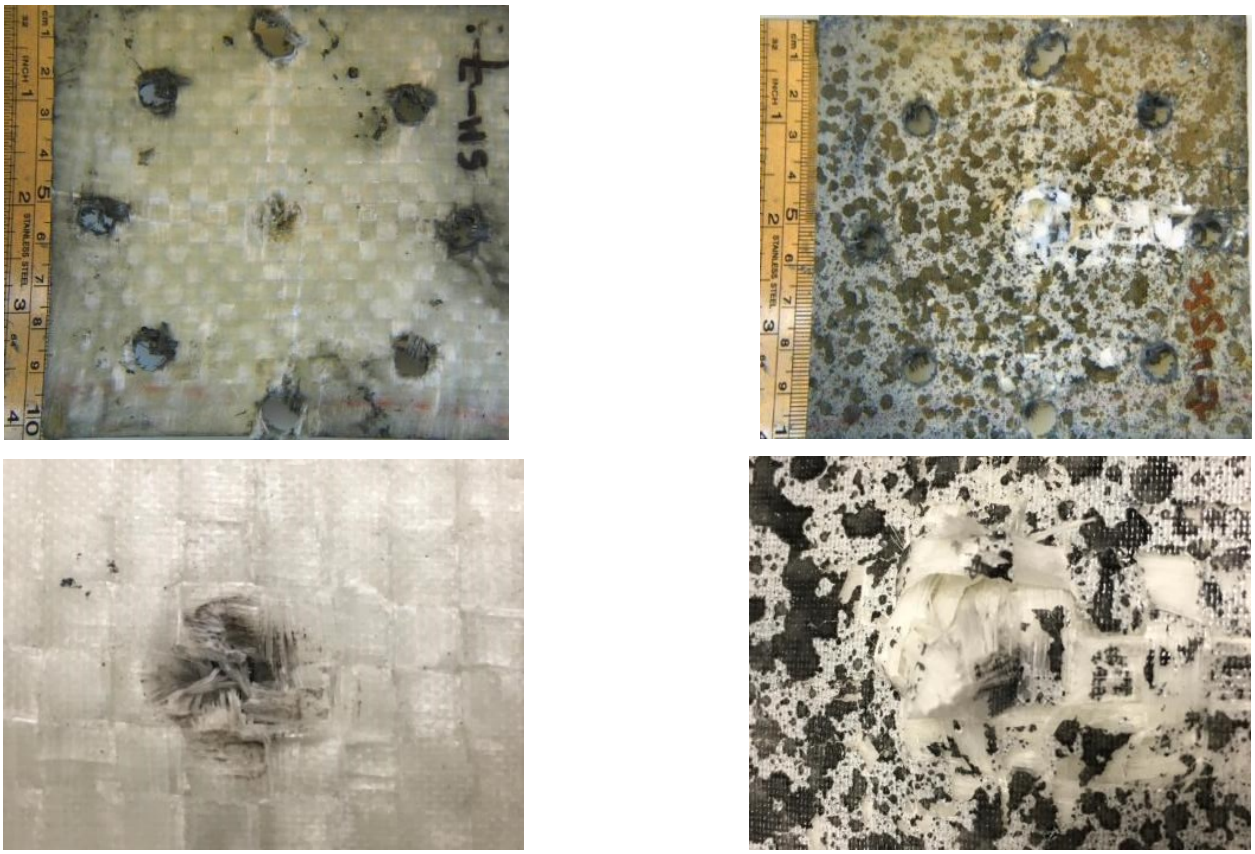

(a)

(b)

Figure 57. (a) Shield Strand S ®/ Epoxy based 2.5 mm thick composite impacted at a velocity of 118.5 m/s with the spherical head projectile (b) Section of impacted composite.

4.2.3 Impact behavior of Twintex® 4.5 mm thick composites with the Spherical head projectile

Figure 58 shows the low magnification optical images of Twintex® based 4.5 mm thick specimen impacted with the spherical head projectile at a velocity of 60.91 m/s. It is evident that on the side and opposite side of impact, there are no signs of major damages and failure.

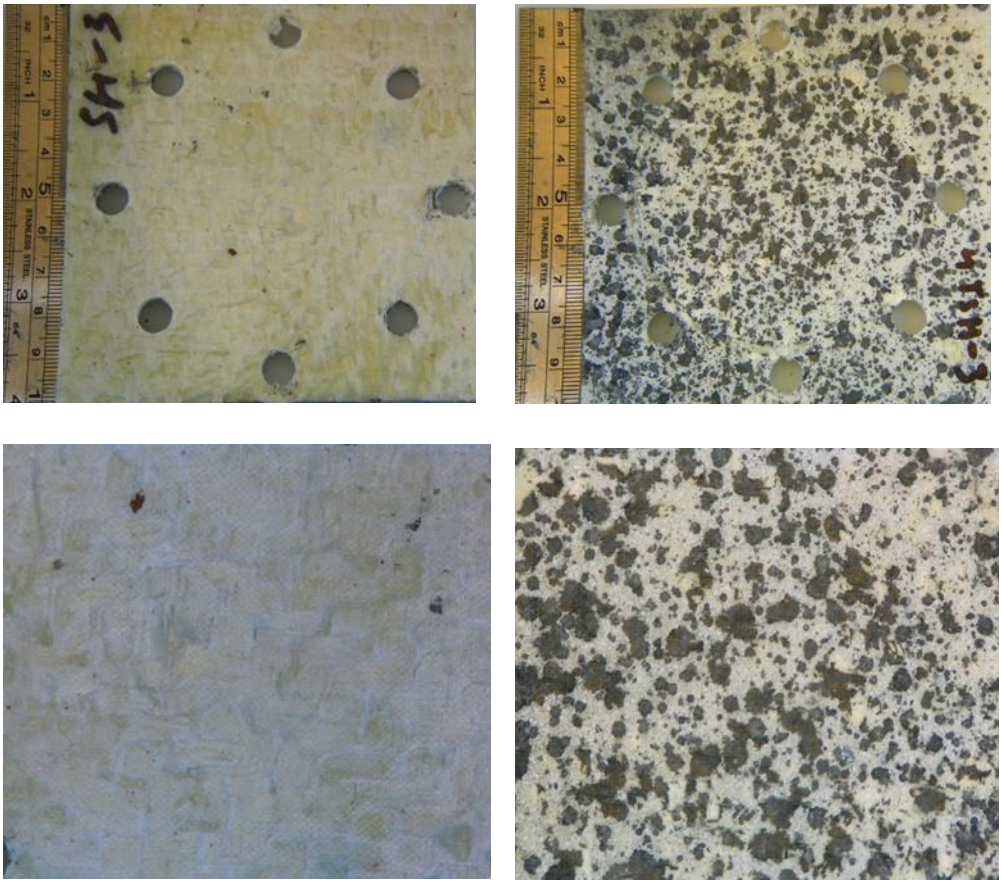

Figure 58. Twintex® based 4.5 mm composite impacted at a velocity of 60.91 m/s with the spherical head projectile.

The maximum transient out-of-plane displacement with stage time for the specimen presented in Figure 59. Here, the maximum out-of-plane displacement reached a value of 7.91 mm. Figure 59 also highlights a impact wave. Here, the amount of impact energy is less to cause major failure in material.

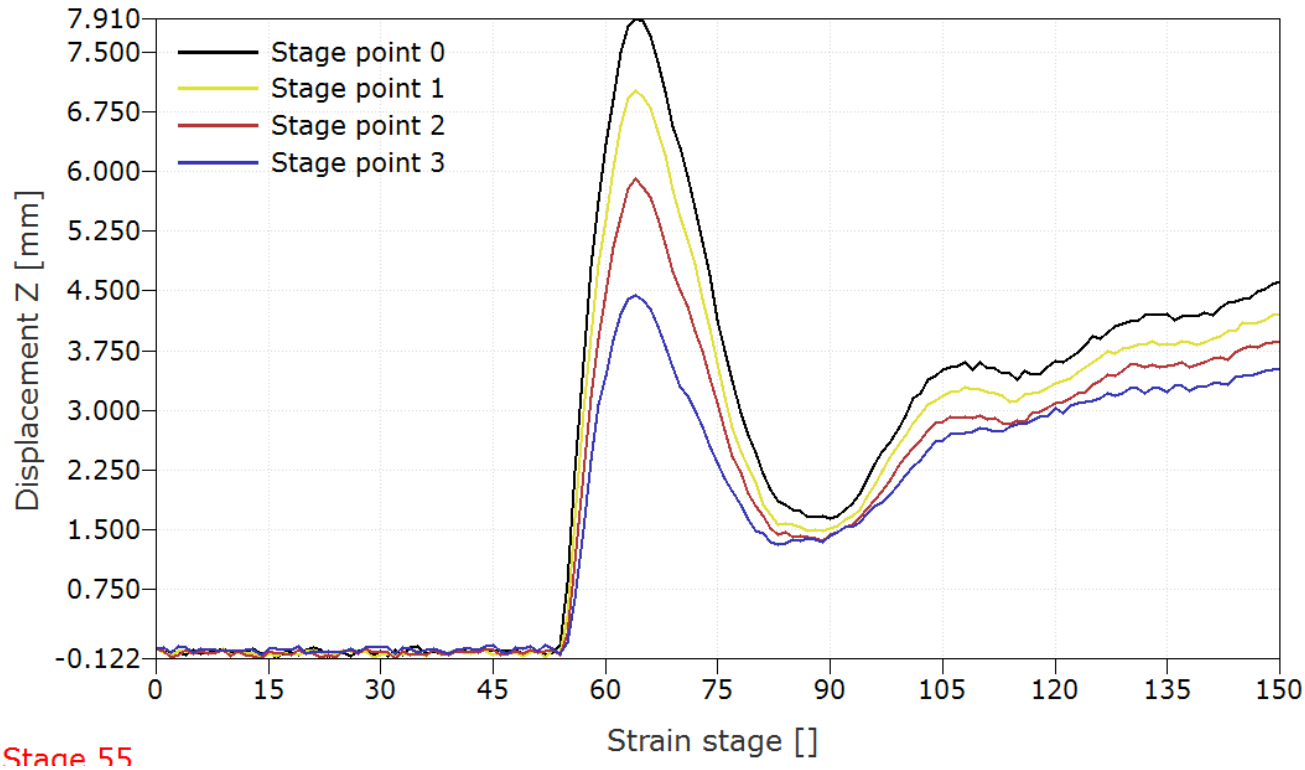

Figure 59. Displacement vs Stage graph of Twintex® based 4.5 mm thick composite impacted at velocity 60.91 m/s with the spherical head projectile.

Figure 60 shows a number of deformation stages representing the impact event on the Twintex® based 4.5 mm thick composite tested at a velocity of 60.91 m/s with the spherical head projectile. From the figure, it is evident how the out-of-plane deformation increased until a value of 7.91 mm was reached in stage 64. Following this, the displacement decreased as shown in stage 94.

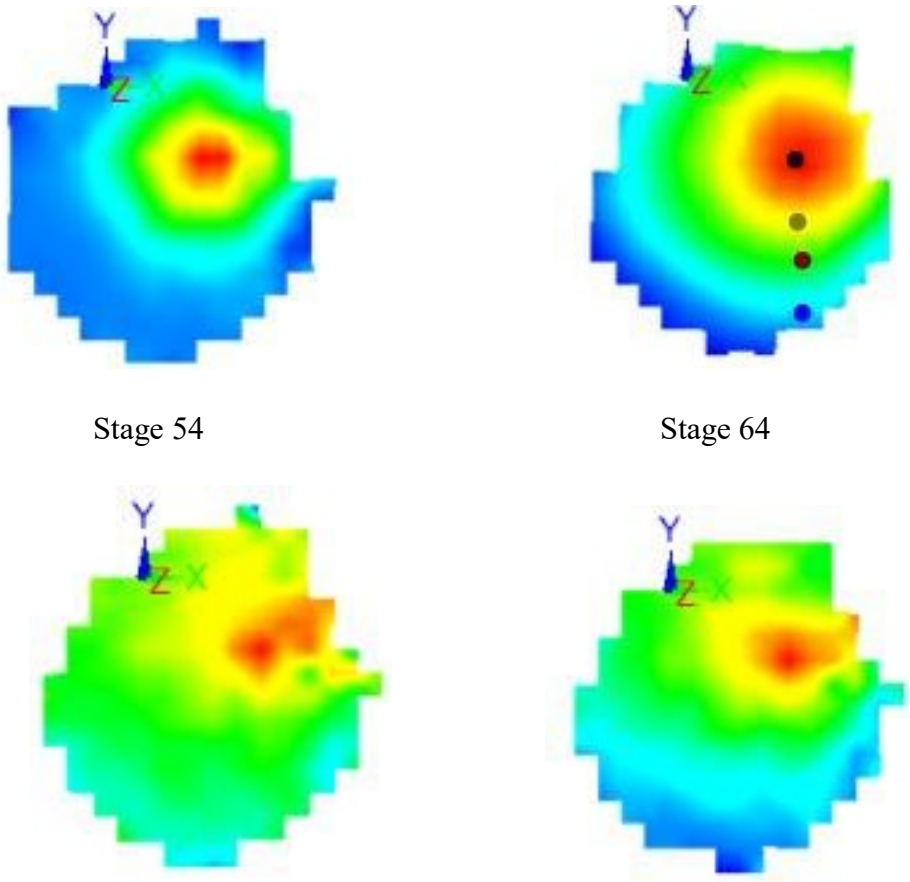

Figure 60. 3D deformation stages of Twintex® based 4.5 mm thick composite impacted at a velocity 60.91 m/s with the spherical head projectile.

Figure 61 shows the impact behavior Twintex® based 4.5 mm thick specimen impacted with the spherical head projectile at a velocity of 75.42 m/s. From the figure, it is evident that there are no signs of damage on the point and region of the impact as well as on the opposite side.

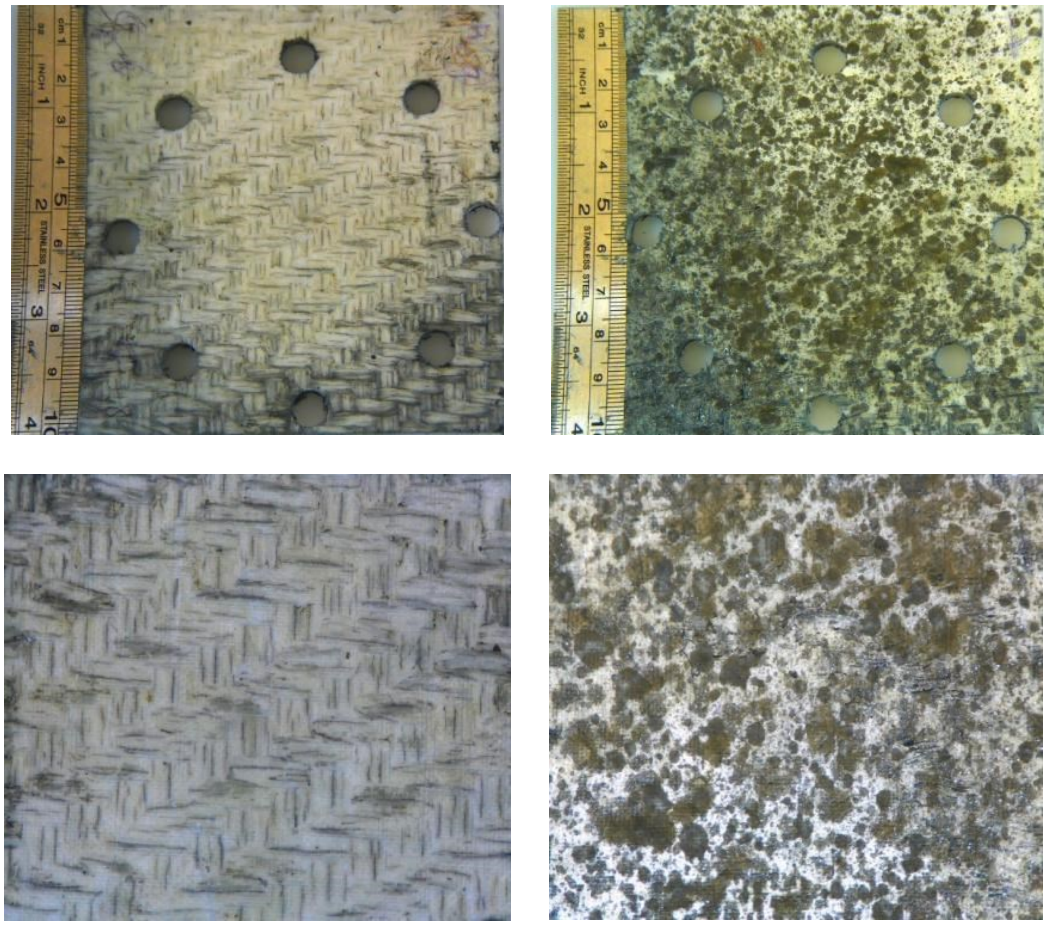

Figure 61. Twintex® based 4.5 mm composite impacted at a velocity of 75.42 m/s with the spherical head projectile.

The maximum transient out-of-plane displacement with stage time for the specimen presented in Figure 62. Here, the maximum out-of-plane displacement reached a value of 8.59 mm. Figure 56 also highlights some impact waves remaining in the specimen after the impact event.

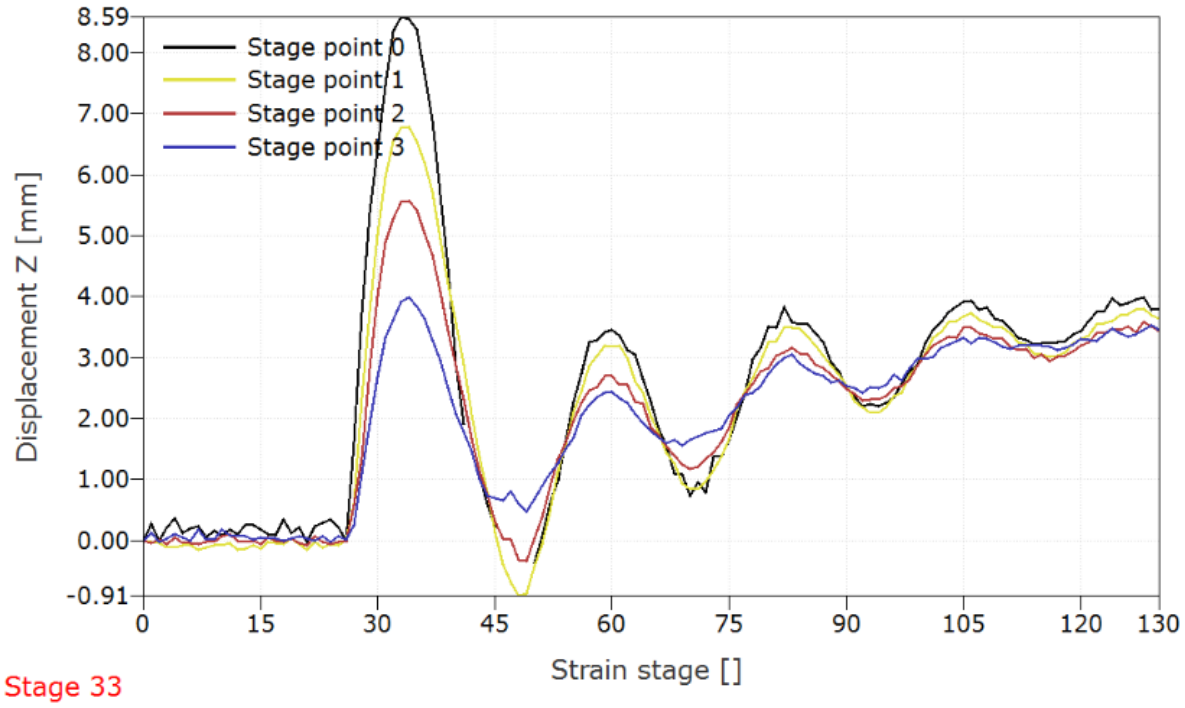

Figure 62. Displacement vs Stage graph of Twintex® based 4.5 mm thick composite impacted at velocity 75.42 m/s with the spherical head projectile.

Figure 63 shows a number of deformation stages representing the impact event on the Twintex® based 4.5 mm thick composite tested at a velocity of 75.42 m/s with the spherical head projectile. From the figure, it is evident how the out-of-plane deformation increased until a value of 8.59 mm was reached. Following this, the displacement decreased as shown in stage 47. The final displacement was close to 4.00 mm at the point of impact.

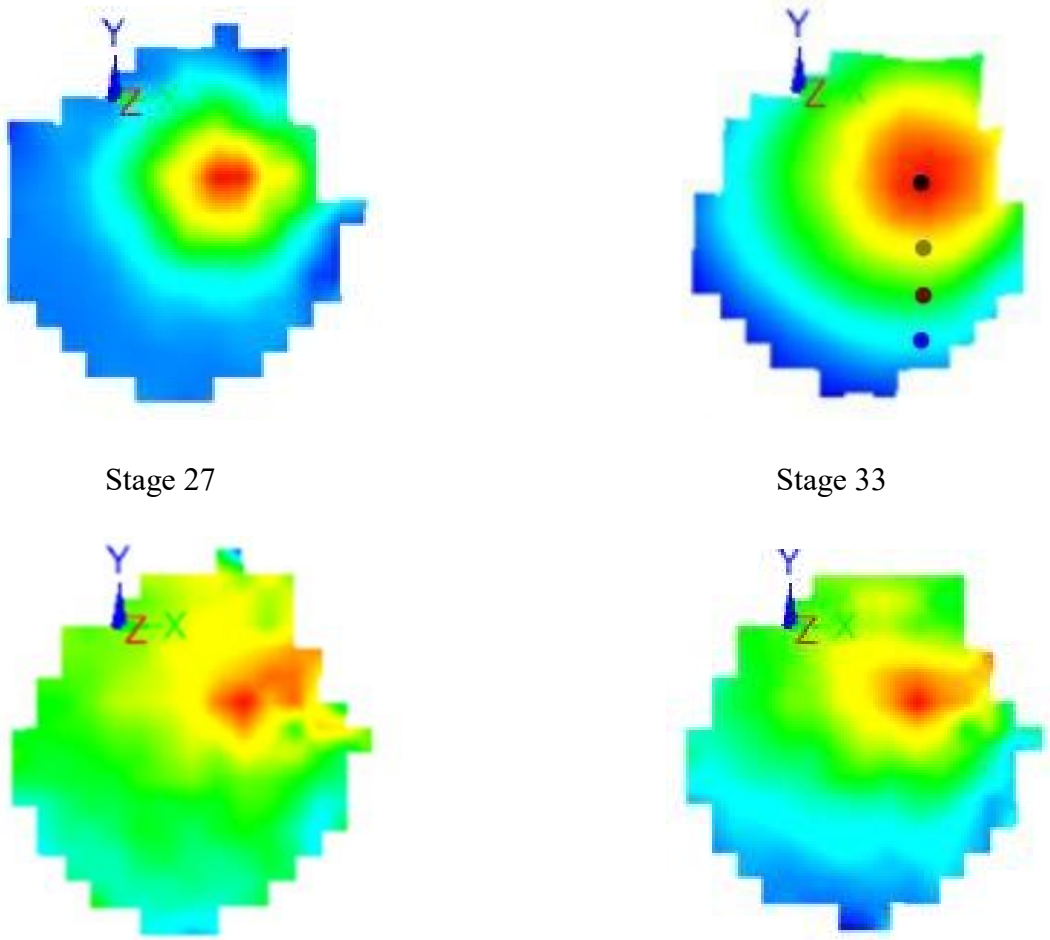

Figure 63. 3D deformation stages of Twintex® based 4.5 mm thick composite impacted at a velocity 75.42 m/s with the spherical head projectile.

Figure 64 shows the low magnification optical images of Twintex® based 4.5 mm thick specimen with the spherical head projectile at a velocity of 87.45 m/s. From the figure, it is noticed that on the point of contact of the projectile, minute splits, as well as signs of minute matrix cracks are evident. On the opposite side, there are no signs of failure.

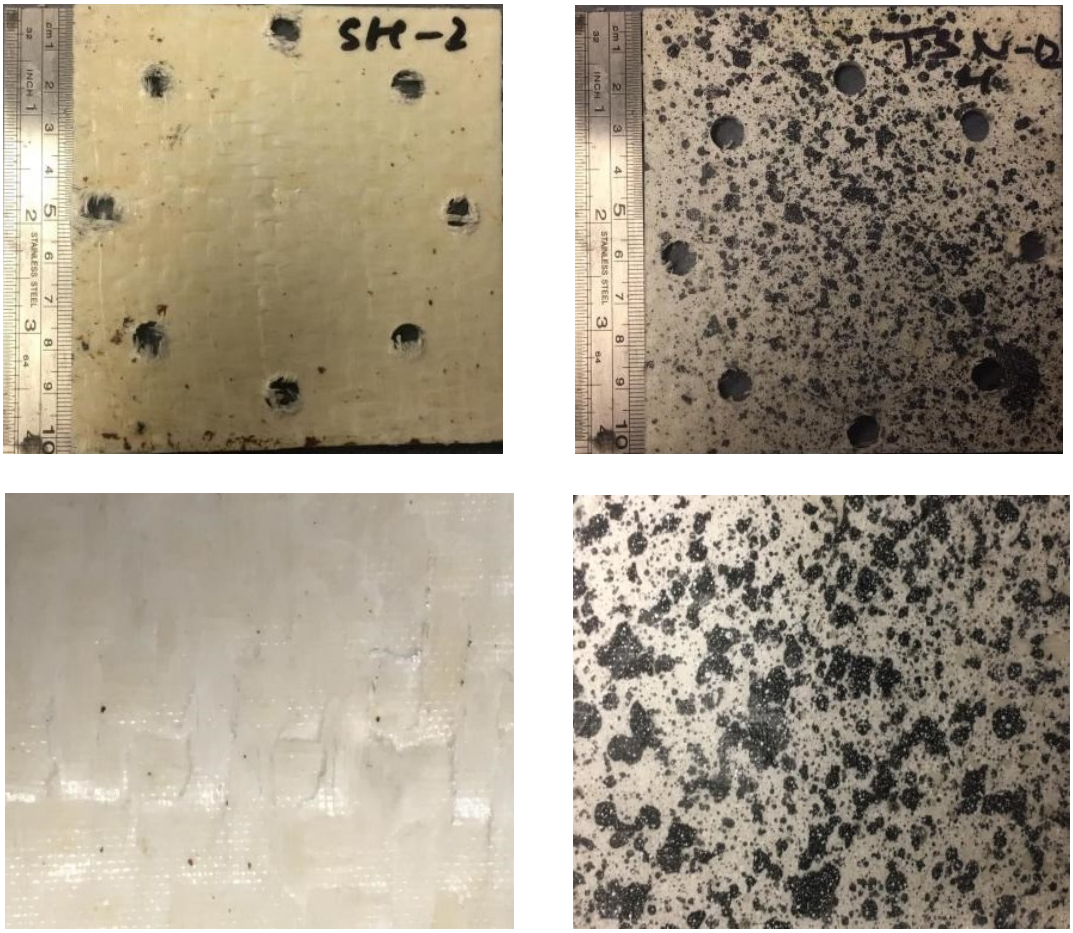

Figure 64. Twintex® based 4.5 mm composite impacted at a velocity of 87.45 m/s with the spherical head projectile.

The maximum transient out-of-plane displacement with stage time for the specimen presented in Figure 65. Here, the maximum out-of-plane displacement reached a value of 12.46 mm. Figure 65 also highlights some impact waves. Here, it was noticed that the number of impact waves are less compared to the same composite when impacted at a velocity of 75.42 m/s.

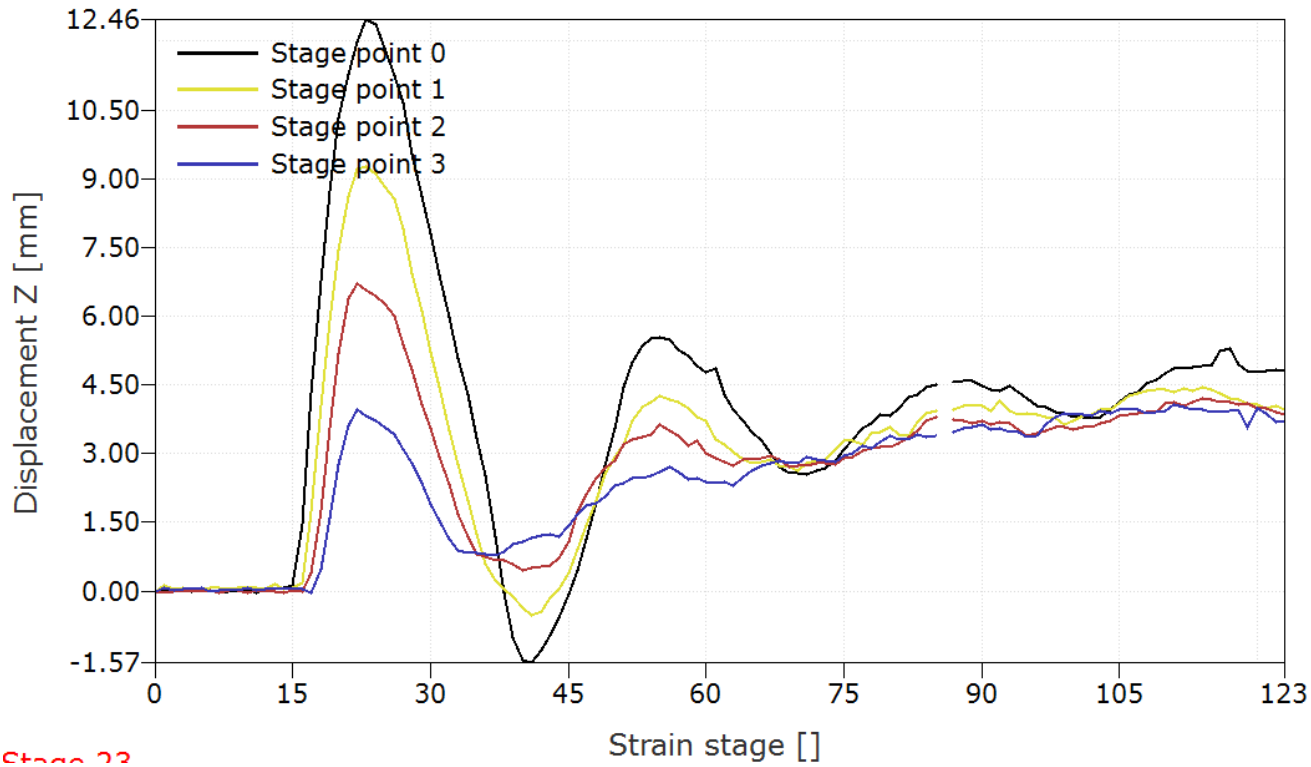

Figure 65. Displacement vs Stage graph of Twintex® based 4.5 mm thick composite impacted at velocity 87.45 m/s with the spherical head projectile.

Figure 66 shows a number of deformation stages representing the impact event on the Twintex® based 4.5 mm thick composite tested at a velocity of 87.45 m/s with the spherical head projectile. Here, it is evident how the out-of-plane deformation increased until a value of 12.46 mm was reached. Following this, the displacement decreased as shown in stage 40. The final displacement was close to 5.00 mm at the point of impact.

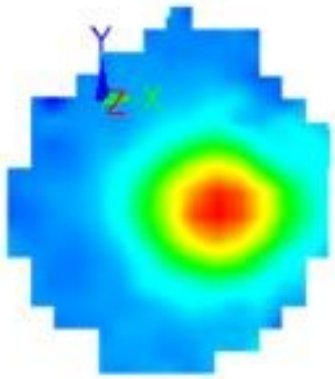

Stage 16

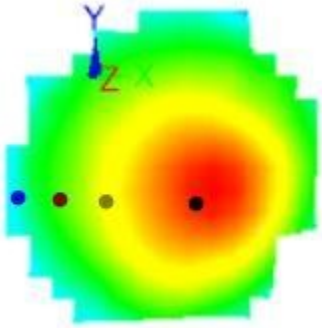

Stage 23

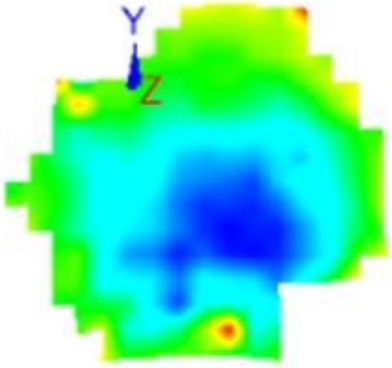

Stage 40

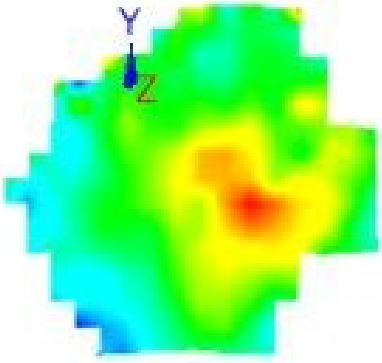

Stage 118

Figure 66. 3D deformation stages of Twintex® based 4.5 mm thick composite impacted at velocity 87.45 m/s with the spherical head projectile.

Figure 67 shows the impact behavior Twintex® based 4.5 mm thick specimen with the spherical head projectile at a velocity of 98.88 m/s. From the figure, it is noticed that there are minute fiber ruptures on the area of impact and on the opposite side, there are no signs of failure.

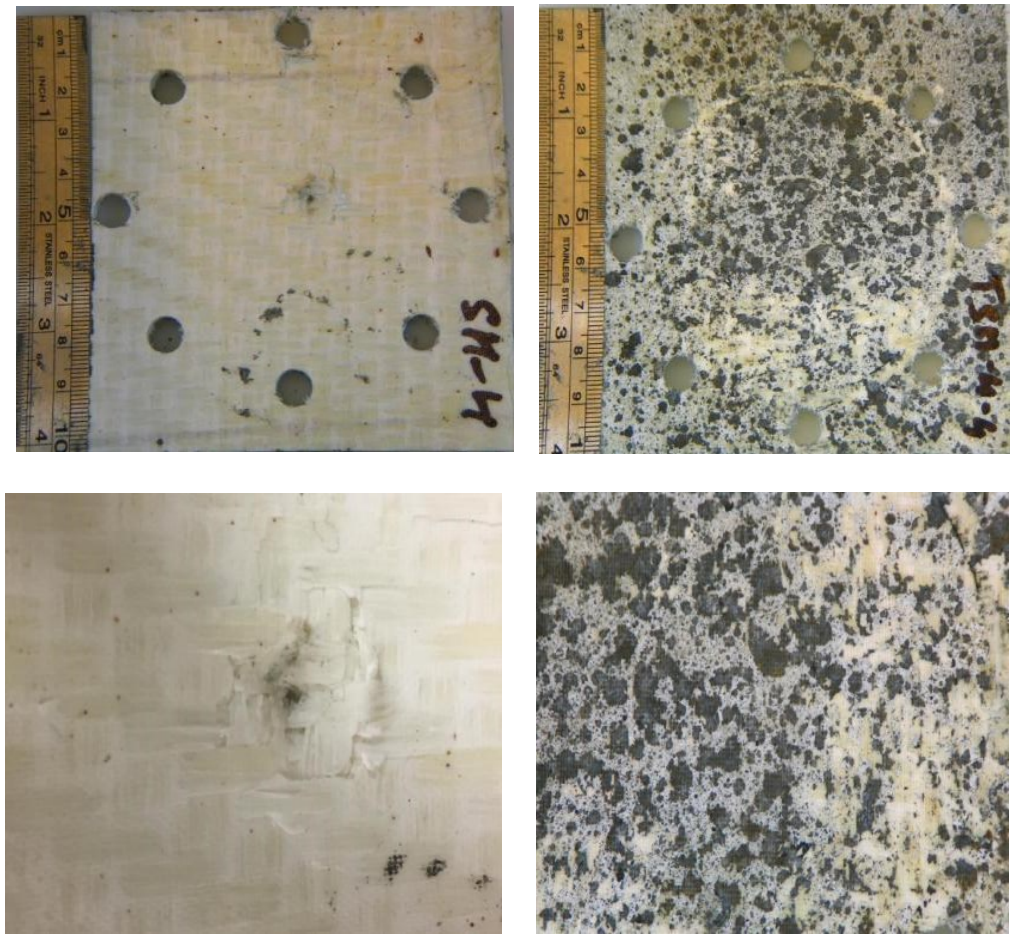

Figure 67. Twintex® based 4.5 mm composite impacted at a velocity of 98.88 m/s with the spherical head projectile.

The maximum transient out-of-plane displacement with stage time for the specimen is presented in Figure 68. Here, the maximum out-of-plane displacement reached a value of 13.80 mm. Figure 68 also highlights a number of impact waves.

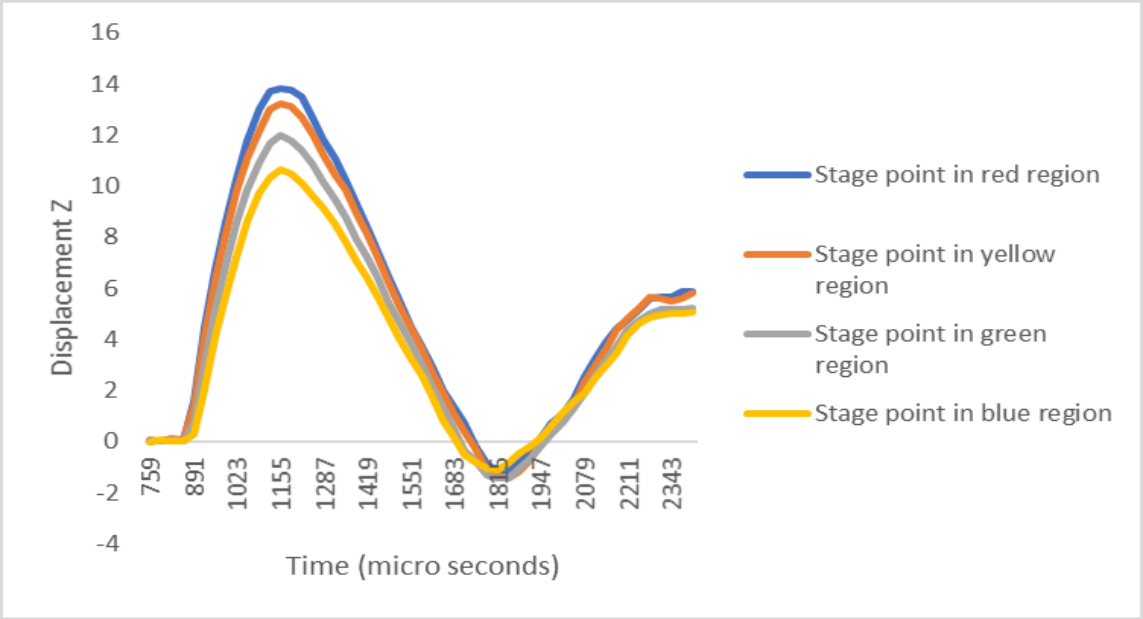

Figure 69. Displacement vs Stage graph of Twintex® based 4.5 mm thick composite impacted at velocity 98.88 m/s with the spherical head projectile.

Figure 69 shows a number of deformation stages representing the impact event on the Twintex® based 4.5 mm thick composite tested at a velocity of 98.88 m/s with the spherical head projectile. Here, it is evident how the out-of-plane deformation increased until a value of 13.80 mm was reached. Following this, the displacement decreased as shown in stage 55. The final displacement was observed to be close to 6.00 mm at the point of impact.

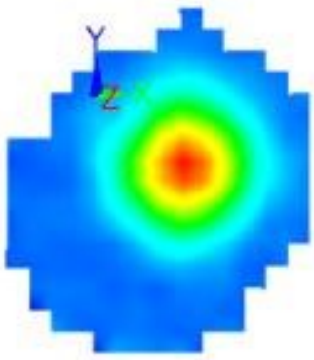

Stage 28

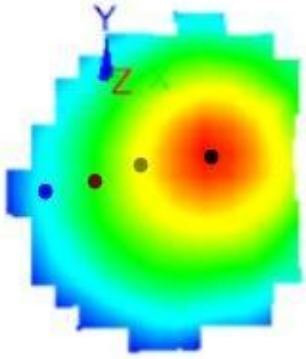

Stage 35

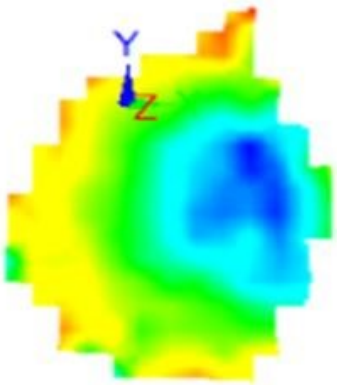

Stage 55

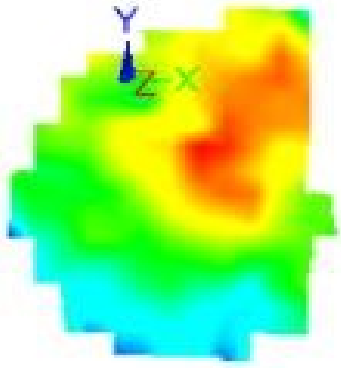

Stage 121

Figure 69. 3D deformation stages of Twintex® based 4.5 mm thick composite impacted at a velocity 98.88 m/s with the spherical head projectile.

Figure 70 shows the low magnification optical images of Twintex® based 4.5 mm thick specimen with the spherical head projectile at a velocity of 107.8 m/s. At this velocity, the specimen attained its ballistic limit. On the area of impact, minute ruptures and matrix cracking are evident along with fiber ruptures at the point of impact. On the speckle pattern side, at the point of impact fiber ruptures with petaling is observed along with minute fragmentation. Matrix cracks are also evident in a few areas on speckle pattern side. Figure 70 includes a optical micrograph of the section of the impacted specimen.

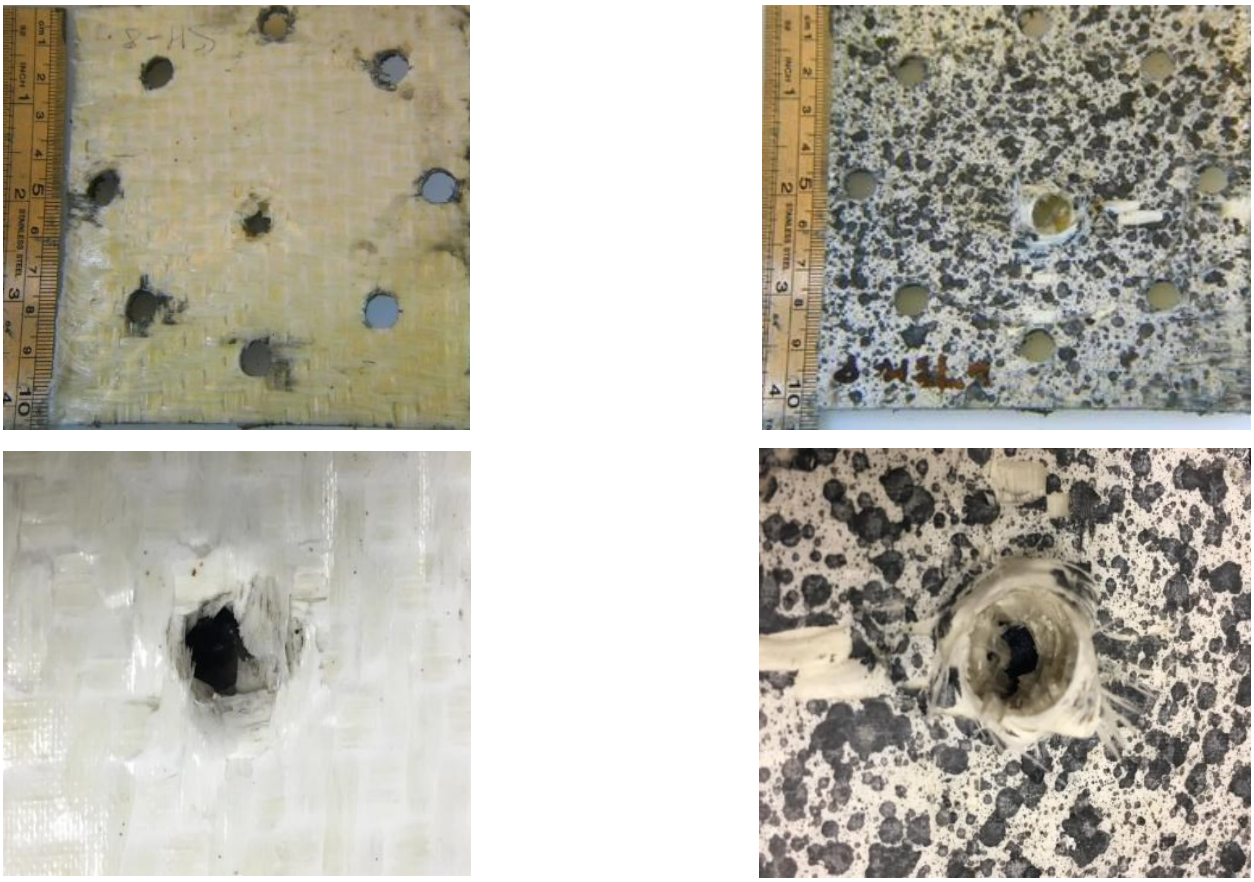

(a)

(b)

Figure 70. (a) Twintex based 4.5 mm composite impacted at a velocity of 107.8 m/s with the spherical head projectile (b) Section of impacted composite.

4.2.4 Impact behavior of Shield Strand S® / Epoxy 4.5 mm thick composites with the Spherical head projectile

Figure 71 shows the low magnification optical images of Shield Strand S® / Epoxy based 4.5 mm thick specimen impacted with the spherical head projectile at a velocity of 79.35 m/s. At this velocity, it was noticed that at the point of contact of the projectile plus (+) shaped delamination occurred with minute matrix cracks on the region of impact. On the speckle pattern side, there are no signs of damage. Plus shaped delamination indicates that the primary yarns absorbed the impact energy of the projectile.

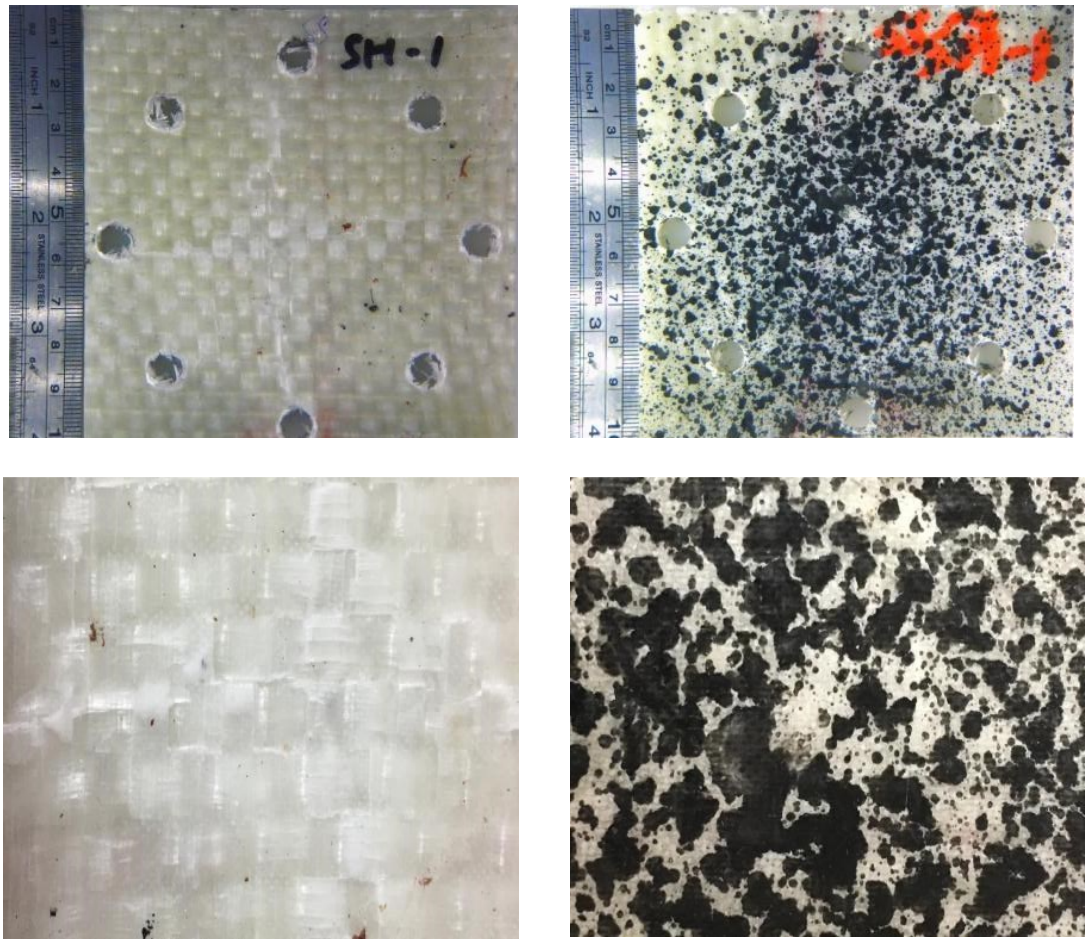

Figure 71. Shield Strand S® / Epoxy based 4.5 mm composite impacted at a velocity of 79.35 m/s with the spherical head projectile.

The maximum transient out-of-plane displacement with stage time for the specimen is presented in Figure 72. Here, the maximum out-of-plane displacement reached a value of 7.74 mm. A couple of impact waves are highlighted. It is interesting to notice that compared with the point of impact, the region near the point of impact took more damage.

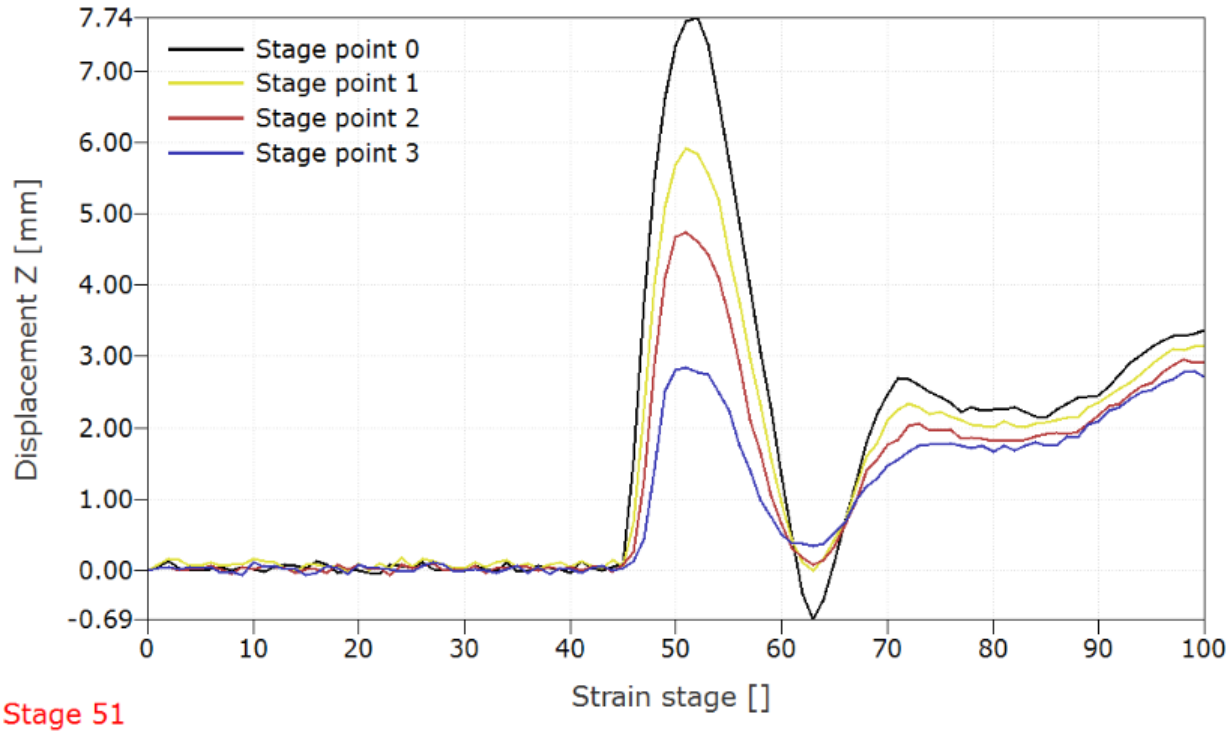

Figure 72. Displacement vs Stage graph of Shield Strand S® /Epoxy based 4.5 mm thick composite impacted at velocity 79.35 m/s with the spherical head projectile.

Figure 73 shows many deformation stages representing the impact event on the Shield Strand S® / Epoxy based 4.5 mm thick composite tested at a velocity of 79.35 m/s with the spherical head projectile. Here, it is evident how the out-of-plane deformation increased until a value of 7.74 mm was reached. Following this, the displacement decreased as shown in stage 63. The final displacement was observed to be close to 3.5 mm at the point of impact.

Stage 46 Stage 51

Stage 63 Stage 100

Figure 73. 3D deformation stages of Shield Strand S® / Epoxy based 4.5 mm thick composite impacted at velocity 79.35 m/s with the spherical head projectile.

Figure 74 shows the low magnification optical images of Shield Strand S ®/ Epoxy based 4.5 mm thick specimen with the spherical head projectile at a velocity of 91.58 m/s. At this velocity, similar to the previous thermoset based 4.5 mm thick specimen impacted with the spherical head projectile, plus shaped delamination is noticed near the point of contact of the projectile. Here, the plus-shaped delamination is more than the previous specimen. On the opposite side, there were no signs of failure.

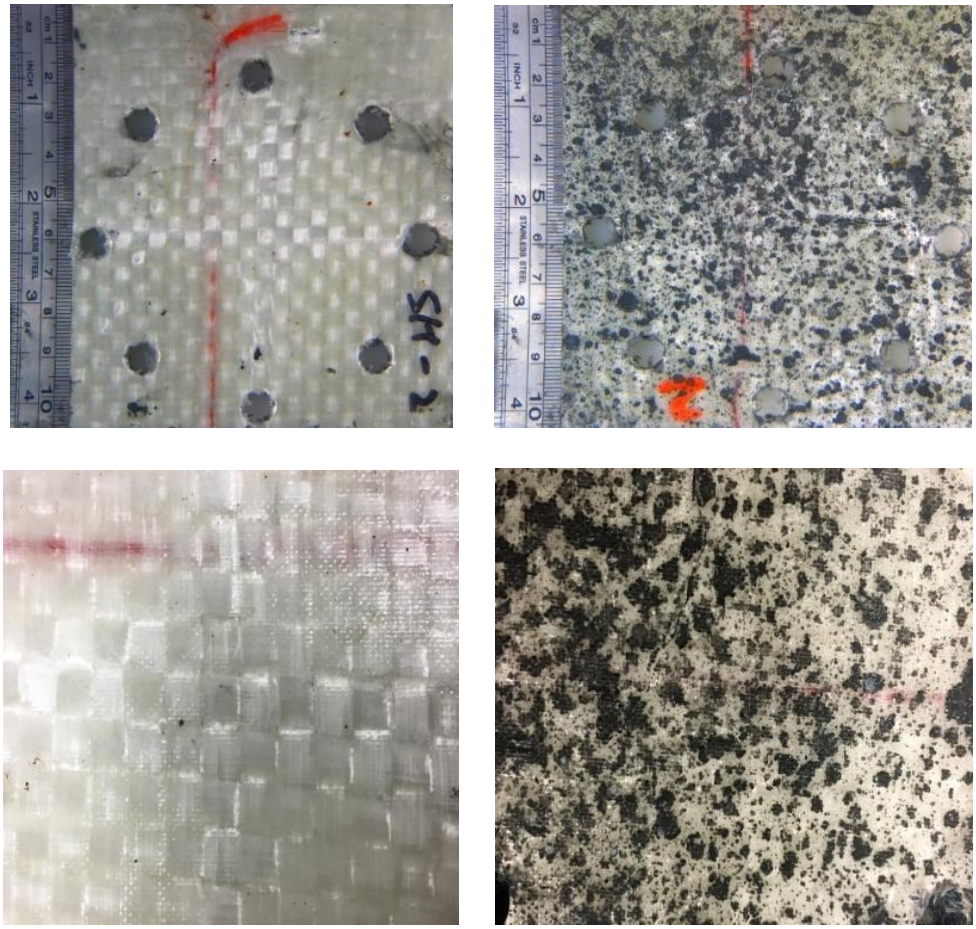

Figure 74. Shield Strand S® / Epoxy based 4.5 mm composite impacted at a velocity of 91.58 m/s with the spherical head projectile.

The maximum transient out-of-plane displacement with stage time for this specimen is presented in Figure 75. Here, the maximum out-of-plane displacement reached a value of 8.8 mm. A couple of impact waves are evident in the Displacement Z vs stage graph.

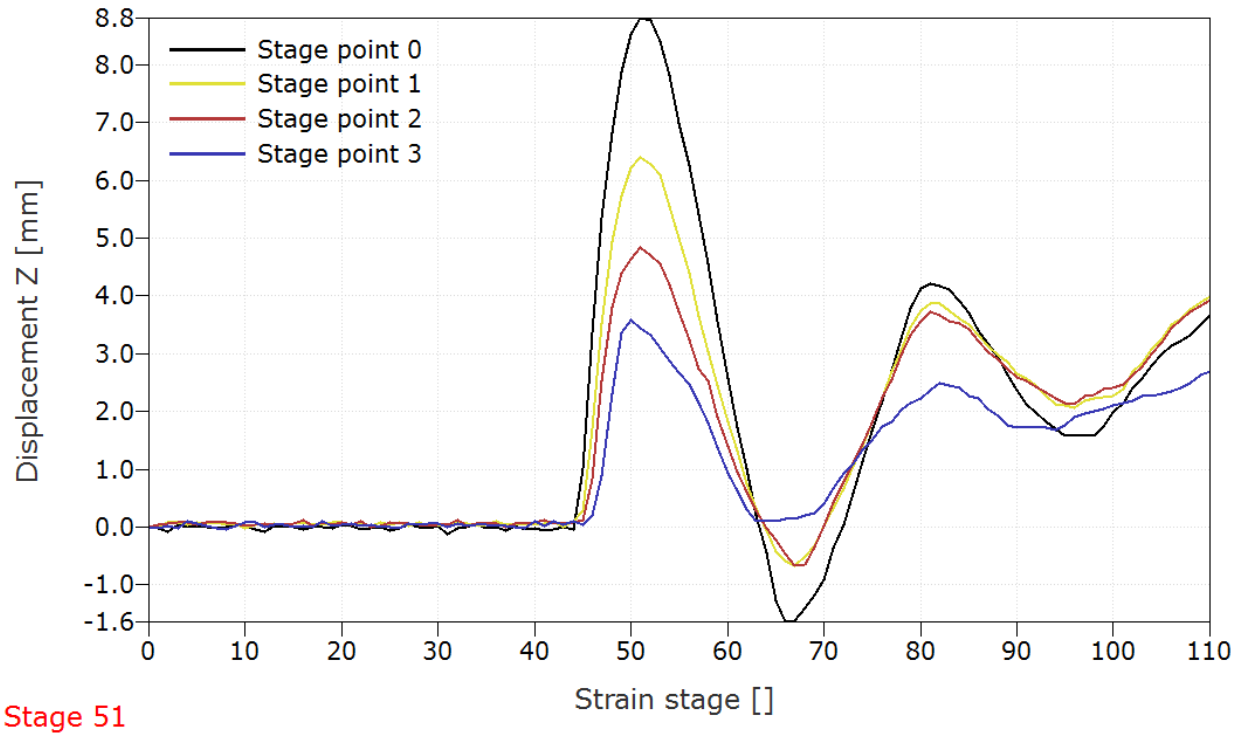

Figure 75. Displacement vs Stage graph of Shield Strand S® / Epoxy based 4.5 mm thick composite impacted at velocity 91.58 m/s with the spherical head projectile.

Figure 76 shows many deformation stages representing the impact event on the Shield Strand S® / Epoxy based 4.5 mm thick composite tested at a velocity of 91.58 m/s with the spherical head projectile. Here, it is evident how the out-of-plane deformation increased until a value of 8.87 mm was reached. Following this, the displacement decreased as shown in stage 68. The final displacement was observed to be close to 4 mm at the point of impact.

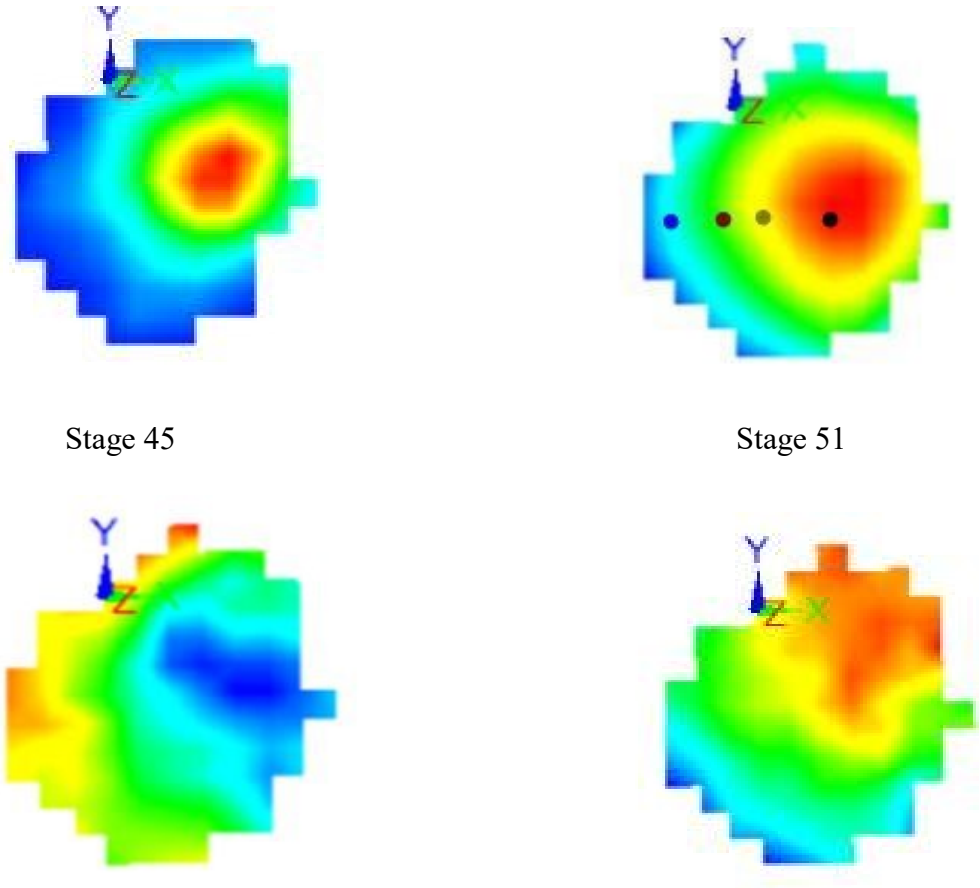

Figure 76. 3D deformation stages of Shield Strand S® / Epoxy based 4.5 mm thick composite impacted at velocity 91.58 m/s with spherical head projectile.

Figure 77 shows the low magnification optical images of Shield Strand S® / Epoxy based 4.5 mm thick specimen with the spherical head projectile at a velocity of 103.7 m/s. From the figure, plus shaped delamination is evident in the region of impact along with signs of matrix cracking. On the opposite side, signs of failure are not visible.

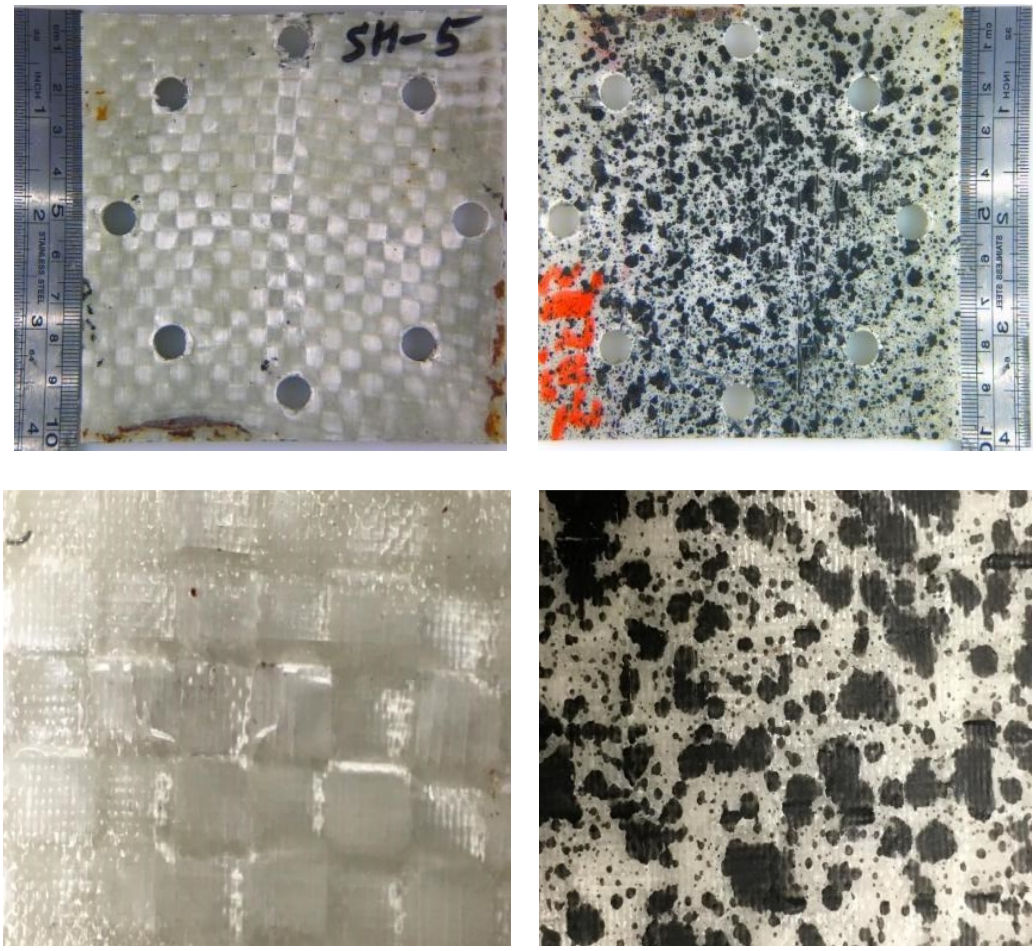

Figure 77. Shield Strand S®/ Epoxy 4.5 mm composite tested at a velocity of 103.7 m/s with the spherical head projectile.

The maximum transient out-of-plane displacement with stage time for this specimen is presented in Figure 78. Here, the maximum out-of-plane displacement reached a value of 10.72 mm. Multiple impact waves are highlighted in Dispalcement vs Stage graph. Here, it is interesting to observe that the number of impact waves increased with increase in the projectile velocity whereas, for the Twintex based 4.5 mm thick specimens impacted with the spherical head projectile, the phenomenon was opposite.

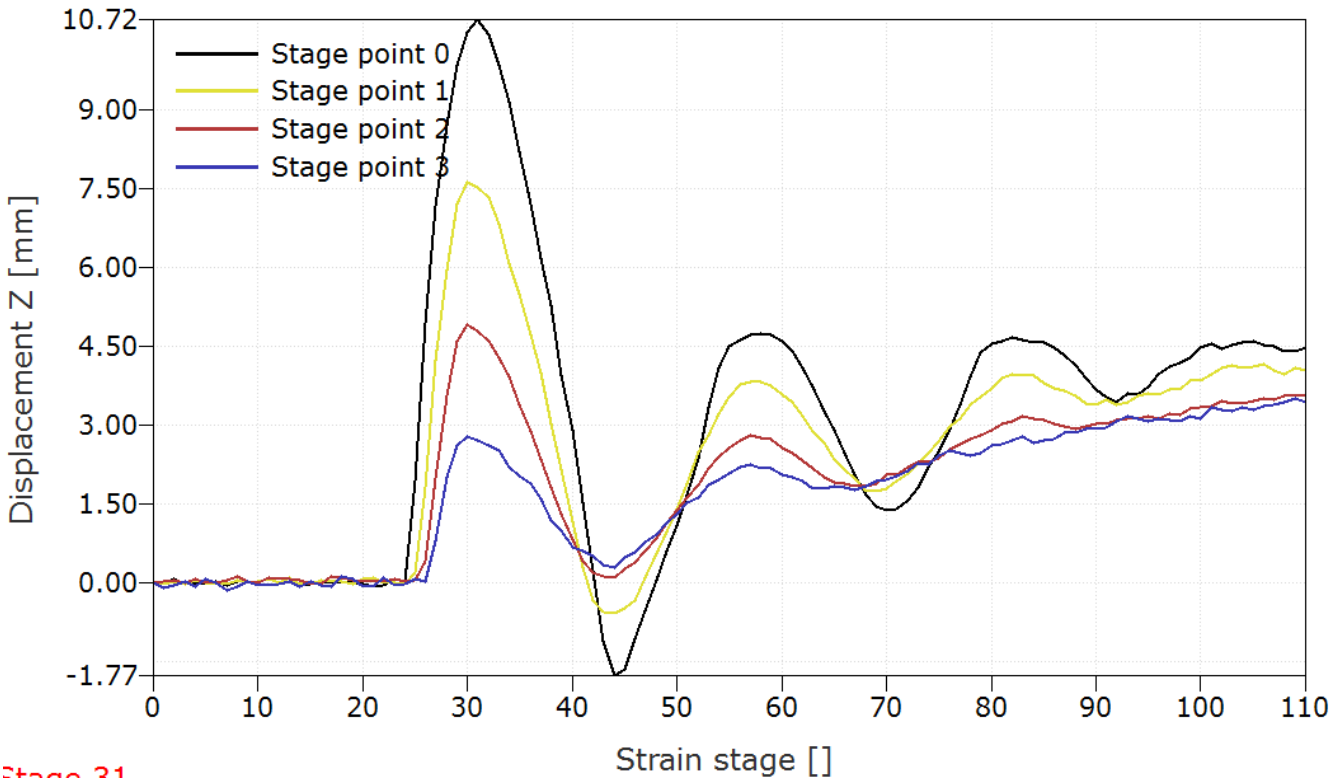

Figure 78. Displacement vs Stage graph of Shield Strand S® / Epoxy based 4.5 mm thick composite impacted at a velocity 103.7 m/s with the spherical head projectile.

Figure 79 shows some deformation stages representing the impact event on the Shield Strand S® / Epoxy based 4.5 mm thick composite tested at a velocity of 103.7 m/s with the spherical head projectile. Here, it is evident how the out-of-plane deformation increased until a value of 10.72 mm was reached. Following this, the displacement decreased as shown in stage 45. The final displacement was observed to be close to 4.5 mm at the point of impact.

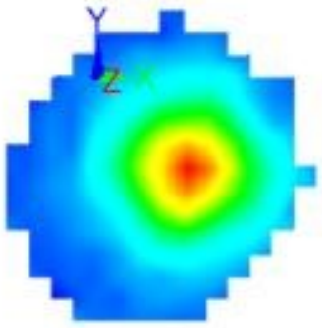

Stage 25

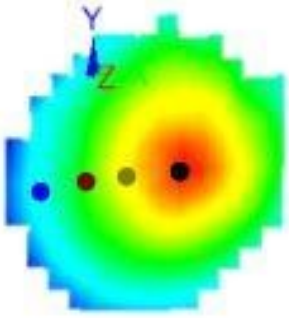

Stage 31

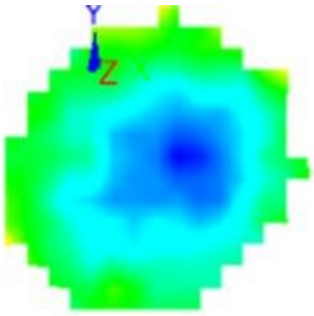

Stage 45

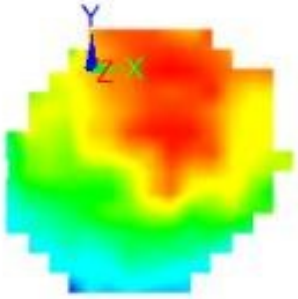

Stage 110

Figure 79. 3D deformation stages of Shield Strand S® / Epoxy based 4.5 mm thick composite impacted at a velocity 103.7 m/s with the spherical head projectile.

Figure 80 shows the low magnification optical images of Shield Strand S® / Epoxy based 4.5 mm thick specimen impacted with the spherical head projectile at a velocity of 116.3 m/s. From the figure, on the point of impact fiber ruptures are noticed along with heavy delamination and multiple matrix cracks in the region of impact. On the opposite side, no signs of damage are noticed.

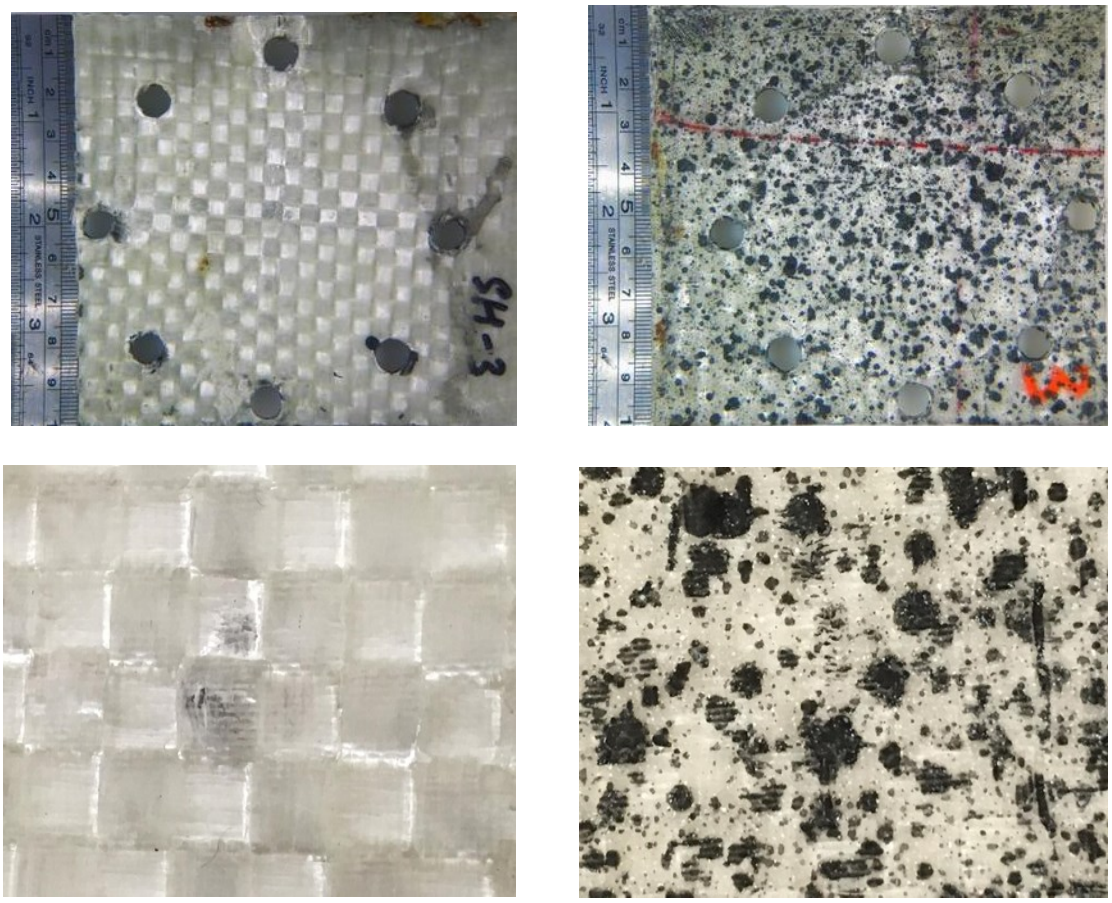

Figure 80. Shield Strand S® / Epoxy based 4.5 mm composite impacted at a velocity of 116.3 m/s with the spherical head projectile.

The maximum transient out-of-plane displacement with stage time for this specimen is presented in Figure 81. Here, the maximum out-of-plane displacement reached a value of 11.88 mm. An impact wave is evident in Figure 81.

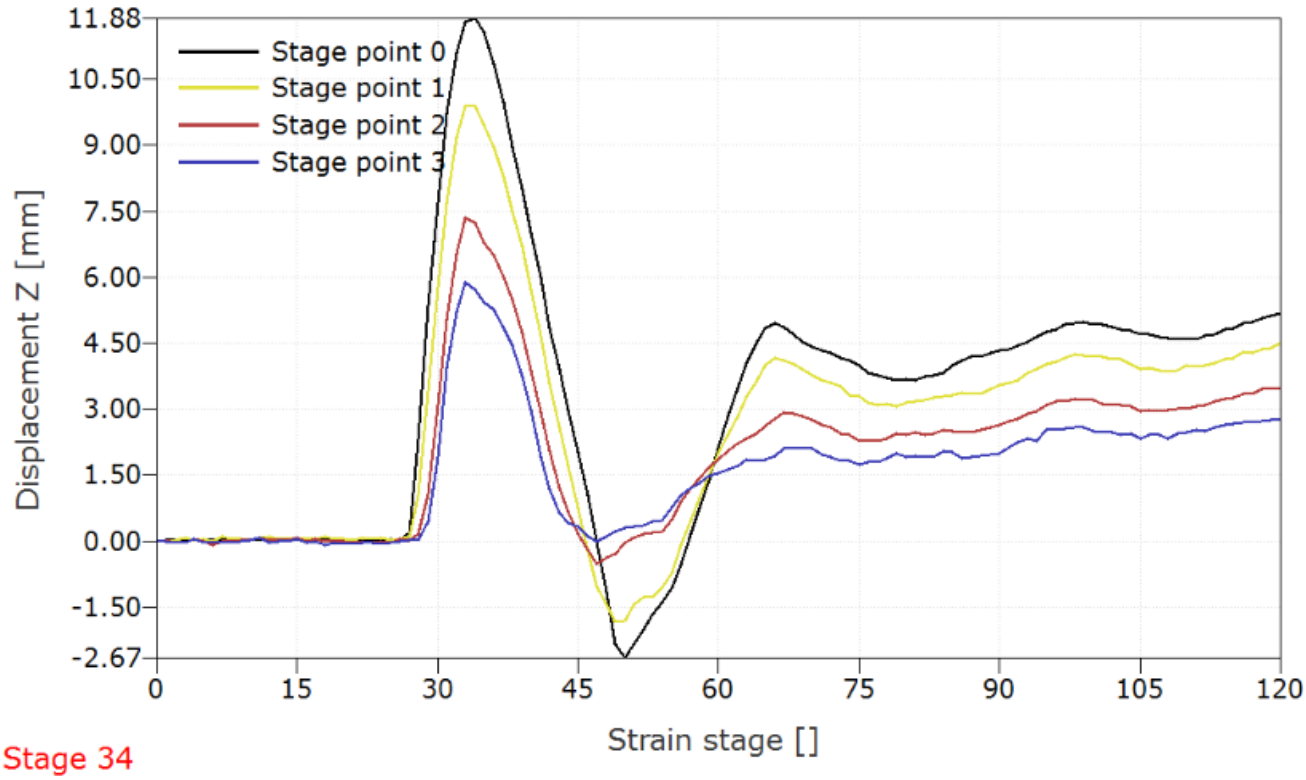

Figure 81. Displacement vs Stage graph of Shield Strand S® / Epoxy based 4.5 mm thick composite impacted at a velocity 116.3 m/s with the spherical head projectile.

Figure 82 shows a number of deformation stages representing the impact event on the Shield Strand S® / Epxoy based 4.5 mm thick composite tested at a velocity of 116.3 m/s with the spherical head projectile. Here, it is evident how the out-of-plane deformation increased until a value of 11.8 mm was reached. Following this, the displacement decreased as shown in stage 49. The final displacement was observed to be close to 5.5 mm at the point of impact.

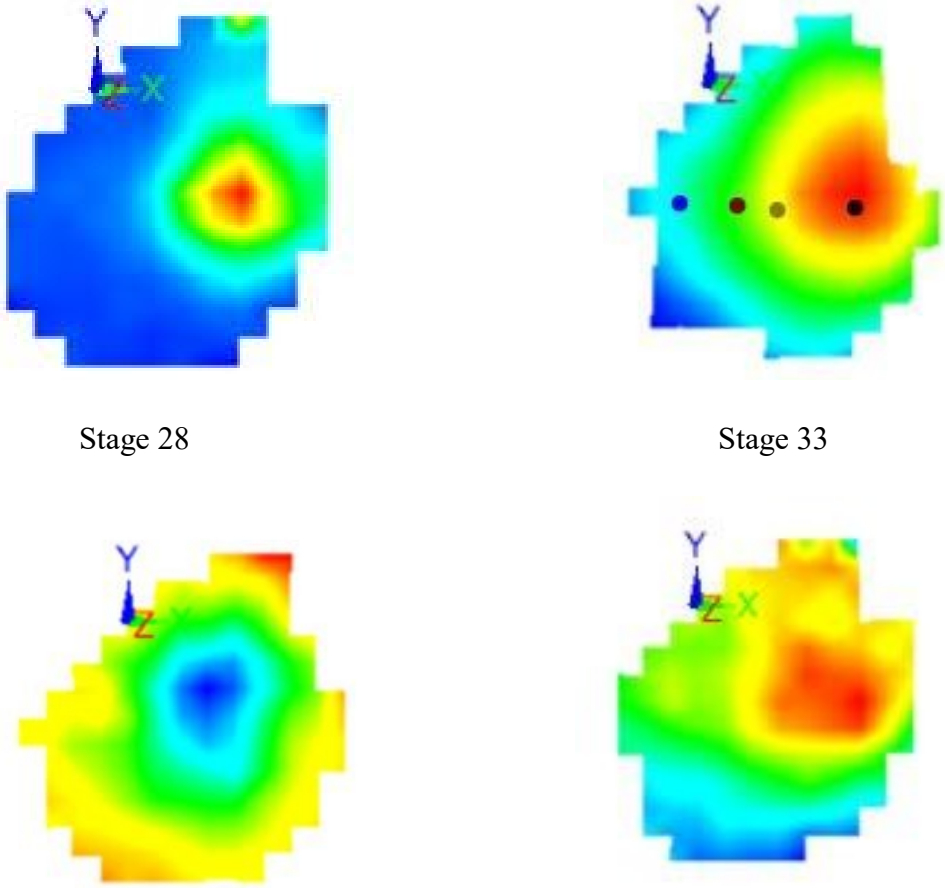

Figure 82. 3D deformation stages of Shield Strand S® / Epoxy based 4.5 mm thick composite impacted at a velocity 116.3 m/s with the spherical head projectile.

Figure 83 shows the low magnification optical images of Shield Strand S® / Epoxy based 4.5 mm thick specimen impacted with the spherical head projectile at a velocity of 126.7 m/s. From the figure, delamination is evident in the region of impact along with matrix cracks and fiber ruptures which are visible in Figure 83. On the opposite side, delamination is noticed.

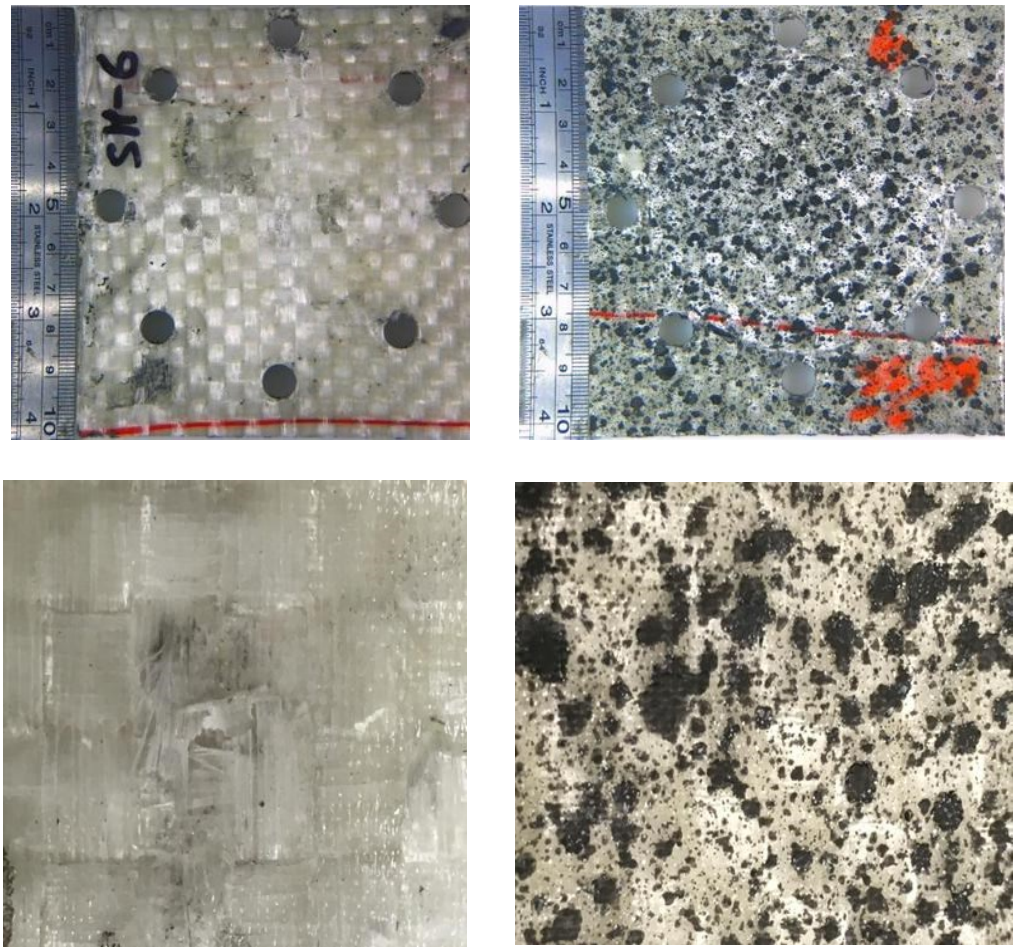

Figure 83. Shield Strand S® / Epoxy based 4.5 mm composite impacted at a velocity of 126.7 m/s with the spherical head projectile.

The maximum transient out-of-plane displacement with stage time for this specimen is presented in Figure 84. It is evident that the maximum out-of-plane displacement reached a value of 13.99 mm. An impact wave is visible in Figure 84.

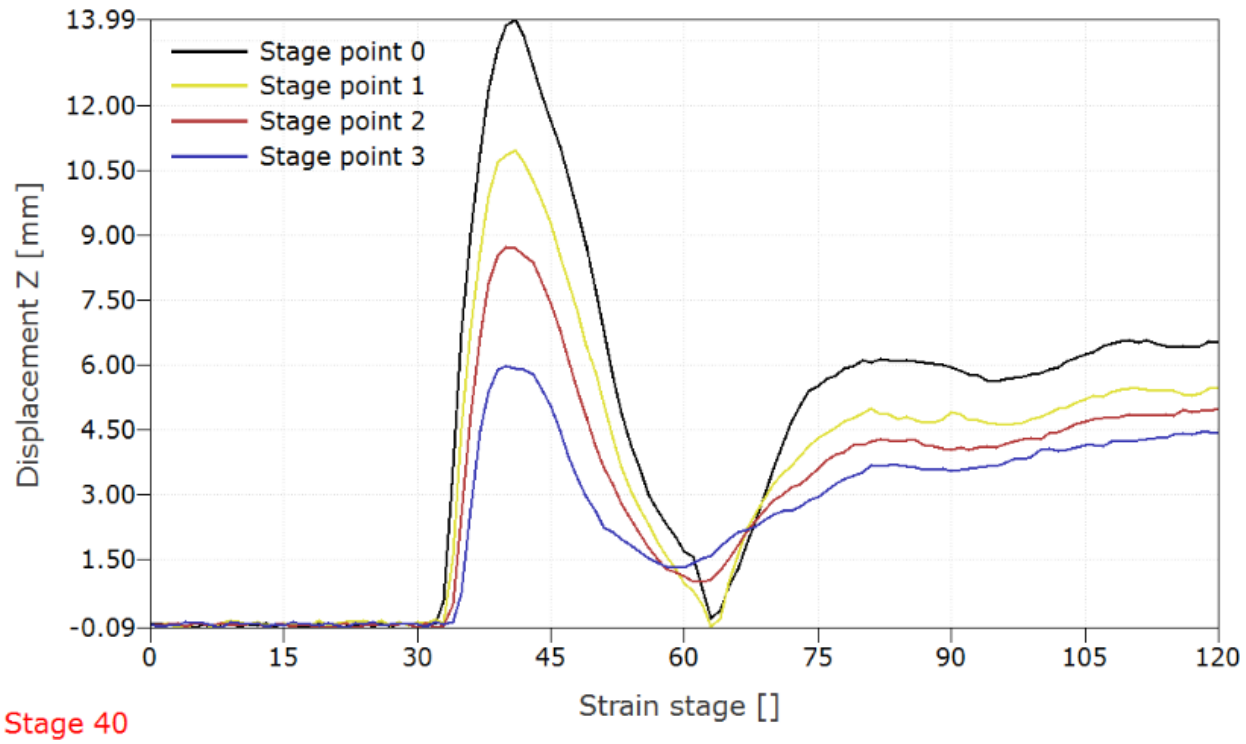

Figure 84. Displacement vs Stage graph of Shield Strand S® / Epoxy based 4.5 mm thick composite impacted at avelocity 126.7 m/s with the spherical head projectile.

Figure 85 shows a number of deformation stages representing the impact event on the Shield Strand S® / Epoxy based 4.5 mm thick composite tested at a velocity of 126.7 m/s with the spherical head projectile. From figure 79, it is evident how the out-of-plane deformation increased until a value of 13.99 mm was reached. Following this, the displacement decreased as shown in stage 62. The final displacement was observed to be close to 6.5 mm at the point of impact.

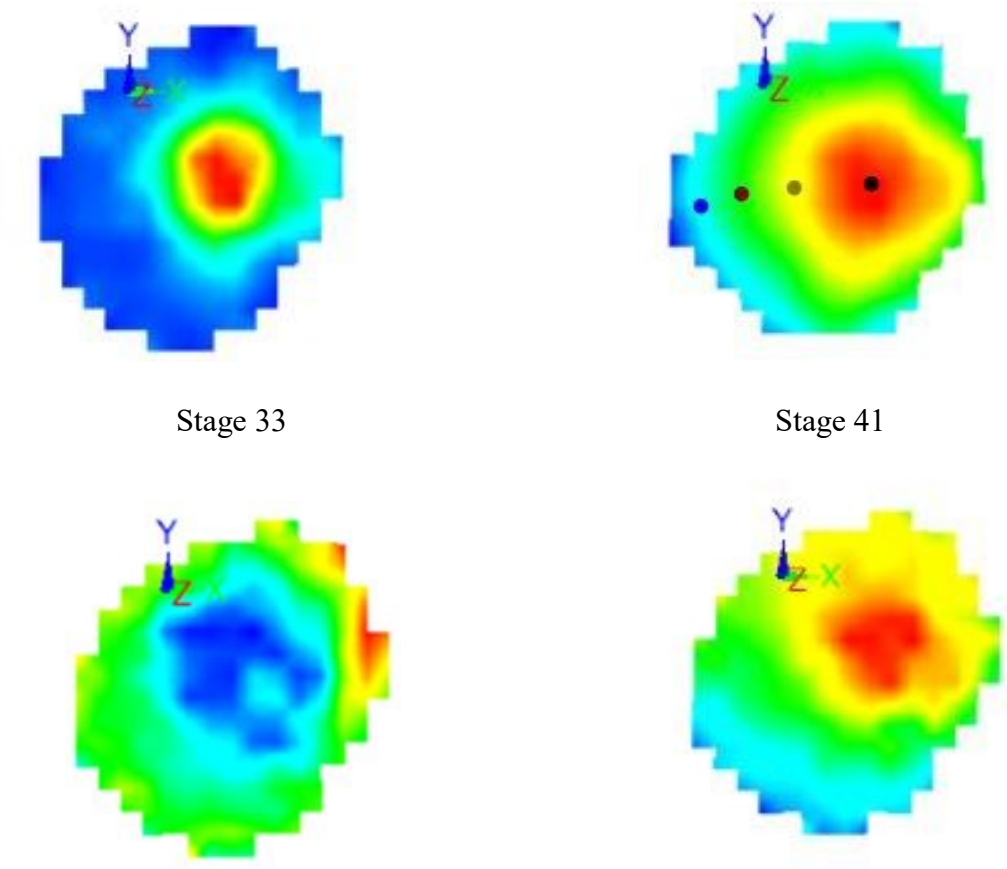

Figure 85. 3D deformation stages of Shield Strand S® / Epoxy based 4.5 mm thick composite impacted at a velocity 126.7 m/s with the spherical head projectile.

Figure 86 shows the low magnification optical images of Shield Strand S® / Epoxy based 4.5 mm thick specimen with the spherical head projectile at a velocity of 144.8 m/s. From the figure, heavy fiber ruptures at point of impact are evident along with delamination and matrix cracking on the region of impact. On the opposite side, delamination is noticed.

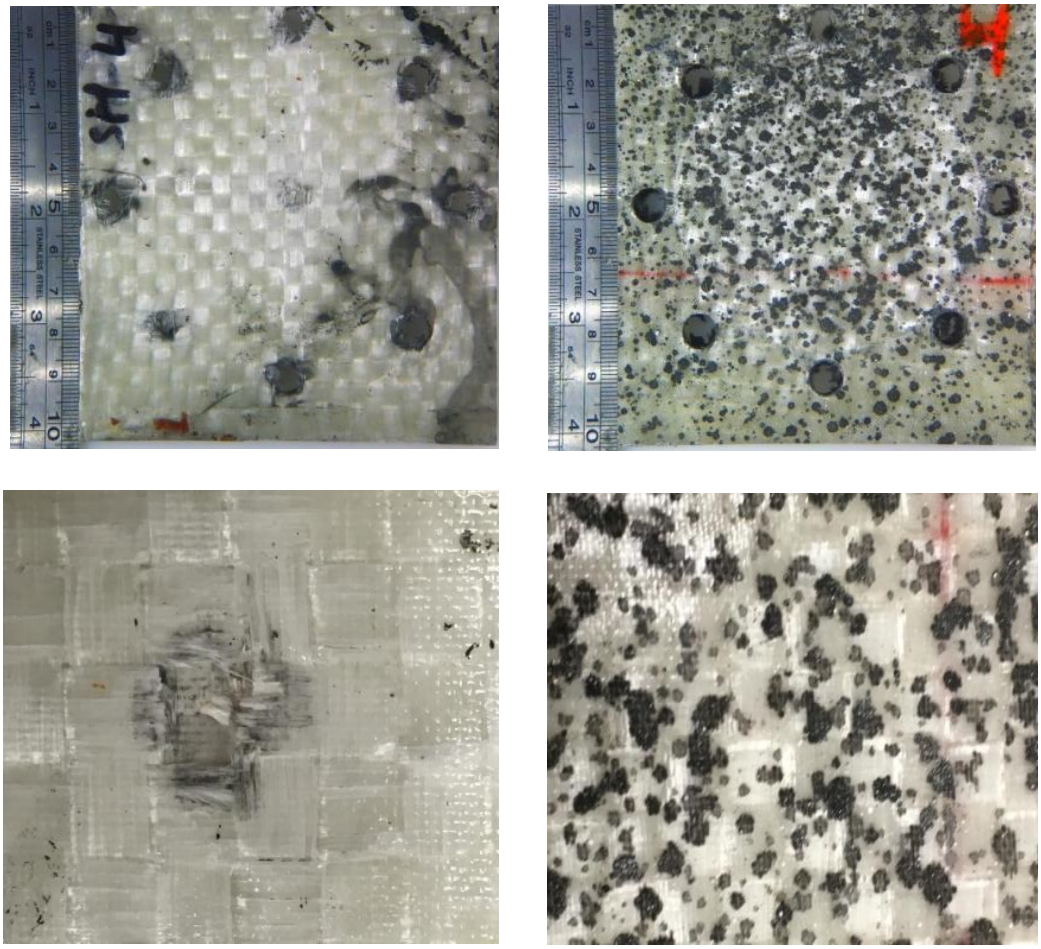

Figure 86. Shield Strand S® / Epoxy based 4.5 mm composite impacted at a velocity of 144.8 m/s with the spherical head projectile.

The maximum transient out-of-plane displacement with stage time for this specimen is presented in Figure 87. It is evident that the maximum out-of-plane displacement reached a value of 14.8 mm. Similar to the previous two thermoset based 4.5 mm thick specimens which are impacted at 116.3 m/s and 126.7 m/s with the spherical head projectile, this specimen also demonstrated a an impact wave as shown in Figure 87.

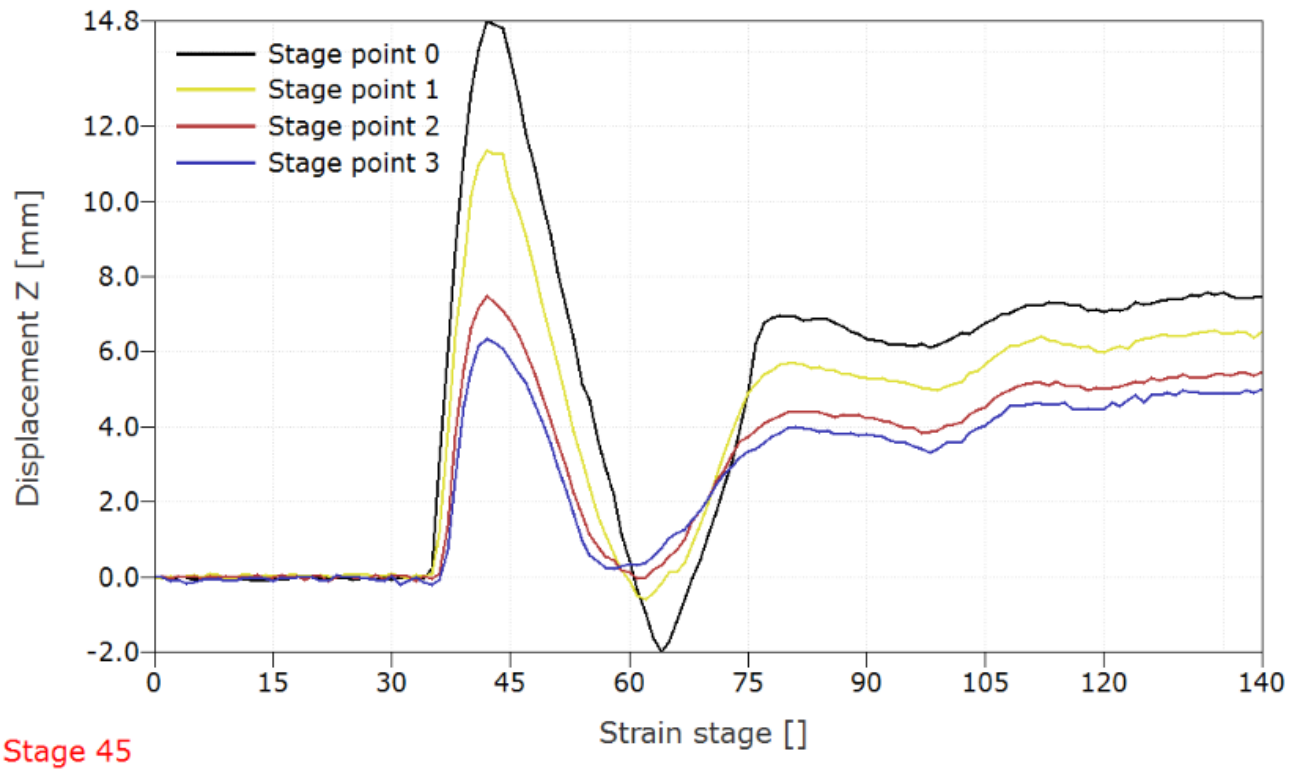

Figure 87. Displacement vs Stage graph of Shield Strand S® / Epoxy based 4.5 mm thick composite impacted at velocity 144.8 m/s with the spherical head projectile.

Figure 88 shows a number of deformation stages representing the impact event on the Shield Strand S® / Epxoy based 4.5 mm thick composite tested at a velocity of 144.8 m/s with the spherical head projectile. From Figure 88, it is evident how the out-of-plane deformation increased until a value of 14.88 mm was reached. Following this, the displacement decreased as shown in stage 64. From Figure 82, final displacement was observed to be close to 8.00 mm at the point of impact.

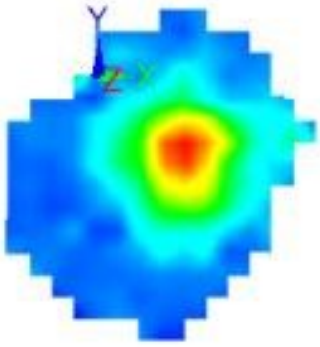

Stage 36

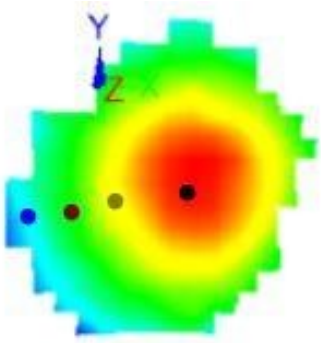

Stage 42

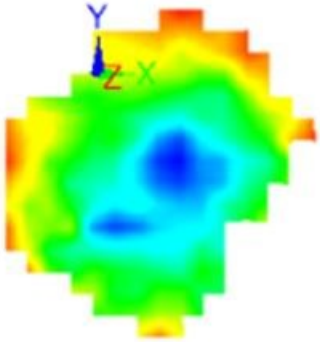

Stage 64

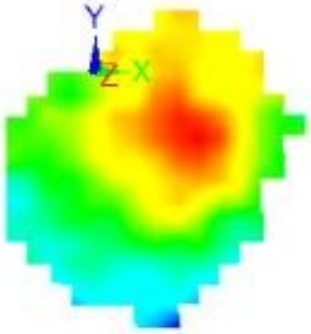

Stage 140

Figure 88. 3D deformation stages of Shield Strand S® / Epoxy based 4.5 mm thick composite impacted at a velocity 144.8 m/s with the spherical head projectile.

Figure 89 shows the low magnification optical images of Shield Strand S® / Epoxy based 4.5 mm thick specimen impacted with the spherical head projectile at a velocity of 156.1 m/s. From the figure, heavy fiber ruptures at the point of impact are evident along with delamination and matrix cracking on the region of impact. On the opposite side, at the point of impact fiber ruptures, matrix cracks, petaling, as well as fragmentation are noticed.

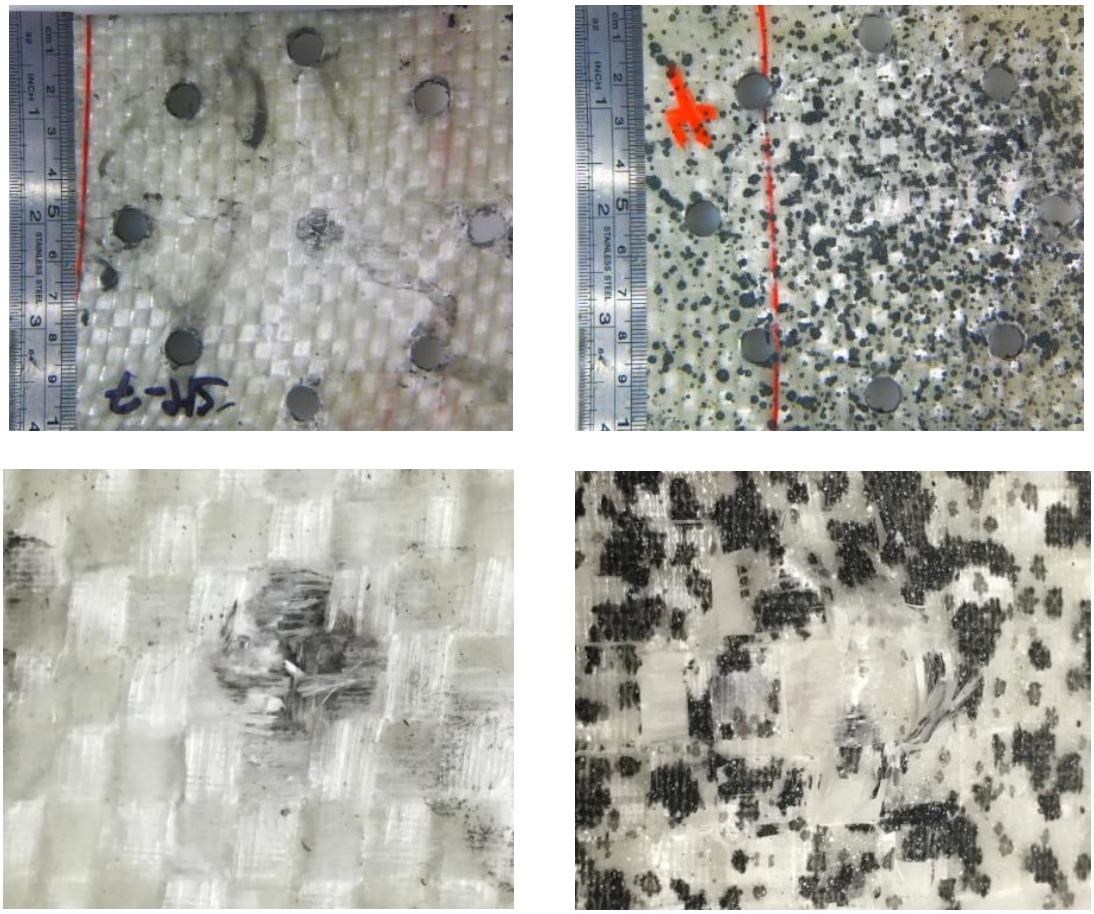

Figure 89. Shield Strand S® / Epoxy based 4.5 mm composite impacted at a velocity of 156.1 m/s with the spherical head projectile.

The maximum transient out-of-plane displacement with stage time for the specimen is presented in Figure 90. It is evident that the maximum out-of-plane displacement reached a value of 15.63 mm. Due to the partial perforation of the projectile through the specimen, no impact waves are evident in Figure 90.

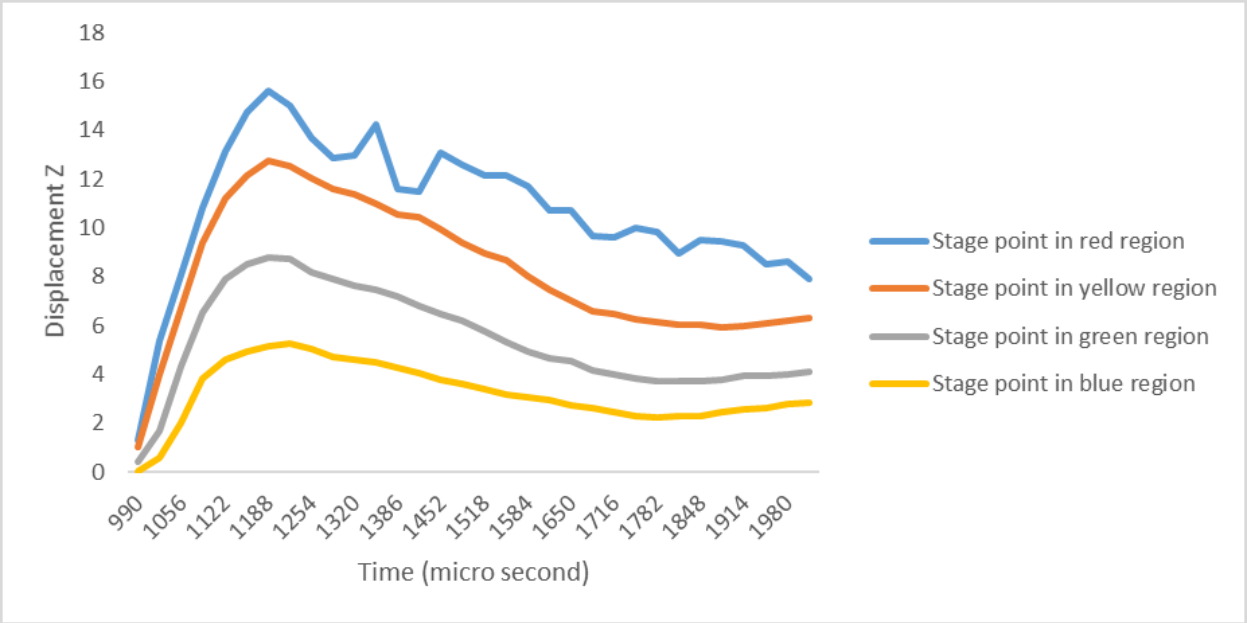

Figure 90. Displacement vs Stage graph of Shield Strand S® / Epoxy based 4.5 mm thick composite impacted at a velocity 156.1 m/s with the spherical head projectile.

Even though there are damages on the opposite side, fortunately, deformation stages are obtained. Figure 91 shows a number of deformation stages representing the impact event on the Shield Strand S® / Epxoy based 4.5 mm thick composite tested at a velocity of 156.1 m/s with the spherical head projectile. From Figure 85, it is evident how the out-of-plane deformation increased until a value of 15.63 mm was reached. Following this, the displacement decreased as shown in stage 55. Due to the serrations in the curve, the final displacement value could not be estimated.

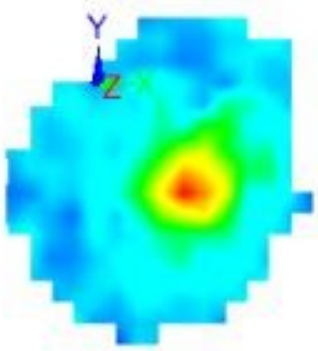

Stage 30

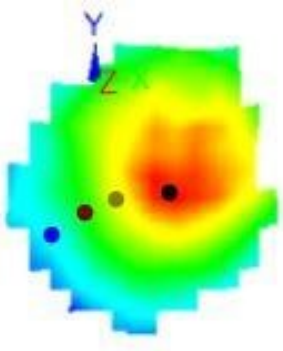

Stage 37

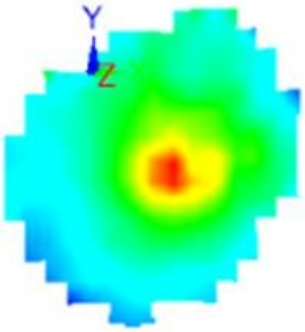

Stage 55

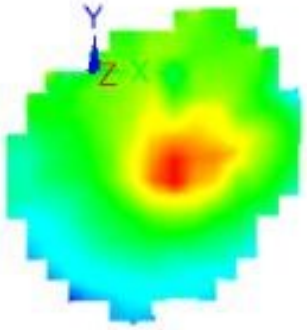

Stage 110

Figure 91. 3D deformation stages of Shield Strand S® / Epoxy based 4.5 mm thick composite impacted at a velocity 156.1 m/s with the spherical head projectile.

Figure 92 shows the low magnification optical images of Shield Strand S® / Epoxy based 4.5 mm thick specimen impacted with the spherical head projectile at a velocity of 164.5 m/s. At this velocity, the specimen attained its ballistic limit. On the point of contact of the projectile, heavy fiber ruptures are evident along with matrix cracking and delamination in the region of impact. On the speckle pattern side, fiber ruptures, petaling, matrix cracking, and delamination are noticed. Figure 92 includes a optical micrograph of the impacted specimen.

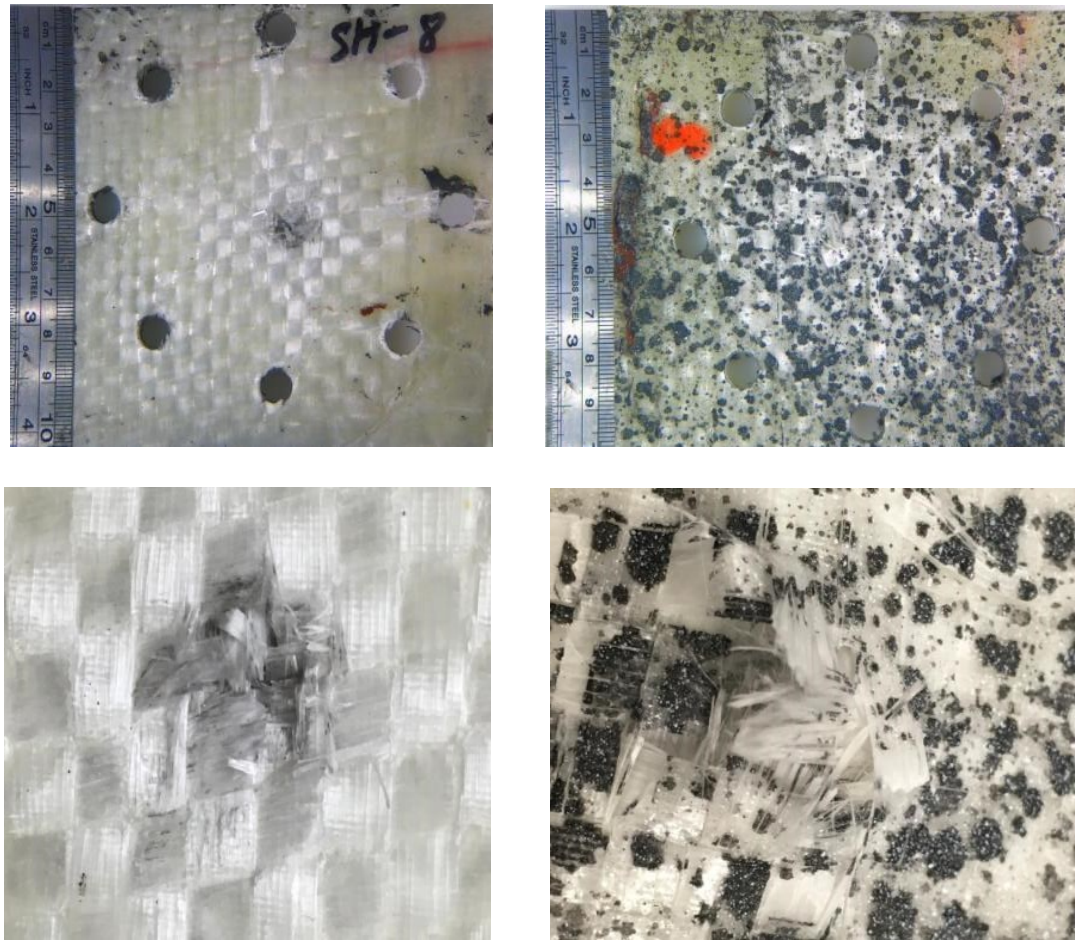

(a)

(b)

Figure 92. (a) Shield Strand S ®/ Epoxy based 4.5 mm thick composite impacted at a velocity of 164.5 m/s with the spherical head projectile (b) Section of impacted composite.

4.2.5 Impact behavior of Twintex® 2.5 mm composites with the Sharp nose projectile

Figure 93 shows the low magnification optical images of the Twintex® based 2.5 mm thick specimen impacted with the sharp nose projectile at a velocity of 60.96 m/s. From the figure, it is evident that on the point of contact of the projectile, fiber ruptures are noticed along with matrix cracks near the point of impact. On the opposite side, fiber ruptures are present as shown in Figure 93.

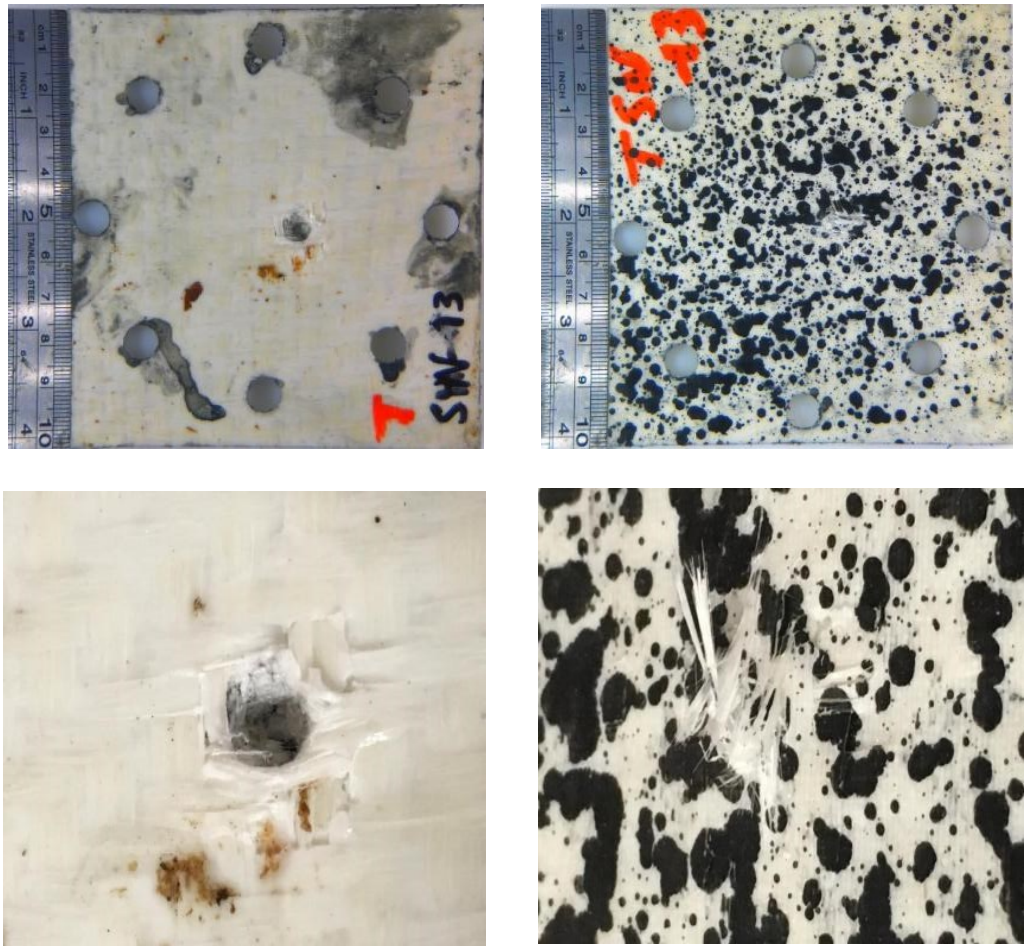

Figure 93. Twintex® based 2.5 mm thick composite impacted at a velocity 60.96 m/s with the sharp nose projectile.

Figure 94 shows the variation of the maximum transient out-of-plane displacement with stage time for the specimen illustrated in Figure 94. For this case, the maximum out of plane displacement was measured as 7.19 mm. Figure 88 also highlights a number of vibrations in stage 0 due to the

heavy fiber ruptures at the point of contact of the projectile. Multiple impact waves are also noticed.

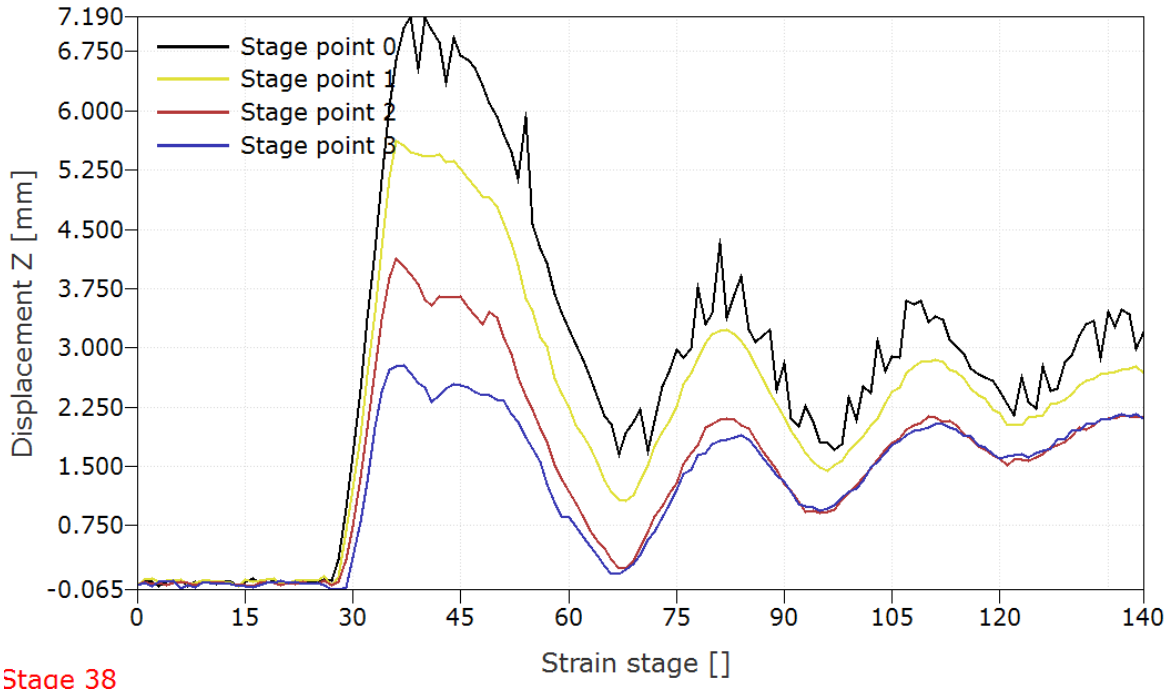

Figure 94. Displacement vs Stage graph of Twintex® based 2.5 mm thick composite impacted at a velocity 60.96 m/s with the sharp nose projectile.

Figure 95 shows a number of deformation stages representing the impact event on the 2.5 mm thick Twintex® based composites tested at a velocity of 60.96 m/s with the sharp nose projectile. From the figure, it is evident how the out-of-plane deformation increased until the maximum transient out-of-plane displacement was reached in stage 38 with a value of 7.1 mm. Following this, the displacement decreased in stage 67. Final displacement could not be accurately known, but approximately the value is close to 3.00 mm.

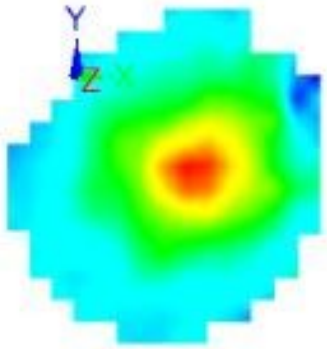

Stage 30

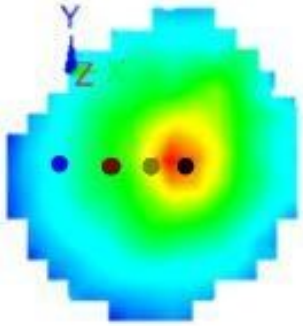

Stage 38

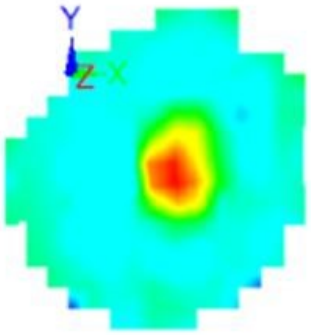

Stage 67

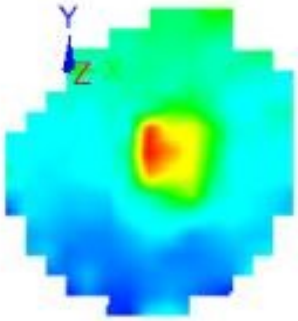

Stage 140

Figure 95. 3D deformation stage of Twintex® based 2.5 mm thick composite impacted at a velocity 60.96 m/s with the sharp nose projectile.

Figure 96 shows the low magnification optical images of the Twintex® based 2.5 mm thick specimen impacted with the sharp nose projectile at a velocity of 71.22 m/s. From the figure, it is evident that on the point of contact of projectile, fiber ruptures were noticed along with matrix cracks near the point of impact. On the opposite side, fiber ruptures are present as well as petaling occurred as shown in Figure 96.

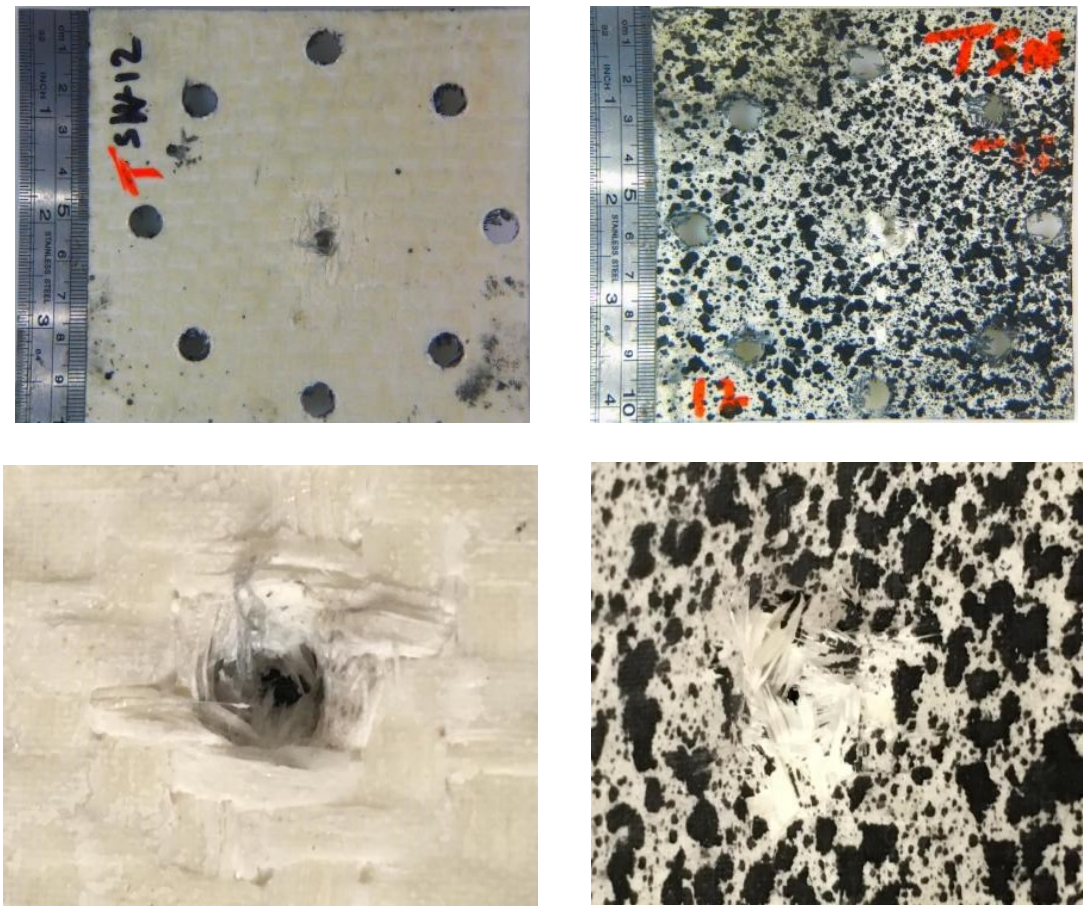

Figure 96. Twintex® based 2.5 mm thick composite impacted at a velocity 71.22 m/s with the sharp nose projectile.

Figure 97 shows the variation of the maximum transient out-of-plane displacement with stage time for the specimen illustrated in Figure 96. For this case, the maximum out of plane displacement was measured as 7.74 mm. Figure 97 also highlights some vibrations in stage 0 due to the heavy fiber ruptures at the point of contact of the projectile. Unlike the previous thermoplastic based 2.5 mm thick specimen which is impacted with velocity 60.96 m/s, there are a less impact waves.

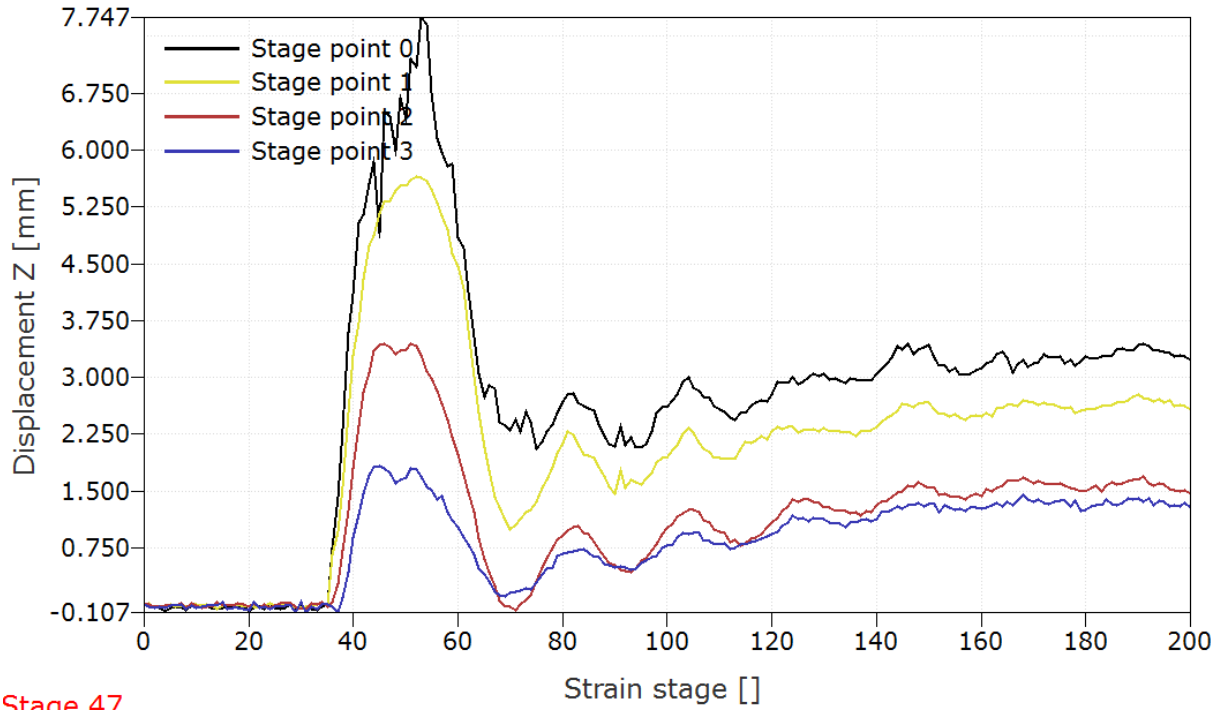

Figure 97. Displacement vs Stage graph of Twintex® based 2.5 mm thick composite impacted at a velocity 71.22 m/s with the sharp nose projectile.

Figure 98 shows many deformation stages representing the impact event on the 2.5 mm thick Twintex® based composites tested at a velocity of 71.22 m/s with the sharp nose projectile. From the figure, it is evident how the out-of-plane deformation increased until the maximum transient out-of-plane displacement was reached in stage 51 with a value of 7.74 mm. Following this, the displacement decreased in stage 72. In this case as well, final displacement could not be accurately known, but approximately the value is close to 3.50 mm.

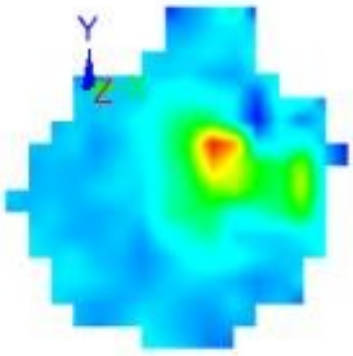

Stage 36

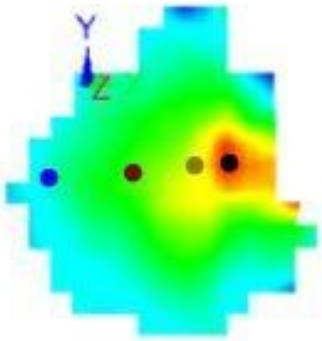

Stage 51

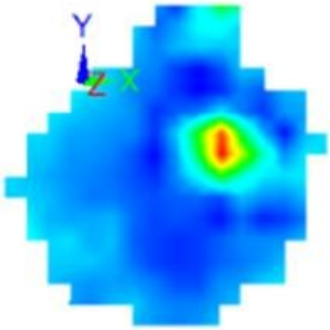

Stage 72

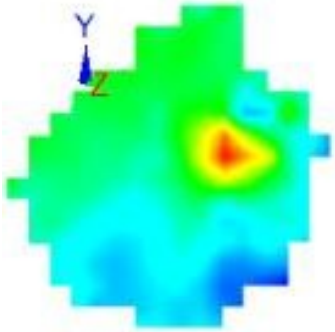

Stage 200

Figure 98. 3D deformation stage of Twintex® based 2.5 mm thick composite impacted at a velocity 71.22 m/s with the sharp nose projectile.

Figure 99 shows the low magnification optical images of the Twintex® based 2.5 mm thick specimen impacted with the sharp nose projectile at a velocity of 81.09 m/s. From the figure, it is evident that on the point of contact of the projectile, fiber ruptures were noticed along with matrix cracks near the point of impact. On the opposite side, heavy fiber ruptures are present with petaling.

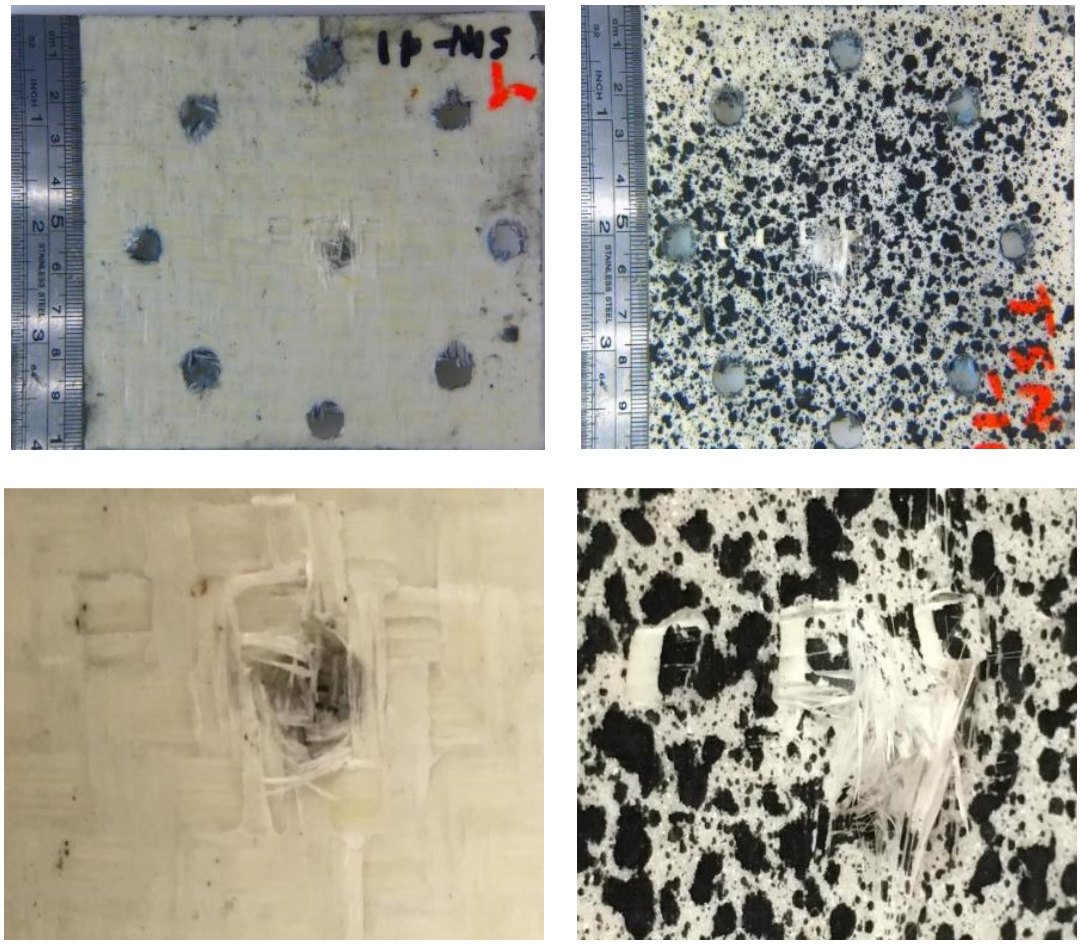

Figure 99. Twintex® based 2.5 mm thick composite impacted at a velocity of 81.09 m/s with the sharp nose projectile.

Figure 100 shows the variation of the maximum transient out-of-plane displacement with stage time for the specimen illustrated in Figure 99. For this case, the maximum out of plane displacement was measured as 12.64 mm. Figure 100 also highlights a number of vibrations in stage 0 due to the heavy fiber ruptures at the point of contact of the projectile, and multiple impact are also evident.

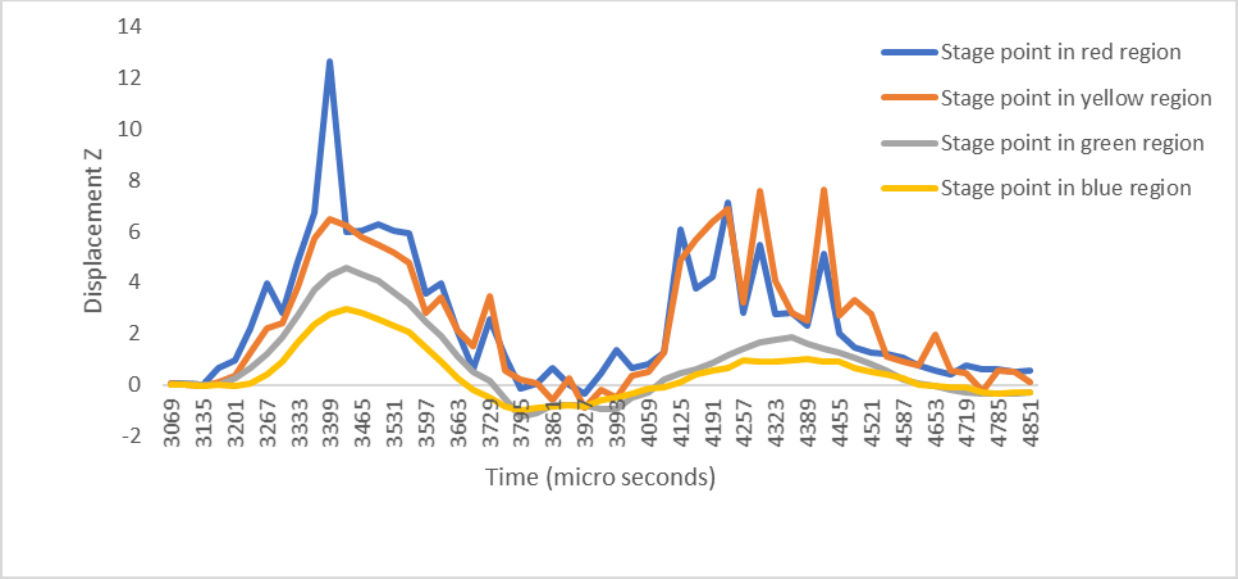

Figure 100. Displacement vs Stage graph of Twintex® based 2.5 mm thick composite impacted at a velocity 81.09 m/s with the sharp nose projectile.

Figure 101 shows a number of deformation stages representing the impact event on the 2.5 mm thick Twintex® based composites tested at a velocity of 81.09 m/s with sharp nose projectile. From the figure, it is evident how the out-of-plane deformation increased until the maximum transient out-of-plane displacement was reached in stage 103 with a value of 12.64 mm. Following this, the displacement decreased in stage 122. The final displacement value could not be estimated due to the heavy serrations in the plot as shown in Figure 101.

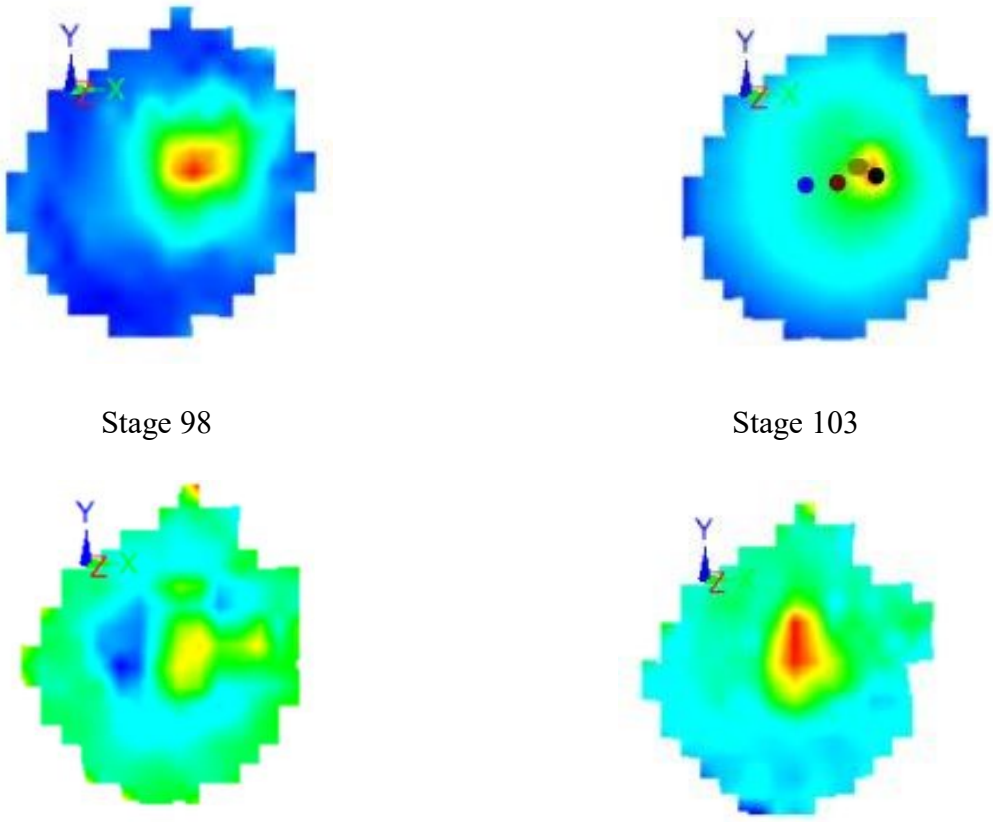

Figure 101. 3D deformation stage of Twintex® based 2.5 mm thick composite impacted at a velocity of 81.09 m/s with the sharp nose projectile.

Figure 102 shows the low magnification optical images of the Twintex® based 2.5 mm thick specimen impacted with the sharp nose projectile at a velocity of 92.1 m/s. At this velocity, specimen reached its ballistic limit. At the point of impact, fiber ruptures are evident along with matrix cracks near the point of impact. On the speckle pattern side, heavy fiber ruptures, as well as petaling, are noticed. Figure 102 includes a optical micrograph of the section of the impacted specimen as well as image of the impact event obtained from the high speed cameras.

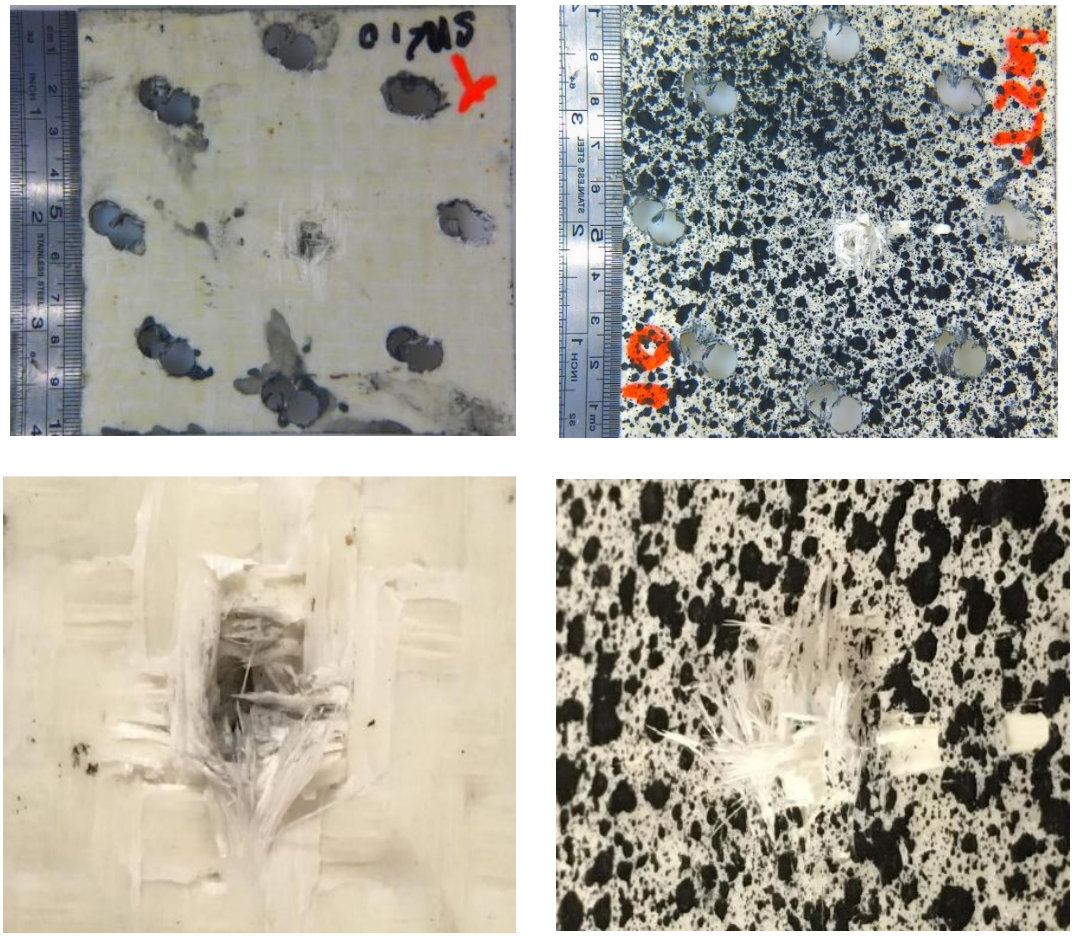

(a)

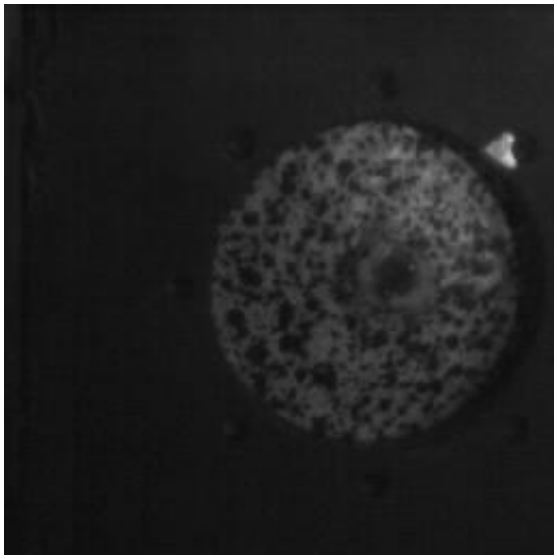

(b)

(c)

Figure 102. (a) Twintex® based 2.5 mm thick composite impacted at a velocity of 92.1 m/s with the sharp nose projectile (b) High speed camera image (c)Section of impacted composite.

4.2.6 Impact behavior of Twintex® 4.5 mm thick composites with the Sharp nose projectile

Figure 103 shows the low magnification optical images of the Twintex® based 4.5 mm thick specimen impacted with the sharp nose projectile at a velocity of 58.07 m/s. Here, at the point of impact, fiber ruptures and matrix cracks are evident along with splitting of layers. On the speckle pattern side, minute fiber ruptures are noticed.

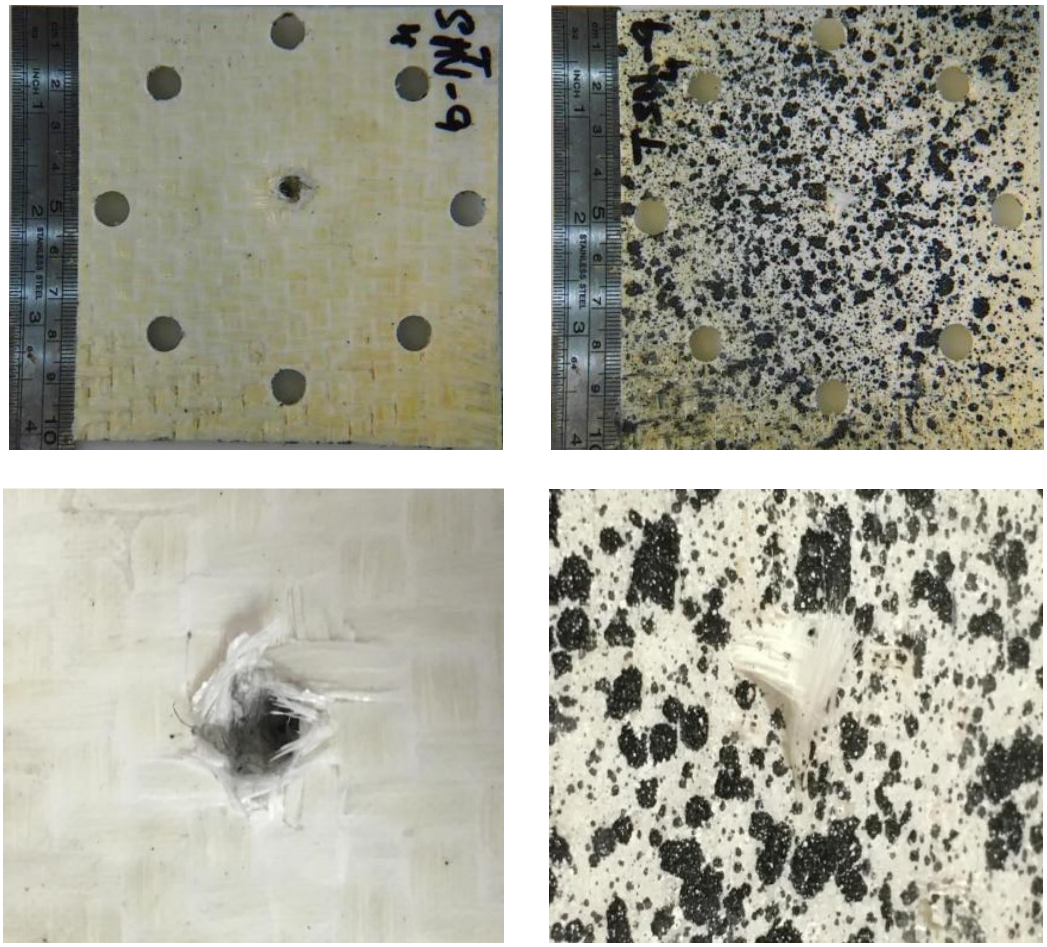

Figure 103. Twintex® based 4.5 mm thick composite tested at a velocity of 58.07 m/s with the sharp nose projectile.

Figure 104 shows the variation of the maximum transient out-of-plane displacement with stage time for the specimen illustrated in Figure 103. Here, the maximum out of plane displacement was measured as 4.87 mm. No impact waves are evident for this specimen.

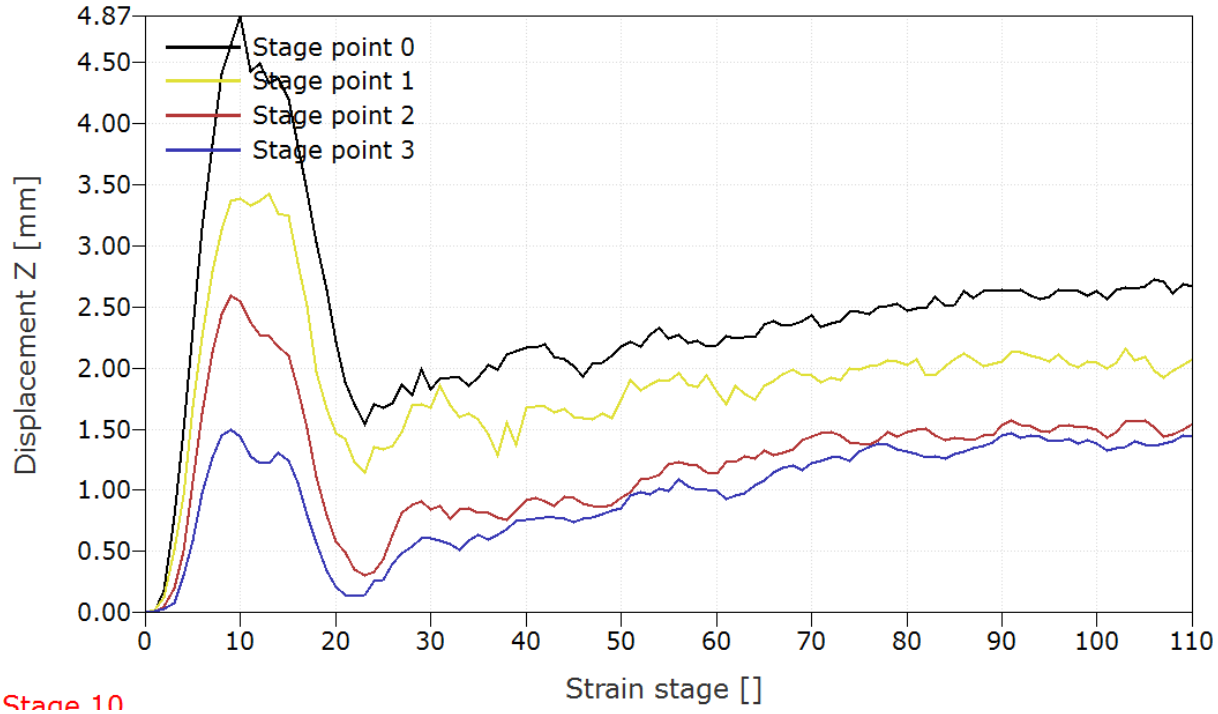

Figure 104. Displacement vs Stage graph of Twintex® based 4.5 mm thick composite impacted at a velocity 58.07 m/s with the sharp nose projectile.

Figure 105 shows a number of deformation stages representing the impact event on the 4.5 mm thick Twintex® based composites tested at a velocity of 58.07 m/s with the sharp nose projectile. From the figure, it is evident how the out-of-plane deformation increased until the maximum transient out-of-plane displacement was reached in stage 11 with a value of 4.87 mm. Following this, the displacement decreased in stage 25. The final displacement took a value close to 2.8 mm.

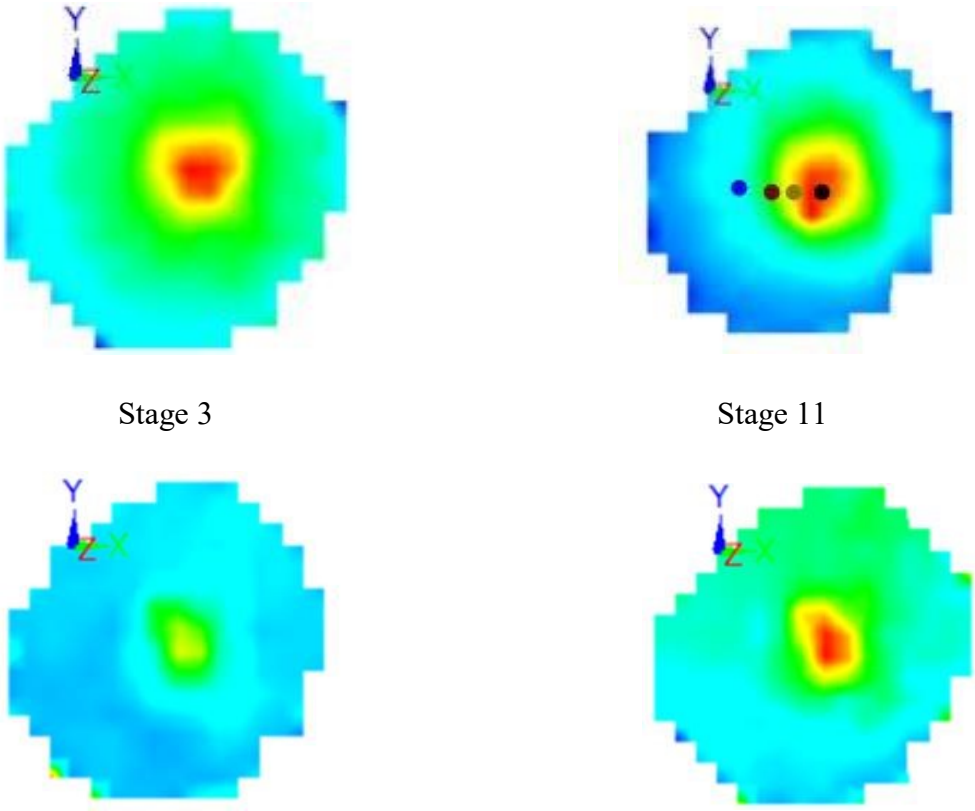

Figure 105. 3D deformation stages of Twintex® based 4.5 mm thick composite impacted at a velocity of 58.07 m/s with the sharp nose projectile.

Figure 106 shows the low magnification optical images of the Twintex® based 4.5 mm thick specimen with the sharp nose projectile at a velocity of 66.35 m/s. Here, at the point of impact, fiber ruptures and matrix cracks are evident along with splitting of layers. On the speckle pattern side, minute fiber ruptures, as well as fragmentation, were noticed.

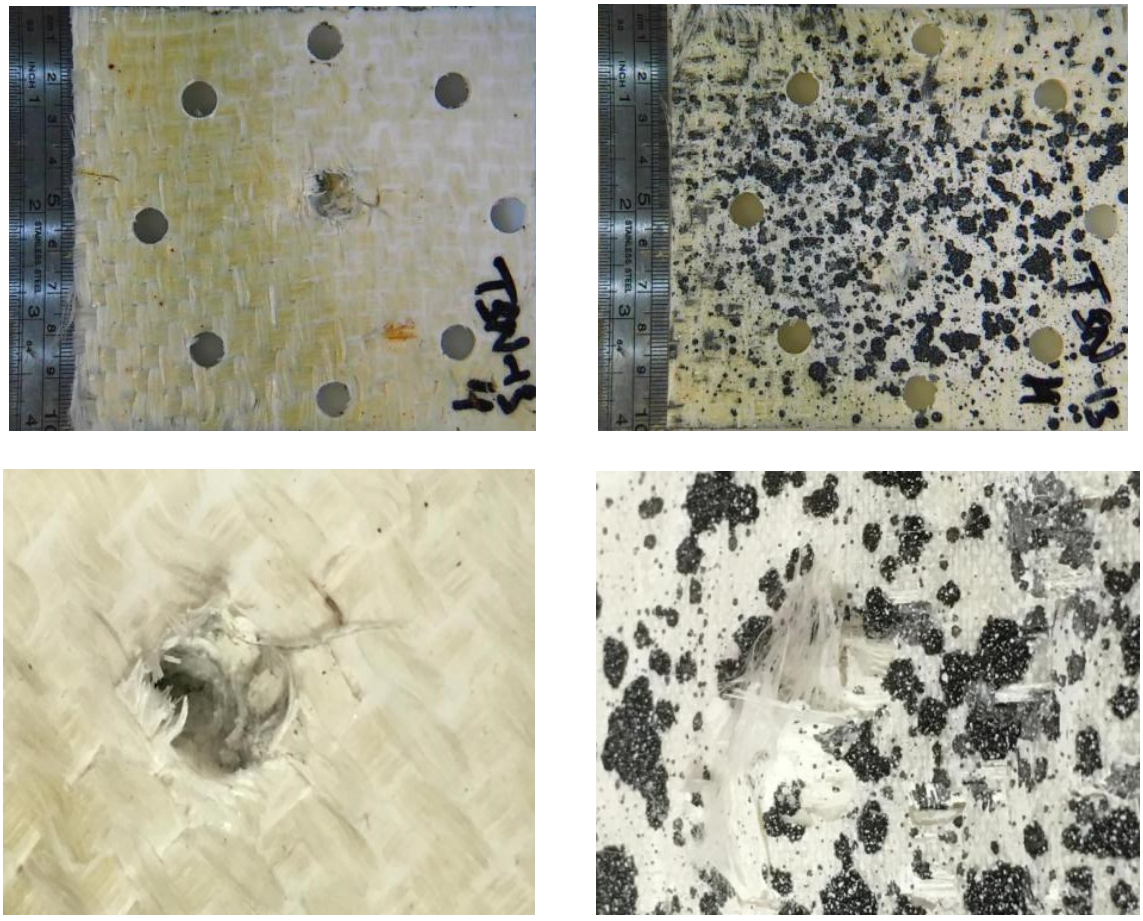

Figure 106. Twintex based 4.5 mm composite impacted at a velocity of 66.35 m/s with the sharp nose projectile.

Figure 107 shows the variation of the maximum transient out-of-plane displacement with stage time for the specimen illustrated in Figure 106. Here, the maximum out of plane displacement was measured as 6.924 mm. A couple of impact waves are evident in the plot as shown in Figure 107.

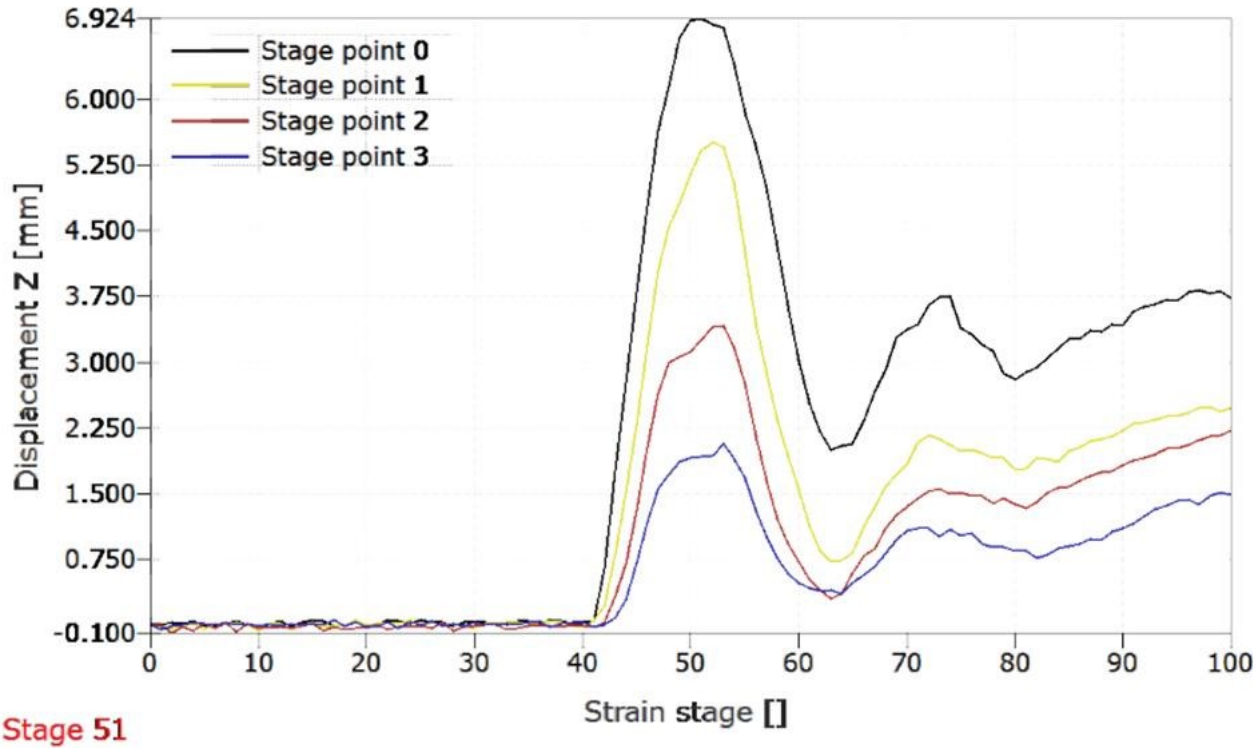

Figure 107. Displacement vs Stage graph of Twintex® based 4.5 mm thick composite impacted at a velocity 66.35 m/s with the sharp nose projectile.

Figure 108 shows a number of deformation stages representing the impact event on the 4.5 mm thick Twintex® based composites tested at a velocity of 66.35 m/s with the sharp nose projectile. From the figure, it is evident how the out-of-plane deformation increased until the maximum transient out-of-plane displacement was reached in stage 51 with a value of 6.92 mm. Following this, the displacement decreased in stage 63. The final displacement took a value close to 3.7 mm.

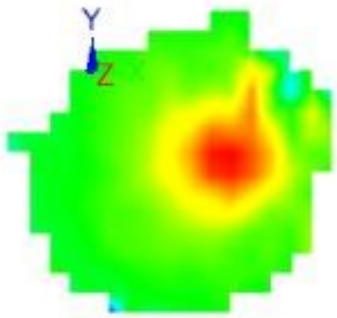

Stage 40

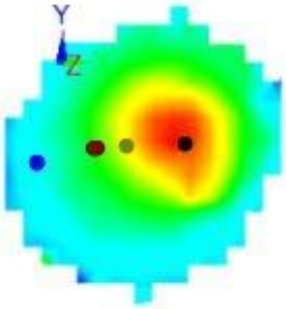

Stage 51

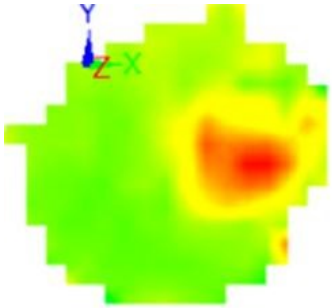

Stage 63

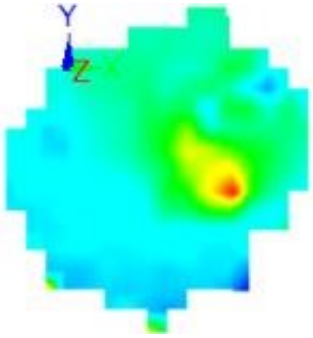

Stage 100

Figure 108. 3D deformation stages of Twintex® based 4.5 mm thick composite impacted at a velocity 66.35 m/s with the sharp nose projectile.

Figure 109 shows the low magnification optical images of the Twintex® based 4.5 mm thick specimen with the sharp nose projectile at a velocity of 74.29 m/s. Here, at the point of impact, fiber ruptures and matrix cracks are evident along with splitting of layers which is more compared with thermoplastic-based 4.5 mm thick specimen impacted at velocity 66.35 m/s with the sharp nose projectile. On the speckle pattern side, fiber ruptures and fragmentation are noticed.

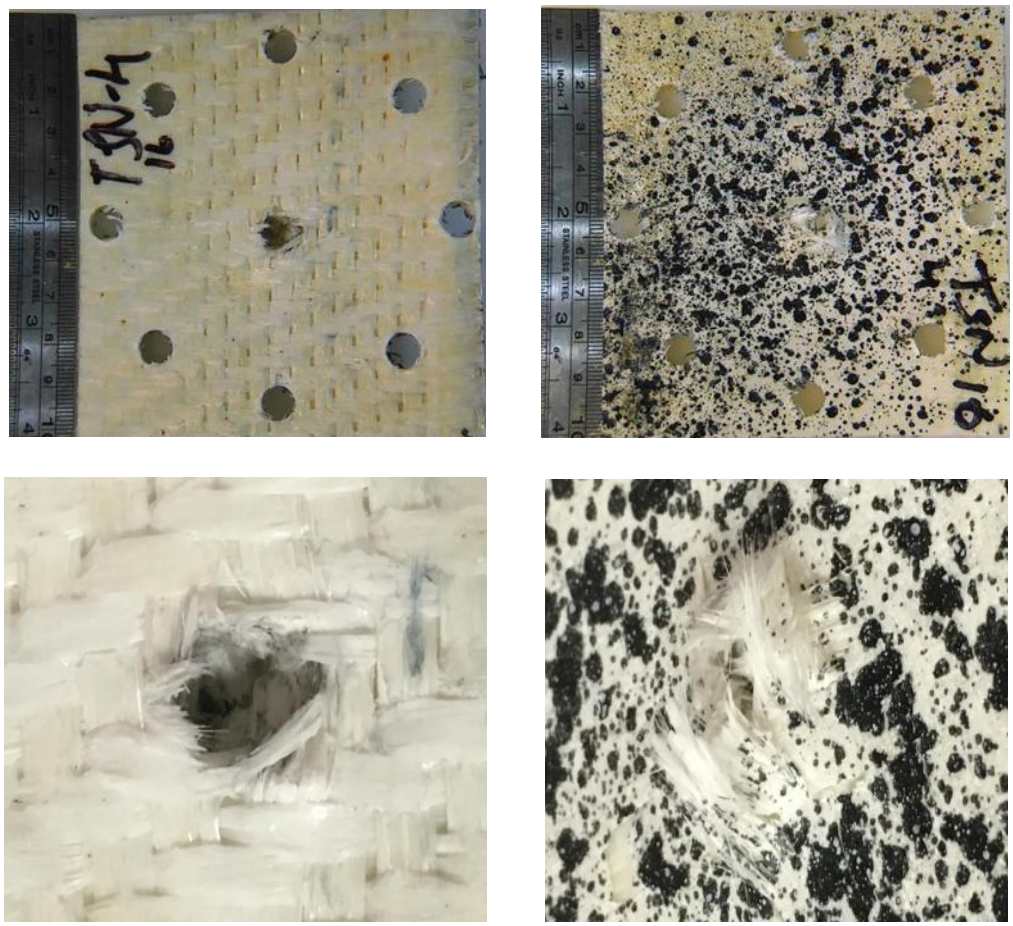

Figure 109. Twintex® based 4.5 mm composite impacted at a velocity of 74.29 m/s with the sharp nose projectile.

Figure 110 shows the variation of the maximum transient out-of-plane displacement with stage time for the specimen thermoplastic-based 4.5 mm thick specimen impacted with the sharp nose projectile at velocity 74.29 m/s. Here, the maximum out of plane displacement was measured as 7.00 mm. Less number of impact waves are noticed in the displacement-stage plot.

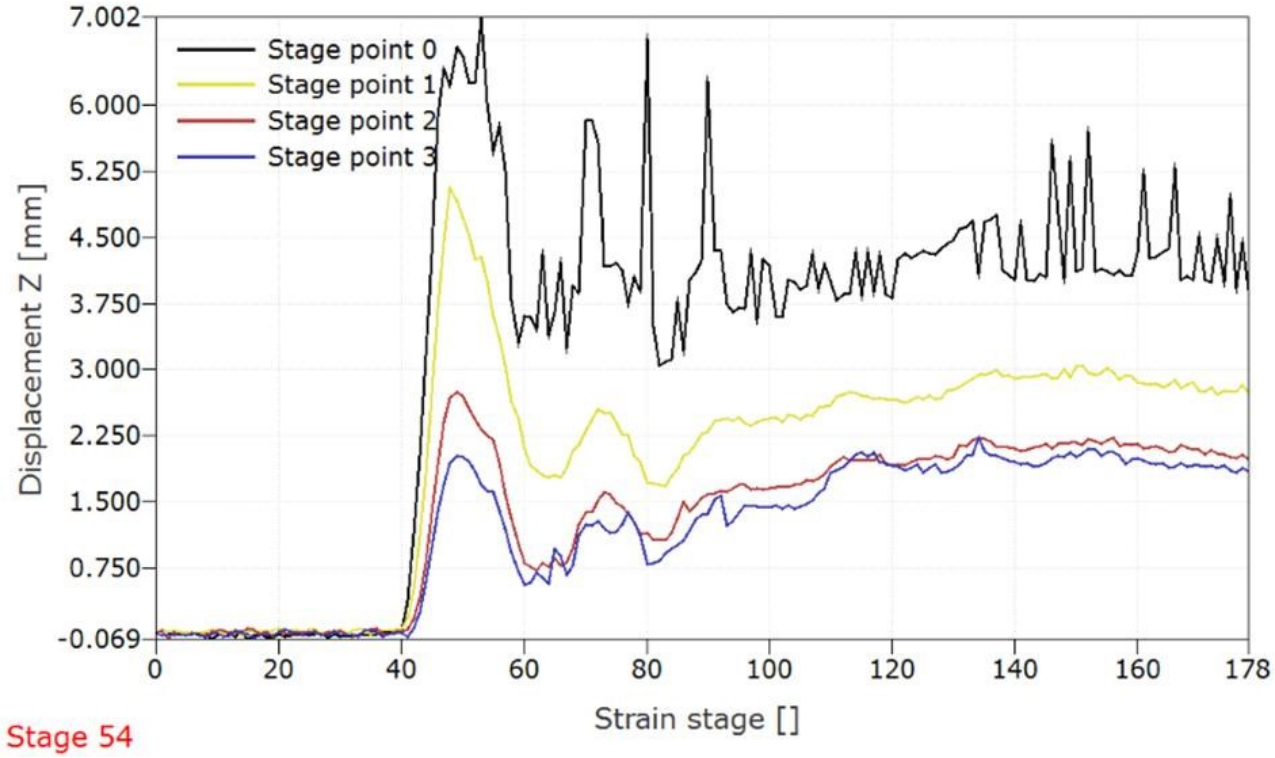

Figure 110. Displacement vs Stage graph of Twintex® based 4.5 mm thick composite impacted at a velocity 74.29 m/s with the sharp nose projectile.

Figure 111 shows a number of deformation stages representing the impact event on the 4.5 mm thick Twintex® based composites tested at a velocity of 74.2 m/s with the sharp nose projectile. From the figure, it is evident how the out-of-plane deformation increased until the maximum transient out-of-plane displacement was reached in stage 49 with a value of 7.00 mm. Following this, the displacement decreased in stage 62. The final displacement is close to 4.00 mm at the the plot at the point of impact.

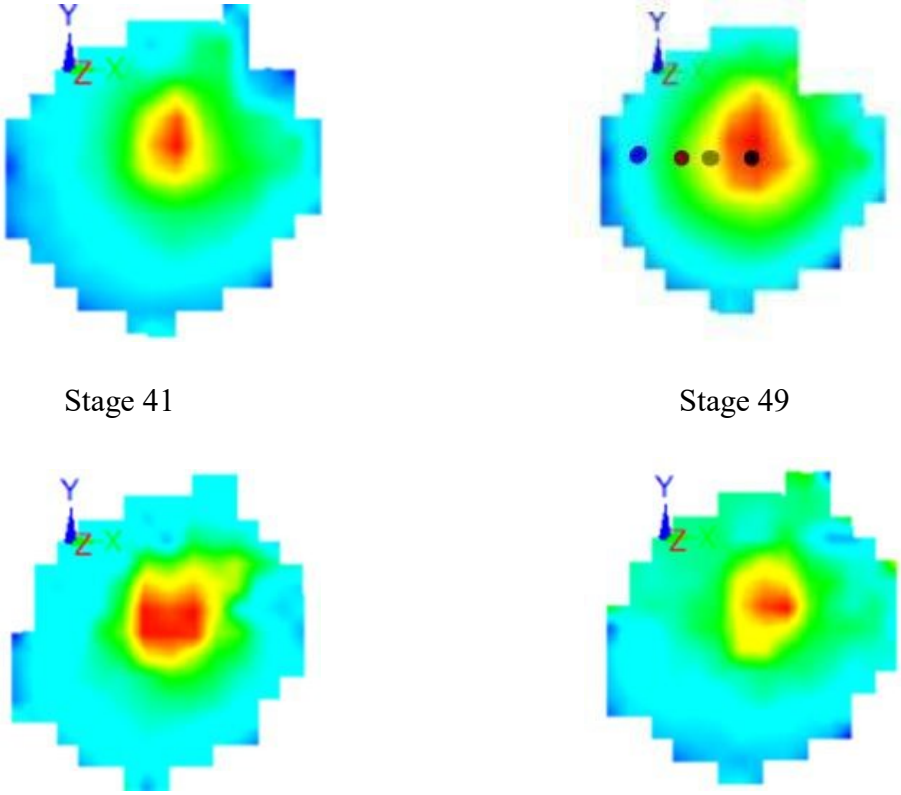

Figure 111. 3D deformation stage of Twintex® based 4.5 mm thick composite impacted at velocity 74.29 m/s with the sharp nose projectile.

Figure 112 shows the low magnification optical images of of the Twintex® based 4.5 mm thick specimen impacted with the sharp nose projectile at a velocity of 93.77 m/s. Here, at the point of impact, fiber ruptures and matrix cracks are evident along with splitting of layers. On the speckle pattern side, fiber ruptures, fragmentation, and petaling are noticed.

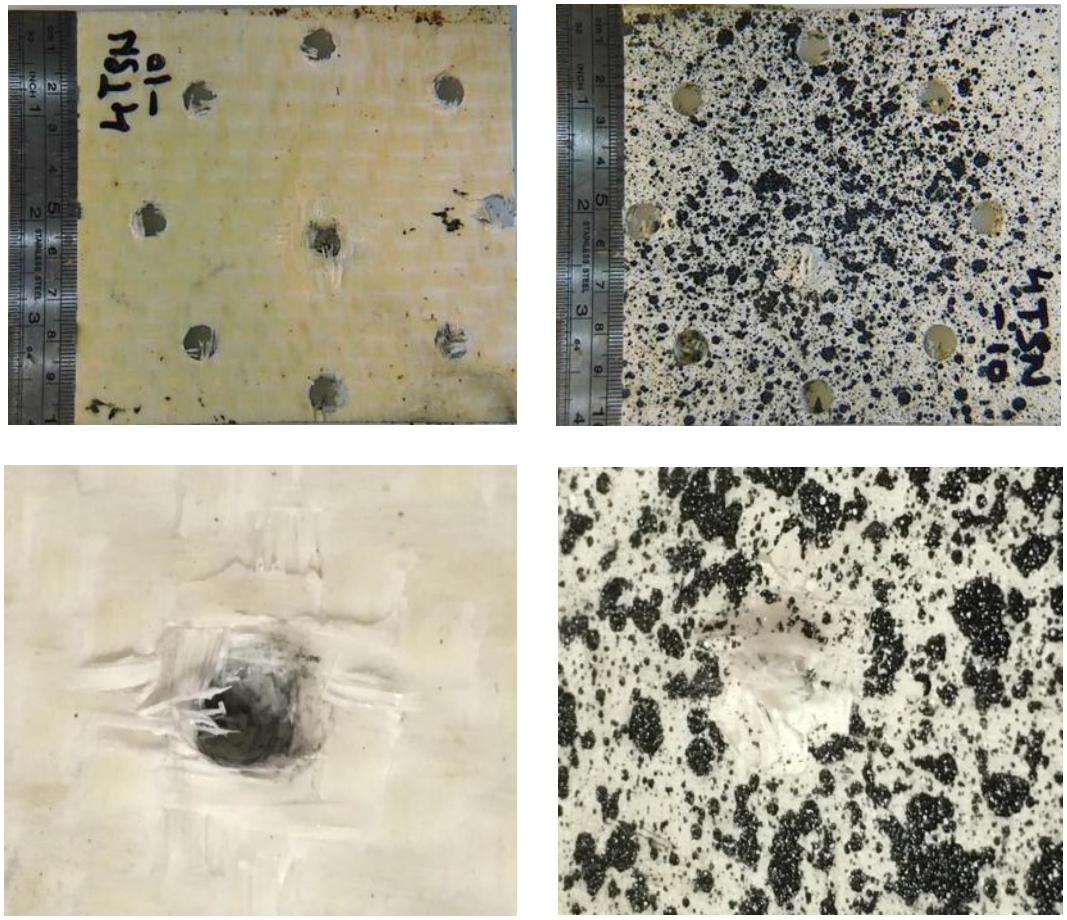

Figure 112. Twintex based 4.5 mm thick composite impacted at a velocity of 93.77 m/s with the sharp nose projectile.

Figure 113 shows the variation of the maximum transient out-of-plane displacement with stage time for the specimen thermoplastic based 4.5 mm thick specimen impacted with the sharp nose projectile at velocity 93.77 m/s. Here, the maximum out of plane displacement was measured as 8.29 mm. There were a less number of impact waves.

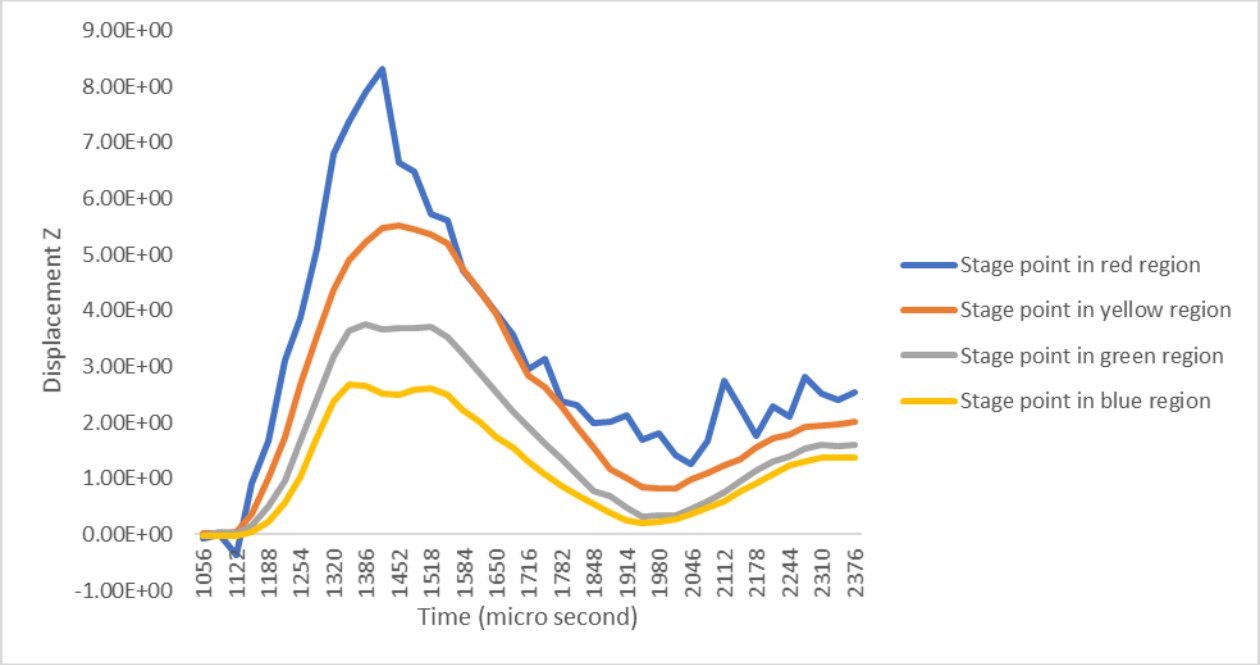

Figure 113. Displacement vs Stage graph of Twintex® based 4.5 mm thick composite impacted at a velocity 93.77 m/s with the sharp nose projectile.

Figure 114 shows a number of deformation stages representing the impact event on the 4.5 mm thick Twintex® based composites tested at a velocity of 93.77 m/s with sharp nose projectile. From the figure, it is evident how the out-of-plane deformation increased until the maximum transient out-of-plane displacement was reached in stage 44 with a value of 8.29 mm. Following this, the displacement decreased in stage 59. The final displacement could not be estimated due to the vibrations in stage 0 of the plot.

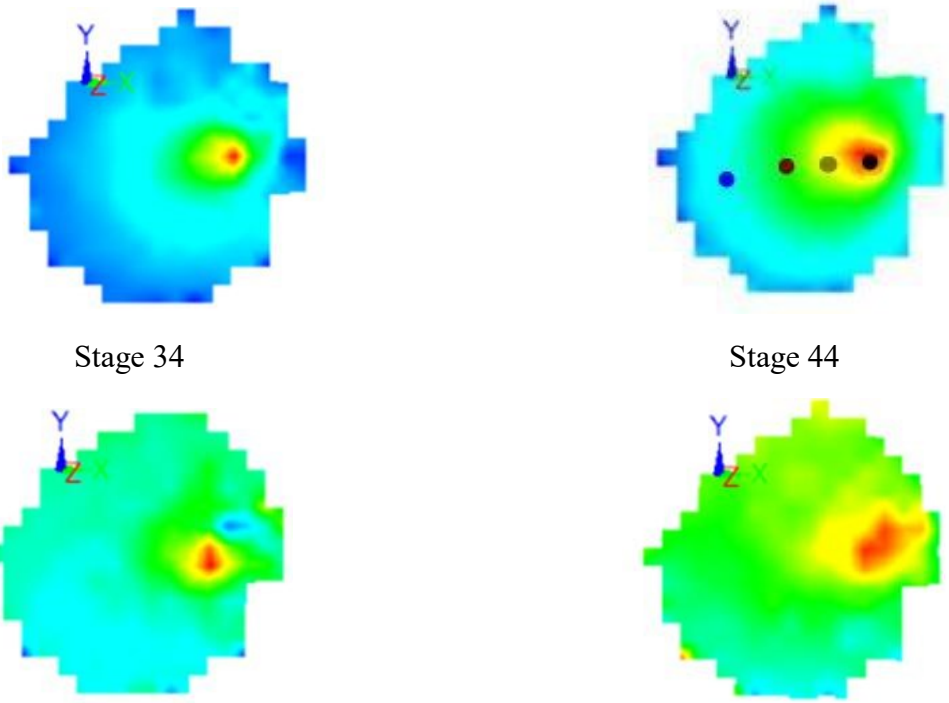

Figure 114. 3D deformation stage of Twintex® based 4.5 mm thick composite tested at a velocity of 93.77 m/s with the sharp nose projectile.

Figure 115 shows the low magnification optical images of the Twintex® based 4.5 mm thick specimen impacted with the sharp nose projectile at a velocity of 103.25 m/s. At this velocity, specimen reached its ballistic limit and at the point of impact of the projectile, fiber ruptures are evident along with matrix cracking near the point of impact. On the speckle pattern side, heavy fiber ruptures, as well as petaling are noticed along with fragmentation. Minute damages in a few areas of speckle pattern are evident due to matrix cracks. Figure 115 includes a optical micrograph of section of the impacted specimen.

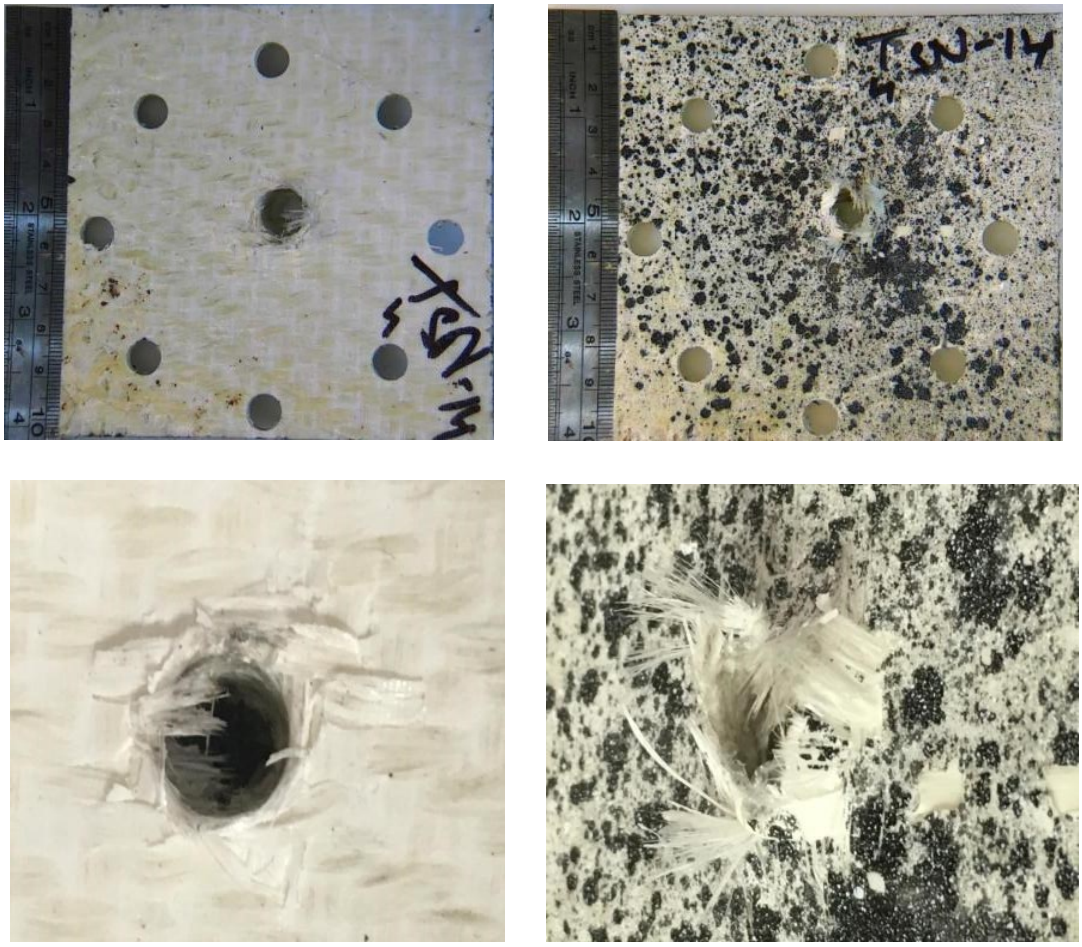

(a)

(b)

Figure 115. (a) Twintex® based 4.5 mm composite impacted at a velocity of 103.25 m/s with the sharp nose projectile (b) Section of impacted composite.

4.2.7 Impact behavior of Shield Strand S®/ Epoxy 2.5 mm thick composites with the Sharp nose projectile

Figure 116 shows the low magnification optical images of Shield Strand S®/Epoxy based 2.5 mm thick specimen impacted with the sharp nose projectile at a velocity of 56.7 m/s. From the figure, it is evident that on the point of contact of the projectile, minute fiber ruptures are present and close to the point of impact, delaminations are also present. On the opposite side (speckle pattern) of the point of contact of the projectile, minute fiber ruptures are evident along with minute fragmentation.

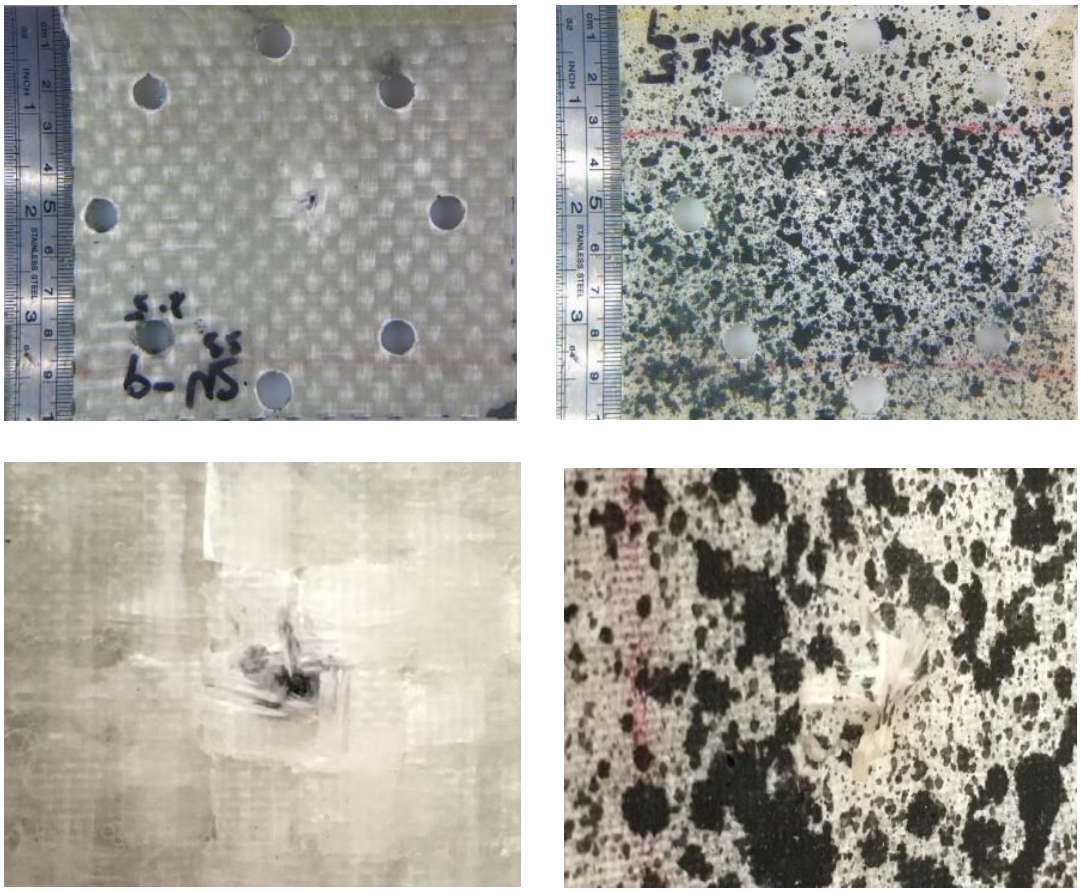

Figure 116. Shield Strand S® / Epoxy based 2.5 mm composite impacted at a velocity of 56.7 m/s with the sharp nose projectile.

The maximum transient out-of-plane displacement with stage time for the specimen presented in Figure 117. In this case, the maximum out-of-plane displacement reached a value of 5.09 mm. Figure 117 also a couple of impact waves.

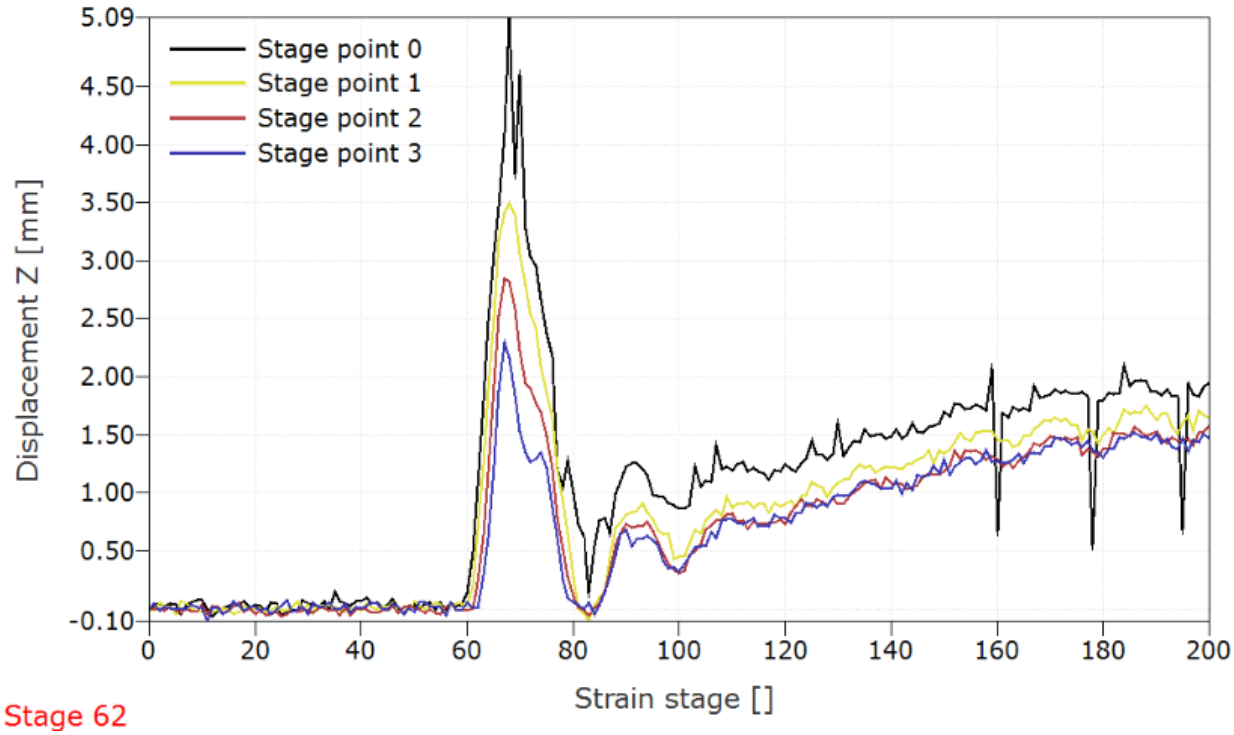

Figure 117. Displacement vs Stage graph of Shield Strand S® / Epoxy 2.5 mm thick composite tested at a velocity 56.7 m/s with the sharp nose projectile.

Figure 118 shows a number of deformation stages representing the impact event on the thermosetting-based composite tested at a velocity of 56.7 m/s with the sharp nose projectile. From the figure, it is evident how the out-of-plane deformation increased until a value of 5.09 mm was reached. Following this, the displacement decreased as shown in stage 83. The final displacement was close to 2.00 mm at the point of impact.

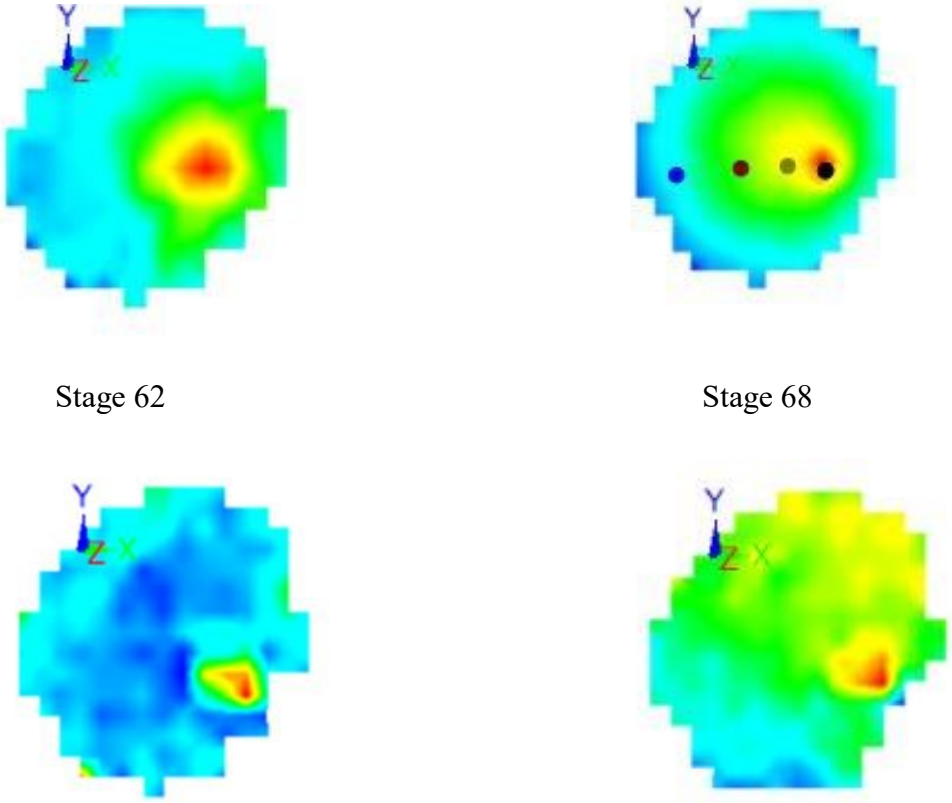

Figure 118. 3D deformation stage of Shield Strand S® / Epoxy based 2.5 mm thick composite impacted at a velocity 56.7 m/s with the sharp nose projectile.

Figure 119 shows the low magnification optical images of Shield Strand S®/Epoxy based 2.5 mm thick specimen impacted with the sharp nose projectile at a velocity of 68.50 m/s. From the figure, it was evident that on the point of contact of the projectile, fiber ruptures are present and close to the point of impact, delamination is also present. On the speckle pattern side of the point of contact of projectile minute, fiber ruptures are evident along with fragmentation.

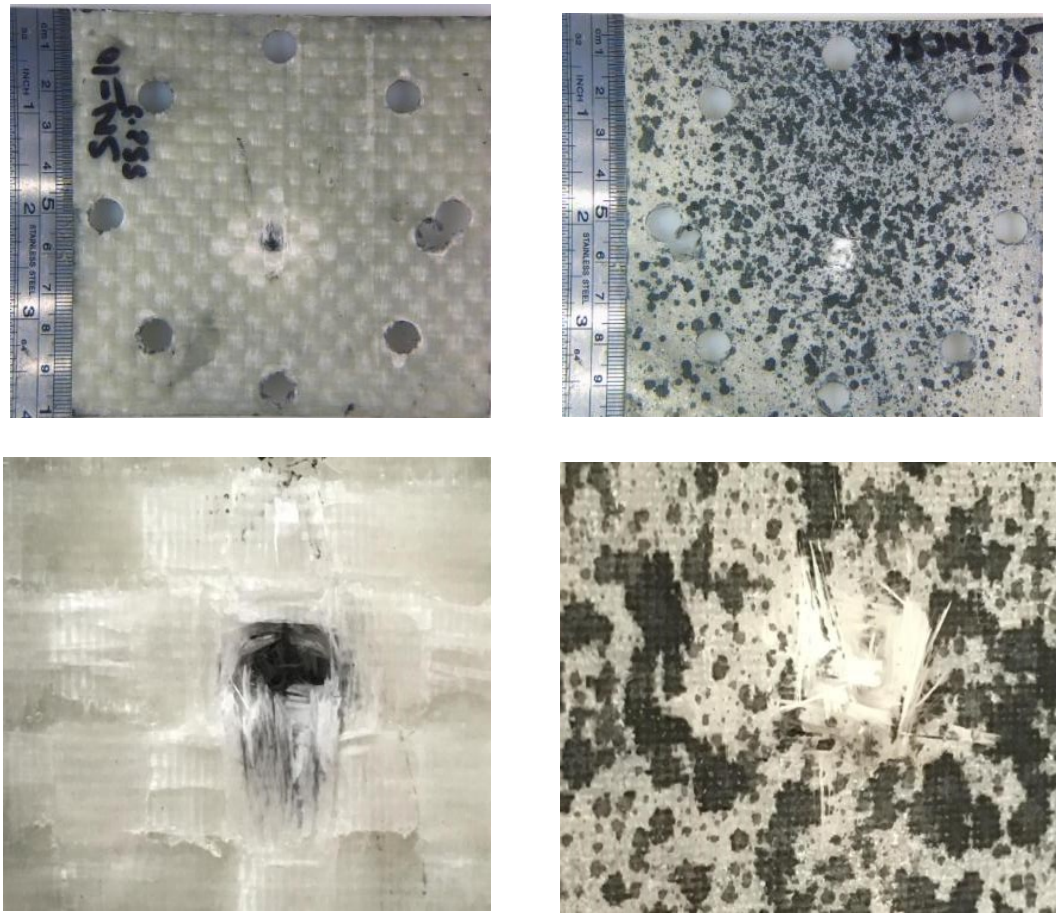

Figure 119. Shield Strand S® / Epoxy based 2.5 mm thick composite impacted at a velocity of 68.50 m/s with the sharp nose projectile.

The maximum transient out-of-plane displacement with stage time for specimen presented is in Figure 120. Here, the maximum out-of-plane displacement reached a value of 6.2 mm. The plot in Figure 120 also highlights a number of impact waves.

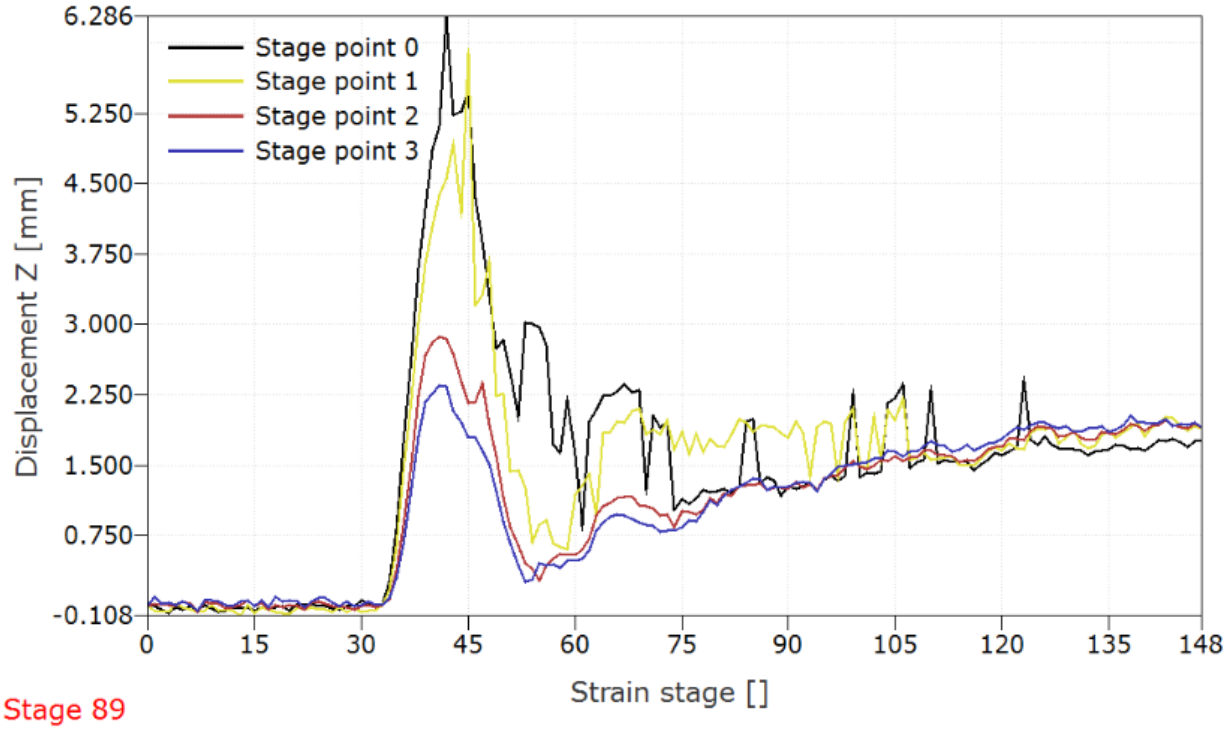

Figure 120. Displacement vs Stage graph of Shield Strand S® / Epoxy based b 2.5 mm thick composite impacted at a velocity 68.50 m/s with the sharp nose projectile.

Figure 121 shows some deformation stages representing the impact event on the thermosetting based composite tested at a velocity of 68.50 m/s with the sharp nose projectile. From the figure, it is evident how the out-of-plane deformation increased until a value of 6.28 mm was reached in stage 42. Following this, the displacement decreased as shown in stage 56. Due to multiple vibrations in the stage 0 at the displacement-stage plot as shown in Figure 121, final displacement could not be estimated.

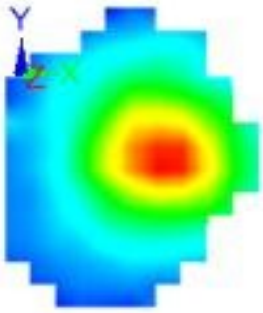

Stage 36

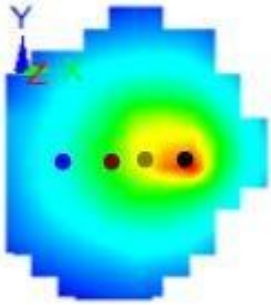

Stage 42

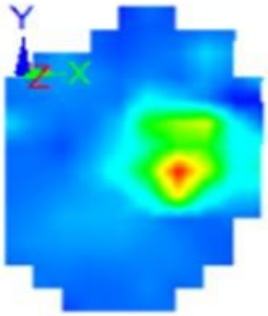

Stage 56

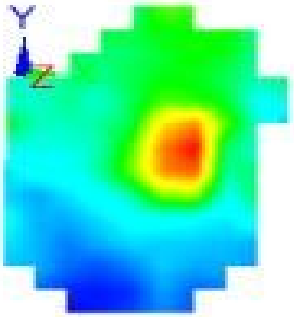

Stage 148

Figure 121. 3D deformation stages of Shield Strand S® / Epoxy based 2.5 mm thick composite impacted at a velocity 68.50 m/s with the sharp nose projectile.

Figure 122 shows the low magnification optical images of Shield Strand S®/Epoxy based 2.5 mm thick specimen impacted with the sharp nose projectile at a velocity of 79.28 m/s. From the figure, it was noticed that on the point of contact of the projectile, fiber ruptures are present and close to the point of impact, delamination is present which is more compared with the previous two thermoset based 2.5 mm thick specimens which were impacted at 56.7 m/s and 68.50 m/s with sharp nose projectile. On the speckle pattern side of the point of contact of projectile, fiber ruptures are evident along with traces of fragmentation.

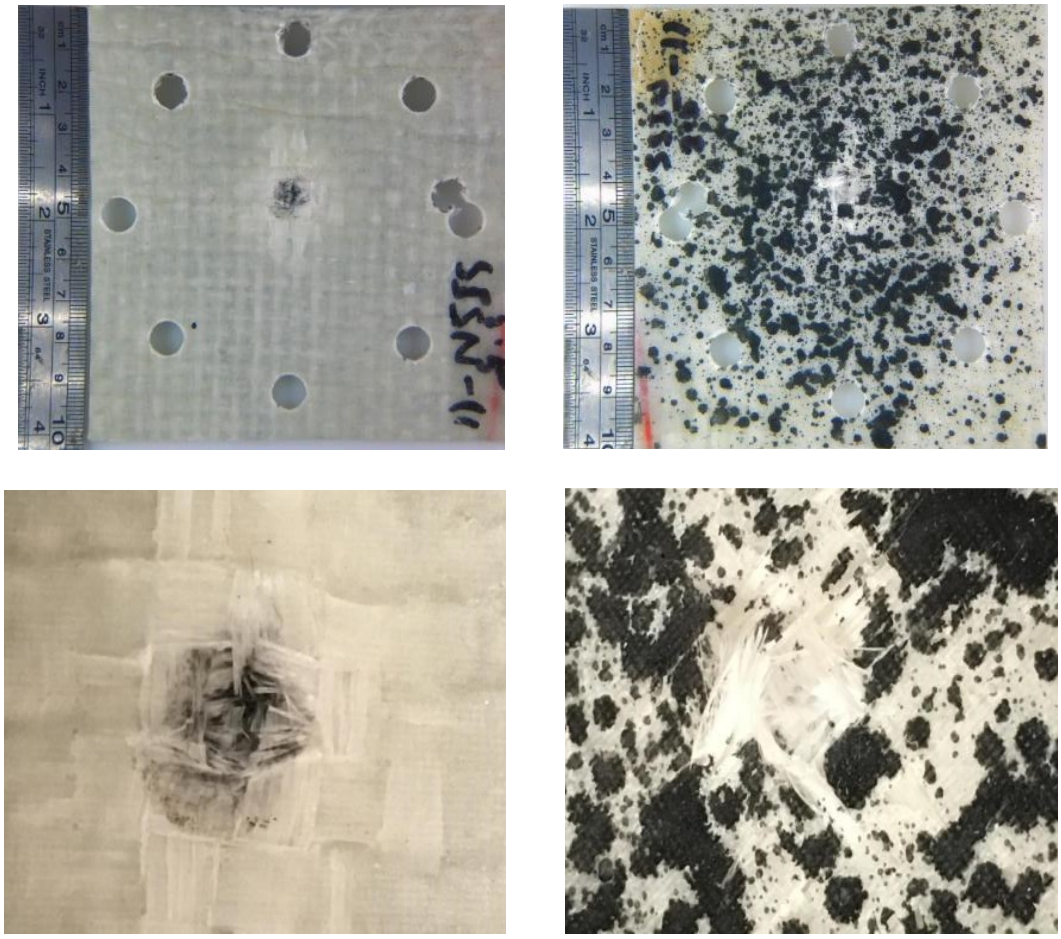

Figure 122. Shield Strand S ®/ Epoxy based 2.5 mm thick composite impacted at a velocity of 79.28 m/s with the sharp nose projectile.

The maximum transient out-of-plane displacement with stage time for specimen presented in Figure 123. Here, the maximum out-of-plane displacement reached a value of 7.6 mm. The plot in Figure 123 highlights a couple of impact waves.

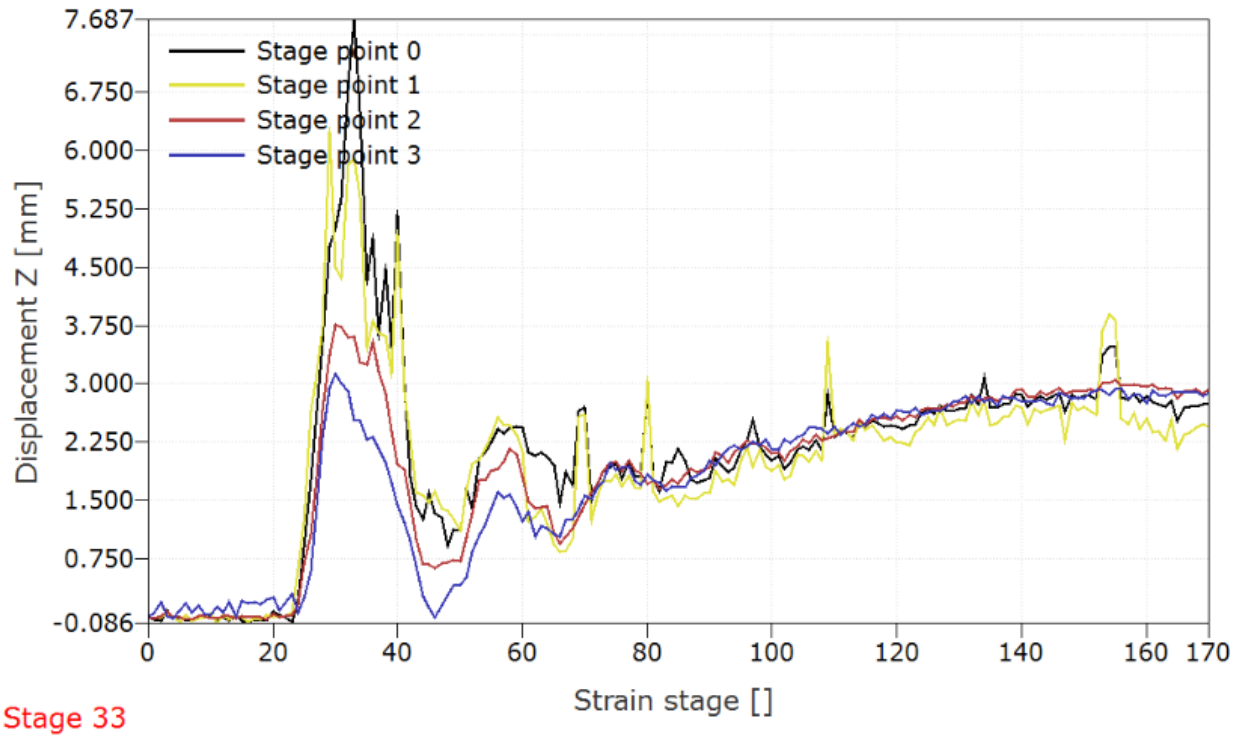

Figure 123. Displacement vs Stage graph of Shield Strand S / Epoxy based 2.5 mm thick composite impacted at a velocity 79.28 m/s with the sharp nose projectile.

Figure 124 shows some deformation stages representing the impact event on the Shield Strand S®/Epoxy based composite tested at a velocity of 79.28 m/s with the sharp nose projectile. From the figure, it is evident how the out-of-plane deformation increased until a value of 7.67 mm was reached in stage 32. Following this, the displacement decreased as shown in stage 45. Due to multiple vibrations in stage 0 at the displacement-stage plot as shown in Figure 124, final displacement could not be estimated. Approximately the value is observed to be close to 3.00 mm.

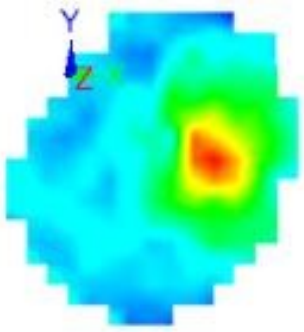

Stage 25

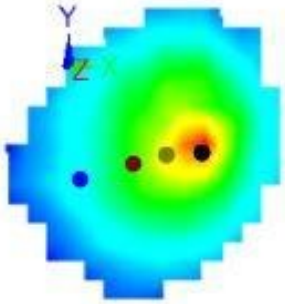

Stage 32

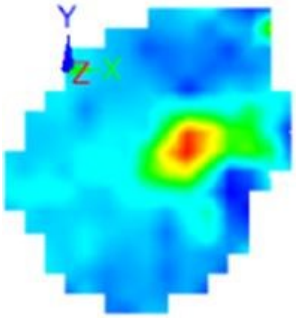

Stage 45

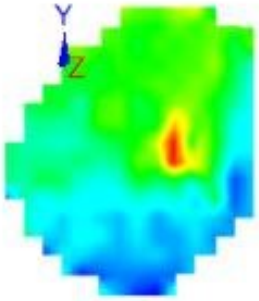

Stage 170

Figure 124. 3D deformation stages of Shield Strand S® / Epoxy based 2.5 mm thick composite impacted at a velocity 79.28 m/s with the sharp nose projectile.

Figure 125 shows the low magnification optical images of Shield Strand S®/Epoxy based 2.5 mm thick specimen impacted with the sharp nose projectile at a velocity of 90.57 m/s. From the figure, it was noticed that on the point of contact of the projectile, fiber ruptures are present and close to the point of impact, heavy delamination is present. On the speckle pattern side of the point of contact of the projectile, fiber ruptures and petaling are evident along with of fragmentation. Damages in the speckle pattern area were also noticed due to matrix cracking.

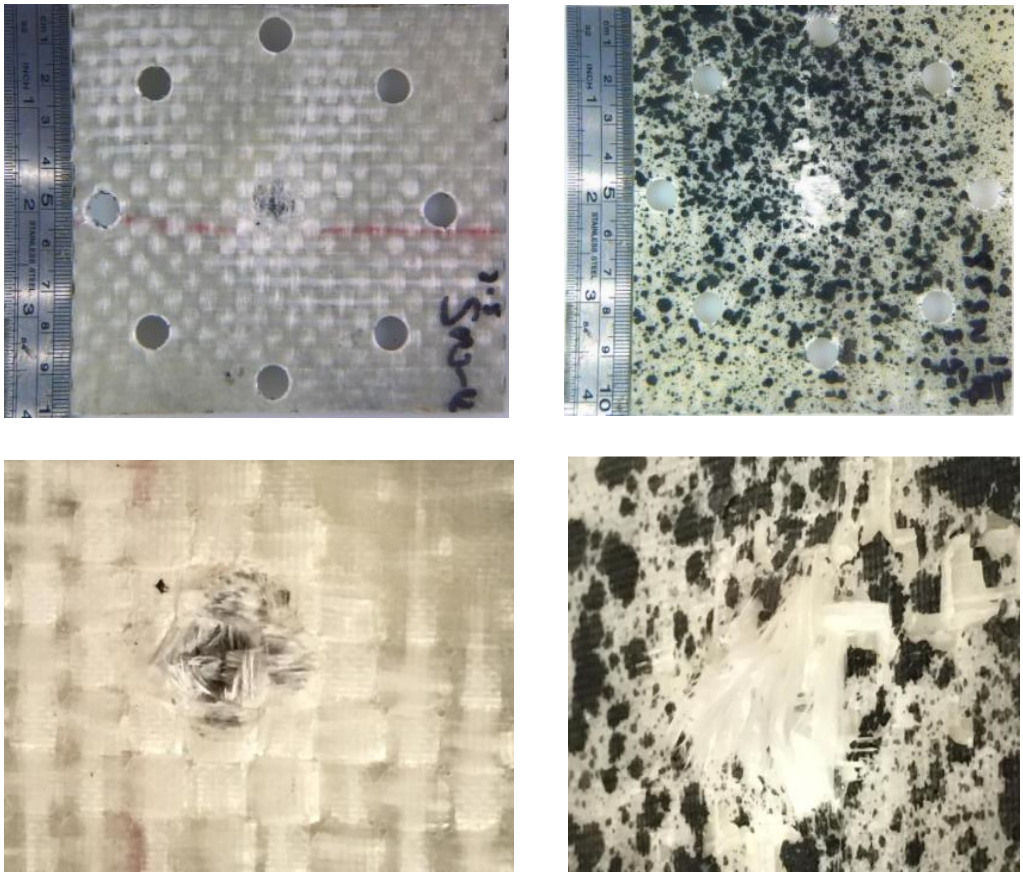

Figure 125. Shield Strand S® / Epoxy based 2.5 mm composite impacted at a velocity of 90.57 m/s with the sharp nose projectile.

The maximum transient out-of-plane displacement with stage time for specimen presented in Figure 126. Here, the maximum out-of-plane displacement reached a value of 7.6 mm. The plot in Figure 126 highlights few impact waves.

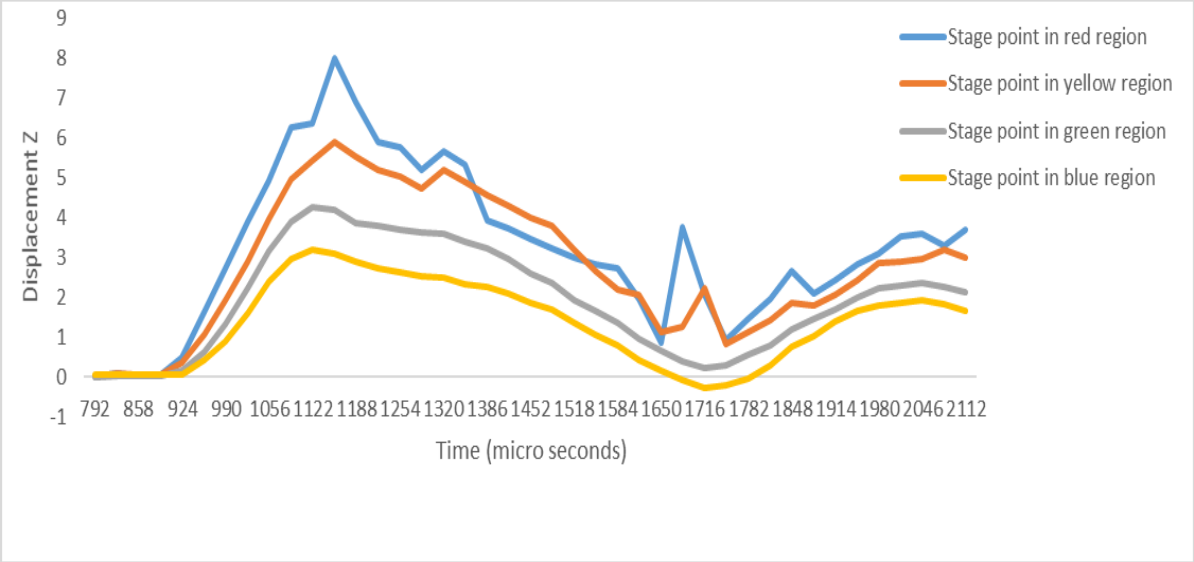

Figure 126. Displacement vs Stage graph of Shield Strand S® / Epoxy 2.5 mm thick composite tested at velocity 90.57 m/s with the sharp nose projectile.

Figure 127 shows some deformation stages representing the impact event on the Shield Strand S®/Epoxy based 2.5 mm thick composite tested at a velocity of 90.57 m/s with the sharp nose projectile. From the figure, it is evident how the out-of-plane deformation increased until a value of 7.99 mm was reached. Following this, the displacement decreased as shown in stage 52. Final displacement could not be accurately known.

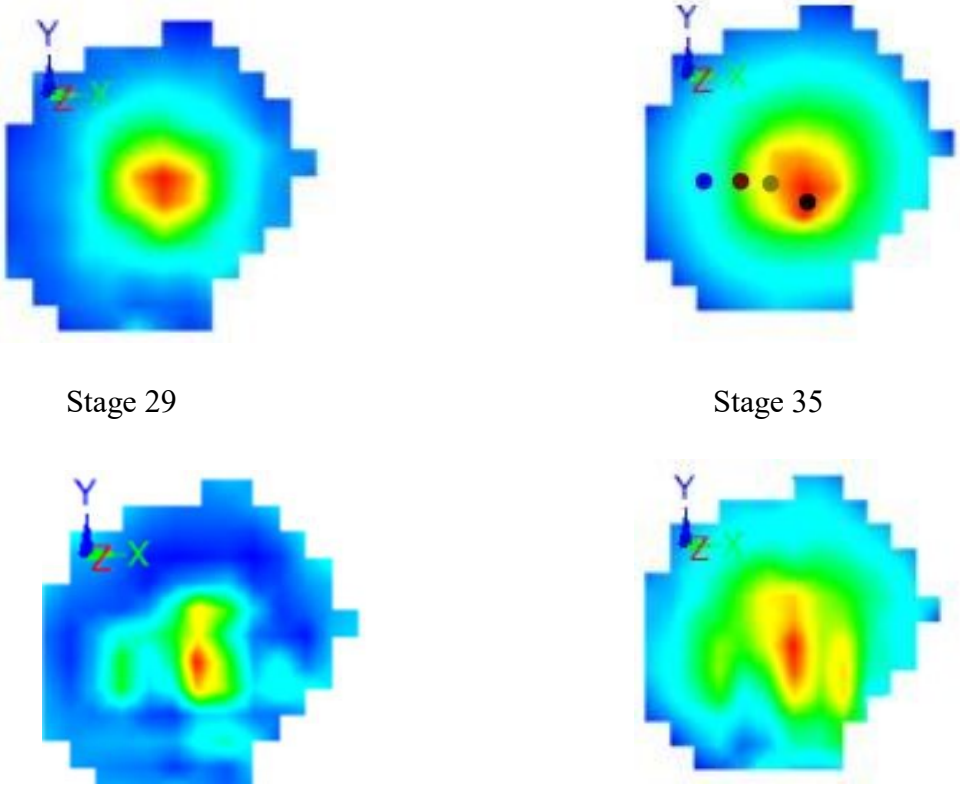

Figure 127. 3D deformation stages of Shield Strand S® / Epoxy 2.5 mm thick composite impacted at a velocity 90.57 m/s with the sharp nose projectile.

Figure 128 shows the low magnification optical images of Shield Strand S® / Epoxy based 2.5 mm thick specimen impacted with the sharp nose projectile at a velocity of 114.4 m/s. From the figure, it is evident that on the point of contact of the projectile, fiber ruptures are present and close to the point of impact, delaminations are also present. On the opposite side (speckle pattern) of the point of contact of the projectile, fiber ruptures and petaling are evident along with delaminations. Also, heavy fragmentation was observed during the impact.

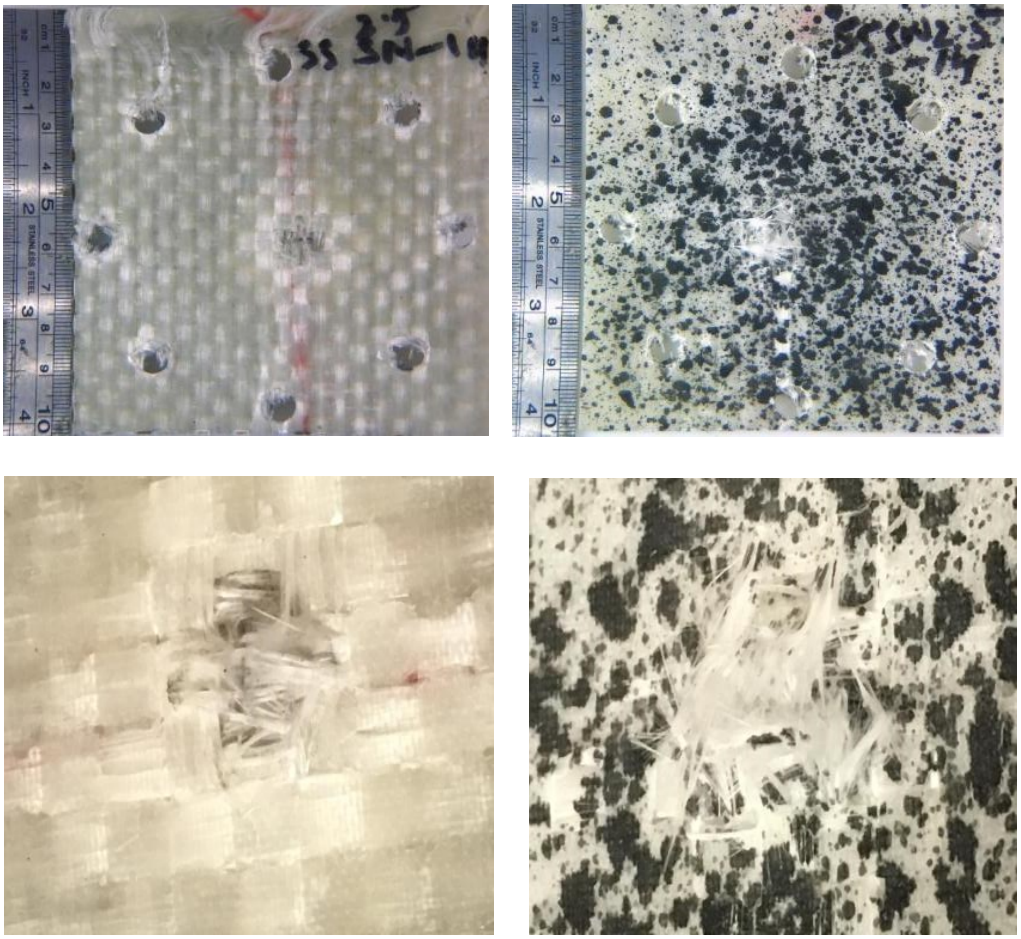

Figure 128. Shield Strand S® /Epoxy based 2.5 mm composite impacted at a velocity of 114.4 m/s with the sharp nose projectile.

Due to the heavy fragmentation and fiber ruptures which affected the speckle pattern, DIC could not process complete deformation and stage time data for this specimen. Only, initial stages of deformation could be obtained as shown in Figure 129.

Initial Stage Stage just before heavy fragmentation and ruptures occurred

Figure 129. 3D deformation stages of Shield Strand S ®/ Epoxy 2.5 mm thick composite impacted at a velocity 114.4 m/s with the sharp nose projectile.

Figure 130 shows the low magnification optical images of the Shield Strand S® / Epoxy based 2.5 mm thick specimen with the sharp nose projectile at a velocity of 125.1 m/s. At this velocity, specimen reached its ballistic limit. At the point of impact of the projectile, fiber ruptures are evident along with matrix cracking as well as delamination near the point of impact. On the speckle pattern side, heavy fiber ruptures, as well as petaling are noticed along with fragmentation. Minute damages in the speckle pattern are evident due to matrix cracks in a few areas. Figure 130 includes optical micrograph of section of the impacted specimen.

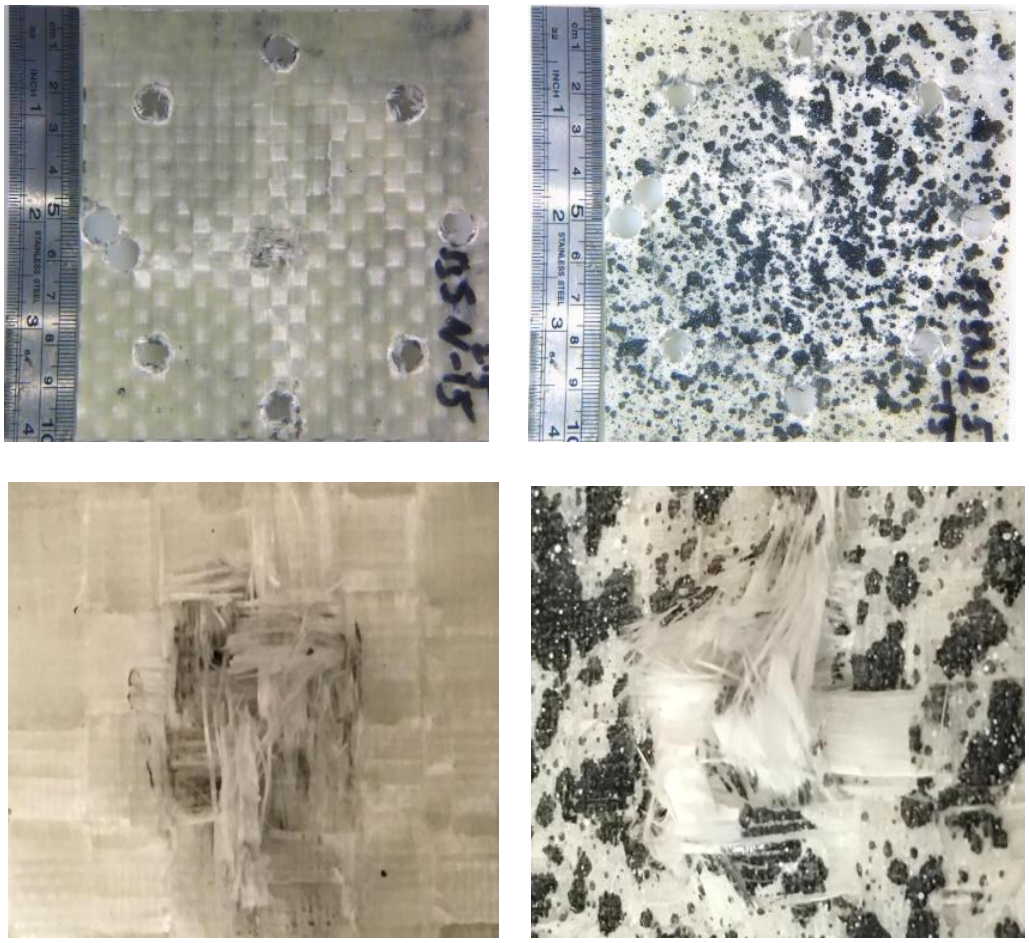

(a)

(b)

Figure 130. (a) Shield Strand S® / Epoxy based 2.5 mm composite impacted at a velocity of 125.1 m/s with the sharp nose projectile (b) Section of impacted composite.

4.2.8 Impact behavior of Shield Strand S®/ Epoxy 4.5 mm thick composites with the Sharp nose projectiles

Figure 131 shows the low magnification optical images of Shield Strand S® / Epoxy based 4.5 mm thick specimen impacted with the sharp nose projectile at a velocity of 80.50 m/s. From the figure, it is noticed that on the point of contact of the projectile, minute fiber ruptures are evident along with minute matrix cracks as well as minute delamination in the region of impact. On the speckle pattern side, no damages are noticed..

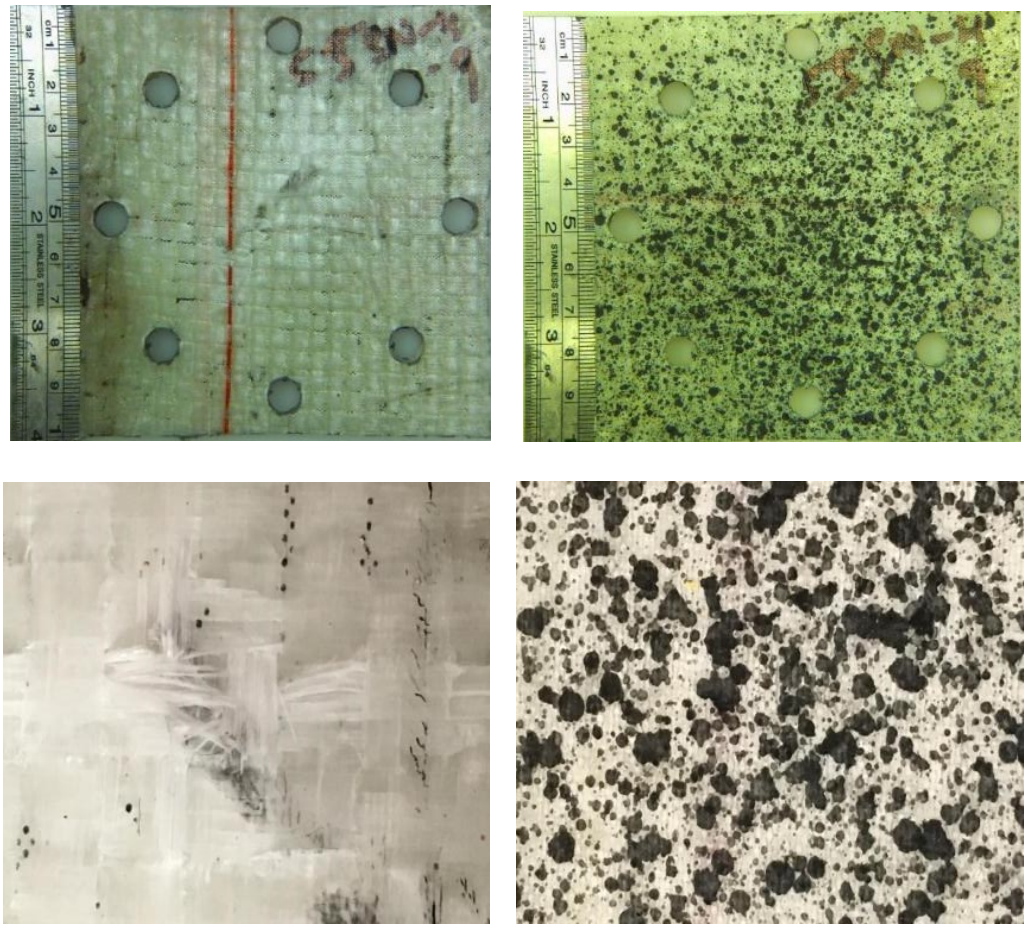

Figure 131. Shield Strand S® / Epoxy based 4.5 mm composite impacted at a velocity of 80.50 m/s with the sharp nose projectile.

The maximum transient out-of-plane displacement with stage time for specimen presented is in Figure 132. Here, the maximum out-of-plane displacement reached a value of 5.08 mm in stage 86. A couple of impact waves are also highlighted in Figure 132.

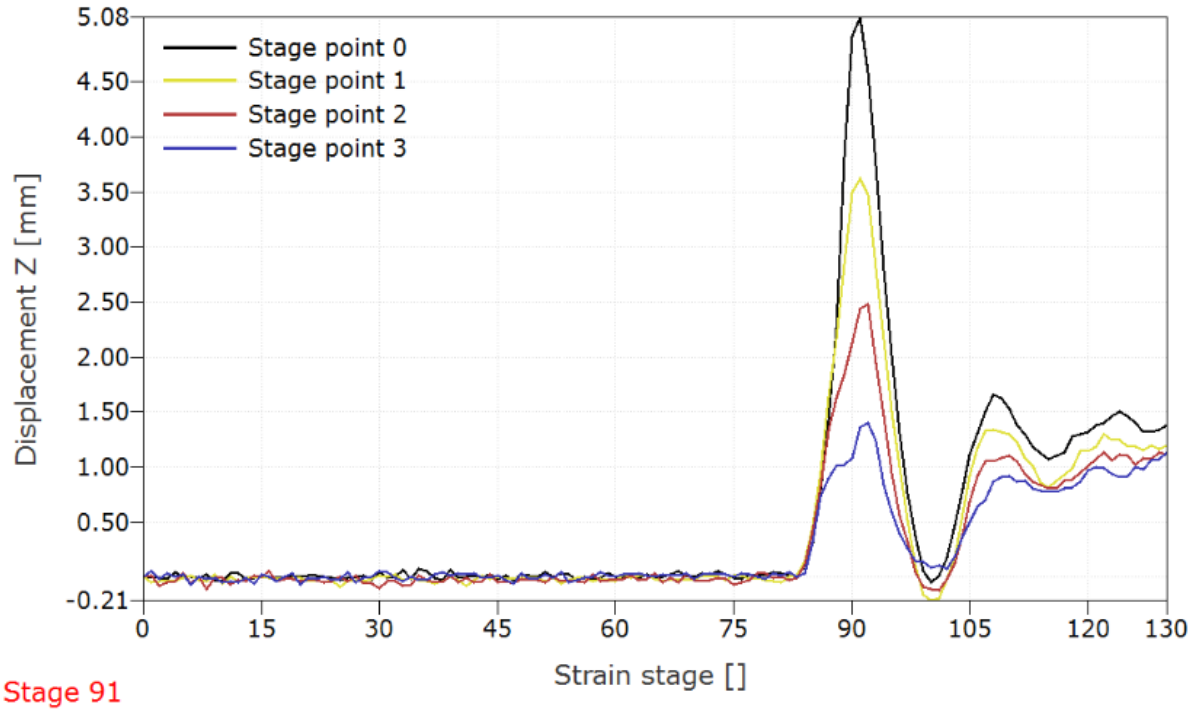

Figure 132. Displacement vs Stage graph of Shield Strand S® / Epoxy based 4.5 mm thick composite impacted at velocity 80.50 m/s with the sharp nose projectile.

Figure 133 shows some deformation stages representing the impact event on the Shield Strand S® / Epoxy based 4.5 mm thick composite impacted at a velocity of 80.50 m/s with the sharp nose projectile. From the figure, it is evident how the out-of-plane deformation increased until a value of 5.08 mm was reached. Following this, the displacement decreased as shown in stage 100. Final displacement took a value close to 1.5 mm at the region of impact.

Figure 133. 3D deformation stages of Shield Strand S® / Epoxy based 4.5 mm thick composite impacted at velocity 80.50 m/s with sharp nose projectile.

Figure 134 shows the low magnification optical images of Shield Strand S® / Epoxy based 4.5 mm thick specimen impacted with the sharp nose projectile at a velocity of 95.69 m/s. From the figure, it is evident that on the point of contact of the projectile, minute fiber ruptures are noticed along with minute matrix cracks as well as minute delamination in the region of impact. On the speckle pattern side, minute fiber ruptures are observed as shown in Figure 134.

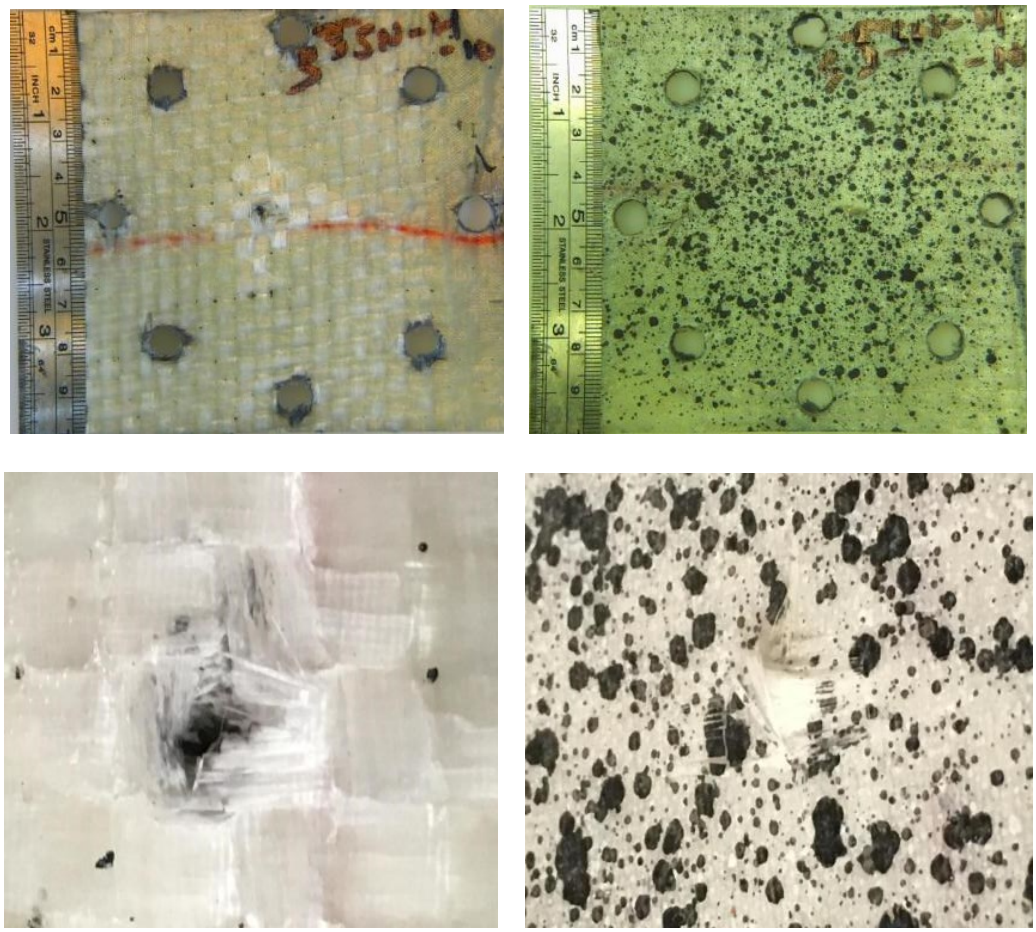

Figure 134. Shield Strand S® / Epoxy based 4.5 mm composite impacted at a velocity of 95.69 m/s with the sharp nose projectile.

The maximum transient out-of-plane displacement with stage time for specimen presented in Figure 135. From the figure , the maximum out-of-plane displacement reached a value of 5.527 mm in stage 36. A couple of impact waves are evident in Figure 135.

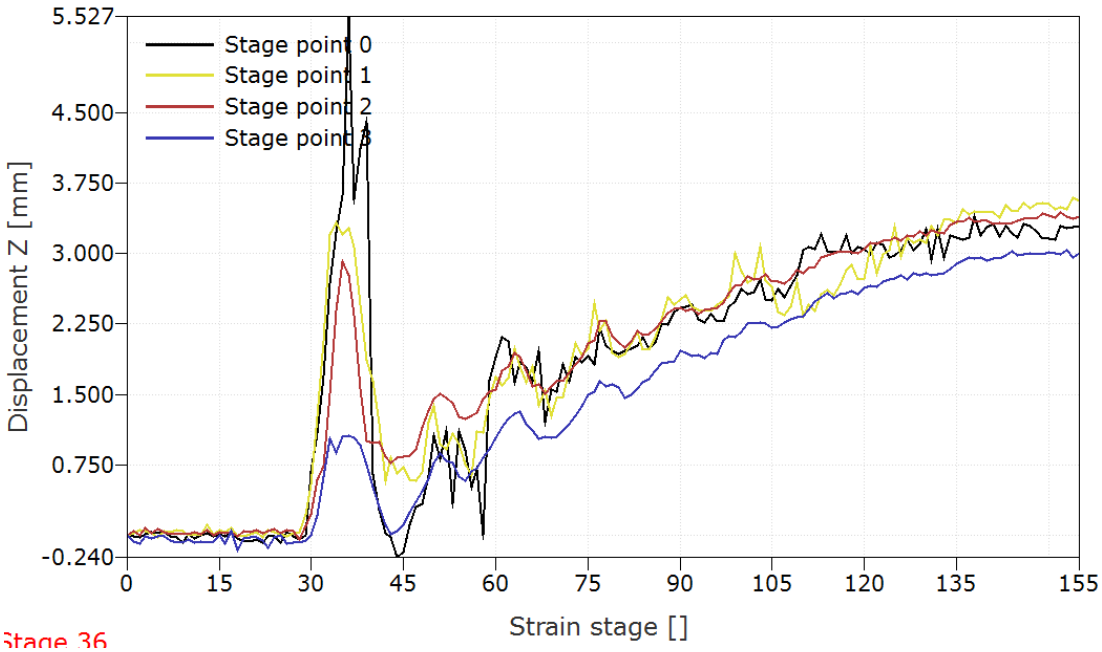

Figure 135. Displacement vs Stage graph of Shield Strand S® /Epoxy based 4.5 mm thick composite impacted at a velocity 95.69 m/s with the sharp nose projectile.

Figure 136 shows some deformation stages representing the impact event on the Shield Strand S® / Epoxy based 4.5 mm thick composite impacted at a velocity of 95.69 m/s with the sharp nose projectile. From the figure, it is evident how the out-of-plane deformation increased until a value of 5.527 mm was reached. Following this, the displacement decreased as shown in stage 45. Final displacement took a value close to 3.00 mm at the region of impact.

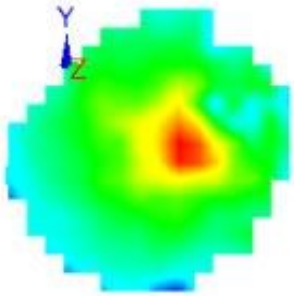

Stage 30

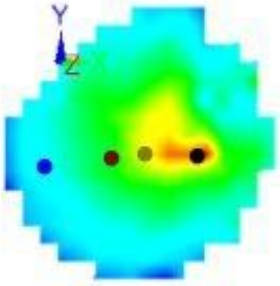

Stage 36

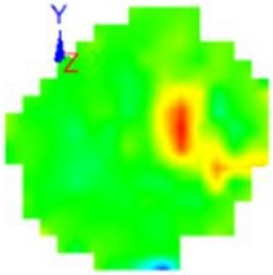

Stage 45

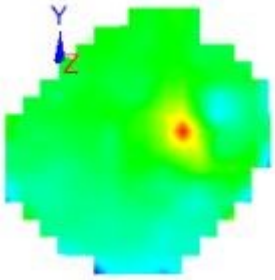

Stage 155

Figure 136. 3D Deformation stages of Shield Strand S® / Epoxy based 4.5 mm thick composite impacted at velocity 80.50 m/s with the sharp nose projectile.

Figure 137 shows the low magnification optical images of Shield Strand S® / Epoxy based 4.5 mm thick specimen impacted with the sharp nose projectile at a velocity of 109.4 m/s. From the figure, it is evident that on the point of contact of the projectile, heavy fiber ruptures are noticed along with minute matrix cracks as well as minute delamination in the region of impact. On the speckle pattern side, fiber ruptures are noticed.

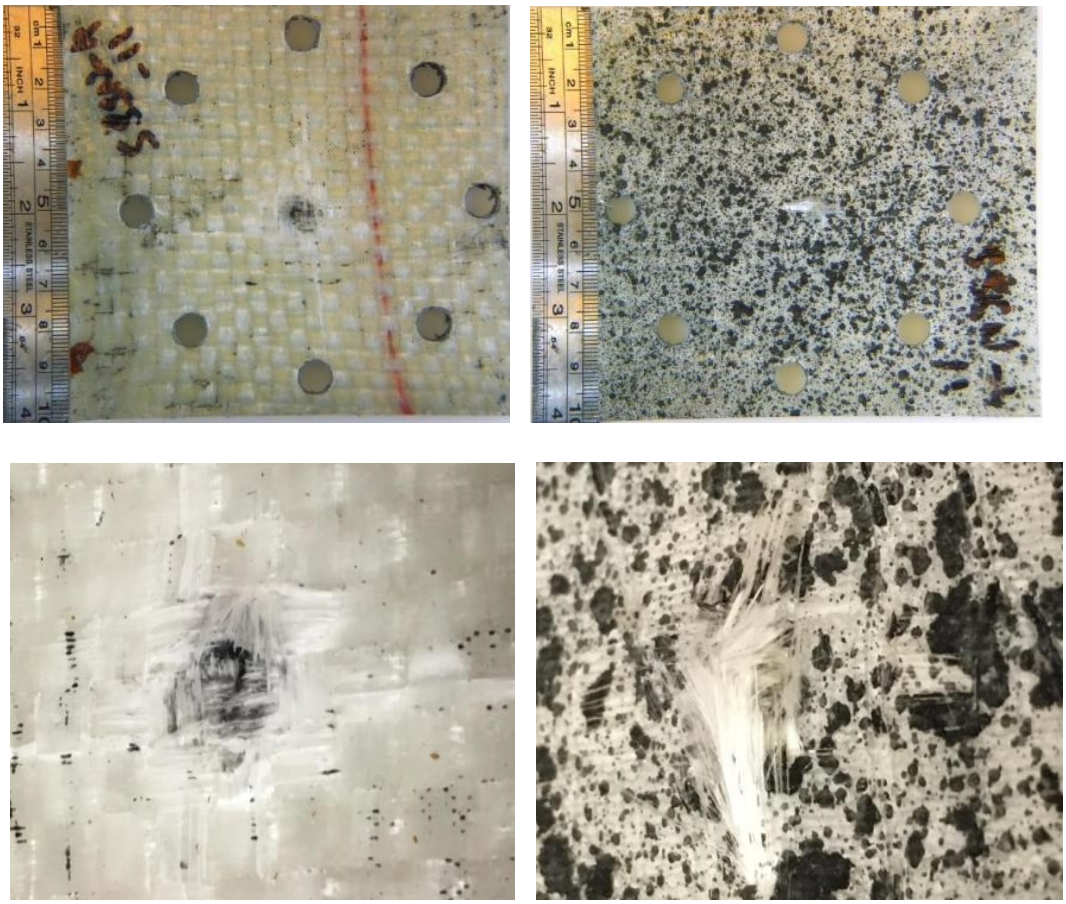

Figure 137. Shield Strand S® / Epoxy based 4.5 mm composite impacted at a velocity of 109.4 m/s with the sharp nose projectile.

The maximum transient out-of-plane displacement with stage time for specimen presented in Figure 138. From the figure , the maximum out-of-plane displacement reached a value of 7.12 mm in stage 29. Multiple impact waves are evident in Figure 138.

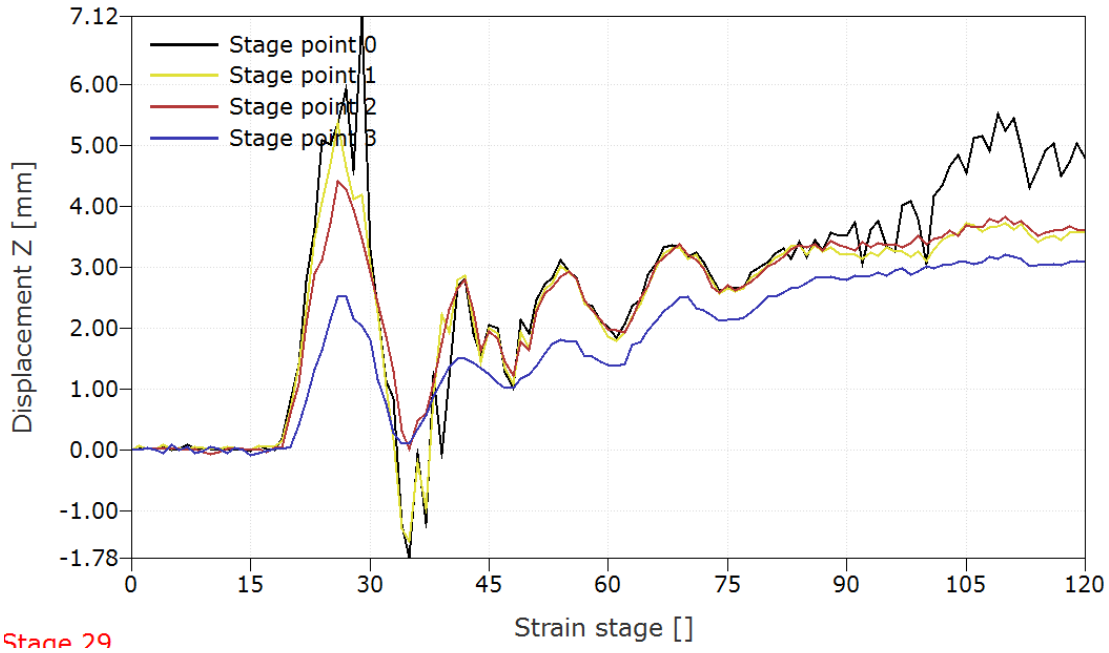

Figure 138. Displacement vs Stage graph of Shield Strand S® / Epoxy based 4.5 mm thick composite impacted at a velocity 109.4 m/s with the sharp nose projectile.

Figure 139 shows a number of deformation stages representing the impact event on the Shield Strand S/Epoxy based 4.5 mm thick composite impacted at the velocity of 109.4 m/s with a sharp nose projectile. From the figure, it is evident how the out-of-plane deformation increased until a value of 7.12 mm was reached in stage 29. Following this, the displacement decreased as shown in stage 37. Due to serrations in displacement-stage plot, final displacement could not be estimated.

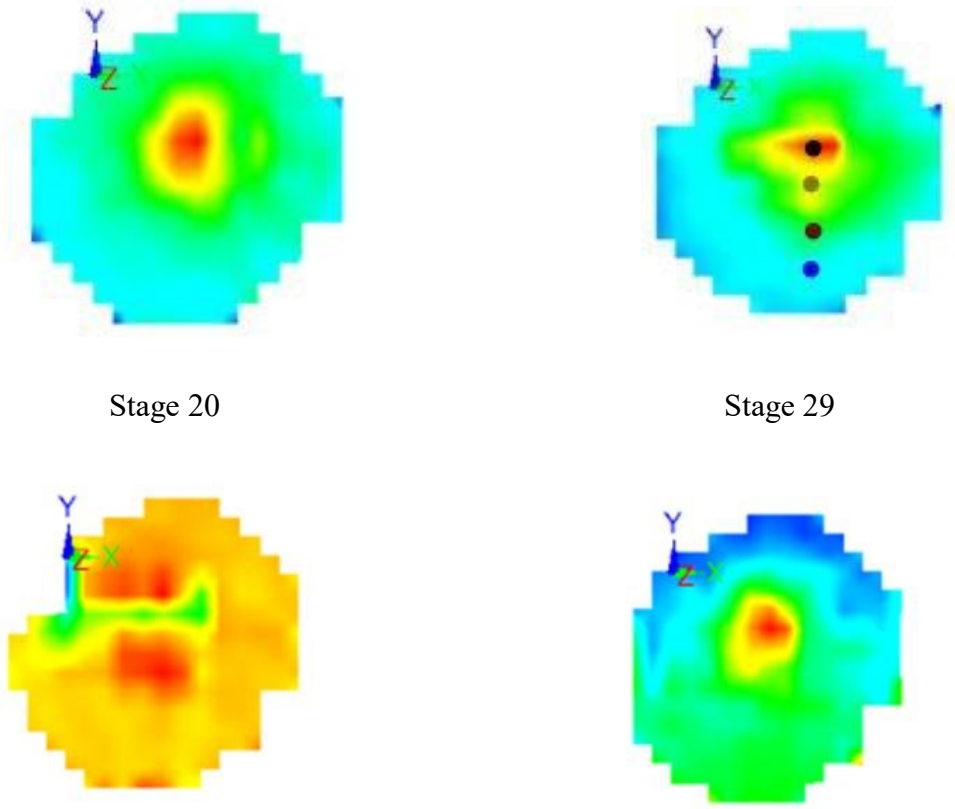

Figure 139. 3D deformation stages of Shield Strand S ®/Epoxy based 4.5 mm thick composite impacted at a velocity 109.4 m/s with the sharp nose projectile.

Figure 140 shows the low magnification optical images of Shield Strand S®/Epoxy based 4.5 mm thick specimen impacted with the sharp nose projectile at a velocity of 121.6 m/s. From the figure, it is evident that on the point of contact of the projectile, heavy fiber ruptures are noticed along with minute matrix cracks as well as delamination in the region of impact. On the speckle pattern side, fiber ruptures are observed, and fragmentation was seen.

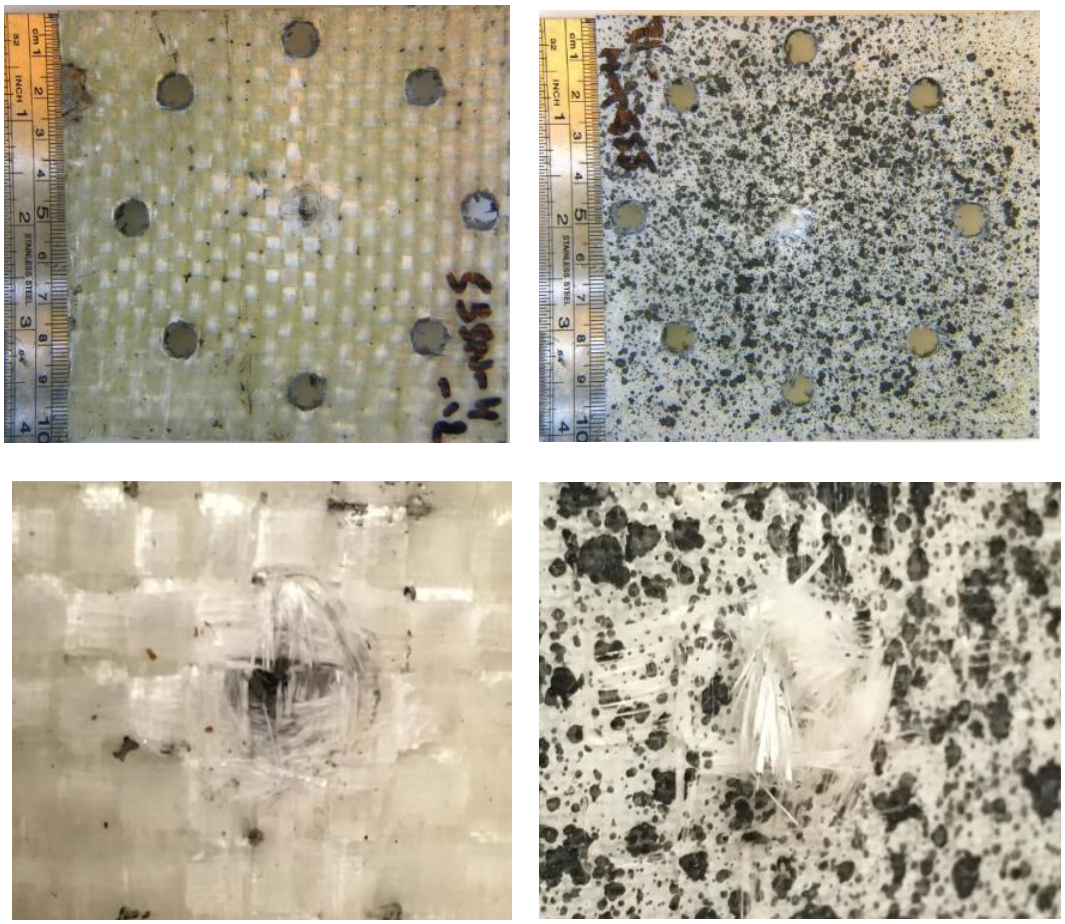

Figure 140. Shield Strand S® / Epoxy based 4.5 mm composite impacted at a velocity of 121.6 m/s with the sharp nose projectile.

The maximum transient out-of-plane displacement with stage time for the specimen presented in Figure 141. From the figure , the maximum out-of-plane displacement reached a value of 8.39 mm in stage 80. Multiple impact waves are evident in Figure 135.

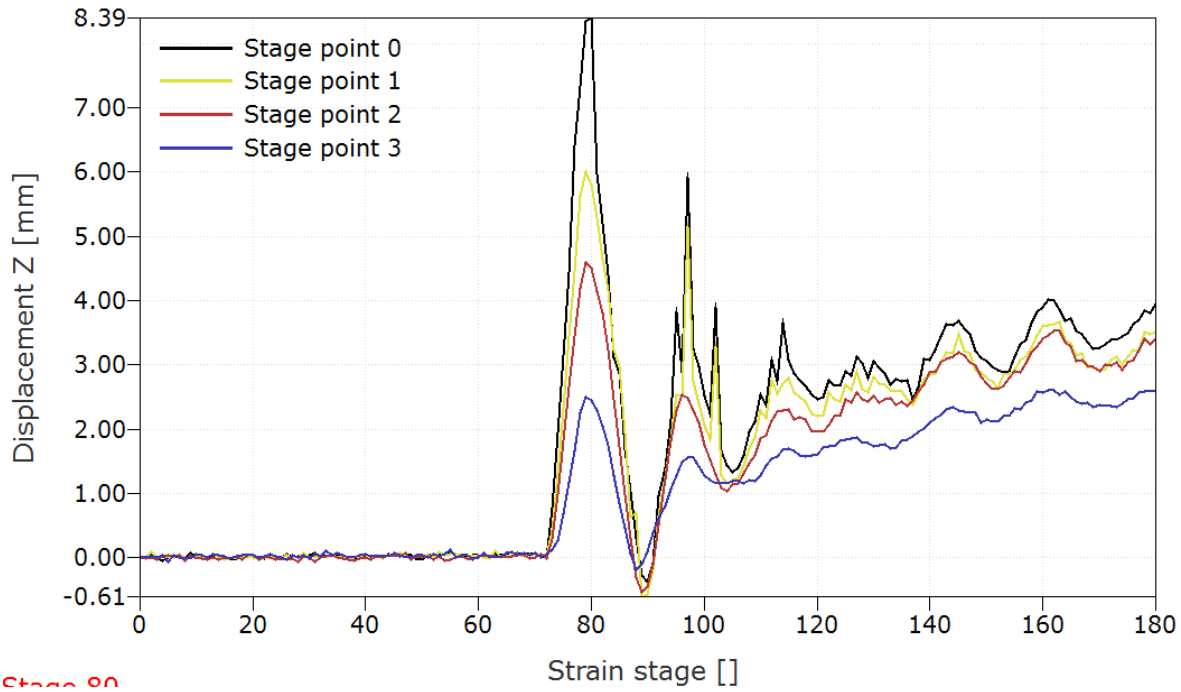

Figure 141. Displacement vs Stage graph of Shield Strand S® /Epoxy based 4.5 mm thick composite impacted at a velocity 121.6 m/s with the sharp nose projectile.

Figure 142 shows some deformation stages representing the impact event on the Shield Strand S® / Epoxy based 4.5 mm thick composite impacted at a velocity of 121.6 m/s with the sharp nose projectile. From the figure, it is evident how the out-of-plane deformation increased until a value of 8.39 mm was reached in stage 80. Following this, the displacement decreased as shown in stage 90. The final displacement took a value approximately close to 4.00 mm.

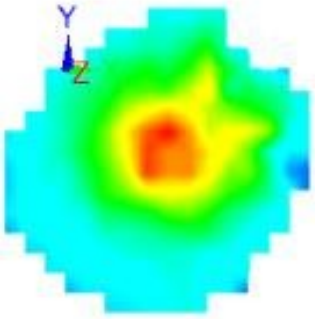

Stage 75

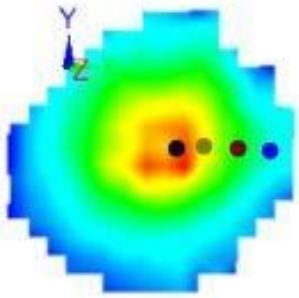

Stage 80

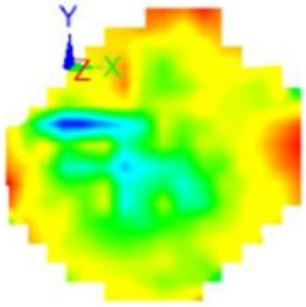

Stage 90

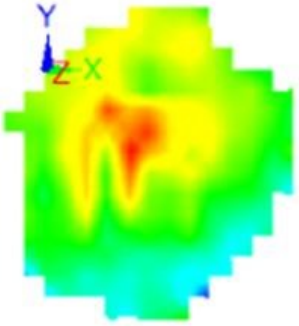

Stage 180

Figure 142. 3D deformation stages of Shield Strand S ®/ Epoxy based 4.5 mm thick composite impacted at a velocity 121.6 m/s with the sharp nose projectile.

Figure 143 shows the low magnification optical images of Shield Strand S® / Epoxy based 4.5 mm thick specimen impacted with the sharp nose projectile at a velocity of 134.24 m/s. From the figure, it is evident that on the point of contact of the projectile, heavy fiber ruptures are noticed along with matrix cracks as well as plus shaped delamination in the region of impact which shows that impact energy is absorbed by the primary yarns at this velocity. On the speckle pattern side, fiber ruptures are observed, and fragmentation was noticed.

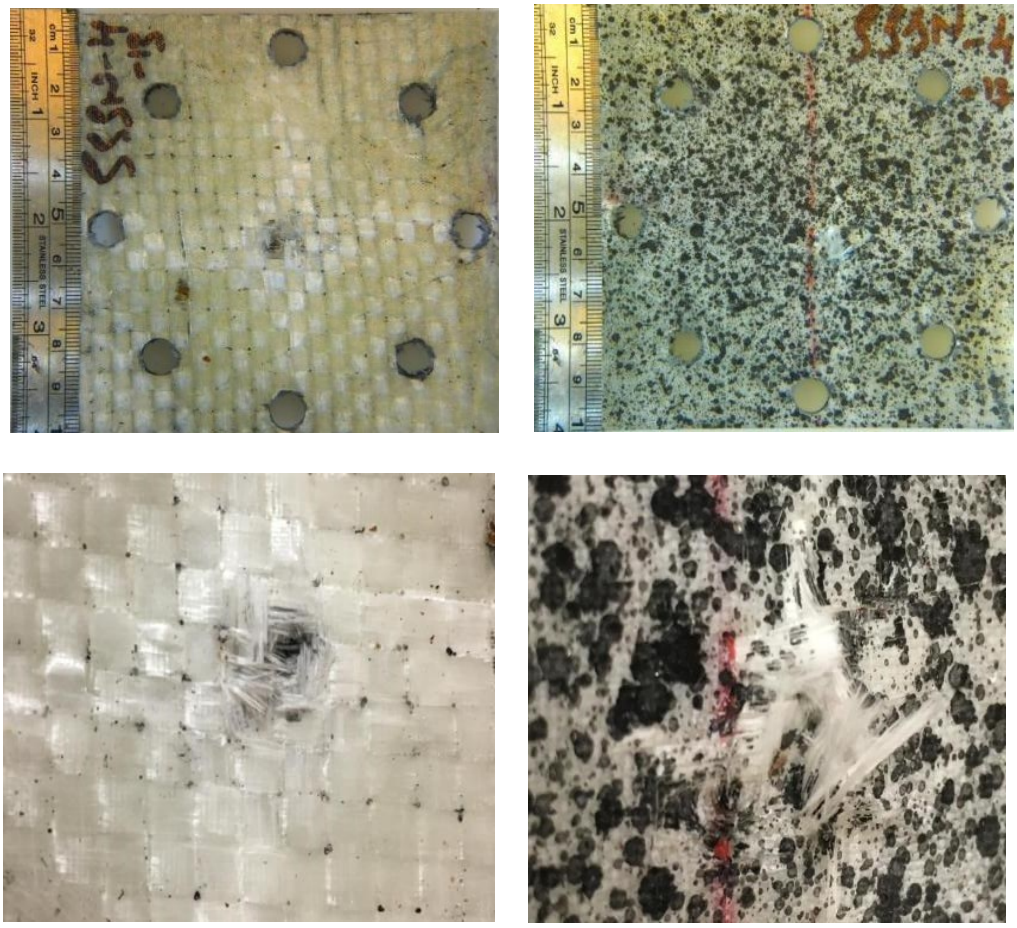

Figure 143. Shield Strand S® / Epoxy based 4.5 mm composite impacted at a velocity of 134.24 m/s with the sharp nose projectile.

The maximum transient out-of-plane displacement with stage time for specimen presented in Figure 144. From the figure, the maximum out-of-plane displacement reached a value of 11.1 mm in stage 66. Multiple impact of waves are evident in the figure.

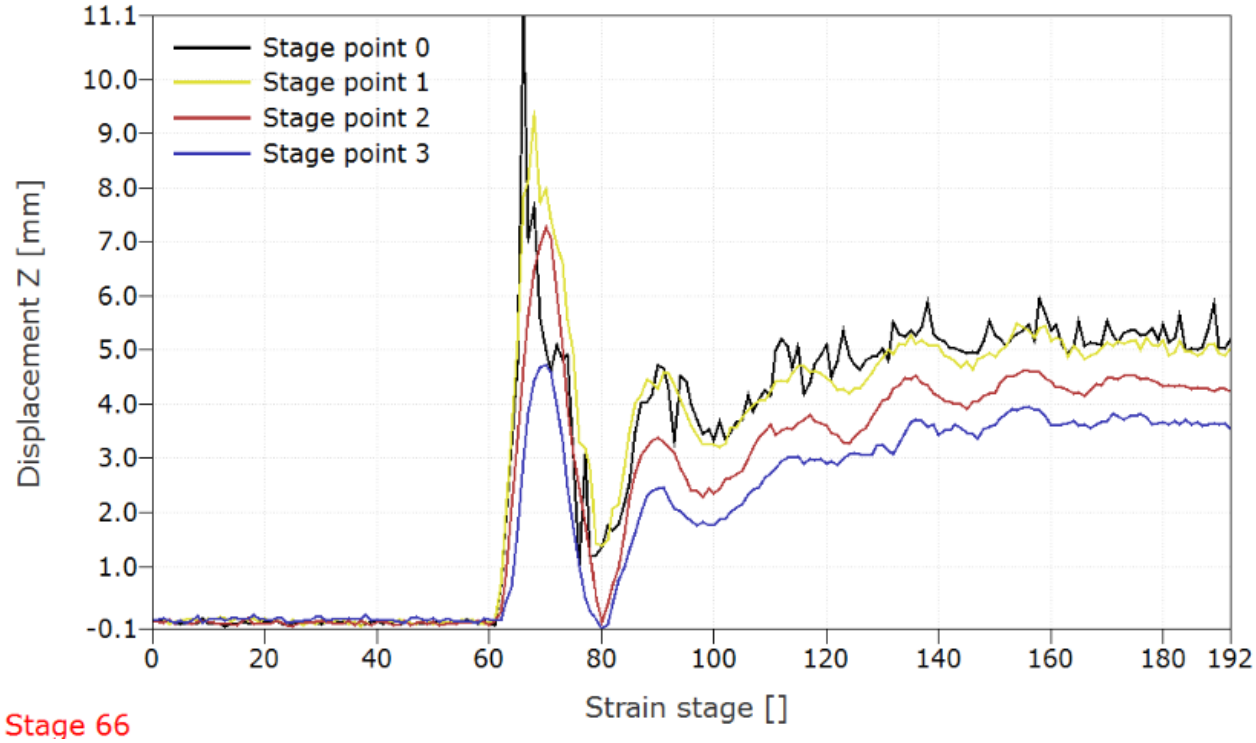

Figure 144. Displacement vs Stage graph of Shield Strand S ®/Epoxy based 4.5 mm thick composite impacted at a velocity 134.24 m/s with the sharp nose projectile.

Figure 145 shows a number of deformation stages representing the impact event on the Shield Strand S®/Epoxy based 4.5 mm thick composite impacted at a velocity of 134.4 m/s with the sharp nose projectile. From the figure, it is evident how the out-of-plane deformation increased until a value of 11.1 mm was reached in stage 66. Following this, the displacement decreased as shown in stage 81. The final displacement took a value approximately close to 5.50 mm.

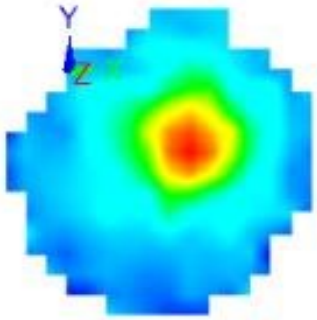

Stage 62

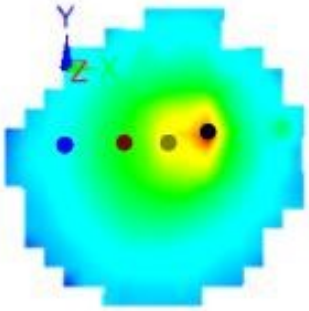

Stage 66

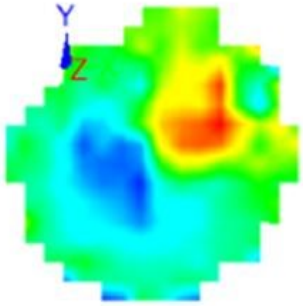

Stage 81

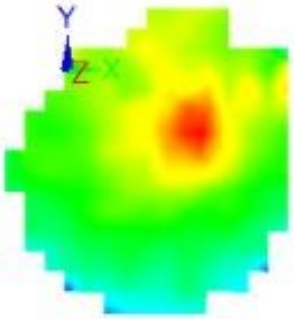

Stage 192

Figure 145. 3D deformation stages of Shield Strand S ®/Epoxy based 4.5 mm thick composite impacted at velocity 134.24 m/s with the sharp nose projectile.

Figure 146 shows the low magnification optical images of Shield Strand S® / Epoxy based 4.5 mm thick specimen impacted with the sharp nose projectile at a velocity of 152.4 m/s. From the figure, it is evident that on the point of contact of the projectile, heavy fiber ruptures are noticed along with matrix cracks as well as plus shaped delamination. On the speckle pattern side, fiber ruptures are observed, and fragmentation was noticed . Matrix cracking in a few areas of speckle pattern side is also evident.

Figure 146. Shield Strand S® / Epoxy based 4.5 mm thick composite impacted at a velocity of 152.4 m/s with the sharp nose projectile.

The maximum transient out-of-plane displacement with stage time for specimen presented in Figure 147. From the figure , the maximum out-of-plane displacement reached a value of 12.6 mm in stage 33. Few impact waves are evident in Figure 147.

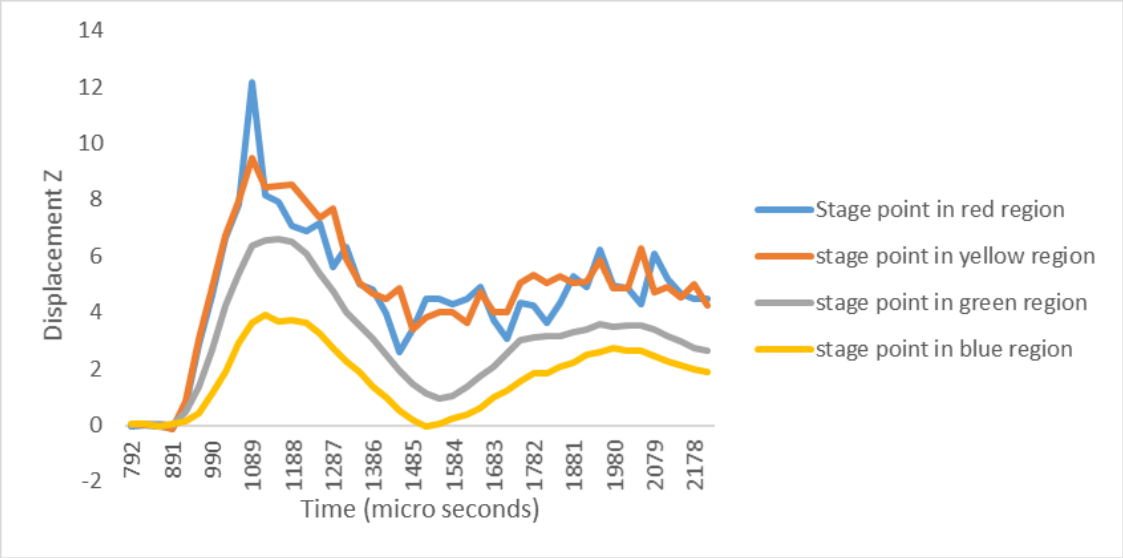

Figure 147. Displacement vs Stage graph of Shield Strand S®/ Epoxy based 4.5 mm thick composite impacted at a velocity 152.4 m/s with the sharp nose projectile.

Figure 148 shows a number of deformation stages representing the impact event on the Shield Strand S®/Epoxy based 4.5 mm thick composite impacted at a velocity of 152.4 m/s with the sharp nose projectile. From the figure, it is evident how the out-of-plane deformation increased until a value of 12.16 mm was reached in stage 33. Following this, the displacement decreased as shown in stage 44. From Figure 148, final displacement could not be estimated due to serrations in the curve but approximately it is assumed to be close to 6.00 mm.

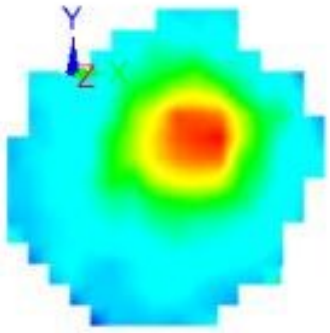

Stage 29

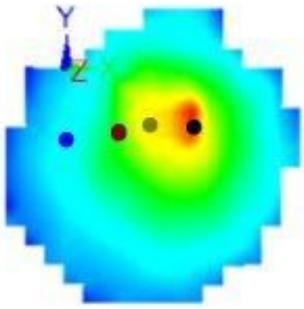

Stage 33

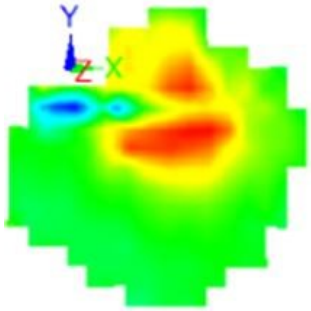

Stage 44

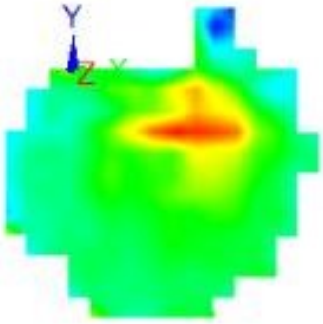

Stage 154

Figure 148. 3D deformation stages of Shield Strand S ®/ Epoxy based 4.5 mm thick composite impacted at a velocity 152.4 m/s with the sharp nose projectile.

Figure 149 shows the low magnification optical images of the Shield Strand S® / Epoxy based 4.5 mm thick specimen with the sharp nose projectile at a velocity of 173.4 m/s. At this velocity, specimen reached its ballistic limit. At the point of impact of the projectile, fiber ruptures are evident, and near the point of impact, matrix cracking, delamination and fiber ruptures are present. On the speckle pattern side, heavy fiber ruptures, as well as petaling, are noticed along with heavy fragmentation. Damages in the speckle pattern are evident due to matrix cracking in a few areas. Figure 149 includes a optical micrograph of section of impacted specimen.

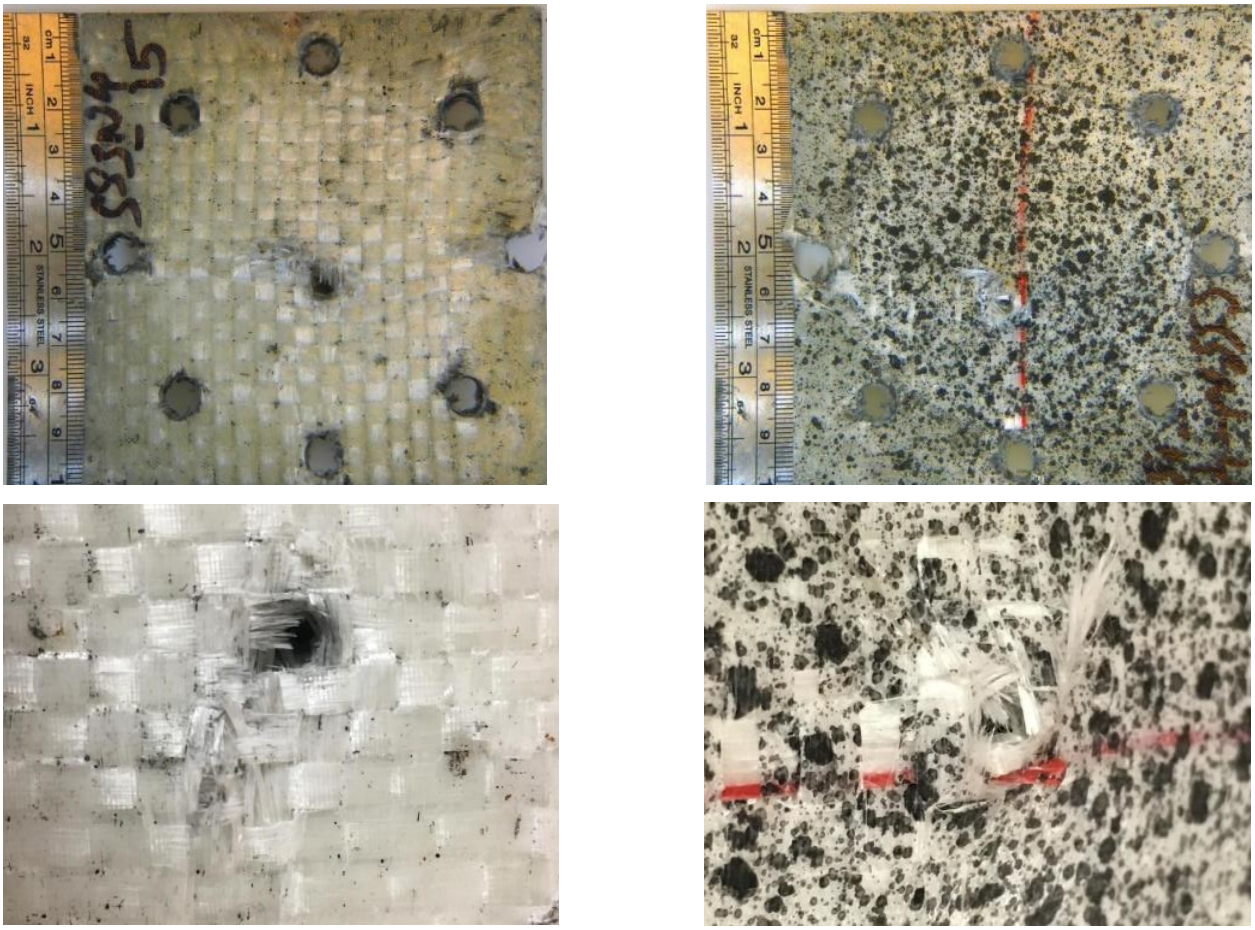

(a)

(b)

Figure 149. (a) Shield Strand S ®/ Epoxy based 4.5 mm composite impacted at a velocity of 173. 4 m/s with the sharp nose projectile (b) Section of impacted composite.

Table 3 shows a summary of the impact energies associated with the impact events for the thermoplastic composites subjected to ballistic testing with a spherical head projectile.

Relation between Impact velocity and Impact energy for Spherical head projectile							
Twintex 2.5 mm thick specimens		Shield Strand S/Epoxy 2.5 mm thick specimens		Twintex 4.5 mm thick specimens		Shield Strand S/Epoxy 4.5 mm thick specimens	
Impact Velocity (m/s)	Impact Energy(J)	Impact Velocity (m/s)	Impact Energy(J)	Impact Velocity (m/s)	Impact Energy(J)	Impact Velocity (m/s)	Impact Energy(J)
76.12	68.3	74.32	65.1	75.42	65.4	79.35	72.4
83.78	82.7	88.4	94.2	87.45	87.9	91.58	98.8
93.86	103	94.2	104.7	98.88	115	103.7	124.6
		101.5	121.5	107.8	133.6	116.3	159.2
		105	130			126.7	186.1
		118.5	165			144.8	247
						156.1	282.1
						164.5	319

Figure 150 shows the relation between perforation energy and specific perforation energy for Twintex® 2.5 mm and 4.5 mm thick composties impacted with the spherical head and sharp nose projectiles.

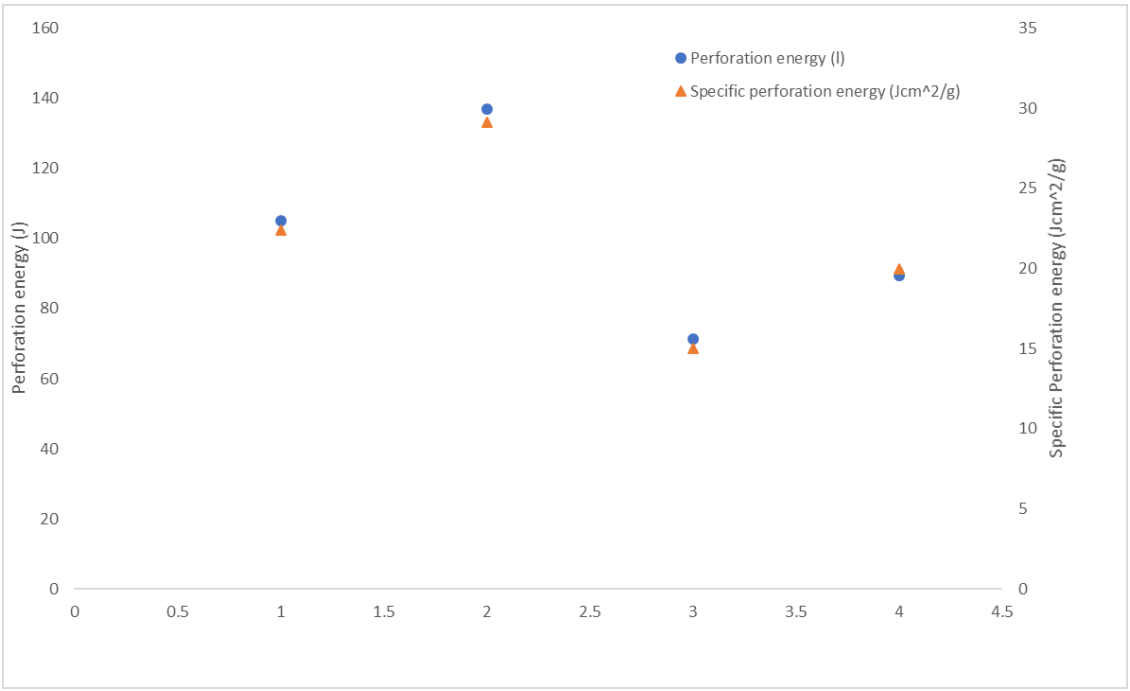

Figure 150. Relation between perforation energy and specific perforation energy for Twintex® composites impacted with the spherical head and sharp nose projectiles.

Table 4 shows a summary of the impact energies associated with the impact events for the thermoplastic composites subjected to ballistic testing with a sharp nose projectile.

Relation between Impact velocity and Impact energy for Sharpnose projectile							
Twintex 2.5 mm thick specimens		Shield Strand S/Epoxy 2.5 mm thick specimens		Twintex 4.5 mm thick specimens		Shield Strand S/Epoxy 4.5 mm thick specimens	
Impact Velocity (m/s)	Impact Energy(J)	Impact Velocity (m/s)	Impact Energy(J)	Impact Velocity (m/s)	Impact Energy(J)	Impact Velocity (m/s)	Impact Energy(J)
60.96	31.3	56.7	27	58.07	28.4	80.5	54.4
71.22	42.8	68.5	39.6	66.35	37	95.69	62
81.09	51.5	79.28	53	74.29	46.6	109.4	101
92.1	71.2	90.57	69.2	93.77	73.8	121.6	124.2
		114.4	110	103.25	89.5	134.24	151.3
		125.1	132			152.4	192
						173.4	252.5

Figure 151 shows the relation between perforation energy and specific perforation energy for Shield Starnd S® / Epoxy 2.5 mm and 4.5 mm thick composties impacted with the spherical head and sharp nose projectiles.

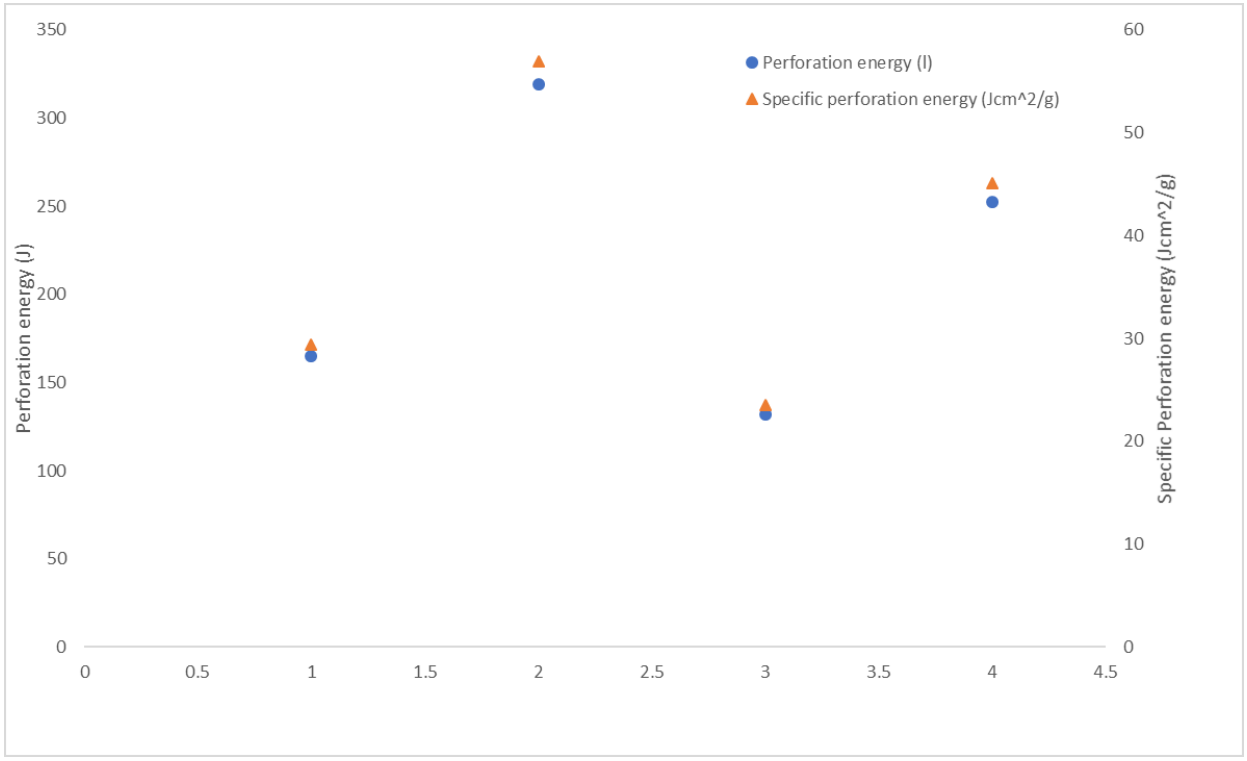

Figure 151. Relation between perforation energy and specific perforation energy for Shield Starnd S® / Epoxy composites impacted with the spherical head and sharp nose projectiles.

From these figures, its evident that the Shield Strand S® / Epoxy based composites offer greater impact resistance when compared to the Twintex® composites for a similar thickness when impacted with the spherical head projectile. Similar conclusions can be drawn from the high velocity impact testing with a sharp nose projectile and even when the thickness of the compsites was increased to 4.5 mm.

The specific perforation energy of the composites was calculated by the areal density of the target. These results also show that the Shield Strand S® / Epoxy based composites offer superior impact resistance to Twintex® based composites when subjected to ballistic loading conditions using spherical and for sharp nose projectiles. This can be attributed to the higher tensile and compressive properties of this S glass fibers used in the manufacturing of the thermoset based composites compared to thye E glass fibers used in the manufacturing of the thermoplastic based composites.

To predict the ballistic limit of the woven composites. In this research, the Reid and Wen analytical model was used [1]. The ballistic limit equation [2,3] is given by

$$V_b = \frac{\pi\Gamma\sqrt{\rho_t \sigma_e}}{4m} D^2 T \left[1 + \sqrt{1 + \frac{8m}{\pi\Gamma^2 \rho_t D^2 T}}\right] \quad [1]$$

Where,

V_b = Velocity at the ballistic limit

D = Diameter of the projectile

T = Total laminate thickness

m = Mass of the projectile

σ_e = Quasistatic linear elastic compression limit

Γ = 1.5 (for spherical head projectile), 0.03 (for sharp nose projectile)

ρ_t = Density of laminate

Here, In order to determine the quasistatic linear elastic compression limit, three-point bending tests are performed on the thermoplastic and thermoset based woven composites [3,4]. The

dimensions of the specimens for testing were considered according to the ASTM D7264 test standard [5] . Testing was performed using a universal testing machine (Instron 5967) at a strain rate of 1 mm/min as shown in Figure 152. For calculating the quasistatic linear elastic compression limit, the average of maximum loads obtained from the flexural testing for respective composite materials was used. Three-point testing results indicated values of σe of 470.5 MPa and 300.3 MPa for the thermoset and thermoplastic woven composites respectively.

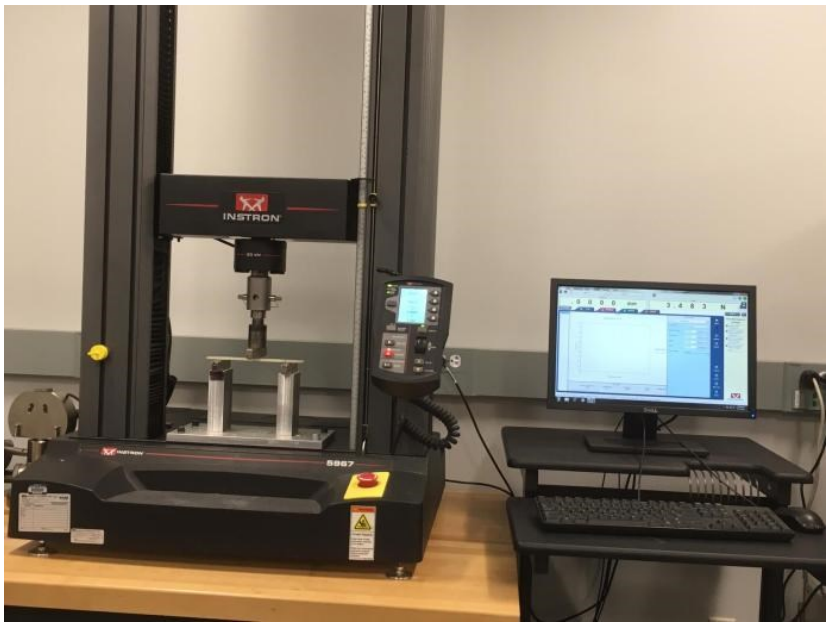

Figure 152. Three point bending testing on composite using an Instron 5967 universal testing machine.

Sample Calculation:

Twintex 2.5 mm thick composite impacted with the spherical head projectile

$$Vb = \frac{\prod * 1.5\sqrt{300.3 * 0.00145}}{4 * 23.6} * (11.9^2)2.5 * [1 + \sqrt{1 + \frac{8 * 23.6}{\prod * (1.5^2) * 0.00145 * (11.9^2) * 2.5}}]$$

$$= 96.348 \text{ m/s}$$

Figure 153 and 154 summarize the results following tests on thermoplastic and thermoset based woven composites with thickness 2.5 mm and 4.5 mm. Included in the figures are the predictions calculated using equation 1.

Figure 153 shows the relation between experimental and theoretical ballistic limit for Twintex® based 2.5 mm and 4.5 mm thick composites impacted with the spherical head and sharp nose projectile.

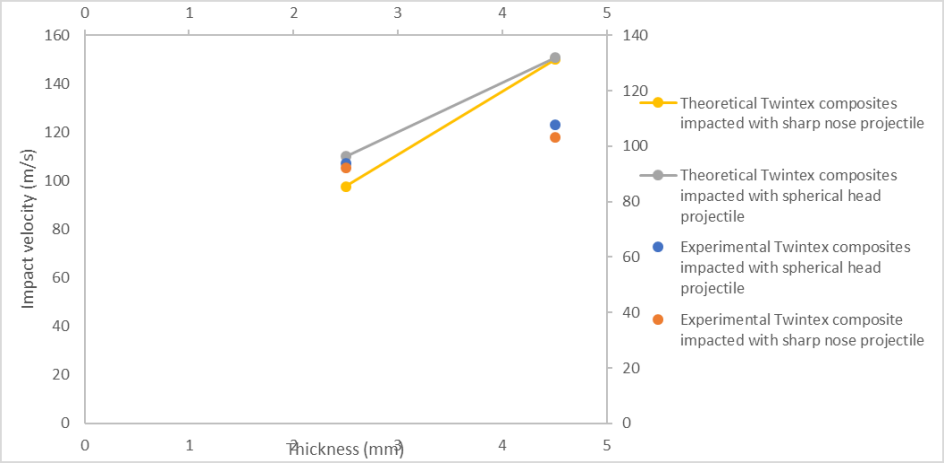

Figure 153. Relation between experimental and theoretical ballistic limit for Twintex® based composites impacted with the spherical head and sharp nose projectile.

Figure 154 shows the relation between experimental and theoretical ballistic limit for Shield Strand S® / Epoxy based 2.5 mm and 4.5 mm thick composites impacted with the spherical head and sharp nose projectile.

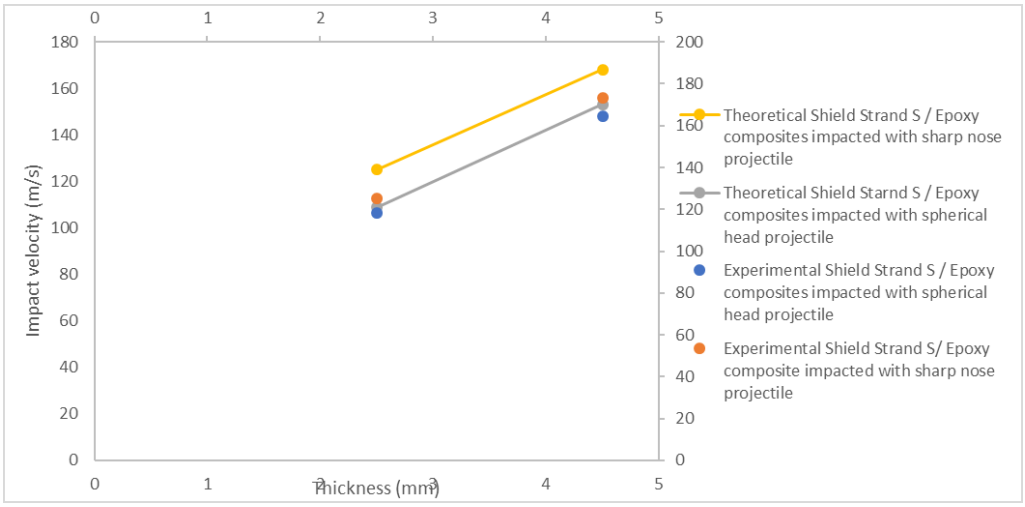

Figure 154. Relation between experimental and theoretical ballistic limit for Shield Strand S® / Epoxy based composites impacted with the spherical head and sharp nose projectile.

From the figures, it is evident that the ballistic limit increases with increasing composite thickness. A similar trend can be observed after testing with the spherical head and sharp nose projectiles. Furthermore, the predictions offered by the analytical model are in good agreement with the experimental data. These results suggest that the ballistic limit of thermoplastic and thermoset woven composites based on E-glass and S glass fibers respectively, using spherical head and sharp nose projectiles can be predicted accurately using Reid and Wen's perforation model [1].

References

[1] S R Reid, H M Wen, 2000, "Perforation of FRP laminates and sandwich panels subjected to missile impact" *A volume in Woodhead Publishing Series in Composites Science and Engineering, Impact Behaviour of Fibre-Reinforced Composite Materials and Structures*, Chapter-8, Pages 239-279

[2] G R Villanueva, WJ Cantwell, 2003, "The high velocity impact response of composite and FML-reinforced sandwich strutures", *Composite Science and Technology* 64 (2004) 35-54

[3] M R Abdullah, WJ Cantwell, 2012, "The high-velocity impact response of thermoplastic–matrix fiber–metal laminates" *J Strain Analysis* 47(7) 432–443

[4] S Yashiro, K Oji, 2011, "High-velocity impact damage behavior of plain-woven SiC/SiC composites after thermal loading" *Elsevier* Composites Part B: Engineering Volume 43, Issue 3, Pages 1353-1362

[5] ASTM D7264/D7264M standards, 2015, "Standard Test Method for Flexural Properties of Polymer Matrix Composite Materials"

CHAPTER 5

CONCLUSIONS

In this project, the ballistic properties of Shield Strand S ® / Epoxy and E-glass fibers / Polypropylene (Twintex ®) based woven composites were investigated using spherical head and sharp nose projectiles. A single stage gas gun setup was used for ballistic testing and a noncontact deformation measurement technique was used to investigate the maximum transient out of plane and final back face displacement of the composites. Many failure modes were highlighted. From the results, it was evident that the thermoset based woven composites exhibited improved impact resistance when compared to the thermoplastic based composites. It was also noticed that the Shield Strand S® / Epoxy 2.5 mm thick composites showed superior ballistic properties compared with the Twintex 4.5 mm thick composites. Furthermore, E-glass fiber reinforced polypropylene exhibited similar values of ballistic limit when subjected to ballistic loading using either the spherical head or the sharp nose projectile highlighting the excellent energy absorbing capabilities of the composite to localized impact loading. In addition, the Shield Strand S® fiber reinforced epoxy exhibited an improved impact response when subjected to ballistic loading using the sharp nose projectile compared to the spherical head projectile. Composites projected with the spherical projectiles had more maximum out of plane displacement when compared to the composites projected with the sharp nose projectiles. It was noticed that thermoset based composites had more maximum out of plane transient displacement when compared with the thermoplastic based composites. It is fascinating to observe that Shield Strand S® / Epoxy 2.5 mm composites showed approximately same maximum out of plane transient displacement when compared to the Twintex® 4.5 mm composites at the same velocities.

An analytical model was successfully used to predict the ballistic limit of the woven composites, results from the analytical model were in good agreement with the experimental results.